

# UC Riverside

## UC Riverside Electronic Theses and Dissertations

### Title

Sulfate Radical-Based Advanced Oxidation Treatment for Groundwater Water Treatment and Potable Water Reuse

### Permalink

<https://escholarship.org/uc/item/4qc8f723>

### Author

Li, Wei

### Publication Date

2017

Peer reviewed|Thesis/dissertation

UNIVERSITY OF CALIFORNIA  
RIVERSIDE

Sulfate Radical-Based Advanced Oxidation Treatment for Groundwater Water Treatment  
and Potable Water Reuse

A Dissertation submitted in partial satisfaction  
of the requirements for the degree of

Doctor of Philosophy

in

Environmental Toxicology

by

Wei Li

September 2017

Dissertation Committee:

Dr. Haizhou Liu, Chairperson

Dr. Sharon Walker

Dr. Dan Schlenk

Copyright by  
Wei Li  
2017

The Dissertation of Wei Li is approved:

---

---

---

Committee Chairperson

University of California, Riverside

## **Acknowledgements**

I would like to thank my adviser Dr. Haizhou Liu for his guidance and support throughout my Ph.D. career. Dr. Liu is a very responsible and knowledgeable PI. He is always seeking opportunities to help his lab grow and supporting his students. He is available for students' questions no matter how big or small. He also provides us with good networking opportunities and takes the time to teach us how to effectively communicate our work beyond the lab. He is very active and patient in helping us write manuscripts and teaching us how to improve writing skills. Under his guidance, I was able to publish three manuscripts on highly impactful journal articles with his help. He is always actively seeking new collaborators for our research projects and exposing us to the more applied side of our work. Dr. Liu's active engagement and enthusiasm for his students encouraged me to be productive and successful in perusing my Ph.D. career.

Additionally, I would like to thank the members of my dissertation committee, Dr. Sharon Walker and Dr. Dan Schlenk, for their support and guidance throughout my research. Dr. Walker treats students like her children. She always spends time with them and cares about their progress and personal lives. She always thinks ahead. Dr. Walker is busy as an associate dean, but she is always prodigal of her care to her students. Dr. Schlenk is the nicest PI I have ever met. He is so supportive and always available to my questions. He provides lab space, equipment, and supplies whenever I needed. Without him, I could not have finished the toxicity study on time.

I also want to give my special thanks to the undergraduate students and high school students, including Heidi Li, Ruben Gonzalez, Natalia Camargos, Katerina Gan, Alex

Numa, Lara Guadalupe, and Kayla Cervera, who worked with me on my research. They helped me a lot in preparing experiments, collecting data, and cleaning the lab equipment afterwards. Without them, I could not complete my research projects so quickly and smoothly.

Parts of this doctoral work have already been published in or submitted to the following journals: Chapter 2 (published in *Environmental Science & Technology*, 2017), Chapter 3 (Submitted to *Environmental Science & Technology*, 2017), Chapter 4 (published in *Environmental Science & Technology: Water Research*, 2016), Chapter 5 (Submitted to *Environmental Science & Technology letters*, 2017).

This research was primarily supported by the University of California, Riverside, the NSF Graduate Research Fellowship, the NSF IGERT fellowship and the Orange County Water District. Any opinion, findings, and conclusions or recommendations in this material are the authors(s) and do not necessarily reflect the views of any these organizations listed above.

## **Dedication**

This dissertation is dedicated to my great mom, Minjie Zhang. She was diagnosed with Lambert-Eaton disease in 2014, a year after I got into the Ph.D. program. Even though her health is getting worse every day, she has never complained about me going home late. She has helped me to raise my kids and relieve my worries about family so that I could be working at full strength. Her supportiveness and dedication pushes me through many difficulties which helped me complete my Ph.D. degree.

I also want to thank my kids, Kingsley and Katrina. I appreciate their understanding, love, and supportiveness. As a single parent, I did not spend much time with them, and sometimes, I had to miss their ceremonies, but they never complained. They also help to take care of their grandma and around the household. Thank you for being with me all these years.

## ABSTRACT OF THE DISSERTATION

Sulfate Radical-Based Advanced Oxidation Treatment for Groundwater Water Treatment  
and Potable Water Reuse

by

Wei Li

Doctor of Philosophy, Graduate Program in Environmental Toxicology  
University of California, Riverside, September 2017  
Dr. Haizhou Liu, Chairperson

Climate change and population growth pose increasing challenges to the availability of fresh water resources. Remediation of contaminated groundwater and recycling of wastewater are two promising solutions to increase fresh water supplies. Persulfate ( $S_2O_8^{2-}$ )-based advanced oxidation processes (AOPs) have gained increasing attention in recent years due to the generation of highly reactive and selective sulfate radicals ( $SO_4^{\bullet-}$ ).  $S_2O_8^{2-}$ -based AOPs have been widely used in *in situ* chemical oxidation (ISCO) for groundwater remediation. UV/ $S_2O_8^{2-}$  is also an alternative to UV/ $H_2O_2$  that can be used to treat recycled wastewater into high quality drinking water.

In this dissertation work, the application of  $S_2O_8^{2-}$ -based AOPs in ISCO and UV/AOPs was examined. First, the effects of important groundwater chemical parameters, *i.e.*, alkalinity, pH and chloride on benzene degradation via heterogeneous  $S_2O_8^{2-}$  activation by three Fe(III)- and Mn(IV)-containing aquifer minerals (*e.g.* ferrihydrite, goethite and pyrolusite) were examined. A comprehensive kinetic model was established to elucidate the mechanisms of radical generation and mineral surface complexation. Results showed

that an increase of alkalinity up to 10 meq/L decreased the rates of persulfate decomposition and benzene degradation. These results were associated with the formation of unreactive surface carbonato complexes. An increase in pH generally accelerated persulfate decomposition due to enhanced formation of reactive surface hydroxo complexation. A change in the chloride level up to 5 mM had a negligible effect on the reaction kinetics. Kinetics modeling also suggested that  $\text{SO}_4^{\bullet-}$  was transformed into hydroxyl radicals ( $\text{HO}^{\bullet}$ ) and carbonate radicals ( $\text{CO}_3^{\bullet-}$ ) at higher pHs.

Secondly, we investigated 1,4-dioxane degradation by  $\text{UV}/\text{S}_2\text{O}_8^{2-}$  in the presence of monochloramine ( $\text{NH}_2\text{Cl}$ ), a membrane anti-fouling reagent. The mixing effects of  $\text{NH}_2\text{Cl}$  and  $\text{S}_2\text{O}_8^{2-}$  on 1,4-dioxane degradation were examined at various oxidant doses, chloride concentrations, solution pHs and dissolved  $\text{O}_2$  levels. Results showed that a  $\text{NH}_2\text{Cl}$ -to- $\text{S}_2\text{O}_8^{2-}$  molar ratio of 0.1 was optimal, beyond which the scavenging effects of  $\text{NH}_2\text{Cl}$  on  $\text{HO}^{\bullet}$ ,  $\text{SO}_4^{\bullet-}$ , and  $\text{Cl}_2^{\bullet-}$  radicals decreased 1,4-dioxane degradation rate. At the optimal ratio, the degradation rate of 1,4-dioxane increased linearly with the total oxidant dose up to 6 mM. The simultaneous photolysis of  $\text{NH}_2\text{Cl}$  and  $\text{S}_2\text{O}_8^{2-}$  was sensitive to the solution's pH, due to a disproportionation of  $\text{NH}_2\text{Cl}$  into less photo-reactive dichloramine ( $\text{NHCl}_2$ ) and radical scavenger  $\text{NH}_4^+$  at pH lower than 6. An increase of chloride concentration transformed reactive  $\text{HO}^{\bullet}$  and  $\text{SO}_4^{\bullet-}$  to less reactive  $\text{Cl}_2^{\bullet-}$ , while the presence of dissolved  $\text{O}_2$  promoted 1,4-dioxane degradation and gaseous nitrogen production by participating in the 1,4-dioxane and  $\text{NH}_4^+$  oxidation steps.

Third, based on the experimental investigations, a kinetic model was developed and

the fundamental mechanisms of contaminant degradation by three UV/AOPs, *i.e.*, UV/hydrogen peroxide ( $\text{H}_2\text{O}_2$ ), UV/ $\text{S}_2\text{O}_8^{2-}$  and UV/chlorine ( $\text{HOCl}$ ) were simulated. Results showed that the treatment efficiency of contaminants generally followed the order of  $\text{UV}/\text{S}_2\text{O}_8^{2-} > \text{UV}/\text{H}_2\text{O}_2 > \text{UV}/\text{HOCl}$  under chemical conditions relevant to reverse osmosis (RO) permeate. The generation of  $\text{HO}^\bullet$  was important in  $\text{UV}/\text{H}_2\text{O}_2$  to degrade contaminants, whereas both  $\text{SO}_4^{\bullet-}$  and  $\text{HO}^\bullet$  contributed to degradation of contaminants in  $\text{UV}/\text{S}_2\text{O}_8^{2-}$ .  $\text{CO}_3^{\bullet-}$  predominated in  $\text{UV}/\text{HOCl}$ . Among the three UV/AOPs, the treatment efficiency of  $\text{UV}/\text{S}_2\text{O}_8^{2-}$  was most sensitive to pH, chloride and inorganic carbon. The results provided guidance on the design and optimization of UV/AOP systems for water reuse under diverse chemical conditions.

Finally, the oxidation byproducts (OBPs) of benzene and 1,4-dioxane by  $\text{S}_2\text{O}_8^{2-}$ -based AOPs were investigated, and the cytotoxicity and genotoxicity levels of the parent compound and oxidation byproducts were compared. Results showed that phenol and aldehyde were the major products from benzene degradation. 1,4-dioxane was transformed into six major intermediates after UV/AOP treatments including ethylene glycol diformate, formaldehyde, glycolaldehyde, glycolic acid, formic acid, and methoxyacetic acid. Toxicity assays showed that the aldehyde and phenol were extremely genotoxic and cytotoxic compared to benzene and 1,4-dioxane. Results suggested that evaluation of the efficiency of any AOPs applied to water treatment must not only include study of the disappearance of the parent compound, but also needs further study of the toxicity of the subsequent oxidation byproducts.

# Table of Contents

Acknowledgements.....	iv
Dedication.....	vi
Abstract.....	vii
List of Schemes.....	xiii
List of Figures.....	xiv
List of Tables.....	xviii
<b>Chapter 1 Introduction.....</b>	<b>1</b>
1.1 Motivation: in Response to Fresh Water Crisis.....	2
1.2 Persulfate-Based ISCO for Groundwater Remediation.....	3
1.3 Persulfate-Based <i>UV/AOPs</i> for Potable Water Reuse.....	7
1.4 Toxicity Assessment for Oxidation Byproducts.....	11
1.5 Experimental Approaches.....	12
1.6 Research Objectives.....	18
<b>Chapter 2 Persulfate-Based ISCO for Groundwater Remediation: Impacts of Alkalinity, pH and Chloride.....</b>	<b>29</b>
2.1 Introduction.....	30
2.2 Materials and Methods.....	32
2.3 Results and Discussion.....	35
2.4 Environmental Implication.....	58
2.5 Acknowledgements.....	58

<b>Chapter 3 Persulfate-Based UV/AOP for Potable Water Reuse: Impact of Chloramine, Chloride, pH, and Oxygen Levels on 1,4-dioxane Removal by UV/Persulfate</b> .....	67
3.1 Introduction .....	68
3.2 Materials and Methods .....	70
3.3 Results and Discussion .....	74
3.4 Engineering Implications.....	88
3.5 Acknowledgements .....	89
<b>Chapter 4 Modeling Approach for A Mechanistic Understanding of the Degradation of Trace Organic Contaminants by UV/Hydrogen Peroxide, UV/Persulfate and UV/Free Chlorine for Water Reuse</b> .....	95
4.1 Introduction .....	96
4.2 Materials and Methods .....	99
4.3 Results and Discussion .....	106
4.4 Engineering Implications.....	129
4.5 Conclusions .....	130
4.6 Acknowledgments .....	131
<b>Chapter 5 Toxicity Assessment of Benzene and 1,4-dioxane Oxidation Byproducts</b> .....	140
5.1 Introduction .....	141
5.2 Materials and Methods .....	143

5.3	Results and Discussion .....	141
5.4	Engineering Implications.....	160
5.5	Acknowledgments .....	161
<b>Chapter 6 Summary and Conclusions .....</b>		<b>169</b>
6.1	Persulfate-Based ISCO for Groundwater Remediation: Impacts of Alkalinity, pH and Chloride .....	170
6.2	$S_2O_8^{2-}$ -Based AOPs for Potable Water Reuse .....	172
6.3	Modeling Approach for Simulating and Comparing Full Scale UV/H <sub>2</sub> O <sub>2</sub> , UV/S <sub>2</sub> O <sub>8</sub> <sup>2-</sup> , and UV/HOCl.....	174
6.4	Toxicity Assessment of Benzene and 1,4-dioxane Oxidation Byproducts ..	176
<b>Appendix A Supplemental Information for Chapter 2 .....</b>		<b>178</b>
<b>Appendix B Supplemental Information for Chapter 3 .....</b>		<b>196</b>
<b>Appendix C Supplemental Information for Chapter 4 .....</b>		<b>216</b>

# List of Scheme

<b>Scheme 1.</b> Interaction of $S_2O_8^{2-}$ with aquifer chemical constituents during ISCO. ....	6
<b>Scheme 2</b> Advanced treatment processes for portable water reuse.....	8
<b>Scheme 3</b> Radical distribution in UV/ $S_2O_8^{2-}$ and UV/ $NH_2Cl$ .....	9
<b>Scheme 4.</b> Experimental set up for persulfate activation by aquifer minerals. ....	14
<b>Scheme 5</b> UV photo reactor. ....	15
<b>Scheme 6</b> Genotoxicity study using HCT-116 human colorectal carcinoma cells ..	18
<b>Scheme 7</b> Radical reaction pathways in UV/persulfate with monochloramine. ....	78
<b>Scheme 8</b> A diagram of the single UV flow-through reactor.....	99
<b>Scheme 9</b> Generation and transformation of radicals from UV/ $H_2O_2$ , UV/ $S_2O_8^{2-}$ and UV/ $HOCl$ in the presence of chloride and inorganic carbon. ....	110
<b>Scheme 10</b> Proposed benzene degradation pathway.....	152
<b>Scheme 11</b> Proposed 1,4-Dioxane degradation pathway in UV/ $S_2O_8^{2-}$ , UV/ $H_2O_2$ , and UV/ $NH_2Cl$ .....	154

<b>Figure 1.</b> Surface area-normalized first-order decay rate constant of persulfate decomposition.....	36
<b>Figure 2.</b> The kinetics of persulfate decomposition and benzene degradation in the presence of different metal oxides.....	36
<b>Figure 3</b> Surface area-normalized first-order rate constants of benzene degradation. ..	40
<b>Figure 4.</b> Correlation between the stoichiometric efficiency of radical yield ( $E_{S_{2O_8^{2-}}}$ ) and the rate of persulfate decomposition ( $k_{S_{2O_8^{2-}}}$ ). .....	40
<b>Figure 5.</b> Impact of alkalinity on persulfate decomposition and benzene degradation by three minerals.....	42
<b>Figure 6</b> Impact of pH on the rates of persulfate decomposition and benzene degradation by three minerals.....	44
<b>Figure 7</b> The impact of pH on persulfate decomposition in the absence of minerals.	46
<b>Figure 8</b> Impact of chloride on the rates of persulfate decomposition and benzene degradation by three minerals.....	49
<b>Figure 9</b> The correlation between the rate of persulfate decomposition and the fraction of carbonate complex on Fe(III) and Mn(IV) mineral.....	54
<b>Figure 10.</b> Correlation between the yields of benzene oxidation products and branching ratio of $SO_4^{\bullet-}$ , $HO^{\bullet}$ and $CO_3^{\bullet-}$ reacting with benzene.....	57
<b>Figure 11</b> Effect of $NH_2Cl$ dose on 1,4-dioxane degradation.....	75
<b>Figure 12</b> Impact of oxidant dosage on 1,4-D degradation.....	76

<b>Figure 13.</b> Effect of $\text{NH}_2\text{Cl}$ dosage on the treatbility of 1,4-dioxane by UV/ $\text{S}_2\text{O}_8^{2-}$ and $\text{NH}_2\text{Cl}$ .....	77
<b>Figure 14.</b> Effect of $\text{NH}_2\text{Cl}$ dosage on 1,4-dioxane degradation by UV/ $\text{S}_2\text{O}_8^{2-}$ and $\text{NH}_2\text{Cl}$ at a fixed chloride concentration. ....	79
<b>Figure 15.</b> Impact of persulfate dosage and oxygen on $\text{NH}_2\text{Cl}$ product distribution. ....	80
<b>Figure 16</b> Persulfate photolysis products.....	81
<b>Figure 17.</b> Impact of total oxidant dosage on the treatment of 1,4-dioxane by UV/ $\text{S}_2\text{O}_8^{2-}$ and $\text{NH}_2\text{Cl}$ .....	83
<b>Figure 18.</b> Impact of chloride on 1,4-dioxane treatment by UV/ $\text{S}_2\text{O}_8^{2-}$ and $\text{NH}_2\text{Cl}$ . (A) Impact of chloride on 1,4-dioxane degradation rate and radical contribution; (B) steady-state concentrations of radicals.....	84
<b>Figure 19</b> Impact of oxygen on 1,4-D treatability by UV/ $\text{S}_2\text{O}_8^{2-}$ and $\text{NH}_2\text{Cl}$ .....	85
<b>Figure 20</b> Impact of pH on 1,4-dioxane treatability by UV/ $\text{S}_2\text{O}_8^{2-}$ and $\text{NH}_2\text{Cl}$ .....	86
<b>Figure 21.</b> Effect of pH on 1,4-dioxane degradation without UV. ....	87
<b>Figure 22.</b> Effect of $\text{NH}_4^+$ on 1,4-dioxane degradation rates.....	87
<b>Figure 23</b> Comparison of UV/ $\text{H}_2\text{O}_2$ , UV/ $\text{S}_2\text{O}_8^{2-}$ and UV/ $\text{HOCl}$ treatment based on the kinetic model.....	107
<b>Figure 24</b> The comparison of three UV/AOP systems on the degradation of six selected trace organic contaminants based on the kinetic model.....	109
<b>Figure 25</b> 1,4-dioxane removal byUV/ $\text{H}_2\text{O}_2$ , UV/ $\text{S}_2\text{O}_8^{2-}$ and UV/ $\text{HOCl}$ .....	114
<b>Figure 26</b> Phenol removal by UV/ $\text{H}_2\text{O}_2$ , UV/ $\text{S}_2\text{O}_8^{2-}$ and UV/ $\text{HOCl}$ . ....	115

<b>Figure 27</b> The effect of pH on the treatment efficiency of UV/S <sub>2</sub> O <sub>8</sub> <sup>2-</sup> based on the kinetic model.....	117
<b>Figure 28</b> Effect of pH on the treatment efficiency of UV/H <sub>2</sub> O <sub>2</sub> based on the kinetic model.....	118
<b>Figure 29</b> Effect of pH on the treatment efficiency of UV/HOCl based on the kinetic model.....	120
<b>Figure 30</b> The effect of chloride on the treatment efficiency of UV/S <sub>2</sub> O <sub>8</sub> <sup>2-</sup> based on the kinetic model.....	122
<b>Figure 31</b> Effect of chloride on the treatment efficiency of UV/H <sub>2</sub> O <sub>2</sub> based on the kinetic model.....	123
<b>Figure 32</b> Effect of chloride on the treatment efficiency of UV/HOCl based on the kinetic model.....	124
<b>Figure 33</b> Effect of inorganic carbon on the treatment efficiency of UV/S <sub>2</sub> O <sub>8</sub> <sup>2-</sup> based on the kinetic model.....	126
<b>Figure 34</b> Effect of inorganic carbon on the treatment efficiency of UV/H <sub>2</sub> O <sub>2</sub> based on the kinetic model.....	127
<b>Figure 35</b> The effect of inorganic carbon on the treatment efficiency of UV/HOCl based on the kinetic model.....	128
<b>Figure 36</b> Calibration curve of DNPH-derivatized glutaraldehyde. ....	145
<b>Figure 37</b> Cytotoxicity and Genotoxicity evolution of 1,4-D during UV/AOPs treatment. ....	149

<b>Figure 38</b> Benzene degradation and products evolution in $S_2O_8^{2-}$ , $H_2O_2$ and $MnO_4^-$ ..	151
.....	
<b>Figure 39.</b> 1,4-D degradation and products evolution in UV/ $S_2O_8^{2-}$ , UV/ $H_2O_2$ , UV/ $NH_2Cl$ .....	153
<b>Figure 40</b> Cytotoxicity and Genotoxicity concentration response curves of benzene, phenol, and aldehyde. Each value represents the mean of three replicates $\pm$ standard deviation. ....	155
<b>Figure 41.</b> Cytotoxicity and Genotoxicity dose response curves of 1,4-dioxane, Formaldehyde, and glycolaldehyde. Each value represents the mean of three replicates $\pm$ standard deviation.....	157
<b>Figure 42</b> Cytotoxicity and Genotoxicity dose response curves of Ethylenen glycol diformate, glycolic acid, formic acid and methoxyacetic acid. Each value represents the mean of three replicates $\pm$ standard deviation. ....	158
<b>Figure 43.</b> Mitomycin Equivalent of genotoxicity evolution during UV/AOPs treatment. ....	160

# List of Tables

<b>Table 1</b> BET surface area of minerals used in this study .....	32
<b>Table 2</b> Major radical chain reactions involving benzene degradation via persulfate activation by Fe(III) and Mn(IV) oxides. ....	37
<b>Table 3</b> Model-predicted steady-state concentrations of radicals generated during heterogeneous persulfate activation.* .....	45
<b>Table 4</b> The impact of pH on the percentile contributions of different reactive radicals to benzene degradation.* .....	46
<b>Table 5</b> The impact of pH on the percentile contributions of different reaction pathways to persulfate decomposition.* .....	47
<b>Table 6</b> The impact of chloride on the percentile contributions of different reactive radicals to benzene degradation.* .....	50
<b>Table 7</b> Model-predicted steady-state concentrations of surface complexes of Fe(III) and Mn(IV) minerals.* .....	53
<b>Table 8</b> Major radical chain reactions that impact the distribution of radicals in UV/AOPs.....	101
<b>Table 9</b> Compound structure and their quantum yield, extinction coefficient and direct photolysis rate .....	102
<b>Table 10</b> Rate constants of reactions between selected organic contaminants and radicals .....	104
<b>Table 11</b> Chemical compositions for selected water matrix. ....	105

<b>Table 12</b> The steady-state concentrations of radicals in three UV/AOPs. The calculation was based on typical RO permeate chemical matrix with 88 $\mu\text{M}$ of oxidant and 1178 $\text{mJ}/\text{cm}^2$ of UV irradiation. ....	113
<b>Table 13</b> Products distribution during UV/AOPs treatment .....	149
<b>Table 14.</b> LC50 and EC50 values of benzen and its degradation products in P53RE-bla CT-116 cell line after 16h exposure.....	156
<b>Table 15.</b> LC50, EC50 and relative effect potency (REP) values of 1,4-dioxane and its degradation products in P53RE-bla CT-116 cell line after 16h exposure.	157

# **Chapter 1**

## **Introduction**

## **1.1 Motivation: in Response to Fresh Water Crisis**

Nearly seventy percent of the earth's surface is covered by water; however, fresh water that is essential for life is extremely limited and mostly stored as glaciers in the Arctic Pole and Antarctica.<sup>1,2</sup> Accessible surface water and groundwater only account for less than 1% of total water on earth. In much of the developing world, fresh water is becoming an increasingly precious resource that requires labor and money to obtain.<sup>3</sup> In the U.S., people have taken water for granted and have become the most inefficient water users. In arid regions, such as California, many water-intensive crops, such as alfalfa and almond trees are grown. The average American water consumption is 300 gallons per day, twice as much as our European counterparts and 100 times more than in developing countries.<sup>4</sup> At the same time, unpredictable climate conditions, uncontrolled population/economic growth, and source water contamination as a result of industrialization exacerbate the water shortages.<sup>2,5,6</sup> Global warming alters precipitation patterns, melts mountain glaciers, and bring more frequent floods and droughts. Population growth is a major contributor to water scarcity. The increase in population means an increasing demand for more water, food, and commodities. The demand for more economic growth seen in nations including China and India has resulted in a need to harness more water for power generation and manufacturing. Economic, industry, and agriculture activities are depleting our fresh water resources, while at the same time dumping wastewater into water bodies. Agricultural runoff, industrial discharge, and untreated sewage are damaging our water quality.<sup>7,8</sup> Water pollution makes a large volume of fresh water unsuitable for use and worsens water scarcity. In response to the crisis, we are exploring water efficiency, desalinating sea water,

expanding wastewater reuse, and repairing damaged water bodies to increase our fresh water supplies. In this dissertation, we are focusing on the emerging chemical oxidation technologies for mitigating contaminated groundwater and recycling wastewater.

## **1.2 Persulfate-Based ISCO for Groundwater Remediation**

Groundwater contamination, which nearly always results from human activities, is difficult and expensive to clean up.<sup>8</sup> Sources of groundwater contamination vary from residential and municipal to industrial and agricultural activities.<sup>9</sup> Leakage of septic systems, sewers and pipelines, improper disposal of hazardous waste, spill from underground petroleum storage tanks, and agricultural runoff that contains pesticide and fertilizer are all possible sources of contamination.<sup>9</sup> Since 1980, the EPA superfund site program has completely remediated more than one thousand heavily contaminated sites. However, there are still more than thirteen hundred superfund sites listed on the National priority list, plus newly discovered sites. Groundwater remediation is still an ongoing challenge.<sup>10</sup> Over the years, research efforts have been directed at advancing and improving the treatment technologies. Examples of these technologies include physical separation, solidification, pump and treat, recycling, phytoremediation, chemical oxidation, thermal treatment, bioremediation, flushing, fracturing, and extraction.<sup>11</sup> Of those technologies, *in situ* Chemical Oxidation (ISCO) is the most rapidly growing remedial technology which is applied at many EPA hazardous waste sites due to its cost-effective performance.<sup>12</sup>

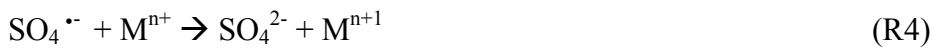
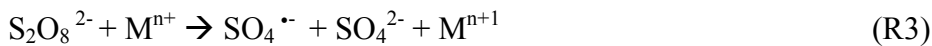
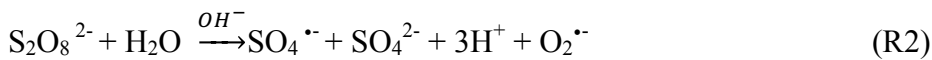
ISCO is a form of advanced chemical oxidation treatment process mostly used for soil or groundwater remediation that utilizes strong oxidants. Example of oxidants used in

ISCO includes catalyzed hydrogen peroxide ( $\text{H}_2\text{O}_2$ ), permanganate ( $\text{KMnO}_4$ ), Ozone ( $\text{O}_3$ ) and persulfate ( $\text{S}_2\text{O}_8^{2-}$ ) to oxidize contaminants to less toxic substances.<sup>13</sup> Catalyzed  $\text{H}_2\text{O}_2$  propagations have been established for years and found to be effective for removing almost all aromatic compounds including halogenated compounds.<sup>14</sup> However, catalyzed  $\text{H}_2\text{O}_2$  has relatively low reactivity with alkanes.<sup>15</sup> Furthermore, the stability of  $\text{H}_2\text{O}_2$  in the subsurface poses a significant shortcoming. The half-life of  $\text{H}_2\text{O}_2$  ranges from a few hours to up to 10 days depending on soil conditions.<sup>16</sup>  $\text{KMnO}_4$  is the oxidant of choice for treating alkenes and chlorinated compounds.<sup>14</sup> However, the solubility of  $\text{KMnO}_4$  is relatively low compared to other oxidants.<sup>17</sup> During its oxidation of organic substances,  $\text{KMnO}_4$  is reduced to solid manganese dioxide, which is in the form of non-soluble crystals. In addition,  $\text{KMnO}_4$  is also rapidly consumed by natural organic matters, hence, the natural oxidant demand for  $\text{KMnO}_4$  is high.<sup>18</sup>  $\text{O}_3$ -based ISCO is less common due to its high cost.<sup>14</sup> Sometimes,  $\text{O}_3$  is combined with  $\text{H}_2\text{O}_2$  to increase the hydroxyl radical ( $\text{HO}^\bullet$ ) yield.<sup>19</sup> However, both  $\text{O}_3$  and  $\text{HO}^\bullet$  are non-selective oxidants, which react with many other non-targeted chemicals.<sup>20</sup>

$\text{S}_2\text{O}_8^{2-}$  is an emerging oxidant used in ISCO. It has gained increasing attention due to its economic feasibility and capacity to remove recalcitrant organic contaminants, such as hydrocarbons<sup>21</sup> and CECs.<sup>22,23</sup> The half-life of persulfate can range from two to hundreds of days depending on the conditions of the soil constituents.<sup>24,25</sup> High solubility of  $\text{S}_2\text{O}_8^{2-}$  enhances the rate of diffusion and transport of  $\text{S}_2\text{O}_8^{2-}$  in the subsurface.  $\text{S}_2\text{O}_8^{2-}$  is also a strong oxidant ( $E_0=2.1\text{V}$ ).<sup>26</sup> Activated persulfate generates  $\text{SO}_4^{\bullet-}$  ( $E_0=2.6\text{V}$ ) to create

highly reactive remediation system to treat contaminants of concern.<sup>6,21,27</sup> Unlike HO•, SO<sub>4</sub>•<sup>-</sup> is more selective towards electron rich organics.<sup>28</sup>

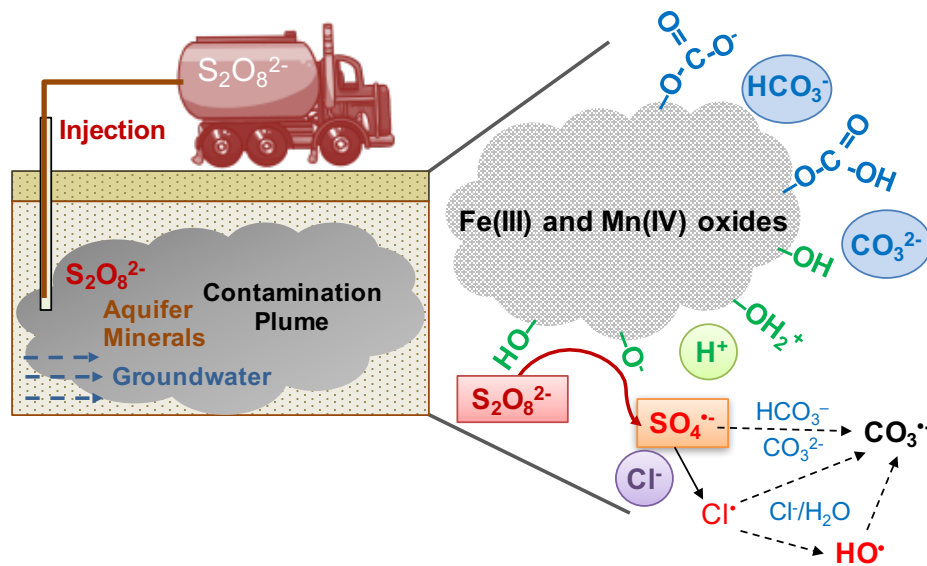
Sulfate radicals can be generated inexpensively through photolytic catalysis of persulfate by UV radiation (R1),<sup>29,30</sup> heat (R1),<sup>31,32</sup> base (R2),<sup>33</sup> and hydrogen peroxide.<sup>34</sup> This strongly oxidative species can also be generated through iron chelate activation (R3).<sup>35</sup> However, the metal activation involves both radical generation and radical scavenging (R3 vs. R4).<sup>36</sup>



Fe(II) and Fe(III) are the most commonly used transitional metals when applying ISCO.<sup>36</sup> Other transition metals such as Cu(I) and Ag(I) are also capable of activating S<sub>2</sub>O<sub>8</sub><sup>2-</sup>, however, the application is limited due to their toxicity.<sup>37</sup> In addition, a few studies have demonstrated the ability of naturally-occurring aquifer minerals such as iron oxides and manganese oxides on S<sub>2</sub>O<sub>8</sub><sup>2-</sup> activation.<sup>38,39</sup> The mechanism involves the oxidization of S<sub>2</sub>O<sub>8</sub><sup>2-</sup> by metal oxides to yield Fe(II) or Mn(III) (R5), which then reduces S<sub>2</sub>O<sub>8</sub><sup>2-</sup> to generate reactive radical species (R3).



Due to the complexity of the aquifer environment, the yield of  $SO_4^{\bullet-}$  and the efficiency of  $S_2O_8^{2-}$ -based ISCO can be impacted by groundwater chemical constituents such as pH,  $Cl^-$  and alkalinity. A few chemical processes can occur. First,  $Cl^-$ ,  $HCO_3^-$  and pH can scavenge  $SO_4^{\bullet-}$  to generate secondary radical species including chlorine atom ( $Cl^{\bullet}$ ), carbonate radical ( $CO_3^{\bullet-}$ ) and  $HO^{\bullet}$  via Reactions 6-8 (**Scheme 1**):<sup>23,40,41</sup>



**Scheme 1** Interaction of  $S_2O_8^{2-}$  with aquifer chemical constituents during ISCO.

The treatment efficiency will therefore depend on the extent of the scavenging effects and the reactivity of secondary radical species with a contaminant.<sup>42-48</sup>  $SO_4^{\bullet-}$ ,  $HO^{\bullet}$  and  $Cl^{\bullet}$  have similar reaction rates with aromatic compounds<sup>49-50</sup> However, the

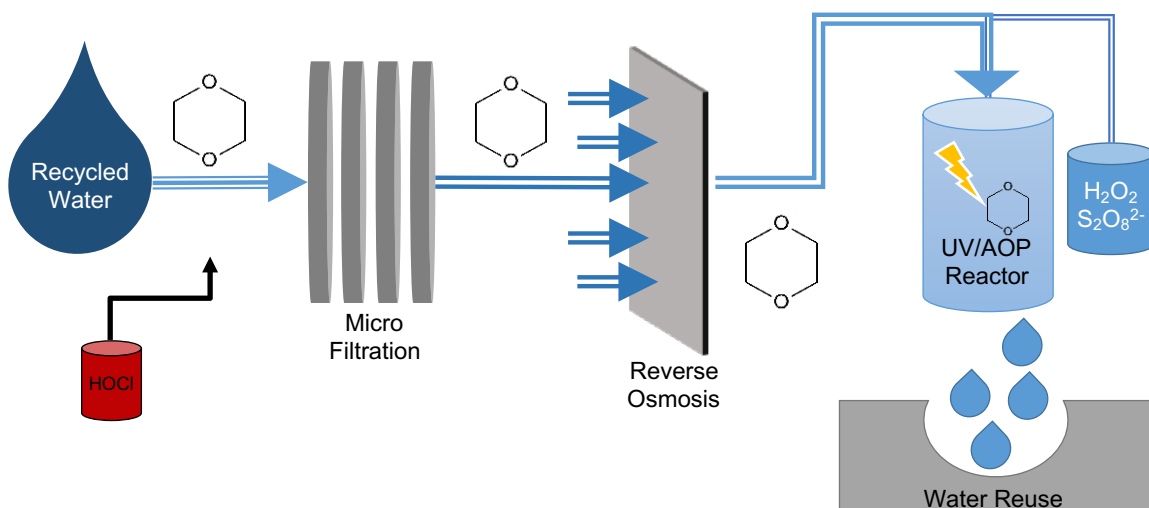
reactivity of  $\text{CO}_3^{\bullet-}$  is usually a few orders of magnitude lower than  $\text{SO}_4^{\bullet-}$ ,  $\text{HO}^{\bullet}$  and  $\text{Cl}^{\bullet}$  towards aromatic compounds.<sup>51</sup> In addition, the presence of  $\text{Cl}^-$  and  $\text{HCO}_3^-$  in groundwater can also form different chloro- and carbonato- surface complexes with Fe(III)- and Mn(IV)-oxides.<sup>52,53</sup> These surface complexes can change the redox reactivities of the surfaces of metal oxides, thus potentially impacting the rate of  $\text{S}_2\text{O}_8^{2-}$  activation and the redox cycle of Fe and Mn-oxides (**Scheme 1**).<sup>54</sup> Thus, it is important to understand the mechanism and consequence of  $\text{S}_2\text{O}_8^{2-}$  interaction with aquifer chemical constituents.

### 1.3 Persulfate-Based UV/AOPs for Potable Water Reuse

Potable water reuse offers a sustainable approach to address water scarcity and mitigate the long-term impacts of climate change.<sup>55,56</sup> However, conventional water and wastewater treatment processes are not sufficient for removing many trace organic contaminants in wastewater.<sup>57</sup> In a typical potable water treatment scheme, the secondary wastewater effluent from a conventional wastewater treatment plant is treated with a series of advanced treatment processes including micro- or nano-filtration,<sup>58</sup> reverse osmosis (RO),<sup>59</sup> activated carbon adsorption,<sup>60</sup> and advanced oxidation.<sup>61</sup>

UV-based AOPs have been widely applied in water industries to remove disinfection byproducts (DBPs) in drinking water and contaminants of emerging concern (CECs) in recycled water.<sup>62-67</sup> When UV-based AOPs are applied to portable reuse scenario, they are often used in the last step to remove trace contaminants that can pass through the filtration steps (**Scheme 2**). For example, small and non-charged molecules such as 1,4-dioxane and acetone can pass through RO membrane and cause potential health effects.<sup>68</sup> Advanced

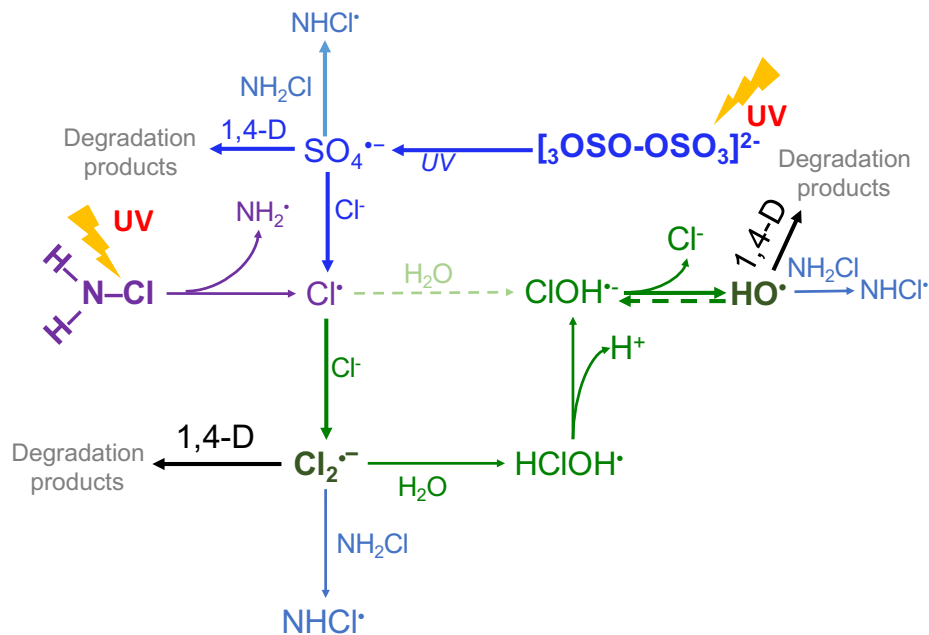
oxidation processes (AOPs) is the ultimate step to eliminate harmful micro organic residues in the final water product.



**Scheme 2** Advanced treatment processes for portable water reuse. Derived from Patton & Li et. al. 2017.

UV/AOPs utilize photo energy to break the bonds of the oxidant precursor, commonly  $\text{H}_2\text{O}_2$ , to produce highly oxidative species such as  $\text{HO}^\bullet$ . UV/ $\text{H}_2\text{O}_2$  is the most common AOP application in the States due to its low cost and non-toxic residual formation.<sup>69</sup> Increasingly stringent regulations urge water utilities to pursue alternative treatment schemes with higher efficacy and lower cost. The current application of  $\text{H}_2\text{O}_2$  as the default oxidant for UV/AOPs may not be the best option due to the non-selectivity of  $\text{HO}^\bullet$ . Replacing  $\text{H}_2\text{O}_2$  with  $\text{S}_2\text{O}_8^{2-}$  might be more energy-efficient. The quantum yield of  $\text{SO}_4^{\bullet-}$  is higher than  $\text{HO}^\bullet$  (0.7 vs. 0.5), and they have similar oxidizing power (2.5-3.1 v vs. 1.9-2.8 v).<sup>5</sup> Furthermore,  $\text{SO}_4^{\bullet-}$  is more selective towards electron-rich contaminants that are typically observed in wastewater effluent.<sup>70,71,72</sup> A prior study has demonstrated that

UV/S<sub>2</sub>O<sub>8</sub><sup>2-</sup> shows better contaminant removal at the same molar concentration of H<sub>2</sub>O<sub>2</sub>.<sup>30</sup> It is also less influenced by other competing water chemical parameters such as alkalinity and chloride concentration.<sup>73</sup> When S<sub>2</sub>O<sub>8</sub><sup>2-</sup> is activated by UV, it generates two SO<sub>4</sub><sup>•-</sup>. In the presence of chloride, SO<sub>4</sub><sup>•-</sup> can be transformed into Cl<sup>•</sup>, Cl<sub>2</sub><sup>•-</sup>, and HO<sup>•</sup> (**Scheme 3**). UV/S<sub>2</sub>O<sub>8</sub><sup>2-</sup> targets a wide range of contaminants of emerging concern, because different radicals have distinct reactivity with specific target contaminants.<sup>50</sup> UV/S<sub>2</sub>O<sub>8</sub><sup>2-</sup> has been reported to successfully degrade phenolic compounds,<sup>74</sup> carboxylic acids,<sup>75</sup> PPCPs,<sup>28</sup> cyanobacterial toxin,<sup>76</sup> and even fluorinate organic compounds.<sup>77</sup> Thus, UV/S<sub>2</sub>O<sub>8</sub><sup>2-</sup> can potentially substitute H<sub>2</sub>O<sub>2</sub> and achieve better treatment efficiency.

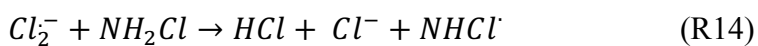
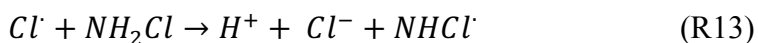


**Scheme 3** Radical distribution in UV/S<sub>2</sub>O<sub>8</sub><sup>2-</sup> and UV/NH<sub>2</sub>Cl

In the advanced water treatment train, monochloramine ( $\text{NH}_2\text{Cl}$ ) residual is often maintained in the feed water to control and minimize membrane fouling. Due to the small molecular size, monochloramine easily passes through RO membrane and undergoes photolysis in UV/AOPs.<sup>78</sup> Despite the vast application of monochloramine in advanced water treatment processes,<sup>79</sup> the fate of monochloramine during UV photolysis, and the impact of monochloramine on the chemistry of parent oxidant in UV/AOPs are not well understood.  $\text{NH}_2\text{Cl}$  has a high UV absorbance coefficient ( $371 \text{ M}^{-1}\text{cm}^{-1}$ )<sup>80</sup> and similar quantum yield as  $\text{S}_2\text{O}_8^{2-}$  ( $0.26\text{-}0.62 \text{ mol E}^{-1}$ )<sup>81-83</sup>. It can be used as a parent oxidant in the AOPs or combined with other parent oxidants to increase the overall radical yield.<sup>82</sup> The current understanding of chloramine aqueous photochemistry is limited to trichloramine photolysis in swimming pools,<sup>84,85</sup> and monochloramine or dichloramine photolysis in the pure water system.<sup>80-83</sup> However, the knowledge of applying the mixed system containing both  $\text{S}_2\text{O}_8^{2-}$  and  $\text{NH}_2\text{Cl}$  in AOPs is underdeveloped<sup>82</sup>. Especially, little is known about the fundamental photochemistry of AOPs involving multiple parent oxidants. In the current AOPs where monochloramine is used as a disinfectant, the presence of monochloramine may alter the solution chemistry, reduce UV transmittance<sup>86</sup> and impact the degradation efficiency of micro-pollutants. In a case where UV/ $\text{S}_2\text{O}_8^{2-}$  is employed, the sulfate radical ( $\text{SO}_4^{\bullet-}$ ) produced from UV activation of  $\text{S}_2\text{O}_8^{2-}$  may further react with monochloramine to form less reactive radical species  $\text{NHCl}^{\bullet}$  (R9).



NH<sub>2</sub>Cl photolysis may also produce NH<sub>2</sub><sup>•</sup> and Cl<sup>•</sup> (R10). However, the reactivity of NH<sub>2</sub><sup>•</sup> with trace organic contaminants in UV/AOPs remained unclear. Furthermore, NH<sub>2</sub>Cl itself may act as a scavenger that decreases the quantum yield of NH<sub>2</sub>Cl (R11-15). Therefore, it is important to understand the role of chloramine in aqueous photochemistry when combined with other oxidants.



#### 1.4 Toxicity Assessment for Oxidation Byproducts

The goal of introducing advanced treatment is to minimize health risks. However, during the application of AOPs, there lies a concern relating to the formation of various transformation byproducts from contaminants oxidized by reactive radicals.<sup>87</sup> To date, most oxidation byproducts of known contaminants and their cumulative toxicity profiles are largely unknown. The disappearance of the original contaminants may therefore not imply that the treatment is efficient, and hence oxidation byproducts of the reactions between oxidants and contaminants must always be considered. With increasing attention on disinfection byproduct formation,<sup>88</sup> the formation of more toxic intermediates or

oxidation products during AOPs has also become an emerging concern. In several instances, the oxidation byproducts in AOPs may preserve the mode of action of the parent compound, and may pose a significant threat to environmental and human health.<sup>89,90</sup> Among numerous oxidation byproducts identified in AOPs-treated water samples, aldehyde compounds have received a great deal of attention from regulatory agencies and scientists due to a high level of carcinogenicity.<sup>91,92</sup> Studies have demonstrated that aldehydes induce nasal carcinomas in animal and humans.<sup>93</sup>

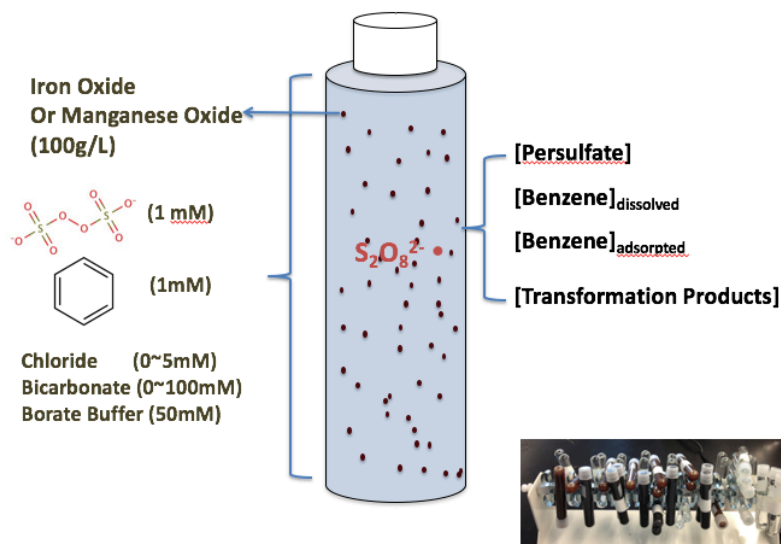
Research has only started to be developed regarding the identification of oxidation byproducts from AOPs, and limited research on the toxicity of these transformation products are available. For a complete risk assessment study on the oxidation byproducts formed during AOPs, identification of the oxidation byproducts and determination of their toxicity is crucial for a comprehensive risk assessment. The present study not only concerns the removal of the parent compounds, benzene and 1,4-dioxane, but also investigates their transformation products, evaluates the toxicity of the products using human cell-based bioassays, and offers recommendations for minimizing the toxic substance formation.

## **1.5 Experimental Approaches**

### ***1.5.1 Examine the impact of groundwater chemistry on persulfate activation by aquifer minerals in ISCO using benzene as model contaminants.***

The natural aquifer is rich in iron oxides and manganese oxides that can act as catalyst to activate  $S_2O_8^{2-}$  by two steps of one-electron redox cycle.<sup>39</sup> To further examine the feasibility of using naturally occurred metal oxides to activate  $S_2O_8^{2-}$  and produce reactive

radical species,  $\text{Fe}(\text{OH})_3$ ,  $\alpha\text{-Fe}(\text{OOH})$ , and  $\beta\text{-MnO}_2$  were first sieved to a uniformed size (38  $\mu\text{m}$  ~150 $\mu\text{m}$ ), and then sterilized to minimize microbes influence. 1mM of  $\text{S}_2\text{O}_8^{2-}$  prepared in MilliQ water was mixed with 100g/L metal oxides with or without the addition of benzene. An aliquot of the mixed solution was transferred to a 9ml-glass tube without head space and rotated in the dark (**Scheme 4**). To examine the impact of chloride, bicarbonate, and pH on  $\text{S}_2\text{O}_8^{2-}$  activation rate, varied levels of chloride (0 to 5mM), bicarbonate (0 to 10mM), and pH (8-13) were prepared with the test solutions. The pH was controlled with 50mM borate buffer or concentrated NaOH, and ionic strength was corrected by adding  $\text{NaClO}_4$  across different pH levels. Samples were collected every five days for a total of 40 days. Collected samples were filtered through a 0.22  $\mu\text{m}$  filter and  $\text{S}_2\text{O}_8^{2-}$  was quantified by colorimetric analysis.<sup>94</sup> Initial chloride concentration was quantified by IC and bicarbonate concentration was monitored by standard sulfuric acid titration method. Benzene was quantified by HPLC using an A Zorbax Eclipse XDB-C18 column (4.6x50mm, 1.8  $\mu\text{m}$  particle size) at a flow rate of 1.0 ml/min. Dissolved ion concentration at different pH levels was measured by ICP-MS. pH changes was monitored using pH meters.

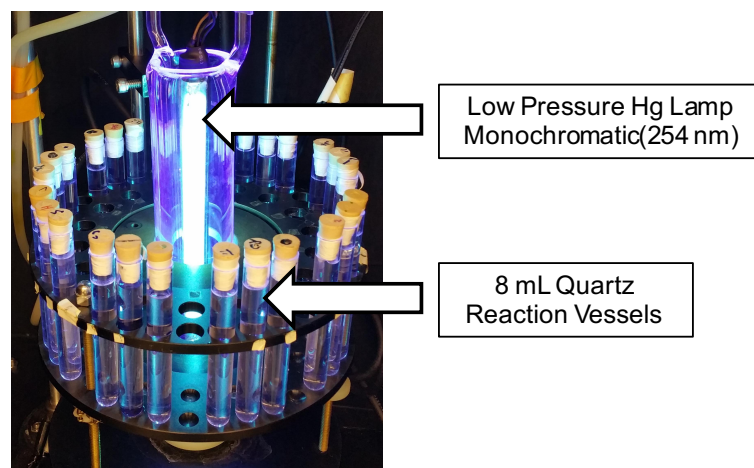


**Scheme 4.** Experimental set up for persulfate activation by aquifer minerals.

**1.5.2 Investigate the application of UV/S<sub>2</sub>O<sub>8</sub><sup>2-</sup> for potable water reuse, and the influence of NH<sub>2</sub>Cl, chloride, pH, and oxygen using 1,4-dioxane as model contaminate**

1,4-dioxane degradation rate by UV/S<sub>2</sub>O<sub>8</sub><sup>2-</sup> in the presence of NH<sub>2</sub>Cl at various concentrations (0-6 mM) was examined. The impact of chloride, pH, and oxygen content was also studied. In general, a requisite amount of 1,4-dioxane, benzoic acid, nitrobenzene, and buffer were first added to a volumetric flask and diluted with deoxygenated MilliQ water at a final concentration of 250 μM, 10 μM, 20 μM, respectively. NH<sub>2</sub>Cl was added lastly to minimize the decay of NH<sub>2</sub>Cl at lower pH. Prepared solutions were transferred to multiple 8 mL sealed quartz tubes without headspace. The tubes were then placed in a carousel UV chamber illuminated with a low-pressure monochromatic Hg lamp (λ=254 nm) at an intensity of 2.1 mW/cm<sup>2</sup> (Phillips TUV6T5, **Scheme 5**). Samples were withdrawn from sacrificial quartz tubes every five minutes for 25 minutes. NH<sub>2</sub>Cl

concentration was measured immediately after sample collection using DPD colorimetric method.<sup>95</sup> The concentration of  $S_2O_8^{2-}$  was measured using KI titration by a UV-Visible Spectrometer (Aqualog, Horiba Scientific).<sup>94</sup> The concentration of 1,4-dioxane, benzoic acid and nitrobenzene were measured by an Agilent 1200 liquid chromatography equipped with a diode array detector, and a Zorbax Eclipse SB-C18 column (4.6×150mm, 5- $\mu$ m particle size). Total nitrogen (TNb) was measured by TOC analyzer (TOC; OI Analytical, College Station, TX). Gaseous nitrogen was determined by calculating the differences between the initial total nitrogen and total nitrogen at each collected data point. Ammonia, Nitrite, and nitrate concentration were measured by colorimetric methods.<sup>95</sup>



**Scheme 5** UV photo reactor.

### ***1.5.3 Modeling approach to simulate UV/ $S_2O_8^{2-}$ , UV/ $H_2O_2$ , and UV/HOCl***

A kinetic model was developed with an open-source software Kintecus 4.55 to simulate the performance of UV/ $S_2O_8^{2-}$ , UV/ $H_2O_2$ , and UV/HOCl, which are the most

popular UV/AOPs in degrading trace organics present in RO permeate. The model was optimized based on the bench-scale experimentally-observed degradation rates of 1,4-dioxane and phenol by UV/S<sub>2</sub>O<sub>8</sub><sup>2-</sup>, UV/H<sub>2</sub>O<sub>2</sub>, and UV/HOCl. The overall degradation rates of six representative trace organic contaminants, 1,4-dioxane, carbamazepine, phenol, 17β-estradiol, aniline, and sulfamethoxazole, in full scale UV/AOP operations were simulated by the model. Three important water chemical parameters associated with RO permeate were examined: pH, chloride, and carbonate. The steady-state concentration of each radical and the contribution of each radical to the oxidation efficiency of trace contaminants were calculated.

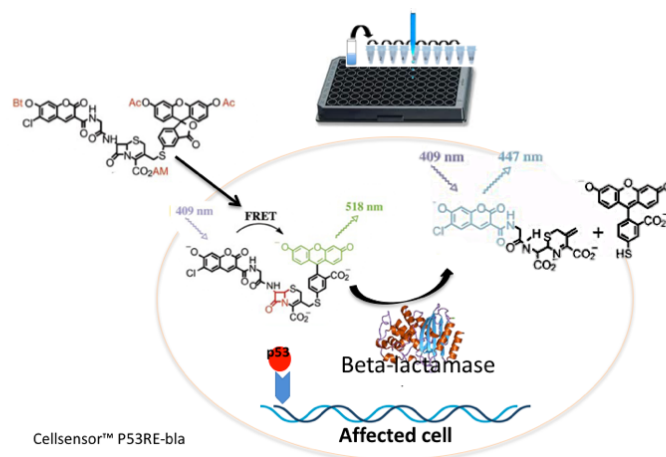
***1.5.4 Investigate the oxidation byproducts of benzene and 1,4-dioxane, and quantify the toxicity potency of the oxidation byproducts using human cell-based assays***

To investigate the impact of different oxidants on product distribution, degradation of benzene by Na<sub>2</sub>S<sub>2</sub>O<sub>8</sub>, H<sub>2</sub>O<sub>2</sub>, and KMnO<sub>4</sub> was investigated. S<sub>2</sub>O<sub>8</sub><sup>2-</sup> and H<sub>2</sub>O<sub>2</sub> at 5mM were activated by the three solids mentioned above with the addition of 1 mM benzene using same glass reactor setup. KMnO<sub>4</sub> at 5mM was directly mixed with 1 mM benzene. All experiments were controlled at pH 8 with 50mM borate buffer. Products were identified and quantified using HPLC, fractionated manually by HPLC, concentrated by purging nitrogen, and finally re-suspended in MilliQ water to a final desired concentration with HPLC solvent containing 0.05% DMSO.

Products of 1,4-dioxane oxidation by UV/S<sub>2</sub>O<sub>8</sub><sup>2-</sup>, UV/H<sub>2</sub>O<sub>2</sub>, and UV/NH<sub>2</sub>Cl were identified using the state-of-arts instruments including HPLC and IC. The concentrations

of 1,4-dioxane, ethylene glycol diformate, formaldehyde, and glycolaldehyde were measured by an Agilent 1200 liquid chromatography equipped with a diode array detector and a Zorbax Eclipse SB-C18 column (4.6×150mm, 5- $\mu$ m particle size). Glycolic acid, formic acid, and methoxyacetic acid were quantified using Dionex 1000 ion chromatograph equipped with a suppressed conductivity detector (Dionex, USA). The chemical standards were purchased based on the identified oxidation byproducts, and the toxicity study was conducted using known standards.

The genotoxicity of the individual transformation products was tested by using HCT-116 human colorectal carcinoma cells with an integrated beta-lactamase reporter gene under the control of p53 response elements (**Scheme 6**). HCT-116 cells after the fourth passage were transferred to each well of the black, clear-bottom, 96 well assay plates at a density of around 50,000 cells per well. The test compounds were then added to the assay plate at gradient concentrations. Mitomycin was used as positive control. The plate was incubated at 37 °C, 5% CO<sub>2</sub> for 16 hours, and then an aliquot of LiveBLAzer™ - FRET B/G substrate mixture was added to each well. The fluorescence intensity at 447 and 520 nm emission was measured with excitation at 405 nm using an EnVision microplate reader. The ratio of emissions at 460nm/530 nm was calculated by Excel and dose response curve was plotted using GraphPad Prism 7.



### Scheme 6 Genotoxicity study using HCT-116 human colorectal carcinoma cells

Cell viability assay was also performed at the same time to test the cytotoxic effect of the compounds. After 16 hours incubation, an aliquot of 10  $\mu\text{L}$  of MTT reagent (Life Technologies) was added to the wells. After 2 hours incubation at 37  $^{\circ}\text{C}$ , the assay medium was then aspirated and 100  $\mu\text{L}$  DMSO was added into each well. After 2 hours incubation at room temperature, the absorbance was recorded at 570 nm and the percentage reduction in cell proliferation (relative cell density) was compared to that achieved in the growth medium controls and vehicle-treated controls. DMSO was used as a positive control to show a dose response curve. LC50 was then calculated using GraphPad Prism 7.

### 1.6 Research Objectives

The overall objective of the study was to conduct a series of applied experiments combined with computational kinetic modeling to explain the basis of  $\text{S}_2\text{O}_8^{2-}$ -based AOPs, and to apply the knowledge obtained from experimental observations to field study. In the meantime, an effort was taken to delve into the toxicity evaluation of the transformation

products during  $S_2O_8^{2-}$  based ISCO and UV/AOPs and develop strategies for controlling the toxic substances formation during the process.

In Chapter 2, the objectives were to (1) investigate the impacts of groundwater alkalinity, pH, and chloride on benzene degradation via heterogeneous  $S_2O_8^{2-}$  activation by Fe(III)- and Mn(IV)-containing minerals were investigated, (2) examine the fundamental mechanisms of radical chain reactions of persulfate activation in diverse chemical conditions, (3) quantify the kinetics and the efficiency of benzene degradation, and (4) assess the distribution of benzene degradation products. (5) A companying objective was to develop a comprehensive kinetic model to elucidate mineral surface complexation and radical chain reactions involving persulfate ISCO under diverse groundwater chemical conditions.

In Chapter 3, the objectives were to (1) quantify the formation of reactive radicals during the simultaneous photolysis of  $NH_2Cl$  and  $S_2O_8^{2-}$ , (2) examine the impact of oxidant dosage, pH, chloride and dissolved  $O_2$  on the degradation of 1,4-dioxane, and (3) develop a kinetic model to predict the radical yield and transformation of with both oxidants.

In Chapter 4, the objectives of the work were to (1) develop a kinetic model to investigate radical generation mechanisms in UV/ $H_2O_2$ , UV/ $S_2O_8^{2-}$  and UV/HOCl, (2) predict the degradation of trace contaminants in complex chemical conditions relevant to potable water reuse by three UV/AOPs, (3) elucidate the impact of individual chemical parameters including pH, chloride and organic carbon on three UV/AOPs.

In Chapter 5, The objectives were to (1) identify the oxidation byproducts of benzene and 1,4-dioxane in  $S_2O_8^{2-}$ -based AOPs, (2) compare the toxicity potency of the

oxidation byproducts to the original contaminant using human cell-based bioassays, (3) Recommend strategies for minimizing toxic byproducts formation.

In Chapter 6, conclusions from the doctoral work are given, as well as discussion on the application of  $S_2O_8^{2-}$ -based AOPs to mitigate the risk of contaminated groundwater and to promote wastewater reuse technology were presented. Chapter two and chapter 4 have been published in peer-reviewed journals. Chapter three and chapter five are currently undergoing the peer-review process with an anticipation of publication.

## Reference:

---

- <sup>1</sup> Oki, T.; Kanae, S. Global hydrological cycles and world water resources. *Science*. **2006**, *313* (5790), 1068-1072.
- <sup>2</sup> Vörösmarty, C. J.; Green, P.; Salisbury, J.; Lammers, R. B. Global water resources: vulnerability from climate change and population growth. *Science*. **2000**, *289* (5477), 284-288.
- <sup>3</sup> Klare, M. *Resource wars: the new landscape of global conflict*. Macmillan, 2002.
- <sup>4</sup> United Nations Development Programme. *Uzbekistan Human Development Report*. UNDP, 2006.
- <sup>5</sup> Trenberth, K.E. Changes in precipitation with climate change. *Climate Research*. 2011, *47*, 123-138.
- <sup>6</sup> Yeston, J.; Coontz, R.; Smith, J.; Ash, C. *A thirsty world*. **2006**, *313* (5790), 1067.
- <sup>7</sup> Rozemeijer, J. C.; Broers, H. P. The groundwater contribution to surface water contamination in a region with intensive agricultural land use (Noord-Brabant, The Netherlands). *Environmental Pollution*. **2007**, *148* (3), 695-706.
- <sup>8</sup> Pye, V. I.; Patrick, R. Ground water contamination in the United States. *Science*. **1983**, *221* (4612), 713-718.
- <sup>9</sup> Pye, V. I.; Kelley, J. The extent of groundwater contamination in the United States. *Groundwater Contamination*. **1984**, *179* (1), 23-33.
- <sup>10</sup> Doty, S. L.; Freeman, J. L.; Cohu, C. M.; Burken, J. G.; Firrincieli, A.; Simon, A., ... & Blaylock, M. J. Enhanced degradation of TCE on a Superfund site using endophyte-assisted poplar tree phytoremediation. *Environmental Science & Technology*. **2017**.
- <sup>11</sup> U.S. Environmental Protection Agency. *Superfund Remedy Report. 14<sup>th</sup> edition*. 2013.
- <sup>12</sup> Krembs, F. J.; Siegrist, R. L.; Crimi, M. L.; Furrer, R. F.; Petri, B. G. ISCO for groundwater remediation: analysis of field applications and performance. *Groundwater Monitoring & Remediation*. **2010**, *30* (4), 42-53.
- <sup>13</sup> Tsitonaki, A.; Petri, B.; Crimi, M.; Mosbæk, H.; Siegrist, R. L. Bjerg, P. L. In situ chemical oxidation of contaminated soil and groundwater using persulfate: a review. *Critical Reviews in Environmental Science and Technology*. **2010**, *40* (1), 55-91.

- 
- <sup>14</sup> Watts, R. J.; Teel, A. L. Treatment of contaminated soils and groundwater using ISCO. *Practice Periodical of Hazardous, Toxic, and Radioactive Waste Management*. **2006**, *10* (1), 2-9.
- <sup>15</sup> Watts, R. J.; Stanton, P. C. Mineralization of sorbed and NAPL-phase hexadecane by catalyzed hydrogen peroxide. *Water Research*. **1999**, *33* (6), 1405-1414.
- <sup>16</sup> Environmental Security Technology Certification Program (ESTCP). *Technology status review: In situ oxidation, environmental security technology certification program*. Arlington, Va: 1999.
- <sup>17</sup> Santos, A.; Rosas, J. M. *In situ* chemical oxidation (ISCO). *Soil Remediation: Applications and New Technologies*. **2016**, 75.
- <sup>18</sup> Wickramanayake, G. B.; Gavaskar, A. R.; Chen, A. S. *Chemical oxidation and reactive barriers: remediation of chlorinated and recalcitrant compounds*. Battelle press, Columbus, Ohio: 2000.
- <sup>19</sup> Watts, R. J.; Teel, A. L. Chemistry of modified Fenton's reagent (catalyzed H<sub>2</sub>O<sub>2</sub> propagations-CHP) for in situ soil and groundwater remediation. *Journal of Environmental Engineering*. **2005**, *131* (4), 612-622.
- <sup>20</sup> Dragun, J.; Chekiri, K. *Elements in North American Soils*. Hazardous Materials Control Resources Institute, Greenbelt, MD: 1991.
- <sup>21</sup> Huling, Scott G.; Bruce E. Pivetz. *In-situ chemical oxidation*. No. EPA/600/R-06/072. USEPA, Washington DC Office of Water, 2006.
- <sup>22</sup> Sra, K. S.; Thomson, N. R.; Barker, J. F. Persistence of persulfate in uncontaminated aquifer materials. *Environmental Science & Technology*. **2010**, *44* (8), 3098-3104.
- <sup>23</sup> Liang, S. H.; Kao, C. M.; Kuo, Y. C.; Chen, K. F.; Yang, B. M. *In situ* oxidation of petroleum-hydrocarbon contaminated groundwater using passive ISCO system. *Water Research*. **2011**, *45* (8), 2496-2506.
- <sup>24</sup> Dahmani, M. A.; Huang, K.; Hoag, G. E. Sodium persulfate oxidation for the remediation of chlorinated solvents (USEPA superfund innovative technology evaluation program). *Water, Air, & Soil Pollution: Focus*. **2006**, *6* (1), 127-141.
- <sup>25</sup> Abranovic, D. J.; Brown, D.; Chemburkar, A. Persulfate stability is limiting factor for ISCO in fine-grained, iron-rich media. *In Proceedings of the Fifth International Conference on Remediation of Chlorinated and Recalcitrant Compounds*. 2006.
- <sup>26</sup> Haynes, W. M. *CRC handbook of chemistry and physics*. CRC press, Boca Raton, FL: 2014.

- 
- <sup>27</sup> Brown, R. A. In situ chemical oxidation: performance, practice, and pitfalls. In *AFCEE Technology Transfer Workshop*. San Antonio, Texas, 2003.
- <sup>28</sup> Huang, K. C.; Couttenye, R. A.; Hoag, G. E. Kinetics of heat-assisted persulfate oxidation of methyl tert-butyl ether (MTBE). *Chemosphere*. 2002, *49* (4), 413-420.
- <sup>29</sup> Gao, Y. Q.; Gao, N. Y.; Deng, Y.; Yang, Y. Q.; Ma, Y. Ultraviolet (UV) light-activated persulfate oxidation of sulfamethazine in water. *Chemical Engineering Journal*. **2012**, *195*, 248
- <sup>30</sup> Wang, C. W.; Liang, C. Oxidative degradation of TMAH solution with UV persulfate activation. *Chemical Engineering Journal*. **2014**, *254*, 472-478.
- <sup>31</sup> Waldemer, R. H.; Tratnyek, P. G.; Johnson, R. L.; Nurmi, J. T. Oxidation of chlorinated ethenes by heat-activated persulfate: kinetics and products. *Environmental Science & Technology*. **2007**, *41* (3), 1010-1015.
- <sup>32</sup> Tan, C.; Gao, N.; Deng, Y.; An, N.; Deng, J. Heat-activated persulfate oxidation of diuron in water. *Chemical Engineering Journal*. **2012**, *203*, 294-300.
- <sup>33</sup> Furman, O. S.; Teel, A. L.; Watts, R. J. Mechanism of base activation of persulfate. *Environmental Science & Technology*. **2010**, *44* (16), 6423-6428.
- <sup>34</sup> House, D. A. Kinetics and mechanism of oxidations by peroxydisulfate. *Chemical Reviews*. **1962**, *62* (3), 185-203.
- <sup>35</sup> Liang, C.; Bruell, C. J.; Marley, M. C.; Sperry, K. L. Persulfate oxidation for in situ remediation of TCE. I. Activated by ferrous ion with and without a persulfate–thiosulfate redox couple. *Chemosphere*. **2004**, *55* (9), 1213-1223.
- <sup>36</sup> Kolthoff, I. M.; Medalia, A. I.; Raaen, H. P. The reaction between ferrous iron and peroxides. IV. Reaction with potassium persulfate. *Journal of the American Chemical Society*. **1951**, *73* (4), 1733-1739.
- <sup>37</sup> Anipsitakis, G. P.; Dionysiou, D. D. Radical generation by the interaction of transition metals with common oxidants. *Environmental Science & Technology*. **2004**, *38* (13), 3705-3712.
- <sup>38</sup> Teel, A. L.; Ahmad, M.; Watts, R. J. Persulfate activation by naturally occurring trace minerals. *Journal of Hazardous Materials*. **2011**, *196*, 153-159.
- <sup>39</sup> Liu, H.; Bruton, T. A.; Doyle, F. M.; Sedlak, D. L. In situ chemical oxidation of contaminated groundwater by persulfate: decomposition by Fe(III)- and Mn(IV)-containing oxides and aquifer materials. *Environmental Science & Technology*. **2014**, *48* (17), 10330-10336.

- 
- <sup>40</sup> Das, T. N. Reactivity and role of  $\text{SO}_5^-$  radical in aqueous medium chain oxidation of sulfite to sulfate and atmospheric sulfuric acid generation. *The Journal of Physical Chemistry A*. **2001**, *105* (40), 9142-9155.
- <sup>41</sup> Dogliotti, L.; Hayon, E. Flash photolysis of persulfate ions in aqueous solutions. The sulfate and ozonide radical anions. *The Journal of Physical Chemistry*. **1967**, *71* (8), 2511-2516.
- <sup>42</sup> Bedient, Philip B.; Rifai, H. S.; Newell, C. J. *Ground water contamination: transport and remediation*. Prentice-Hall International, Inc.: **1994**.
- <sup>43</sup> Buxton, G.V.; Greenstock, C.; Hellman, W.P.; Ross, A.B. Critical review of rate constants for reactions of hydrated electrons, hydrogen atoms, and hydroxyl radicals ( $\cdot\text{OH}/\cdot\text{O}^-$ ) in aqueous solution. *Journal of Physical and Chemical Reference Data*. **1988**, *17* (2) 513-886.
- <sup>44</sup> Pignatello, J.J. Dark and photoassisted  $\text{Fe}^{3+}$  catalyzed degradation of chlorophenoxyl herbicides by hydrogen peroxide. *Environmental Science & Technology*. **1992**, *26* (5) 944-951.
- <sup>45</sup> Lipczynska-Kochany, E.; Gregor, S.; Harms, S. Influence of some groundwater and surface waters constituents on the degradation of 4-chlorophenol by the Fenton reaction. *Chemosphere*. **1995**, *30* (1), 9-20.
- <sup>46</sup> Tang, W. Z.; Huang, C. P. 2, 4-Dichlorophenol oxidation kinetics by Fenton's reagent. *Environmental Technology*. **1996**, *17* (12) 1371-1378.
- <sup>47</sup> Lu, M. C.; Chen, J. N.; Chang, C. P. Effect of inorganic ions on the oxidation of dichlorvos insecticide with Fenton's reagent. *Chemosphere*. **1997**, *35* (10), 2285-2293.
- <sup>48</sup> Kiwi, J.; Lopez, A.; Nadtochenko, V. Mechanism and kinetics of the OH-radical intervention during Fenton oxidation in the presence of a significant amount of radical scavenger ( $\text{Cl}^-$ ). *Environmental Science & Technology*. **2000**, *34* (11), 2162-2168.
- <sup>49</sup> Grebel, J. E.; Pignatello, J. J.; Mitch, W. A., Effect of halide ions and carbonates on organic contaminant degradation by hydroxyl radical-based advanced oxidation processes in saline waters. *Environmental Science & Technology*. **2010**, *44* (17), 6822-6828.
- <sup>50</sup> NIST Standard Reference Database 40: NDRL/NIST Solutions Kinetics Database V. 3.0, Gaithersburg, MD.

- 
- <sup>51</sup> Chen, S. N.; Hoffman, M. Z.; Parsons Jr. G. H. Reactivity of the carbonate radical toward aromatic compounds in aqueous solution. *The Journal of Physical Chemistry*. **1975**, 79 (18), 1911-1912.
- <sup>52</sup> De Laat, J.; Truong Le, G.; Legube, B. A comparative study of the effects of chloride, sulfate and nitrate ions on the rates of decomposition of H<sub>2</sub>O<sub>2</sub> and organic compounds by Fe (II)/H<sub>2</sub>O<sub>2</sub> and Fe (III)/ H<sub>2</sub>O<sub>2</sub>. *Chemosphere*. **2004**, 55 (5), 715-723.
- <sup>53</sup> Valentine, R. L.; Wang, H.C. A. Iron oxide surface catalyzed oxidation of quinoline by hydrogen peroxide. *Journal of Environmental Engineering*. **1998**, 124 (1), 31-38.
- <sup>54</sup> Liu, H.; Korshin, G. V.; Ferguson, J. F. Investigation of the kinetics and mechanisms of the oxidation of cerussite and hydrocerussite by chlorine. *Environmental Science & Technology*. **2008**, 42 (9), 3241-3247.
- <sup>55</sup> Sedlak, D. L. *Water 4.0: The past, present, and future of the world's most vital resource*; Yale University Press: **2014**.
- <sup>56</sup> National Research Council of the National Academies. *Water reuse: potential for expanding the nation's water supply through reuse of municipal wastewater*. The national Academies Press. Washington DC: 2012.
- <sup>57</sup> McClellan, K.; Halden, R. U. Pharmaceuticals and personal care products in archived US biosolids from the 2001 EPA national sewage sludge survey. *Water Research*. **2010**, 44 (2), 658-668.
- <sup>58</sup> Alturki, A. A.; Tadkaew, N.; McDonald, J. A.; Khan, S. J.; Price, W. E.; Nghiem, L. D. Combining MBR and NF/RO membrane filtration for the removal of trace organics in indirect potable water reuse applications. *Journal of Membrane Science*. **2010**, 365 (1), 206-215.
- <sup>59</sup> del Pino, M. P.; Durham, B. Wastewater reuse through dual-membrane processes: opportunities for sustainable water resources. *Desalination*. **1999**, 124 (1), 271-277.
- <sup>60</sup> Snyder, S. A.; Adham, S.; Redding, A. M.; Cannon, F. S.; DeCarolis, J.; Oppenheimer, J.; ... & Yoon, Y. Role of membranes and activated carbon in the removal of endocrine disruptors and pharmaceuticals. *Desalination*. **2007**, 202 (1-3), 156-181.
- <sup>61</sup> Comninellis, C.; Kapalka, A.; Malato, S.; Parsons, S. A.; Poullos, I.; Mantzavinos, D. Advanced oxidation processes for water treatment: advances and trends for R&D. *Journal of Chemical Technology and Biotechnology*. **2008**, 83 (6), 769-776.
- <sup>62</sup> Raut-Jadhav, S.; Saharan, V. K.; Pinjari, D.; Sonawane, S.; Saini, D.; Pandit, A. Synergetic effect of combination of AOP's (hydrodynamic cavitation and H<sub>2</sub>O<sub>2</sub>) on the degradation of neonicotinoid class of insecticide. *Journal of Hazardous Materials*. **2013**,

---

261, 139-147.

- <sup>63</sup> Saharan, V.; Badve, M.; Pandit, A. Degradation of Reactive Red 120 dye using hydrodynamic cavitation, *Chemical Engineering Journal*. **2011**, *178*, 100-107.
- <sup>64</sup> Lee, C.; Sedlak, D. L. A novel homogeneous Fenton-like system with Fe(III)–phosphotungstate for oxidation of organic compounds at neutral pH values. *Journal of Molecular Catalysis A: Chemical*. **2009**, *311*, 1-6.
- <sup>65</sup> An, J.; Zhu, L.; Zhang, Y.; Tang, H. Efficient visible light photo-Fenton-like degradation of organic pollutants using in situ surface-modified BiFeO<sub>3</sub> as a catalyst. *Journal of Environmental Sciences*. **2013**, *25*, 213-225.
- <sup>66</sup> Bahnmüller, S.; Loi, C.; Linge, K.; von Gunten, U., Canonica, S. Degradation rates of benzotriazoles and benzothiazoles under UV-C irradiation and the advanced oxidation process UV/H<sub>2</sub>O<sub>2</sub>. *Water Research*. **2015**, *74*, 143-154.
- <sup>67</sup> Moreira, F.; Boaventuraa; R.; Brillasb; E., Vilar V. Remediation of a winery wastewater combining aerobic biological oxidation and electrochemical advanced oxidation processes. *Water Research*. **2015**, *75*, 95-108.
- <sup>68</sup> Kegel, F. S.; Rietman, B. M.; Verliefe, A. R. D. Reverse osmosis followed by activated carbon filtration for efficient removal of organic micropollutants from river bank filtrate. *Water Science and Technology*. **2010**, *61* (10), 2603-2610.
- <sup>69</sup> Souza, B. S.; Dantas, R. F.; Agulló-Barceló, M.; Lucena, F.; Sans, C.; Esplugas, S.; Dezotti, M. Evaluation of UV/H<sub>2</sub>O<sub>2</sub> for the disinfection and treatment of municipal secondary effluents for water reuse. *Journal of Chemical Technology and Biotechnology*. **2013**, *88* (9), 1697-1706.
- <sup>70</sup> Minisci, F.; Citterio, A.; Giordano, C. Electron-transfer processes: peroxydisulfate, a useful and versatile reagent in organic chemistry. *Accounts of Chemical Research*. **1983**, *16*, 27-32.
- <sup>71</sup> Neta, P.; Madhavan, V.; Zemel, H.; Fessenden, R. W. Rate constants and mechanism of reaction of sulfate radical anion with aromatic compounds. *Journal of the American Chemical Society*. **1977**, *99*, 163-164.
- <sup>72</sup> Peyton, G. R. The free-radical chemistry of persulfate-based total organic carbon analyzers. *Marine Chemistry*. **1993**, *41*, 91-103.
- <sup>73</sup> Liang, C.; Wang, Z. S.; Mohanty, N. Influences of carbonate and chloride ions on persulfate oxidation of trichloroethylene at 20C. *Science of the Total Environment*. **2006**, *370* (2), 271-277.

- 
- <sup>74</sup> Lin, Y. T.; Liang, C.; Chen, J. H. Feasibility study of ultraviolet activated persulfate oxidation of phenol. *Chemosphere*. **2011**, *82* (8), 1168-1172.
- <sup>75</sup> Criquet, J.; Leitner, N. K. V. Degradation of acetic acid with sulfate radical generated by persulfate ions photolysis. *Chemosphere*. **2009**, *77* (2), 194-200.
- <sup>76</sup> He, X.; Armah, A.; Dionysiou, D. D. Destruction of cyanobacterial toxin cylindrospermopsin by hydroxyl radicals and sulfate radicals using UV-254nm activation of hydrogen peroxide, persulfate and peroxydisulfate. *Journal of Photochemistry and Photobiology A: Chemistry*. **2013**, *251*, 160-166.
- <sup>77</sup> Hori, H.; Yamamoto, A.; Hayakawa, E.; Taniyasu, S.; Yamashita, N.; Kutsuna, S.; ... & Arakawa, R. Efficient decomposition of environmentally persistent perfluorocarboxylic acids by use of persulfate as a photochemical oxidant. *Environmental Science & Technology*. **2005**, *39* (7), 2383-2388.
- <sup>78</sup> Patton, S.; Li, W.; Couch, K.; Mezyk, S.; Ishida, K.; Liu, H. The impact of the UV photolysis of monochloramine on 1,4-dioxane removal: implications on potable water reuse. *Environmental Science & Technology Letters*. **2017**, *4* (1), 26-30.
- <sup>79</sup> Sedlak, D. L.; Deeb, R. A.; Hawley, E. L.; Mitch, W. A.; Durbin, T. D.; Mowbray, S.; Carr, S. Sources and fate of nitrosodimethylamine and its precursors in municipal wastewater treatment plants. *Water Environment Research*. **2005**, *77* (1), 32-39.
- <sup>80</sup> De Laat, J.; Boudiaf, N.; Sossier-Berne, F. Effect of dissolved oxygen on the photodecomposition of monochloramine and dichloramine in aqueous solution by UV irradiation at 253.7 nm. *Water Research*. **2010**, *44* (10), 3261-3269.
- <sup>81</sup> Cooper, W. J.; Jones, A. C.; Whitehead, R.F.; Zika, R.G.; Sunlight-induced photochemical decay of oxidants in natural waters: implications in ballast water treatment. *Environmental Science & Technology*. **2007**, *41* (10), 3728-3733.
- <sup>82</sup> Watts, M. J.; Linden, K. G. Chlorine photolysis and subsequent OH radical production during UV treatment of chlorinated water. *Water Research*. **2007**, *41* (13), 2871-2878.
- <sup>83</sup> Li, J.; Blatchley, E. R. UV photodegradation of inorganic chloramines. *Environmental Science & Technology*. **2009**, *43* (1), 60-65.
- <sup>84</sup> Soltermann, F.; Widler, T.; Canonica, S.; von Gunten, U. Photolysis of inorganic chloramine and efficiency of trichloramine abatement by UV treatment of swimming pool water. *Water Research*. **2014**, *56*, 280-291.
- <sup>85</sup> Hansen, K. M. S.; Zortea, R.; Piketty, A.; Vega, S. R.; Andersen, H. R. Photolytic removal of DBPs by medium pressure UV in swimming pool water. *Science of the Total Environment*. **2013**, *443*, 850-856.

- 
- <sup>86</sup> Cushings, R. S.; Mackey, E. D.; Bolton, J. R.; Stefan, M. I. Impact of common water treatment chemicals on UV disinfection. In *Proceedings AWWA Annual Conference and Exposition, Washington DC*: 2001.
- <sup>87</sup> Fatta-Kassinos, D.; Vasquez, M. I.; Kümmerer, K. Transformation products of pharmaceuticals in surface waters and wastewater formed during photolysis and advanced oxidation processes—degradation, elucidation of byproducts and assessment of their biological potency. *Chemosphere*. **2011**, *85* (5), 693-709.
- <sup>88</sup> Richardson, S. D. Disinfection by-products and other emerging contaminants in drinking water. *TrAC Trends in Analytical Chemistry*. **2003**, *22* (10), 666-684.
- <sup>89</sup> Rosal, R.; Gonzalo, M. S.; Boltes, K.; Letón, P.; Vaquero, J. J.; García-Calvo, E. Identification of intermediates and assessment of ecotoxicity in the oxidation products generated during the ozonation of clofibric acid. *Journal of Hazardous Materials*. **2009**, *172* (2), 1061-1068.
- <sup>90</sup> Radjenović, J.; Sirtori, C.; Petrović, M.; Barceló, D.; Malato, S. Characterization of intermediate products of solar photocatalytic degradation of ranitidine at pilot-scale. *Chemosphere*. **2010**, *79* (4), 368-376.
- <sup>91</sup> Graham, J. L.; Striebich, R.; Patterson, C. L.; Krishnan, E. R.; Hought, R. C. MTBE oxidation byproducts from the treatment of surface waters by ozonation and UV-ozonation. *Chemosphere*. **2004**, *54* (7), 1011-1016.
- <sup>92</sup> Herner, H. A.; Trosko, J. E.; Masten, S. J. The epigenetic toxicity of pyrene and related ozonation byproducts containing an aldehyde functional group. *Environmental Science & Technology*. **2001**, *35* (17), 3576-3583.
- <sup>93</sup> Feron, V. J.; Til, H. P.; De Vrijer, F.; Woutersen, R. A.; Cassee, F. R.; Van Bladeren, P. J. Aldehydes: occurrence, carcinogenic potential, mechanism of action and risk assessment. *Mutation Research/Genetic Toxicology*. **1991**, *259* (3-4), 363-385.
- <sup>94</sup> Liang, C.; Huang, C. F.; Mohanty, N.; Kurakalva, R. M. A rapid spectrophotometric determination of persulfate anion in ISCO. *Chemosphere*. **2008**, *73* (9), 1540-1543.
- <sup>95</sup> Standard Methods for the Examination of Water and Wastewater. 14th Edition. Method 403. **1975**, 278.

## **Chapter 2**

# **Persulfate-Based ISCO for Groundwater Remediation: Impacts of Alkalinity, pH and Chloride**

**Previously Published in *Environmental Science & Technology***

Li, Wei, Ruben Orozco, Natalia Camargos, and Haizhou Liu. “Mechanisms on the Impacts of Alkalinity, pH and Chloride on Persulfate-based Groundwater Remediation.” *Environmental Science & Technology* 51, no. 7 (2017): 3948-3959.

## 2.1 Introduction

Groundwater contamination is a global challenge due to rapid industrialization and population growth.<sup>1-2</sup> In particular, carcinogenic petroleum hydrocarbons including benzene are widely present in groundwater at hazardous waste sites.<sup>3-6</sup> A variety of physical, chemical and biological approaches have been developed to remediate groundwater.<sup>7-10</sup> *In situ* chemical oxidation (ISCO) using persulfate ( $S_2O_8^{2-}$ ) has been increasingly applied as a novel chemical remediation approach.<sup>11-17</sup> Besides base activation, persulfate can also be heterogeneously activated by Fe(III)- and Mn(IV)-containing minerals via Fenton-like reactions to generate sulfate radical ( $SO_4^{\bullet-}$ ).<sup>18-21</sup> Compared to hydroxyl radical ( $HO^{\bullet}$ ),  $SO_4^{\bullet-}$  is similarly oxidative but more selective towards electron-rich organic contaminants.<sup>22-24</sup> In addition, the half-life of persulfate in the aquifer is orders of magnitude longer than other conventional oxidants including hydrogen peroxide ( $H_2O_2$ ) and permanganate ( $MnO_4^-$ ).<sup>25-29</sup> These unique features can lead to an efficient delivery of persulfate to the contamination plumes at hazardous waste sites.<sup>20,21</sup>

Despite inherent advantages, persulfate-based ISCO remediation is affected by the presence of major groundwater chemical constituents, especially alkalinity, pH and chloride; however, the impacts of these important chemical parameters on the efficiency and kinetics of persulfate-based remediation are not well understood. Contaminated groundwater typically has chloride and alkalinity levels ranging from micro- to milli-mole, and pH from neutral to extremely high levels impacted by the base activation of persulfate.<sup>30,31</sup> Prior studies also reported inconclusive effects of pH and chloride on the

efficiency of contaminant degradation by  $\text{SO}_4^{\bullet-}$ . For example, some contaminants were degraded more quickly at higher pHs while others at lower pHs.<sup>32-34</sup> The effect of chloride on the degradation of organic contaminants was reported to be either negligible, inhibitive or positive at varying concentrations.<sup>32,35-37</sup> A better understanding of the impacts of groundwater chemical conditions on persulfate activation will significantly benefit large-scale remediation efforts.

In principle, a variety of groundwater constituents can transform  $\text{SO}_4^{\bullet-}$  into chlorine atom ( $\text{Cl}^{\bullet}$ ), carbonate radical ( $\text{CO}_3^{\bullet-}$ ),  $\text{HO}^{\bullet}$  and other radicals.<sup>23,38,39</sup> The reactivities of different radicals can vary by orders of magnitude.<sup>22,40-43</sup> Furthermore, alkalinity and pH affect the formation of carbonate and hydroxo complexes on the mineral surfaces and their redox reactivity.<sup>44</sup> In addition, Fe(III)- and Mn(IV)-containing minerals that are widely present in aquifer exhibit distinct rates of persulfate decomposition and efficiencies of radical yield.<sup>20-21</sup> However, the fundamental mechanisms controlling the impacts of groundwater chemical matrix on heterogeneous persulfate activation remain unknown.

The main objectives of this study were to investigate the impacts of groundwater alkalinity, pH and chloride on benzene degradation via heterogeneous persulfate activation by Fe(III)- and Mn(IV)-containing minerals, examine the fundamental mechanisms of radical chain reactions of persulfate activation in diverse chemical conditions, quantify the kinetics and the efficiency of benzene degradation, and assess the distribution of benzene degradation products. A accompanying objective was to develop a comprehensive kinetic model to elucidate mineral surface complexation and radical chain reactions involving

persulfate ISCO under diverse groundwater chemical conditions. 2.2. Materials and Methods

## 2.2 Materials and Methods

### 2.2.1 Experimental system

All chemicals were purchased as ACS grade from Fisher Chemical or Sigma-Aldrich. Three Fe(III) and Mn(IV) minerals were employed in this study to simulate typical aquifer conditions: ferrihydrite  $\text{FeO}(\text{OH})_{(\text{s})}$ , goethite  $\alpha\text{-FeO}(\text{OH})_{(\text{s})}$  and pyrolusite  $\beta\text{-MnO}_{2(\text{s})}$ . In particular, pyrolusite represents a Mn(IV)-containing aquifer mineral because it is present in the subsurface and exhibits a strong catalytic effect to activate persulfate.<sup>21,45-47</sup> Ferrihydrite and pyrolusite were purchased from Sigma-Aldrich. Goethite was synthesized by precipitating  $\text{Fe}(\text{NO}_3)_3$  with  $\text{NaOH}$ .<sup>48</sup> All metal oxides were grounded and sieved through No. 100 and 400 sieves with a nominal particle size between 38 and 150  $\mu\text{m}$ . Additional information on mineral preparation can be found in a previous study.<sup>21</sup> The surface area of each mineral was directly measured, and details are provided in **Table 1** and **Appendix A-1**.

**Table 1** BET surface area of minerals used in this study.

<b>Mineral</b>	<b>BET Surface Area (<math>\text{m}^2/\text{g}</math>)</b>
Goethite ( $\alpha\text{-FeO}(\text{OH})_{(\text{s})}$ )	21
Ferrihydrite ( $\text{FeO}(\text{OH})_{(\text{s})}$ )	180
Pyrolusite ( $\beta\text{-MnO}_{2(\text{s})}$ )	0.11

To prepare persulfate activation and benzene degradation experiments, a 1-mM benzene solution was prepared directly in a 1-L volumetric flask with deionized (DI) water containing 50 mM borate buffer at pH 8.0 with no headspace. Chloride concentrations varying between 0 and 5 mM was prepared by adding a requisite amount of 100 mM NaCl. The solution pH was adjusted between 8 and 13 by adding 50 mM borate buffer and 5 M NaOH. Solution alkalinity was adjusted between  $1.6 \times 10^{-2}$  and 10 meq/L with a 0.5 M  $\text{NaHCO}_3$  stock solution. The ionic strength was 10 mM in most experiments except that it was 100 mM in experiments with varying pH levels. Pure  $\text{K}_2\text{S}_2\text{O}_8$  crystals were added to the flask to reach the targeted  $\text{S}_2\text{O}_8^{2-}$  concentration of 1 mM. After mixing, the solution was quickly transferred to 10-mL glass vials without headspace. The vials were pre-loaded with 100 g/L of Fe(III) or Mn(IV) minerals, a typical dosage to simulate ISCO performance.<sup>20,21</sup> Each vial was then placed on an automatic rotator and left at 23 °C in darkness. All experiments were performed in duplicates or triplicates.

Samples were withdrawn from the sacrificial glass vials every five days, centrifuged at 2000 g for 5 minutes and filtered through 0.22- $\mu\text{m}$  syringe filters before analysis.<sup>21</sup> The concentration of persulfate was measured using potassium iodine (KI) titration with a Horiba UV spectrometer.<sup>49</sup> Benzene and its oxidation product phenol were analyzed by an Agilent 1200 liquid chromatography (**Appendix A- 2**). Another major benzene degradation product, an aldehyde compound, was characterized by nuclear magnetic resonance (NMR) and liquid chromatography-mass spectrometry (LC-MS).<sup>20</sup> Chloride was measured by a Dionex 1000 ion chromatography equipped with a

conductivity detector. Alkalinity was measured by the standard sulfuric acid titration method.<sup>50</sup>

### ***2.2.2. Development of a kinetic model***

A comprehensive kinetic model of heterogeneous persulfate activation was established using the Kintecus software.<sup>51</sup> Details on the kinetic model were provided in **Appendix A-3**. In short, a total of 77 and 56 reactions were established to model persulfate decomposition by Fe(III) and Mn(IV) oxide, respectively (**Appendix A-5**). All rate constants were directly obtained from prior literature, except that the rate constants of four reactions involving homogeneous persulfate activation by soluble Fe(III) were optimized using experimental data from persulfate activation by soluble Fe(III). Rate constants of six reactions involving heterogeneous persulfate activation by ferrihydrite and goethite and three reactions involving heterogeneous persulfate activation by pyrolusite were optimized using experimental data at different alkalinity, pH and chloride levels. Metal surface hydroxo and carbonato complexes were modeled based on known equilibrium constants without considering the surface electrostatic interactions. The model ensured the surface hydroxo and carbonato complexes reactions reached equilibria instantaneously throughout the reaction regardless the presence or absence of persulfate in all conditions. The best model fitting was achieved by minimizing the root mean squares (RMS) between experimental and modeled data using Powell non-restricted algorithms. The steady-state concentrations of metal surface complexes and radicals were calculated based on the fully optimized kinetic model.

## 2.3 Results and Discussion

### 2.3.1 *Radical chain reactions during persulfate activation by aquifer minerals*

In the presence of 1 mM benzene, 100 g/L of minerals, negligible levels of alkalinity and chloride, and at pH 8, the surface area-normalized rates of persulfate decomposition followed the order of pyrolusite > goethite > ferrihydrite (**Figure 1A**). The high reactivity of pyrolusite was mainly associated with its surface hydroxo complexation and crystalline structure.<sup>3,21,52-56</sup> The activation of persulfate by ferrihydrite and goethite resulted from Fenton-like reactions involving the reduction of surface Fe(III) to Fe(II) by persulfate (Reaction 1-2 in **Table 2**; all subsequently referred reactions are listed in **Table 2**), followed by the oxidation of surface Fe(II) by persulfate to generate  $\text{SO}_4^{\bullet-}$  (Reaction 3-4). Similar reactions involving surface Mn(IV) and Mn(III) took place for pyrolusite involving Mn(IV) and Mn(III) (Reactions 5-6).<sup>20,21,57</sup> Based on the kinetic model prediction, a predominant fraction of persulfate loss (>80%) was attributed to Fenton-like reactions involving oxidized and reduced surfaces sites of metal oxides (**Figure 1**), and the rest of persulfate was decomposed via thermal decomposition at 25 °C (Reactions 7).

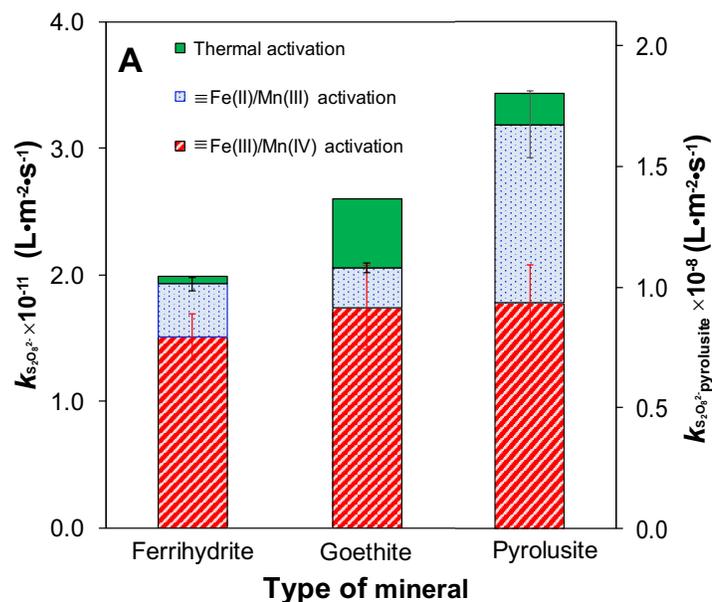


**Figure 1.** Surface area-normalized first-order decay rate constant of persulfate decomposition (pyrolusite rates on the secondary y-axis);  $[S_2O_8^{2-}] = 1$  mM,  $[benzene] = 1$  mM,  $[Cl^-] = 0$  mM,  $pH = 8.0$  [alkalinity] =  $1.6 \times 10^{-2}$  meq/L, dosage of mineral = 100 g/L, ionic strength = 10 mM.

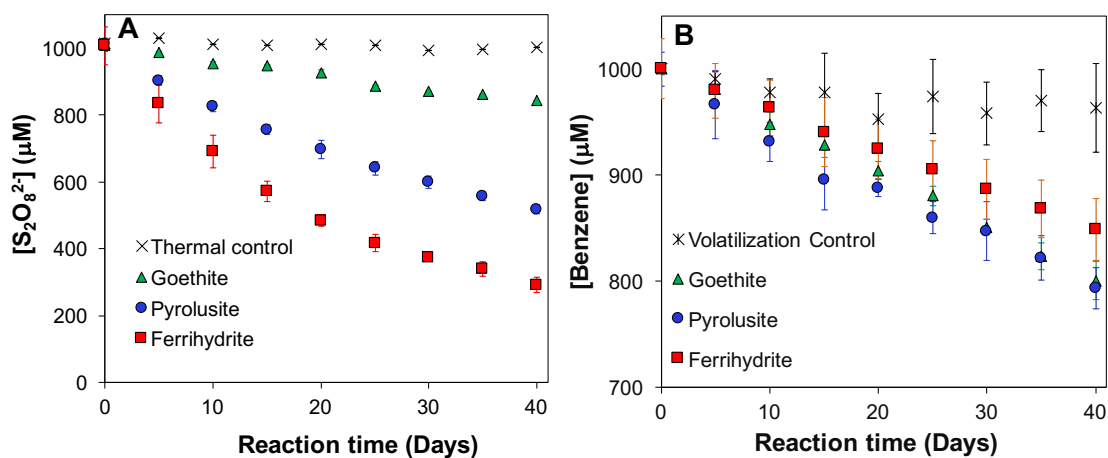


**Figure 2.** The kinetics of persulfate decomposition and benzene degradation in the presence of different metal oxides. (A) Persulfate decomposition time profile; (B) Benzene degradation time profile.  $[S_2O_8^{2-}] = 1$  mM,  $[benzene] = 1$  mM, [alkalinity] =  $1.6 \times 10^{-2}$  meq/L,  $[Cl^-] = 0$  mM,  $pH = 8.0$ , dosage of metal oxides = 100 g/L, ionic strength = 12 mM.

**Table 2** Major radical chain reactions involving benzene degradation via persulfate activation by Fe(III) and Mn(IV) oxides.

No.	Reaction	Rate constant ( $M^{-1}s^{-1}$ )	Reference <sup>*</sup>
1	$\equiv Fe(III) - OH + S_2O_8^{2-} \rightarrow \equiv Fe(II) - OH + S_2O_8^-$	$(6.0 \pm 0.6) \times 10^{-6}$	
2	$\equiv Fe(III) - O^- + S_2O_8^{2-} \rightarrow \equiv Fe(II) - O^- + S_2O_8^-$	$(2.8 \pm 0.8) \times 10^{-6}$	
3	$\equiv Fe(II) - OH + S_2O_8^{2-} \rightarrow \equiv Fe(III) - OH + SO_4^- + SO_4^{2-}$	$(1.8 \pm 0.2) \times 10^{-4}$	
4	$\equiv Fe(II) - O^- + S_2O_8^{2-} \rightarrow \equiv Fe(III) - O^- + SO_4^- + SO_4^{2-}$	$(2.2 \pm 0.3) \times 10^{-5}$	
5	$\equiv Mn(IV) - O^- + S_2O_8^{2-} \rightarrow \equiv Mn(III) - O^- + S_2O_8^-$	$(2.2 \pm 0.4) \times 10^{-3}$	
6	$\equiv Mn(III) - O^- + S_2O_8^{2-} \rightarrow \equiv Mn(IV) - O^- + SO_4^- + SO_4^{2-}$	$(4.9 \pm 1.3) \times 10^{-3}$	
7	$S_2O_8^{2-} \rightarrow 2SO_4^-$ (25 °C)	$1.2 \times 10^{-8}$	21 <sup>a</sup>
8	$C_6H_6 + SO_4^- \rightarrow C_6H_6^+ + SO_4^{2-}$	$3.0 \times 10^9$	58
9	$S_2O_8^{2-} + SO_4^- \rightarrow S_2O_8^- + SO_4^{2-}$	$6.6 \times 10^5$	59
10	$SO_4^- + H_2O \rightarrow HSO_4^- + HO^\cdot$	$1.2 \times 10^1$	60 <sup>a</sup>
11	$SO_4^- + OH^- \rightarrow SO_4^{2-} + HO^\cdot$	$7.0 \times 10^7$	23
12	$SO_4^- + HCO_3^- \rightarrow CO_3^- + SO_4^{2-} + H^+$	$9.1 \times 10^6$	39
13	$HO^\cdot + HCO_3^- \rightarrow CO_3^- + H_2O$	$8.6 \times 10^6$	61
14	$\equiv Fe(II) - OH + SO_4^- \rightarrow \equiv Fe(III) - O^- + SO_4^{2-}$	$(9.5 \pm 1.0) \times 10^7$	
15	$\equiv Fe(II) - O^- + SO_4^- \rightarrow \equiv Fe(III) - O^- + SO_4^{2-}$	$(1.0 \pm 5.0) \times 10^8$	
16	$\equiv Mn(III) - O^- + SO_4^- \rightarrow \equiv Mn(IV) - O^- + SO_4^{2-}$	$(5.6 \pm 1.5) \times 10^{10}$	
17	$SO_4^- + Cl^- \rightarrow SO_4^{2-} + Cl^\cdot$	$6.6 \times 10^8$	62
18	$Cl^\cdot + H_2O \rightarrow ClOH^\cdot + H^+$	$4.5 \times 10^3$	63 <sup>a</sup>
19	$Cl^\cdot + OH^- \rightarrow ClOH^\cdot$	$1.8 \times 10^{10}$	64
20	$Cl^\cdot + Cl^- \rightarrow Cl_2^-$	$8.5 \times 10^9$	63
21	$Cl_2^- + H_2O \rightarrow HClOH^\cdot + Cl^-$	$2.4 \times 10^0$	63 <sup>a</sup>
22	$HClOH^\cdot \rightarrow H^+ + ClOH^\cdot$	$1.0 \times 10^8$	63 <sup>a</sup>

23	$ClOH^- \rightarrow Cl^- + HO^\cdot$	$6.1 \times 10^9$	65 <sup>a</sup>
24	$Cl^\cdot + HCO_3^- \rightarrow CO_3^{\cdot-} + H^+ + Cl^-$	$2.2 \times 10^8$	66
25	$\equiv Fe(III) - OH + CO_3^{2-} + H^+ \rightarrow \equiv Fe(III) - OCO_2^- + H_2O$	$1.0 \times 10^{15}$	75 <sup>b</sup>
26	$\equiv Fe(III) - OCO_2^- + H_2O \rightarrow \equiv Fe(III) - OH + CO_3^{2-} + H^+$	$1.7 \times 10^2$	75 <sup>a</sup>
27	$\equiv Mn(IV) - OH + CO_3^{2-} + H^+ \rightarrow \equiv Mn(IV) - OCO_2^- + H_2O$	$1.0 \times 10^{15}$	76 <sup>b</sup>
28	$\equiv Mn(IV) - OCO_2^- + H_2O \rightarrow \equiv Mn(IV) - OH + CO_3^{2-} + H^+$	$7.1 \times 10^0$	76 <sup>a</sup>
29	$\equiv Fe(III) - OH + CO_3^{2-} + 2H^+ \rightarrow \equiv Fe(III) - OCO_2H^0 + H_2O$	$1.0 \times 10^{20}$	75 <sup>c</sup>
30	$\equiv Fe(III) - OCO_2H^0 + H_2O \rightarrow \equiv Fe(III) - OH + CO_3^{2-} + 2H^+$	$4.3 \times 10^{-1}$	75 <sup>a</sup>
31	$\equiv Mn(IV) - OH + CO_3^{2-} + 2H^+ \rightarrow \equiv Mn(IV) - OCO_2H^0 + H_2O$	$1.0 \times 10^{20}$	76 <sup>c</sup>
32	$\equiv Mn(IV) - OCO_2H^0 + H_2O \rightarrow \equiv Mn(IV) - OH + CO_3^{2-} + 2H^+$	$2.2 \times 10^{-3}$	76 <sup>a</sup>
33	$\equiv Fe(III) - OH_2^+ \rightarrow \equiv Fe(III) - OH + H^+$	$2.6 \times 10^2$	78 <sup>a</sup>
34	$\equiv Fe(III) - OH + H^+ \rightarrow \equiv Fe(III) - OH_2^+$	$5.0 \times 10^9$	78
35	$\equiv Mn(IV) - OH_2^+ \rightarrow \equiv Mn(IV) - OH + H^+$	$1.3 \times 10^9$	79 <sup>a</sup>
36	$\equiv Mn(IV) - OH + H^+ \rightarrow \equiv Mn(IV) - OH_2^+$	$5.0 \times 10^9$	79
37	$\equiv Fe(III) - OH \rightarrow \equiv Fe(III) - O^- + H^+$	$5.9 \times 10^0$	78 <sup>a</sup>
38	$\equiv Fe(III) - O^- + H^+ \rightarrow \equiv Fe(III) - OH$	$5.0 \times 10^9$	78
39	$\equiv Mn(IV) - OH \rightarrow \equiv Mn(IV) - O^- + H^+$	$1.3 \times 10^7$	79 <sup>a</sup>
40	$\equiv Mn(IV) - O^- + H^+ \rightarrow \equiv Mn(IV) - OH$	$5.0 \times 10^9$	79

\* Reaction rate constants without references were obtained in this study from the kinetic model. All rate constants on Fe(III) in this table are for ferrihydrite. Rate constants for goethite are listed in **Appendix A-5**.

<sup>a</sup> rate constants are in unit of  $s^{-1}$

<sup>b</sup> rate constants are in unit of  $M^{-2} s^{-1}$

<sup>c</sup> rate constants are in unit of  $M^{-3} s^{-1}$

After 40 days of reaction, 16% to 70% of persulfate was decomposed and approximately 20% of benzene was degraded (**Figure 2**). Surface area-normalized rates of benzene degradation followed the same order as persulfate decomposition for different minerals, and  $\text{SO}_4^{\cdot-}$  was the major oxidative species (**Figure 3**).  $\text{SO}_4^{\cdot-}$  predominantly reacted with benzene than with persulfate (Reaction 8 vs. 9). Although both  $\text{HO}^{\cdot}$  and  $\text{CO}_3^{\cdot-}$  were produced via  $\text{SO}_4^{\cdot-}$  chain reactions (Reactions 10-13), they negligibly contributed to benzene degradation due to low steady-state concentrations (**Appendix A-4**).

Because benzene was the major sink for  $\text{SO}_4^{\cdot-}$ , its degradation was used to calculate the stoichiometric efficiency of  $\text{SO}_4^{\cdot-}$  yield (denoted as  $E_{S_2O_8^{2-}}$ ) in persulfate decomposition:

$$E_{S_2O_8^{2-}} = \frac{\Delta[\text{Benzene}]}{\Delta[S_2O_8^{2-}]} \times 100\% \quad (1)$$

The experimentally observed stoichiometric efficiency of  $\text{SO}_4^{\cdot-}$  yield was inversely correlated with the rate of persulfate decomposition for the three minerals (**Figure 4**). This trend was consistent with our prior observations on the reactivity of minerals.<sup>20,21</sup> As persulfate was decomposed and  $\text{SO}_4^{\cdot-}$  was generated via heterogeneous activation by mineral surfaces,  $\text{SO}_4^{\cdot-}$  was also scavenged by reactive mineral surface complexes (Reactions 14-16), which eventually lowered the radical yield.

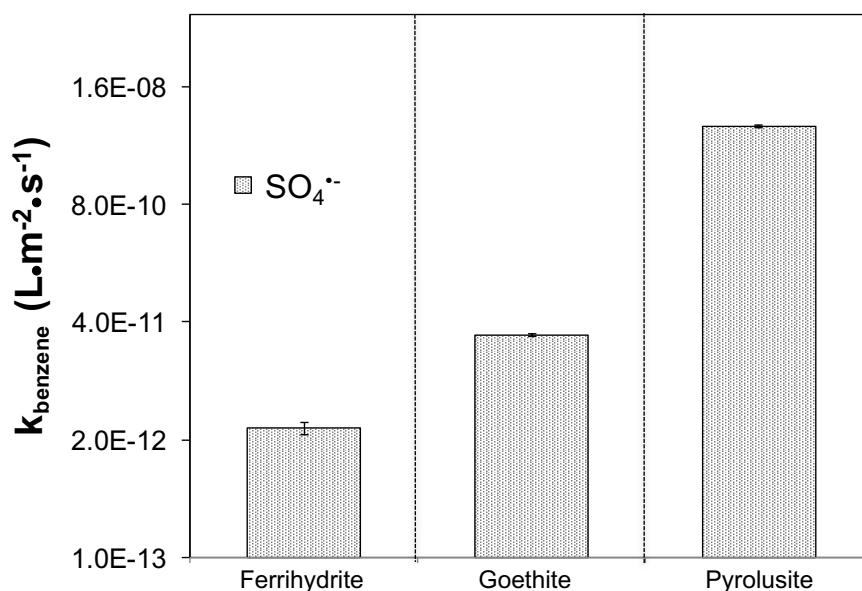


**Figure 3** Surface area-normalized first-order rate constants of benzene degradation. Initial  $[\text{S}_2\text{O}_8^{2-}] = 1 \text{ mM}$ , initial  $[\text{benzene}] = 1 \text{ mM}$ ,  $[\text{Cl}^-] = 0 \text{ mM}$ ,  $[\text{alkalinity}] = 1.6 \times 10^{-2} \text{ meq/L}$ ,  $\text{pH} = 8.0$ , dose of metal oxides = 100 g/L, ionic strength = 12 mM. The benzene degradation was predominantly contributed by  $\text{SO}_4^{\cdot-}$  oxidation, calculated from kinetic model predictions.

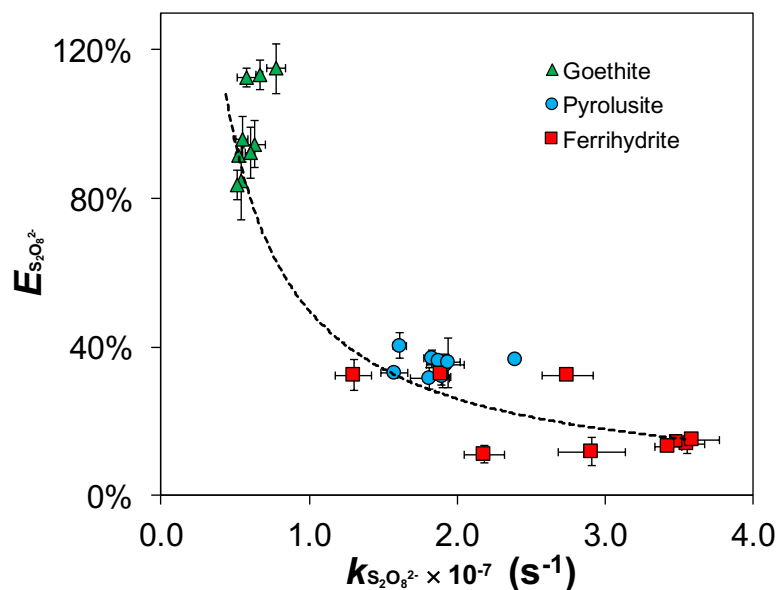


**Figure 4.** Correlation between the stoichiometric efficiency of radical yield ( $E_{\text{S}_2\text{O}_8^{2-}}$ ) and the rate of persulfate decomposition ( $k_{\text{S}_2\text{O}_8^{2-}}$ ).  $[\text{S}_2\text{O}_8^{2-}] = 1 \text{ mM}$ ,  $[\text{benzene}] = 1 \text{ mM}$ ,  $[\text{Cl}^-] = 0 \text{ mM}$ ,  $\text{pH} = 8.0$ ,  $[\text{alkalinity}] = 1.6 \times 10^{-2} \text{ meq/L}$ , dosage of mineral = 100 g/L, ionic strength = 10 mM.

### ***2.3.2 Impact of groundwater chemistry on benzene degradation and persulfate decomposition***

The impact of groundwater chemical parameters on persulfate decomposition was systematically investigated on the basis of alkalinity, pH and chloride levels. When alkalinity increased from  $1.6 \times 10^{-2}$  meq/L (*i.e.*, the background level in air-saturated condition) to 10 meq/L, the rates of persulfate decomposition decreased by 40%, 3% and 15% in ferrihydrite, goethite and pyrolusite system, respectively (**Figure 5A, C and E**). Rates of benzene degradation also decreased by 24% and 15% in ferrihydrite and pyrolusite systems, and remained unchanged in goethite system (**Figure 5B, D and F**). The kinetic model predicted that the presence of alkalinity led to a transformation of  $\text{SO}_4^{\bullet-}$  and  $\text{HO}^{\bullet}$  to  $\text{CO}_3^{\bullet-}$  (Reactions 12-13). Specifically,  $[\text{SO}_4^{\bullet-}]_{\text{ss}}$  decreased by 12%-32%,  $[\text{HO}^{\bullet}]_{\text{ss}}$  decreased by 20%-38%, and  $[\text{CO}_3^{\bullet-}]_{\text{ss}}$  increased by three orders of magnitude with increasing alkalinity (). Different radicals exhibit distinct reactivities with organic contaminants. For example,  $\text{SO}_4^{\bullet-}$ ,  $\text{HO}^{\bullet}$  and  $\text{Cl}^{\bullet}$  have comparable reaction rates with aromatic compounds.<sup>42</sup> However,  $\text{CO}_3^{\bullet-}$  is much less reactive except for reacting with amine-containing compounds.<sup>67-68</sup>

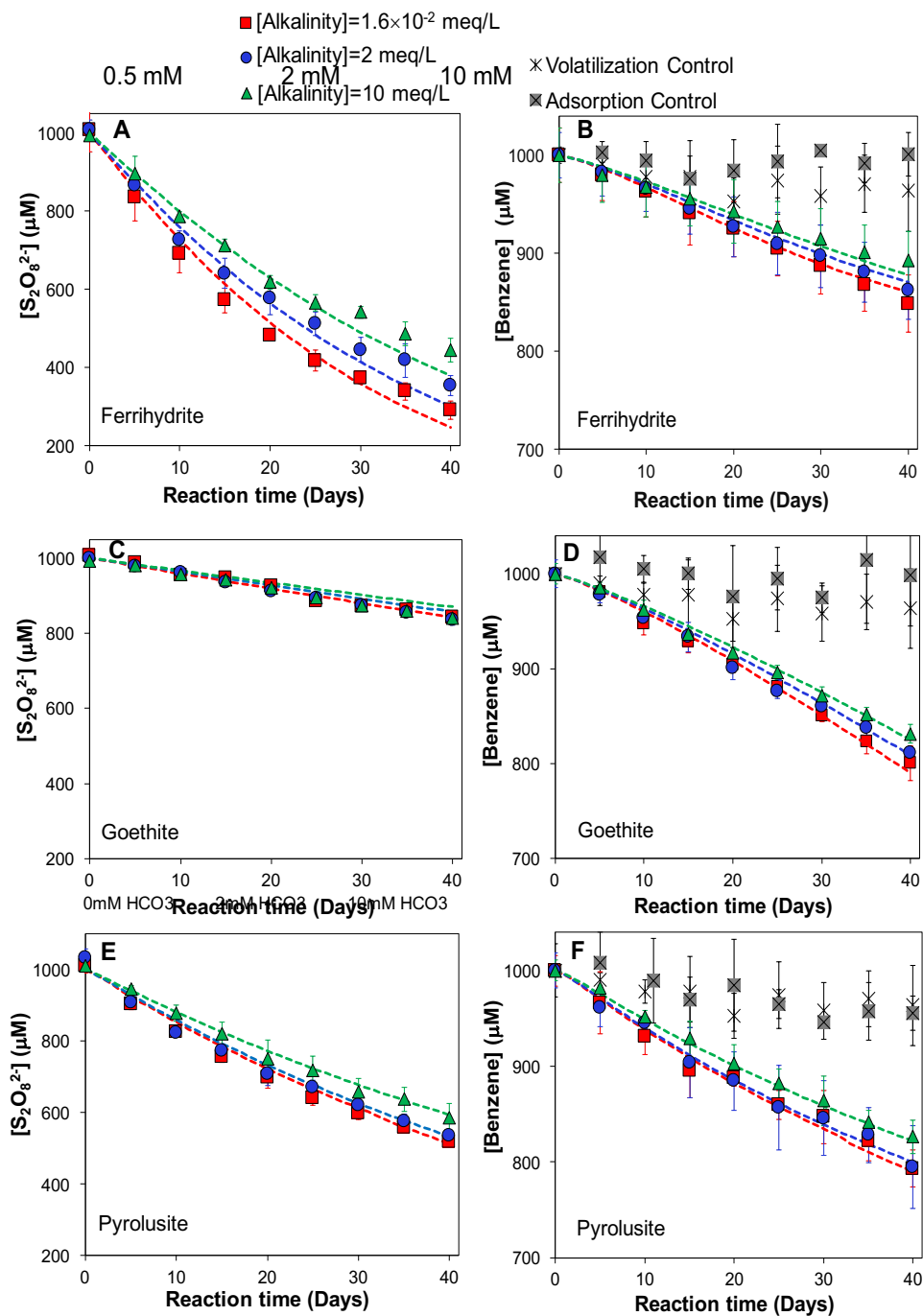


**Figure 5.** Impact of alkalinity on persulfate decomposition and benzene degradation by three minerals. (A, C, E) Persulfate decomposition; (B, D, F) Benzene degradation.  $[S_2O_8^{2-}] = 1$  mM,  $[benzene] = 1$  mM, mineral dosage = 100 g/L, pH = 8.0, ionic strength = 10 mM. Data points represent the experimental results. Dash lines represent the model-fitted values.

Solution pH significantly impacted the reaction kinetics. For all three minerals, when pH was increased from 8 to 12, the rates of persulfate decomposition increased by as much as 200% (**Figure 6A, C and E**), and the rates of benzene degradation was enhanced by up to 70% (**Figure 6B, D and F**). A further pH rise from 12 to 13 decreased the reaction kinetics. As the pH increased from 8 to 12,  $\text{SO}_4^{\cdot-}$  was transformed to  $\text{HO}^{\cdot}$  (Reaction 11). Consequently,  $[\text{HO}^{\cdot}]_{\text{ss}}$  increased by more than 2 orders of magnitude for all three minerals (**Table 3**), corresponding to an 20% increase of the contribution of  $\text{HO}^{\cdot}$  to benzene degradation (**Table 4**). Meanwhile,  $\text{CO}_3^{\cdot-}$  was generated as a result of the scavenging effect of bicarbonate on  $\text{SO}_4^{\cdot-}$  and  $\text{HO}^{\cdot}$  (Reactions 12-13), and  $[\text{CO}_3^{\cdot-}]_{\text{ss}}$  increased dramatically at higher pHs (**Table 3**). Because of the low reactivity of  $\text{CO}_3^{\cdot-}$ , benzene degradation slowed down from pH 12 to 13.

In addition, the change of pH did not significantly impact the solubility of metal oxides. The contribution of soluble Fe(III) due to dissolution of metal oxides to persulfate decomposition was minimal except at pH 13 (**Table 5**). Furthermore, control experiments in the absence of minerals showed that homogeneous persulfate decomposition was slow and not sensitive to pH ranging from 8 to 13 (**Figure 7**). This is consistent with previous observations that only extremely alkaline conditions at pH above 13 accelerated the base activation of persulfate in a homogeneous system.<sup>14</sup>

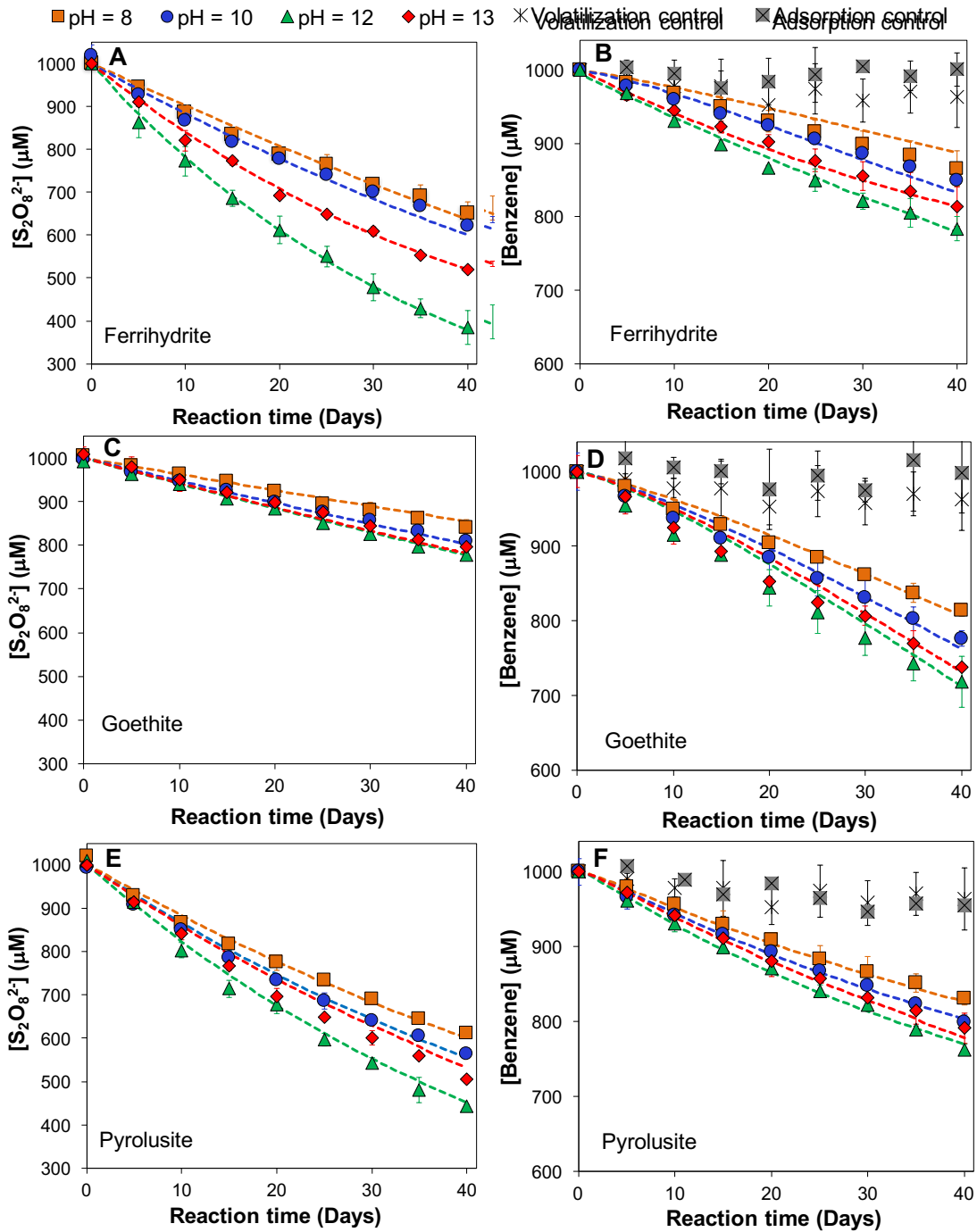


**Figure 6** Impact of pH on the rates of persulfate decomposition and benzene degradation by three minerals. (A, C, E) Persulfate decomposition; (B, D, F) Benzene degradation.  $[S_2O_8^{2-}] = 1$  mM, [benzene] = 1 mM, mineral dosage = 100 g/L, ionic strength = 100 mM. Data points represent the experimental results. Dash lines represent the model fitted values.

**Table 3** Model-predicted steady-state concentrations of radicals generated during heterogeneous persulfate activation. \*

Ferrhydrite	[Alkalinity] (meq/L)				pH				[Chloride] (mM)			
	1.6×10 <sup>-2</sup>	2	10	10	8	10	12	13	0	1	2	5
[SO <sub>4</sub> ] <sup>•-</sup> <sub>ss</sub>	1.7×10 <sup>-17</sup>	1.4×10 <sup>-17</sup>	1.2×10 <sup>-17</sup>	1.7×10 <sup>-17</sup>	1.7×10 <sup>-17</sup>	8.2×10 <sup>-18</sup>	4.2×10 <sup>-18</sup>	1.7×10 <sup>-18</sup>	1.7×10 <sup>-17</sup>	9.7×10 <sup>-18</sup>	9.1×10 <sup>-18</sup>	6.7×10 <sup>-18</sup>
[HO] <sup>•</sup> <sub>ss</sub>	1.7×10 <sup>-21</sup>	1.5×10 <sup>-21</sup>	1.3×10 <sup>-21</sup>	1.7×10 <sup>-21</sup>	1.7×10 <sup>-21</sup>	8.5×10 <sup>-21</sup>	4.4×10 <sup>-19</sup>	2.1×10 <sup>-19</sup>	1.7×10 <sup>-21</sup>	1.8×10 <sup>-20</sup>	3.0×10 <sup>-20</sup>	4.9×10 <sup>-20</sup>
[CO <sub>3</sub> ] <sup>•-</sup> <sub>ss</sub>	1.7×10 <sup>-18</sup>	2.2×10 <sup>-16</sup>	1.3×10 <sup>-15</sup>	1.7×10 <sup>-18</sup>	1.7×10 <sup>-18</sup>	3.3×10 <sup>-16</sup>	7.0×10 <sup>-15</sup>	2.8×10 <sup>-13</sup>	1.7×10 <sup>-18</sup>	1.6×10 <sup>-15</sup>	3.7×10 <sup>-15</sup>	7.2×10 <sup>-15</sup>
[Cl] <sup>•</sup> <sub>ss</sub>	-	-	-	-	-	-	-	-	-	2.1×10 <sup>-19</sup>	2.4×10 <sup>-19</sup>	2.1×10 <sup>-19</sup>
Goethite	[Alkalinity] (meq/L)				pH				[Chloride] (mM)			
	1.6×10 <sup>-2</sup>	2	10	10	8	10	12	13	0	1	2	5
[SO <sub>4</sub> ] <sup>•-</sup> <sub>ss</sub>	2.3×10 <sup>-17</sup>	2.2×10 <sup>-17</sup>	2.1×10 <sup>-17</sup>	2.3×10 <sup>-17</sup>	2.3×10 <sup>-17</sup>	2.4×10 <sup>-17</sup>	2.9×10 <sup>-17</sup>	8.3×10 <sup>-18</sup>	2.3×10 <sup>-17</sup>	2.2×10 <sup>-17</sup>	2.1×10 <sup>-17</sup>	1.8×10 <sup>-17</sup>
[HO] <sup>•</sup> <sub>ss</sub>	2.3×10 <sup>-21</sup>	2.2×10 <sup>-21</sup>	2.1×10 <sup>-21</sup>	2.3×10 <sup>-21</sup>	2.3×10 <sup>-21</sup>	2.5×10 <sup>-20</sup>	3.0×10 <sup>-18</sup>	1.0×10 <sup>-18</sup>	3.4×10 <sup>-21</sup>	3.2×10 <sup>-20</sup>	5.5×10 <sup>-20</sup>	1.1×10 <sup>-19</sup>
[CO <sub>3</sub> ] <sup>•-</sup> <sub>ss</sub>	4.3×10 <sup>-17</sup>	5.5×10 <sup>-15</sup>	2.8×10 <sup>-14</sup>	4.3×10 <sup>-17</sup>	5.7×10 <sup>-17</sup>	1.5×10 <sup>-16</sup>	1.2×10 <sup>-14</sup>	8.6×10 <sup>-13</sup>	5.7×10 <sup>-17</sup>	2.9×10 <sup>-14</sup>	6.1×10 <sup>-14</sup>	1.0×10 <sup>-13</sup>
[Cl] <sup>•</sup> <sub>ss</sub>	-	-	-	-	-	-	-	-	-	4.6×10 <sup>-19</sup>	5.6×10 <sup>-19</sup>	5.5×10 <sup>-19</sup>
Pyrolusite	[Alkalinity] (meq/L)				pH				[Chloride] (mM)			
	1.6×10 <sup>-2</sup>	2	10	10	8	10	12	13	0	1	2	5
[SO <sub>4</sub> ] <sup>•-</sup> <sub>ss</sub>	2.2×10 <sup>-17</sup>	1.7×10 <sup>-17</sup>	1.5×10 <sup>-17</sup>	2.2×10 <sup>-17</sup>	2.2×10 <sup>-17</sup>	1.8×10 <sup>-17</sup>	1.9×10 <sup>-17</sup>	7.6×10 <sup>-18</sup>	2.2×10 <sup>-17</sup>	1.9×10 <sup>-17</sup>	1.9×10 <sup>-17</sup>	1.9×10 <sup>-17</sup>
[HO] <sup>•</sup> <sub>ss</sub>	2.4×10 <sup>-21</sup>	2.1×10 <sup>-21</sup>	1.9×10 <sup>-21</sup>	2.4×10 <sup>-21</sup>	2.4×10 <sup>-21</sup>	2.2×10 <sup>-20</sup>	1.9×10 <sup>-18</sup>	9.4×10 <sup>-19</sup>	2.4×10 <sup>-21</sup>	4.1×10 <sup>-20</sup>	4.8×10 <sup>-20</sup>	1.3×10 <sup>-19</sup>
[CO <sub>3</sub> ] <sup>•-</sup> <sub>ss</sub>	7.2×10 <sup>-17</sup>	7.6×10 <sup>-15</sup>	3.5×10 <sup>-14</sup>	7.2×10 <sup>-17</sup>	7.2×10 <sup>-17</sup>	1.8×10 <sup>-15</sup>	2.7×10 <sup>-14</sup>	1.1×10 <sup>-12</sup>	7.2×10 <sup>-17</sup>	4.2×10 <sup>-14</sup>	6.8×10 <sup>-14</sup>	7.2×10 <sup>-14</sup>
[Cl] <sup>•</sup> <sub>ss</sub>	-	-	-	-	-	-	-	-	-	5.3×10 <sup>-19</sup>	5.5×10 <sup>-19</sup>	5.8×10 <sup>-19</sup>

\* When alkalinity varied between 1.6×10<sup>-2</sup> and 10 meq/L; [Cl<sup>-</sup>]=0 mM, pH=8.0; when pH varied between 8 and 13; [Cl<sup>-</sup>]=0 mM, [alkalinity]= 1.6×10<sup>-2</sup> meq/L; when chloride concentration varied between 0 and 5 mM, [alkalinity]=1.6×10<sup>-2</sup> meq/L, pH=8.0.

**Table 4** The impact of pH on the percentile contributions of different reactive radicals to benzene degradation.\*

Ferrihydrite pH				Goethite pH				Pyrolusite pH			
8	10	12	13	8	10	12	13	8	10	12	13
100%	100%	77%	24%	100%	100%	76%	30%	100%	100%	78%	27%
0%	0%	21%	8%	0%	0%	22%	8%	0%	0%	20%	9%
0%	0%	2%	68%	0%	0%	2%	62%	0%	0%	2%	64%

\* Experimental condition: mineral dosage=100 g/L; alkalinity= $1.6 \times 10^{-2}$  meq/L; no chloride added.

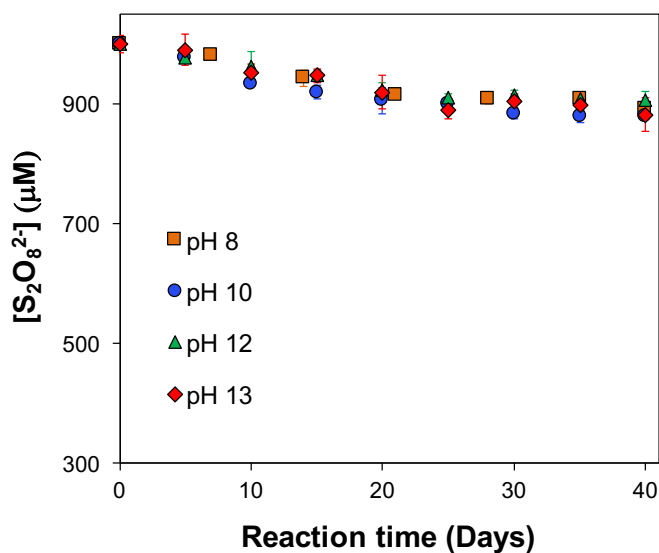


**Figure 7** The impact of pH on persulfate decomposition in the absence of minerals. [S<sub>2</sub>O<sub>8</sub><sup>2-</sup>]=1 mM, [benzene]=1 mM, [Cl<sup>-</sup>]=0 mM, [alkalinity]= $1.6 \times 10^{-2}$  -125 meq/L, ionic strength=100 mM.

**Table 5** The impact of pH on the percentile contributions of different reaction pathways to persulfate decomposition. \*

Reaction pathway for persulfate activation	Ferrihydrite			Goethite			Pyrolusite					
	pH			pH			pH					
	8	10	12	13	8	10	12	13	8	10	12	13
$\equiv\text{Fe(III)-OH}$ or $\equiv\text{Mn(IV)-OH}$	57%	4%	0%	0%	63%	45%	1%	0%	0%	0%	0%	0%
$\equiv\text{Fe(II)-OH}$ or $\equiv\text{Mn(III)-OH}$	24%	2%	0%	0%	10%	5%	0%	0%	0%	0%	0%	0%
$\equiv\text{Fe(III)-O}^-$ or $\equiv\text{Mn(IV)-O}^-$	11%	83%	76%	41%	1%	30%	70%	71%	55%	52%	52%	51%
$\equiv\text{Fe(II)-O}^-$ or $\equiv\text{Mn(III)-O}^-$	1%	3%	5%	2%	0%	5%	13%	13%	38%	42%	41%	42%
Thermal activation	8%	7%	5%	5%	26%	15%	16%	16%	7%	7%	7%	7%
Soluble Fe(III) or Mn(IV)	0%	1%	14%	54%	0%	0%	0%	0%	0%	0%	0%	0%

\* Experimental condition: mineral dosage=100 g/L, alkalinity=1.6×10<sup>-2</sup> meq/L at pH 8, alkalinity=1.3×10<sup>-1</sup> meq/L at pH 10, alkalinity=1.5 meq/L at pH 12, alkalinity=1.25 ×10<sup>2</sup> meq/L at pH 13, no chloride added.

With respect to chloride, a change of chloride level up to 5 mM had no discernible effect on either persulfate decomposition or benzene degradation (**Figure 8**). The presence of chloride generated reactive chlorine atom radical ( $\text{Cl}^\bullet$ ) via the scavenging reaction between chloride and  $\text{SO}_4^{\bullet-}$  (Reaction 17). Although chain reactions involving  $\text{Cl}^\bullet$  yielded reactive  $\text{HO}^\bullet$  (Reactions 18-23),  $\text{Cl}^\bullet$  also reacted strongly with bicarbonate and produced non-reactive  $\text{CO}_3^{\bullet-}$  (Reaction 24), leading to a simultaneous increase of both  $[\text{HO}^\bullet]_{\text{ss}}$  and  $[\text{CO}_3^{\bullet-}]_{\text{ss}}$  (). As a result, the overall reactivity of the system remained more or less the same (), and benzene degradation was still mostly attributable to its reaction with  $\text{SO}_4^{\bullet-}$  (**Table 6**). Prior literature reported the conversion of chloride to chlorate ( $\text{ClO}_3^-$ ) by  $\text{SO}_4^{\bullet-}$  and  $\text{HO}^\bullet$  via radical-radical chain reactions in UV/persulfate system.<sup>69</sup> However, the steady-state concentrations of  $\text{SO}_4^{\bullet-}$  and  $\text{HO}^\bullet$  were very low in ISCO persulfate system (), and the extent of radical-radical reaction and the subsequent formation of chlorate was negligible.

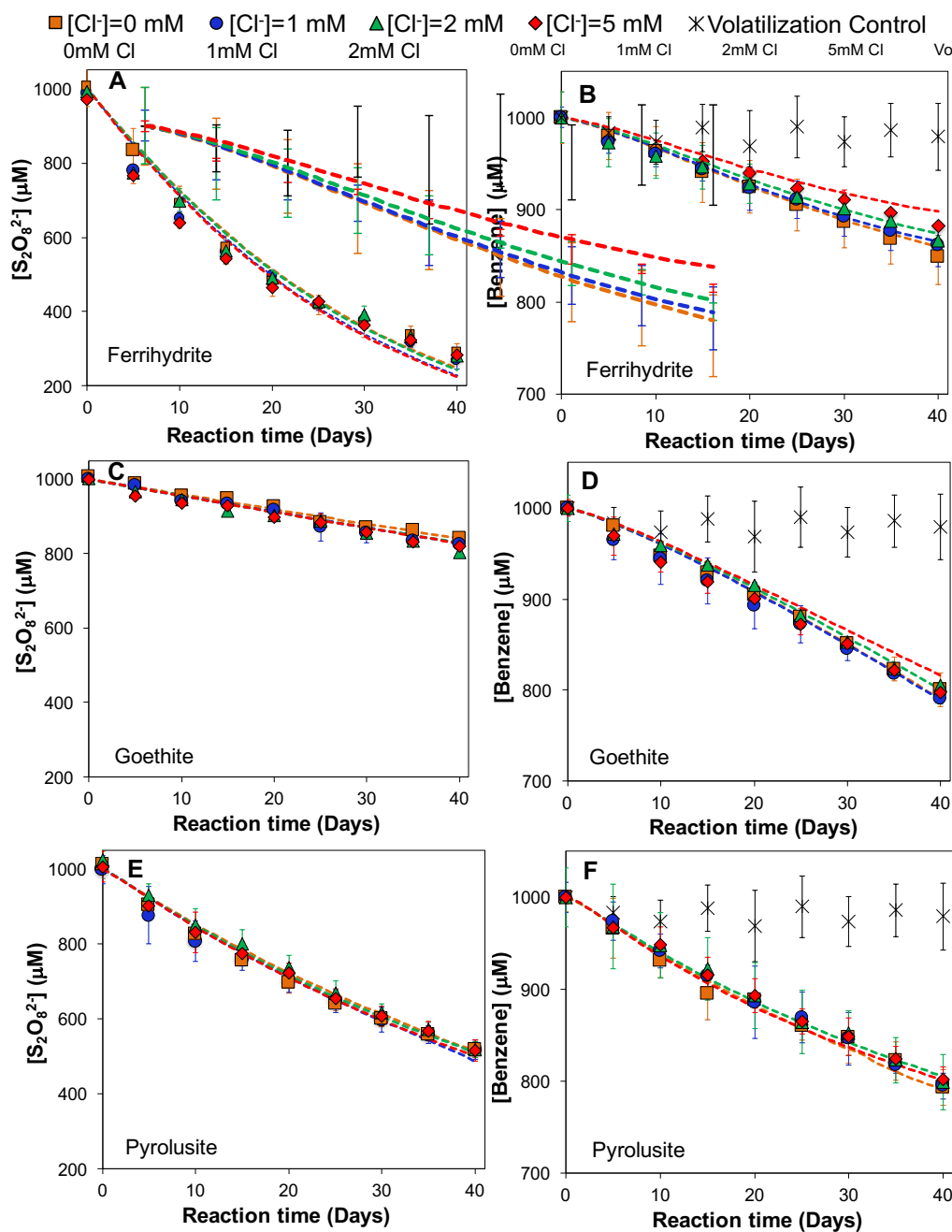


**Figure 8** Impact of chloride on the rates of persulfate decomposition and benzene degradation by three minerals. (A, C, E) Persulfate decomposition; (B, D, F) Benzene degradation.  $[S_2O_8^{2-}] = 1 \text{ mM}$ ,  $[\text{benzene}] = 1 \text{ mM}$ ,  $[\text{alkalinity}] = 1.6 \times 10^{-2} \text{ meq/L}$ ,  $\text{pH} = 8.0$ , mineral dosage = 100 g/L. Data points represent the experimental data. Dash lines represent the model-fitted values.

**Table 6** The impact of chloride on the percentile contributions of different reactive radicals to benzene degradation.\*

Reactive radical	Ferrihydrite [Cl] (mM)				Goethite [Cl] (mM)				Pyrolusite [Cl] (mM)			
	0	1	2	5	0	1	2	5	0	1	2	5
SO <sub>4</sub> <sup>•-</sup>	100%	96%	94%	91%	100%	94%	90%	85%	100%	91%	89%	88%
HO <sup>•</sup>	0%	0%	1%	2%	0%	0%	1%	1%	0%	1%	1%	2%
Cl <sup>•</sup>	0%	4%	5%	6%	0%	4%	5%	5%	0%	5%	5%	5%
CO <sub>3</sub> <sup>•-</sup>	0%	0%	1%	2%	0%	2%	4%	8%	0%	3%	5%	5%

\* Experimental condition: mineral dosage=100 g/L; alkalinity=1.6×10<sup>-2</sup> meq/L; pH=8.0.

### 2.3.3 The impact of mineral surface complexation on persulfate activation

The reactivity of Fe(III) and Mn(IV) minerals on persulfate decomposition is mainly associated with metal surface complexation, especially carbonato and hydroxo complexes. Metal carbonato complexes including  $\equiv\text{Me-OCO}_2\text{H}^0$  and  $\equiv\text{Me-OCO}_2^-$  exist at the surface of Fe(III) and Mn(IV) oxides.<sup>70-74</sup> For example, ferrihydrite possesses  $\equiv\text{Fe(III)-OCO}_2\text{H}^0$  and  $\equiv\text{Fe(III)-OCO}_2^-$  surface carbonato complexes, each of which accounts for 28% and 72% of total carbonato complexes at varying pHs, respectively. The log value of equilibrium constant for  $\equiv\text{Me-OCO}_2^-$  surface carbonato complexation reaction (denoted as  $\log\beta_1$ ) is 12.78, 12.76 and 14.15 for ferrihydrite, goethite and pyrolusite, respectively (forward and reverse reactions of the equilibria are shown in Reactions 25-28).<sup>75-77</sup> The log value of equilibrium constant for  $\equiv\text{Me-OCO}_2\text{H}^0$  surface carbonato complexation reaction (denoted as  $\log\beta_2$ ) is 20.37, 18.30 and 22.65 for ferrihydrite, goethite and pyrolusite, respectively (Reactions 29-32). The formation of metal carbonato surface complexes can decrease the surface redox reactivity, because the carboxylic groups

possess high electron density that can prevent their reactions with persulfate. Consequently, heterogeneous persulfate decomposition tends to slow down by surface carbonato complexation. This is consistent with prior observation that the formation of metal surface carbonato complexes decreased the redox reactivity on mineral surfaces.<sup>44</sup>

Furthermore, three hydroxo complexes exist at the mineral surfaces at solution pH ranging between 8 and 13:  $\equiv\text{Me}-\text{OH}_2^+$ ,  $\equiv\text{Me}-\text{OH}^0$  and  $\equiv\text{Me}-\text{O}^-$ . The equilibrium constants associated with the two steps of protonation (defined as  $\text{pK}_1$  and  $\text{pK}_2$ ) are 7.29 and 8.93 for ferrihydrite, 6.90 and 10.9 for goethite, and 0.6 and 2.6 for pyrolusite, respectively (forward and reverse reactions of the equilibria are shown in Reactions 33-40).<sup>77-79</sup> On the basis of pK values and the relevant range of groundwater pH, both  $\equiv\text{Fe(III)-OH}$  and  $\equiv\text{Fe(III)-O}^-$  hydroxo complexes are important for ferrihydrite and goethite, and only  $\equiv\text{Me}-\text{O}^-$  is relevant for pyrolusite. The deprotonated  $\equiv\text{Fe(III)-O}^-$  is likely less reactive than the protonated  $\equiv\text{Fe(III)-OH}$  with persulfate for two reasons. First, the negative charges on  $\equiv\text{Fe(III)-O}^-$  repulse the same negatively charged persulfate anion. Second,  $\equiv\text{Fe(III)-O}^-$  possesses a higher electron density due to  $-\text{O}^-$  groups, Therefore, it is less prone to withdraw additional electrons from persulfate to initiate the first step of activation.<sup>80</sup> The kinetic model fitting also showed that the rate constants of  $\equiv\text{Fe(III)-OH}$  reacting with persulfate was two times higher than those of  $\equiv\text{Fe(III)-O}^-$  (Reaction 1 vs. 2 for ferrihydrite in **Table 2**; Reaction 54 vs. 56 for goethite in **Appendix A-5**).

With an increase of alkalinity up to 10 meq/L, the model-predicted steady-state concentrations (*i.e.*, equilibrium concentrations) of hydroxo surface complexes  $\equiv\text{Me}-\text{OH}$

and  $\equiv\text{Me}-\text{O}^-$  decreased by 10%-45%, and the equilibrium concentrations of carbonato surface complexes  $\equiv\text{Fe(III)}-\text{OCO}_2\text{H}^0$  and  $\equiv\text{Fe(III)}-\text{OCO}_2^-$  increased by nearly three orders of magnitude (**Table 7**). This significant increase of unreactive carbonato surface complexation with increasing alkalinity slowed down persulfate decomposition and decreased the yield of  $\text{SO}_4^{\bullet-}$  (**Table 3**).

With an increase of pH from 8 to 12, model predictions suggested that the equilibrium concentrations of unreactive carbonato surface complexes  $\equiv\text{Me}-\text{OCO}_2\text{H}^0$  and  $\equiv\text{Me}-\text{OCO}_2^-$  decreased by several orders of magnitude, and reactive hydroxo complexes are predominant and remained relatively constant (**Table 7**). The combined effects are consistent with the observed acceleration of persulfate decomposition with increasing pH up to 12 (**Figure 6**). However, the concentrations of reactive hydroxo surface complex  $\equiv\text{Me}-\text{OH}$  decreased by 10 times from pH 12 to 13 due to hydroxo surface equilibrium (**Table 7**). This reversed change of surface reactivity is consistent with the experimentally observed decrease of persulfate decomposition from pH 12 to 13 (**Figure 6A, C and E**).

In addition, a variation in chloride levels had a negligible effect on the speciation of metal surface hydroxo or carbonato complexes (**Table 7**). The impact of chloride mainly resulted in changes of solution radical chain reactions. As  $\text{Cl}^\bullet$  was generated via chloride (Reaction 17),  $\text{HCO}_3^-$  was transformed to  $\text{CO}_3^{\bullet-}$  by  $\text{Cl}^\bullet$  (Reaction 24) instead of forming carbonato surface complexes (Reactions 25-32). These competing reactions slightly decreased the equilibrium concentrations of carbonato surface complexes, but the overall rates of persulfate decomposition and benzene degradation were not affected regardless

**Table 7** Model-predicted steady-state concentrations of surface complexes of Fe(III) and Mn(IV) minerals. \*

Ferrhydrite	[Alkalinity] (meq/L)					pH					[Chloride] (mM)				
	1.6×10 <sup>-2</sup>	2	10	8	10	12	13	0	1	2	5	0	1	2	5
[Fe(III)-OH <sup>0</sup> ] <sub>ss</sub>	5.1×10 <sup>-2</sup>	5.0×10 <sup>-2</sup>	4.4×10 <sup>-2</sup>	5.1×10 <sup>-2</sup>	5.3×10 <sup>-3</sup>	5.7×10 <sup>-5</sup>	5.7×10 <sup>-6</sup>	5.1×10 <sup>-2</sup>							
[Fe(III)-O] <sub>ss</sub>	6.0×10 <sup>-3</sup>	5.8×10 <sup>-3</sup>	5.1×10 <sup>-3</sup>	6.0×10 <sup>-3</sup>	6.2×10 <sup>-2</sup>	6.7×10 <sup>-2</sup>	6.7×10 <sup>-2</sup>	6.0×10 <sup>-3</sup>							
[Fe(III)-OHCO <sub>2</sub> <sup>0</sup> ] <sub>ss</sub>	4.3×10 <sup>-6</sup>	5.3×10 <sup>-4</sup>	2.7×10 <sup>-3</sup>	4.3×10 <sup>-6</sup>	3.0×10 <sup>-7</sup>	2.0×10 <sup>-11</sup>	1.7×10 <sup>-12</sup>	4.3×10 <sup>-6</sup>	4.2×10 <sup>-6</sup>	4.1×10 <sup>-6</sup>	4.0×10 <sup>-6</sup>	4.3×10 <sup>-6</sup>	4.2×10 <sup>-6</sup>	4.1×10 <sup>-6</sup>	4.0×10 <sup>-6</sup>
[Fe(III)-OCO <sub>2</sub> ] <sub>ss</sub>	1.1×10 <sup>-5</sup>	1.4×10 <sup>-3</sup>	6.8×10 <sup>-3</sup>	1.1×10 <sup>-5</sup>	7.7×10 <sup>-5</sup>	5.0×10 <sup>-7</sup>	4.3×10 <sup>-7</sup>	1.1×10 <sup>-5</sup>							
[Fe(II)-OH <sup>0</sup> ] <sub>ss</sub>	5.1×10 <sup>-4</sup>	4.8×10 <sup>-7</sup>	4.2×10 <sup>-4</sup>	2.1×10 <sup>-4</sup>	1.8×10 <sup>-5</sup>	1.8×10 <sup>-7</sup>	2.1×10 <sup>-8</sup>	5.1×10 <sup>-4</sup>	5.2×10 <sup>-4</sup>	5.0×10 <sup>-4</sup>	5.2×10 <sup>-4</sup>	5.1×10 <sup>-4</sup>	5.2×10 <sup>-4</sup>	5.0×10 <sup>-4</sup>	5.2×10 <sup>-4</sup>
[Fe(II)-O] <sub>ss</sub>	3.4×10 <sup>-5</sup>	3.5×10 <sup>-5</sup>	3.4×10 <sup>-5</sup>	3.7×10 <sup>-5</sup>	3.2×10 <sup>-4</sup>	5.3×10 <sup>-4</sup>	3.7×10 <sup>-4</sup>	3.4×10 <sup>-5</sup>	3.5×10 <sup>-5</sup>	3.6×10 <sup>-5</sup>	3.5×10 <sup>-5</sup>	3.4×10 <sup>-5</sup>	3.5×10 <sup>-5</sup>	3.6×10 <sup>-5</sup>	3.5×10 <sup>-5</sup>
Goethite	[Alkalinity] (meq/L)					pH					[Chloride] (mM)				
	1.6×10 <sup>-2</sup>	2	10	8	10	12	13	0	1	2	5	0	1	2	5
[Fe(III)-OH <sup>0</sup> ] <sub>ss</sub>	2.0×10 <sup>-3</sup>	1.7×10 <sup>-3</sup>	1.1×10 <sup>-3</sup>	2.0×10 <sup>-3</sup>	2.5×10 <sup>-3</sup>	5.5×10 <sup>-5</sup>	5.6×10 <sup>-6</sup>	2.0×10 <sup>-3</sup>							
[Fe(III)-O] <sub>ss</sub>	1.6×10 <sup>-5</sup>	1.4×10 <sup>-5</sup>	8.8×10 <sup>-6</sup>	1.6×10 <sup>-5</sup>	2.0×10 <sup>-3</sup>	4.4×10 <sup>-3</sup>	4.5×10 <sup>-3</sup>	1.6×10 <sup>-5</sup>							
[Fe(III)-OHCO <sub>2</sub> <sup>0</sup> ] <sub>ss</sub>	2.0×10 <sup>-8</sup>	2.3×10 <sup>-6</sup>	7.4×10 <sup>-6</sup>	2.0×10 <sup>-8</sup>	1.1×10 <sup>-10</sup>	1.6×10 <sup>-13</sup>	1.4×10 <sup>-14</sup>	2.0×10 <sup>-8</sup>	1.5×10 <sup>-8</sup>	9.3×10 <sup>-9</sup>	2.1×10 <sup>-9</sup>	2.0×10 <sup>-8</sup>	1.5×10 <sup>-8</sup>	9.3×10 <sup>-9</sup>	2.1×10 <sup>-9</sup>
[Fe(III)-OCO <sub>2</sub> ] <sub>ss</sub>	5.8×10 <sup>-6</sup>	6.6×10 <sup>-4</sup>	2.1×10 <sup>-3</sup>	5.8×10 <sup>-6</sup>	3.2×10 <sup>-6</sup>	4.7×10 <sup>-7</sup>	4.0×10 <sup>-7</sup>	5.8×10 <sup>-6</sup>	4.2×10 <sup>-6</sup>	2.7×10 <sup>-6</sup>	6.1×10 <sup>-7</sup>	5.8×10 <sup>-6</sup>	4.2×10 <sup>-6</sup>	2.7×10 <sup>-6</sup>	6.1×10 <sup>-7</sup>
[Fe(II)-OH <sup>0</sup> ] <sub>ss</sub>	2.3×10 <sup>-4</sup>	2.0×10 <sup>-4</sup>	1.7×10 <sup>-4</sup>	2.3×10 <sup>-4</sup>	1.7×10 <sup>-4</sup>	6.4×10 <sup>-6</sup>	6.0×10 <sup>-7</sup>	2.3×10 <sup>-4</sup>	2.5×10 <sup>-4</sup>	2.5×10 <sup>-4</sup>	2.7×10 <sup>-4</sup>	2.3×10 <sup>-4</sup>	2.5×10 <sup>-4</sup>	2.5×10 <sup>-4</sup>	2.7×10 <sup>-4</sup>
[Fe(II)-O] <sub>ss</sub>	1.3×10 <sup>-6</sup>	1.1×10 <sup>-6</sup>	6.7×10 <sup>-7</sup>	1.3×10 <sup>-6</sup>	1.3×10 <sup>-4</sup>	3.5×10 <sup>-4</sup>	3.4×10 <sup>-4</sup>	1.3×10 <sup>-6</sup>							
Pyrolusite	[Alkalinity] (meq/L)					pH					[Chloride] (mM)				
	1.6×10 <sup>-2</sup>	2	10	8	10	12	13	0	1	2	5	0	1	2	5
[Mn(IV)-OH <sup>0</sup> ] <sub>ss</sub>	1.9×10 <sup>-10</sup>	1.9×10 <sup>-10</sup>	1.9×10 <sup>-10</sup>	1.6×10 <sup>-10</sup>	1.5×10 <sup>-12</sup>	1.5×10 <sup>-14</sup>	1.5×10 <sup>-15</sup>	1.9×10 <sup>-10</sup>	1.8×10 <sup>-10</sup>	1.8×10 <sup>-10</sup>	1.8×10 <sup>-10</sup>	1.9×10 <sup>-10</sup>	1.8×10 <sup>-10</sup>	1.8×10 <sup>-10</sup>	1.8×10 <sup>-10</sup>
[Mn(IV)-O] <sub>ss</sub>	4.6×10 <sup>-5</sup>	4.6×10 <sup>-5</sup>	4.5×10 <sup>-5</sup>	4.0×10 <sup>-5</sup>	3.8×10 <sup>-5</sup>	3.9×10 <sup>-5</sup>	3.8×10 <sup>-5</sup>	4.6×10 <sup>-5</sup>	4.5×10 <sup>-5</sup>						
[Mn(IV)-OHCO <sub>2</sub> <sup>0</sup> ] <sub>ss</sub>	6.4×10 <sup>-11</sup>	8.2×10 <sup>-9</sup>	4.1×10 <sup>-8</sup>	5.6×10 <sup>-11</sup>	2.3×10 <sup>-14</sup>	1.0×10 <sup>-18</sup>	8.3×10 <sup>-12</sup>	6.4×10 <sup>-11</sup>	3.5×10 <sup>-11</sup>	2.2×10 <sup>-11</sup>	1.4×10 <sup>-12</sup>	6.4×10 <sup>-11</sup>	3.5×10 <sup>-11</sup>	2.2×10 <sup>-11</sup>	1.4×10 <sup>-12</sup>
[Mn(IV)-OCO <sub>2</sub> ] <sub>ss</sub>	2.0×10 <sup>-11</sup>	2.6×10 <sup>-9</sup>	1.3×10 <sup>-8</sup>	1.8×10 <sup>-11</sup>	7.1×10 <sup>-13</sup>	3.2×10 <sup>-15</sup>	2.6×10 <sup>-15</sup>	2.0×10 <sup>-11</sup>	1.1×10 <sup>-11</sup>	7.1×10 <sup>-12</sup>	4.4×10 <sup>-13</sup>	2.0×10 <sup>-11</sup>	1.1×10 <sup>-11</sup>	7.1×10 <sup>-12</sup>	4.4×10 <sup>-13</sup>
[Mn(III)-O] <sub>ss</sub>	1.3×10 <sup>-5</sup>	1.2×10 <sup>-5</sup>	1.2×10 <sup>-5</sup>	1.9×10 <sup>-5</sup>	2.1×10 <sup>-5</sup>	2.1×10 <sup>-5</sup>	2.1×10 <sup>-5</sup>	1.3×10 <sup>-5</sup>	1.4×10 <sup>-5</sup>						

\* When alkalinity varied between 1.6×10<sup>-2</sup> and 10 meq/L: [Cl<sup>-</sup>]=0 mM, pH=8.0; when pH varied between 8 and 13: [Cl<sup>-</sup>]=0 mM,

[alkalinity]= 1.6×10<sup>-2</sup> meq/L; when chloride concentration varied between 0 and 5 mM: [alkalinity]=1.6×10<sup>-2</sup> meq/L, pH=8.0

of the chloride level (**Figure 8**).

In accord with these observations, the fraction of carbonato surface complexes, denoted as  $\alpha$ , was calculated as:

$$\alpha = \frac{[\equiv\text{Me}-\text{OCO}_2\text{H}^0]_{\text{SS}} + [\equiv\text{Me}-\text{OCO}_2^-]_{\text{SS}}}{[\equiv\text{Me}-\text{OH}_2^+]_{\text{SS}} + [\equiv\text{Me}-\text{OH}^0]_{\text{SS}} + [\equiv\text{Me}-\text{O}^-]_{\text{SS}} + [\equiv\text{Me}-\text{OCO}_2\text{H}^0]_{\text{SS}} + [\equiv\text{Me}-\text{OCO}_2^-]_{\text{SS}}} = \frac{K_1\beta_1[\text{CO}_3^{2-}][\text{H}^+]^2 + K_1\beta_2[\text{CO}_3^{2-}][\text{H}^+]^3}{[\text{H}^+]^2 + K_1[\text{H}^+] + K_1K_2 + K_1\beta_1[\text{CO}_3^{2-}][\text{H}^+]^2 + K_1\beta_2[\text{CO}_3^{2-}][\text{H}^+]^3} \quad (2)$$

$[\equiv\text{Me}-\text{OCO}_2\text{H}^0]_{\text{SS}}$ ,  $[\equiv\text{Me}-\text{OCO}_2^-]_{\text{SS}}$ ,  $[\equiv\text{Me}-\text{OH}_2^+]_{\text{SS}}$ ,  $[\equiv\text{Me}-\text{OH}]_{\text{SS}}$  and  $[\equiv\text{Me}-\text{O}^-]_{\text{SS}}$  are the equilibrium concentrations of the surface carbonato complex with bicarbonate, carbonate, and protonated and deprotonated hydroxo groups, respectively.  $K_i$  and  $\beta_i$  are surface hydroxo and carbonato complexation equilibrium constants.

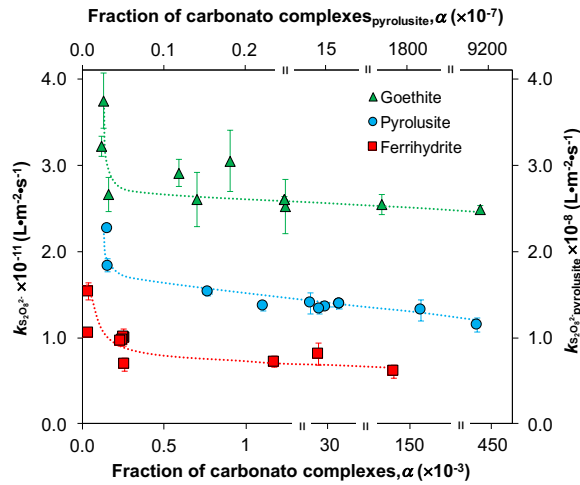


**Figure 9** The correlation between the rate of persulfate decomposition and the fraction of carbonato complex on Fe(III) and Mn(IV) mineral (data for pyrolusite shown as secondary x- and y-axes).  $[\text{S}_2\text{O}_8^{2-}] = 1 \text{ mM}$ ,  $[\text{benzene}] = 1 \text{ mM}$ , mineral dosage = 100 g/L, pH = 8.0, ionic strength = 10 mM. Data points represent the experimental results. Dash lines are the trend lines.

The experimentally observed rate of persulfate decomposition was associated with the model-predicted fraction of unreactive carbonato complexes in an inversely exponential relationship (**Figure 9**). The reactivity of minerals with persulfate decomposition plummeted by as much as 40% when a small fraction of mineral surface sites was occupied by carbonato complexes. This initial sharp decrease of reactivity was associated with a high sensitivity of surface speciation to carbonato complexation at pHs higher than 10. Under this chemical condition, the equilibrium concentration of reactive  $\equiv\text{Me-OH}$  reached a minimum, and a small extent of carbonato complex formation drastically decreased the surface reactivity. In contrast, as the fraction of carbonato complexes increased (this corresponded to conditions with solution pHs lower than 10),  $\equiv\text{Fe(III)-OH}$  and  $\equiv\text{Mn(IV)-O}^-$  remained as the predominant reactive surface complexes. Consequently, the redox reactivity of mineral surface became less sensitive to carbonato complexation and exhibited a small variation (**Figure 9**).

#### ***2.3.4 Product distribution of benzene oxidation via heterogeneous persulfate activation***

Two major oxidation products were simultaneously generated from benzene degradation, *i.e.*, phenol and a six-carbon aldehyde ring-cleavage product. The correlation between the yields of oxidation products and the branching ratio of  $\text{SO}_4^{\cdot-}$  reacting with benzene exhibited a positively exponential relationship (**Figure 10A-B**). On the contrary, an inverse relationship existed between the yield of oxidation products and the branching ratio of  $\text{HO}^\bullet$  or  $\text{CO}_3^{\cdot-}$  (**Figure 10C-F**). These results indicated that  $\text{SO}_4^{\cdot-}$  had a distinct oxidation pathway on benzene degradation compared to that of  $\text{HO}^\bullet$  or  $\text{CO}_3^{\cdot-}$ . Prior studies

reported the distinct oxidation mechanisms for different radicals. For example,  $\text{SO}_4^{\cdot-}$  reacted with benzene via direct electron transfer,  $\text{HO}^{\cdot}$  reacted with benzene via OH addition, and  $\text{CO}_3^{\cdot-}$  reacted via hydrogen abstraction.<sup>42,43,81-84</sup> The data suggested that  $\text{SO}_4^{\cdot-}$ -driven oxidation likely favored pathways that involve fewer steps of hydroxylation that accumulated phenol and aldehyde products, whereas  $\text{HO}^{\cdot}$  or  $\text{CO}_3^{\cdot-}$  oxidation promoted multiple steps of sequential hydroxylation of benzene and generated low-carbon-chain products. For example, a further oxidation of phenol can produce benzoquinone and hydroquinone intermediates.<sup>85-86</sup> The toxicity implications of the  $\text{SO}_4^{\cdot-}$ -driven oxidation products will be examined in the future.

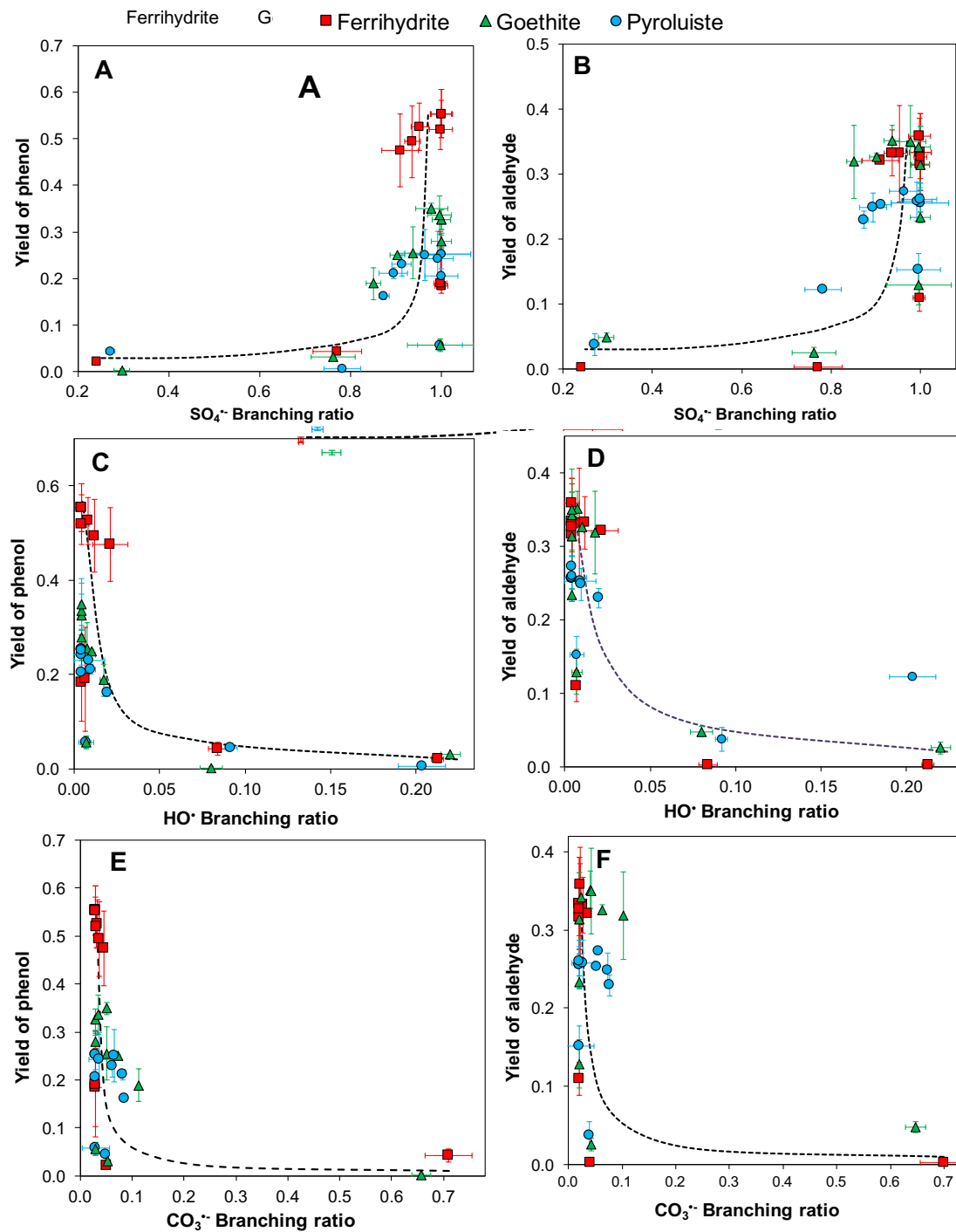


**Figure 10.** Correlation between the yields of benzene oxidation products and branching ratio of  $\text{SO}_4^{\bullet-}$ ,  $\text{HO}^{\bullet}$  and  $\text{CO}_3^{\bullet-}$  reacting with benzene. (A,C,E) phenol; (B,D,F) aldehyde. Data points are experimental observations; dash lines are the trend lines.

## **2.4 Environmental Implications**

One salient finding from this study is that persulfate-based ISCO remediation efforts need special attention to native alkalinity and pH levels in contaminated groundwater, because these chemical parameters indicate the in situ redox reactivity in the aquifer and the effectiveness on persulfate activation. Alkalinity and pH mainly impact the surface complexation of Fe(III)- and Mn(IV)-containing aquifer minerals. Higher alkalinity favors the formation of unreactive surface carbonato complexes, which tends to inhibit persulfate activation, while higher pH favors the formation of reactive surface hydroxo complexes and accelerates remediation efforts. Chloride in groundwater is found to impact solution radical distributions, but it poses a negligible effect on persulfate decomposition and contaminant removal. This indicates that persulfate ISCO is applicable to groundwater with elevated salinity. Results also suggest that aquifers with abundant goethite can increase the persistence of persulfate and increase remediation efficiency. Although aquifer minerals with higher abundance of ferrihydrite and pyrolusite can accelerate persulfate decomposition, these minerals tend to have lower stoichiometric efficiency of radical yields.

## **2.5 Acknowledgement**

This research was partially supported by grants to W.L. from the National Science Foundation Graduate Research Fellowship and IGERT Water Sense Fellowship and to H.L. from the UC Riverside Faculty Initiation Research Fund.

## Reference:

- 
- <sup>1</sup> Giordano, M. Global groundwater: Issues and solutions. *Annual Review of Environment and Resources*. **2009**, 34, 153-178.
  - <sup>2</sup> Foster, S. S. D.; Chilton, P. J. Groundwater: the processes and global significance of aquifer degradation. *Philosophical Transactions of the Royal Society B: Biological Sciences*. **2003**, 358 (1440), 1957-1972.
  - <sup>3</sup> Miller, C. M.; Valentine, R. L. Hydrogen peroxide decomposition and quinoline degradation in the presence of aquifer material. *Water Research*. **1995**, 29 (10), 2353-2359.
  - <sup>4</sup> Fay, R. M.; Mumtaz, M. M. Development of a priority list of chemical mixtures occurring at 1188 hazardous waste sites, using the HazDat database. *Food and Chemical Toxicology*. **1996**, 34 (11), 1163-1165.
  - <sup>5</sup> Uzochukwu, G.; Schimmel, K.; Chang, S.Y.; Kabadi, V.; Luster-Teasley, S.; Reddy, G.; Nzewi, E. Proceedings of the 2007 national conference on environmental science and technology. Springer-Verlag: New York, 2009.
  - <sup>6</sup> Maltoni, C.; Conti, B.; Cotti, G. Benzene: A multipotential carcinogen. results of long-term bioassays performed at the bologna institute of oncology. *American Journal of Industrial Medicine*. **1983**, 4 (5), 589-630.
  - <sup>7</sup> McKinney, D. C.; Lin, M. D. Pump-and-treat ground-water remediation system optimization. *Journal of Water Resources Planning and Management*. **1996**, 122 (2), 128-136.
  - <sup>8</sup> Yoon, J. H.; Shoemaker, C. A. Comparison of optimization methods for ground-water bioremediation. *Journal of Water Resources Planning and Management*. **1999**, 125 (1), 54-63.
  - <sup>9</sup> Krembs, F. J.; Siegrist, R. L.; Crimi, M. L.; Furrer, R. F.; Petri, B. G. ISCO for groundwater remediation: analysis of field applications and performance. *Groundwater Monitoring & Remediation*. **2010**, 30 (4), 42-53.
  - <sup>10</sup> Hyman, M.; Dupont, R. R. *Groundwater and soil remediation: process design and cost estimating of proven technologies*. ASCE Press, 2001.
  - <sup>11</sup> Siegrist, R. L.; Crimi, M.; Simpkin, T. J. In situ chemical oxidation: technology, description and status. In situ chemical oxidation for groundwater remediation; Springer Media, LLC: New York City, **2011**; Chapter 1.

- 
- <sup>12</sup> Liang, C.; Bruell, C. J.; Marley, M. C.; Sperry, K. L. Persulfate oxidation for in situ remediation of TCE. I. Activated by ferrous ion with and without a persulfate–thiosulfate redox couple. *Chemosphere*. **2004**, *55* (9), 1213-1223.
- <sup>13</sup> Yang, Q.; Choi, H.; Chen, Y.; Dionysiou, D. D. Heterogeneous activation of peroxymonosulfate by supported cobalt catalysts for the degradation of 2, 4-dichlorophenol in water: the effect of support, cobalt precursor, and UV radiation. *Applied Catalysis B: Environmental*. **2008**, *77* (3), 300-307.
- <sup>14</sup> Furman, O. S.; Teel, A. L.; Watts, R. J. Mechanism of base activation of persulfate. *Environmental Science & Technology*. **2010**. *44* (16), 6423-6428.
- <sup>15</sup> Interstate Technology and Regulatory Council (ITRC). Technical and Regulatory Guidance for In Situ Chemical Oxidation of Contaminated Soil and Groundwater, 2nd ed.; **2005**; <http://www.itrcweb.org>.
- <sup>16</sup> Huling, Scott G.; Pivetz, B. E. In-situ chemical oxidation. No. EPA/600/R-06/072. *Environmental Protection Agency Washington DC Office of Water*. **2006**.
- <sup>17</sup> Liang, C. J.; Bruell, C. J.; Marley, M. C.; Sperry, K. L. Thermally activated persulfate oxidation of trichloroethylene (TCE) and 1, 1, 1-trichloroethane (TCA) in aqueous systems and soil slurries. *Soil and Sediment Contamination: An International Journal*. **2003**, *12* (2), 207-228.
- <sup>18</sup> Sra, K. S.; Thomson, N. R.; Barker, J. F. Persistence of persulfate in uncontaminated aquifer materials. *Environ. Sci. Technol.* **2010**, *44* (8), 3098–3104.
- <sup>19</sup> Block, P. A.; Brown, R. A.; Robinson, D. Novel activation technologies for sodium persulfate in situ chemical oxidation. In proceedings of the fourth international conference on the remediation of chlorinated and recalcitrant compounds. (pp. 24-27). Columbus, OH: Battelle Press, **2004**.
- <sup>20</sup> Liu, H.; Bruton, T. A.; Li, W.; Van Buren, J.; Prasse, C.; Doyle, F. M.; Sedlak, D. L. Oxidation of benzene by persulfate in the presence of Fe(III)-and Mn(IV)-containing oxides: stoichiometric efficiency and transformation products. *Environmental Science & Technology*. **2016**, *50* (2), 890–898.
- <sup>21</sup> Liu, H.; Bruton, T. A.; Doyle, F. M.; Sedlak, D. L. In situ chemical oxidation of contaminated groundwater by persulfate: decomposition by Fe (III)-and Mn (IV)-containing oxides and aquifer materials. *Environmental Science & Technology*. **2014**, *48* (17), 10330-10336.
- <sup>22</sup> Yang, Y.; Pignatello, J. J.; Ma, J.; Mitch, W. A. Comparison of halide impacts on the efficiency of contaminant degradation by sulfate and hydroxyl radical-based advanced

- 
- oxidation processes (AOPs). *Environmental Science & Technology*. **2014**, *48* 2344-2351.
- <sup>23</sup> Minisci, F.; Citterio, A.; Giordano, C. Electron-transfer processes: peroxydisulfate, a useful and versatile reagent in organic chemistry. *Accounts of Chemical Research*. **1983**, *16*, 27-32.
- <sup>24</sup> Neta, P.; Madhavan, V.; Zemel, H.; Fessenden, R. W. Rate constants and mechanism of reaction of sulfate radical anion with aromatic compounds. *Journal of the American Chemical Society*. **1977**, *99*, 163-164.
- <sup>25</sup> Valentine, R. L.; Wang, H.C. A. Iron oxide surface catalyzed oxidation of quinoline by hydrogen peroxide. *Journal of environmental engineering*. **1998**, *124* (1), 31-38.
- <sup>26</sup> Petri, B. G.; Watts, R. J.; Teel, A. L.; Huling, S. G.; Brown, R. A. Fundamentals of ISCO using hydrogen peroxide. *In Situ Chemical Oxidation for Groundwater Remediation*. Springer New York, **2011**.
- <sup>27</sup> Urynowicz, M. A.; West, O. R.; Crimi, M. L.; Lowe, K. S. *Principles and practices of in situ chemical oxidation using permanganate*. Vol. 505. Columbus, OH: Battelle Press, **2001**.
- <sup>28</sup> Lee, E. S.; Seol, Y.; Fang, Y. C.; Schwartz, F. W. Destruction efficiencies and dynamics of reaction fronts associated with the permanganate oxidation of trichloroethylene. *Environmental Science & Technology*. **2003**, *37* (11), 2540-2546.
- <sup>29</sup> Waldemer, R. H.; Tratnyek, P. G. Kinetics of contaminant degradation by permanganate. *Environmental Science & Technology*. **2006**, *40* (3), 1055-1061.
- <sup>30</sup> Deutsch, W. J.; Siegel, R. *Groundwater geochemistry: fundamentals and applications to contamination*; CRC press: New York, 1997.
- <sup>31</sup> Furman, O. S.; Teel, A. L.; Ahmad, M.; Merker, M. C.; Watts, R. J. Effect of basicity on persulfate reactivity. *Journal of Environmental Engineering*. **2010**, *137* (4), 241-247.
- <sup>32</sup> Lin, Y. T.; Liang, C.; Chen, J. H. Feasibility study of ultraviolet activated persulfate oxidation of phenol. *Chemosphere*. **2011**, *82* (8), 1168-1172.
- <sup>33</sup> Zhao, D.; Liao, X.; Yan, X.; Huling, S. G.; Chai, T.; Tao, H. Effect and mechanism of persulfate activated by different methods for PAHs removal in soil. *Journal of Hazardous Materials*. **2013**. *254*, 228-235.
- <sup>34</sup> Lee, Y.; Lo, S.; Kuo, J.; Hsieh, C. Decomposition of perfluorooctanoic acid by microwave-activated persulfate: Effects of temperature, pH, and chloride ions. *Frontiers of Environmental Science & Engineering*. **2012**, *6* (1), 17-25.

- 
- <sup>35</sup> Liang, C.; Wang, Z. S.; Mohanty, N. Influences of carbonate and chloride ions on persulfate oxidation of trichloroethylene at 20 °C. *Science of the Total Environment*. **2006**, *370* (2), 271-277.
- <sup>36</sup> Yuan, R.; Ramjaun, S. N.; Wang, Z.; Liu, J. Effects of chloride ion on degradation of Acid Orange 7 by sulfate radical-based advanced oxidation process: implications for formation of chlorinated aromatic compounds. *Journal of Hazardous Materials*. **2011**, *196*, 173-179.
- <sup>37</sup> Fang, G. D.; Dionysiou, D. D.; Wang, Y.; Al-Abed, S. R.; Zhou, D. M. Sulfate radical-based degradation of polychlorinated biphenyls: effects of chloride ion and reaction kinetics. *Journal of Hazardous Materials*. **2012**, *227*, 394-401.
- <sup>38</sup> Das, T. N. Reactivity and role of  $\text{SO}_5^-$  radical in aqueous medium chain oxidation of sulfite to sulfate and atmospheric sulfuric acid generation. *The Journal of Physical Chemistry A*. **2001**, *105* (40), 9142-9155.
- <sup>39</sup> Dogliotti, L.; Hayon, E. Flash photolysis of persulfate ions in aqueous solutions. The sulfate and ozonide radical anions. *The Journal of Physical Chemistry*. **1967**, *71* (8), 2511-2516.
- <sup>40</sup> Buxton, G.V.; Greenstock, C.; Hellman, W.P.; Ross, A.B. Critical review of rate constants for reactions of hydrated electrons, hydrogen atoms, and hydroxyl radicals ( $\cdot\text{OH}/\cdot\text{O}^-$ ) in aqueous solution. *Journal of Physical and Chemical Reference Data*. **1988**, *17* (2), 513-886.
- <sup>41</sup> Kiwi, J.; Lopez, A.; Nadtochenko, V. Mechanism and kinetics of the OH radical intervention during Fenton oxidation in the presence of a significant amount of radical scavenger (Cl<sup>-</sup>). *Environmental Science & Technology*. **2000**, *34* (11), 2162-2168.
- <sup>42</sup> Grebel, J. E.; Pignatello, J. J.; Mitch, W. A. Effect of halide ions and carbonates on organic contaminant degradation by hydroxyl radical-based advanced oxidation processes in saline waters. *Environmental Science & Technology*. **2010**, *44* (17), 6822-6828.
- <sup>43</sup> Chen, S. N.; Hoffman, M. Z.; Parsons Jr. G. H. Reactivity of the carbonate radical toward aromatic compounds in aqueous solution. *The Journal of Physical Chemistry*. **1975**, *79* (18), 1911-1912.
- <sup>44</sup> Liu, H.; Korshin, G. V.; Ferguson, J. F. Investigation of the kinetics and mechanisms of the oxidation of cerussite and hydrocerussite by chlorine. *Environmental Science & Technology*. **2008**, *42* (9), 3241-3247.
- <sup>45</sup> Teel, A. L.; Ahmad, M.; Watts, R. J. Persulfate activation by naturally occurring trace minerals. *Journal of Hazardous Materials*. **2011**, *196*, 153-159.

- 
- <sup>46</sup> Do, S. H.; Kwon, Y. J.; Kong, S. H. Effect of metal oxides on the reactivity of persulfate/Fe (II) in the remediation of diesel-contaminated soil and sand. *Journal of Hazardous Materials*. **2010**, 182 (1), 933-936.
- <sup>47</sup> Teel, A. L.; Finn, D. D.; Schmidt, J. T.; Cutler, L. M.; Watts, R. J. Rates of trace mineral-catalyzed decomposition of hydrogen peroxide. *Journal of Environmental Engineering*. **2007**, 133 (8), 853-858.
- <sup>48</sup> Schwertmann, U.; Cambier, P.; Murad, E. Properties of goethite of varying crystallinity. *Clays and Clay Minerals*. **1985**, 33 (5), 369-378.
- <sup>49</sup> Liang, C.; Huang, C. F.; Mohanty, N.; Kurakalva, R. M. A rapid spectrophotometric determination of persulfate anion in ISCO. *Chemosphere*. **2008**, 73 (9), 1540-1543.
- <sup>50</sup> Standard Methods for the Examination of Water and Wastewater. 14th Edition. Method 403. **1975**, p278.
- <sup>51</sup> Lanni, J. C., Kintecus, Windows version 4.55. www.kintecus.com. **2012**.
- <sup>52</sup> Pham, A. L. T.; Doyle, F. M.; Sedlak, D. L. Kinetics and efficiency of H<sub>2</sub>O<sub>2</sub> activation by iron-containing minerals and aquifer materials. *Water Research*. **2012**, 46 (19), 6454-6462.
- <sup>53</sup> Malati, M. A. Solid state properties of manganese oxides. *Chemistry & Industry*. **1971**, (17), 446.
- <sup>54</sup> Hasegawa, S.; Yasuda, K.; Mase, T.; Kawaguchi, T. Surface active sites for dehydrogenation reaction of isopropanol on manganese dioxide. *Journal of Catalysis*. **1977**, 46 (2), 125-131.
- <sup>55</sup> Kanungo, S. B. Physicochemical properties of MnO<sub>2</sub> and MnO<sub>2</sub>CuO and their relationship with the catalytic activity for H<sub>2</sub>O<sub>2</sub> decomposition and CO oxidation. *Journal of Catalysis*. **1979**, 58 (3), 419-435.
- <sup>56</sup> Pham, A. L. T.; Doyle, F. M.; Sedlak, D. L. Inhibitory effect of dissolved silica on H<sub>2</sub>O<sub>2</sub> decomposition by iron (III) and manganese (IV) oxides: implications for H<sub>2</sub>O<sub>2</sub>-based in situ chemical oxidation. *Environmental Science & Technology*. **2011**, 46 (2), 1055-1062.
- <sup>57</sup> Lin, S. S.; Gurol, M. D. Catalytic decomposition of hydrogen peroxide on iron oxide: kinetics, mechanism, and implications. *Environmental Science & Technology*. **1998**, 32 (10), 1417-1423.
- <sup>58</sup> Neta, P.; Madhavan, V.; Zemel, H.; Fessenden, R. W. Rate constants and mechanism of reaction of sulfate radical anion with aromatic compounds. *Journal of the American Chemical Society*. **1977**, 99 (1), 163-164.

- 
- <sup>59</sup> Jiang, P. Y.; Katsumura, Y.; Domae, M.; Ishikawa, K.; Nagaishi, R.; Ishigure, K.; Yoshida, Y. Pulse radiolysis study of concentrated phosphoric acid solutions. *Journal of the Chemical Society. Faraday Transactions*. **1992**, 88 (22), 3319-3322.
- <sup>60</sup> Herrmann, H.; Reese, A.; Zellner, R. Time-resolved UV/VIS diode-array absorption spectroscopy of  $\text{SO}_x^-$  ( $x=3, 4, 5$ ) radical anions in aqueous solution. *Journal of Molecular Structure*. **1995**, 348, 183-186.
- <sup>61</sup> Peyton, G. R. The free-radical chemistry of persulfate-based total organic carbon analyzers. *Marine Chemistry*. **1993**, 41 (1-3), 91-103.
- <sup>62</sup> McElroy, W. J. A laser photolysis study of the reaction of  $\text{SO}_4^{\bullet-}$  with  $\text{Cl}^-$  and the subsequent decay of  $\text{Cl}_2^{\bullet-}$  in aqueous solution. *Journal of Physical Chemistry*. **1990**, 94 (6), 2435-2441.
- <sup>63</sup> Jayson, G.; Parsons, B.; Swallow, A. J. Some simple, highly reactive, inorganic chlorine derivatives in aqueous solution. Their formation using pulses of radiation and their role in the mechanism of the Fricke dosimeter. *Journal of the Chemical Society. Faraday Transaction 1: Physical Chemistry in Condensed Phases*. **1973**, (69), 1597- 1607.
- <sup>64</sup> Klaining, U. K.; Wolff, T. Laser flash photolysis of  $\text{HClO}$ ,  $\text{ClO}^-$ ,  $\text{HBrO}$  and  $\text{BrO}^-$  in aqueous solutions. *Berichte der Bunsen-Gesellschaft fur Physikalische Chemmie*. **1985**, 89, 243-245.
- <sup>65</sup> Jayson, G.; Parsons, B.; Swallow, A. J. Some simple, highly reactive, inorganic chlorine derivatives in aqueous solution. Their formation using pulses of radiation and their role in the mechanism of the Fricke dosimeter. *Journal of the Chemical Society. Faraday Transaction 1: Physical Chemistry in Condensed Phases*. **1973**, (69), 1597- 1607.
- <sup>66</sup> Mertens, R.; von Sonntag, C. Photolysis ( $\lambda= 354$  nm) of tetrachloroethene in aqueous solutions. *Journal of Photochemistry and Photobiology A: Chemistry*. **1995**, 85, (1), 1-9.
- <sup>67</sup> Chen, S. N.; Hoffman, M. Z.; Parsons Jr. G. H. Reactivity of the carbonate radical toward aromatic compounds in aqueous solution. *The Journal of Physical Chemistry*. **1975**, 79 (18), 1911-1912.
- <sup>68</sup> NIST Standard Reference Database 40: NDRL/NIST Solutions Kinetics Database V. 3.0, Gaithersburg, MD.
- <sup>69</sup> Qian, Y.; Guo, X.; Zhang, Y.; Peng, Y.; Sun, P.; Huang, C. H.; Niu, J; Zhou, X; Crittenden, J. C. Perfluorooctanoic Acid Degradation Using UV–Persulfate Process: Modeling of the Degradation and Chlorate Formation. *Environmental Science & Technology*. **2015**, 50 (2), 772-781.

- 
- <sup>70</sup> Van Cappellen, P.; Charlet, L.; Stumm, W.; Wersin, P. A surface complexation model of the carbonate mineral-aqueous solution interface. *Geochimica et Cosmochimica Acta*. **1993**, *57* (15), 3505-3518.
- <sup>71</sup> Zachara, J. M.; Girvin, D. C.; Schmidt, R. L.; Resch, C. T. Chromate adsorption on amorphous iron oxyhydroxide in the presence of major groundwater ions. *Environmental Science & Technology*. **1987**, *21* (6), 589-594.
- <sup>72</sup> Russell, J. D.; Paterson, E.; Fraser, A. R.; Farmer, V. C. Adsorption of carbon dioxide on goethite ( $\alpha$ -FeOOH) surfaces, and its implications for anion adsorption. *Journal of the Chemical Society, Faraday Transactions 1: Physical Chemistry in Condensed Phases*. **1975**, *71*, 1623-1630.
- <sup>73</sup> Harrison, J. B.; Berkheiser, V. E. Anion interactions with freshly prepared hydrous iron oxides. *Clays Clay Miner*. **1982**, *30* (2), 97-102.
- <sup>74</sup> van Geen, A.; Robertson, A. P.; Leckie, J. O. Complexation of carbonate species at the goethite surface: Implications for adsorption of metal ions in natural waters. *Geochimica et Cosmochimica Acta*. **1994**, *58* (9), 2073-2086.
- <sup>75</sup> Appelo, C. A. J.; Van der Weiden, M. J. J.; Tournassat, C.; Charlet, L. Surface complexation of ferrous iron and carbonate on ferrihydrite and the mobilization of arsenic. *Environmental Science & Technology*. **2002**, *36* (14), 3096-3103.
- <sup>76</sup> Pokrovsky, O. S.; Schott, J. Surface chemistry and dissolution kinetics of divalent metal carbonates. *Environmental Science & Technology*. **2002**, *36* (3), 426-432.
- <sup>77</sup> Villalobos, M.; Leckie, J. O. Surface complexation modeling and FTIR study of carbonate adsorption to goethite. *Journal of Colloid and Interface Science*. **2001**, *235* (1), 15-32.
- <sup>78</sup> Dzombak, D. A.; Morel, F. M. Surface complexation modeling: hydrous ferric oxide. 1990. John Wiley & Sons.
- <sup>79</sup> Wang, Z.; Lee, S. W.; Catalano, J. G.; Lezama-Pacheco, J. S.; Bargar, J. R.; Tebo, B. M.; Giammar, D. E. Adsorption of uranium (VI) to manganese oxides: X-ray absorption spectroscopy and surface complexation modeling. *Environmental Science & Technology*. **2012**, *47* (2), 850-858.
- <sup>80</sup> Arena, F.; Gatti, G.; Martra, G.; Coluccia, S.; Stievano, L.; Spadaro, L.; Famulari, P.; Parmaliana, A. Structure and reactivity in the selective oxidation of methane to formaldehyde of low-loaded FeOx/SiO<sub>2</sub> catalysts. *Journal of Catalysis*. **2005**, *231* (2), 365-380.

- 
- <sup>81</sup> Anipsitakis, G. P.; Dionysiou, D. D.; Gonzalez, M. A. Cobalt-mediated activation of peroxymonosulfate and sulfate radical attack on phenolic compounds. Implications of chloride ions. *Environmental Science & Technology*. **2006**, *40*, 1000-1007.
- <sup>82</sup> Norman, R. O. C.; Storey, P. M.; West, P. R. Electron spin resonance studies. Part XXV. Reactions of the sulphate radical anion with organic compounds. *Journal of the Chemical Society. B*. **1970**, 1087-1095.
- <sup>83</sup> Huie, R. E.; Shoute, L. C. T.; Neta, P. Temperature dependence of the rate constants for reactions of the carbonate radical with organic and inorganic reductants. *International Journal of Chemical Kinetics*. **1991**, *23* (6), 541-552.
- <sup>84</sup> Augusto, O.; Bonini, M. G.; Amanso, A. M.; Linares, E.; Santos, C. C.; De Menezes, S. L. Nitrogen dioxide and carbonate radical anion: two emerging radicals in biology. *Free Radical Biology and Medicine*. **2002**, *32* (9), 841-859.
- <sup>85</sup> Lu, M. C.; Chen, J. N.; Chang, C. P. Effect of inorganic ions on the oxidation of dichlorvos insecticide with Fenton's reagent. *Chemosphere*. **1997**, *35* (10), 2285-2293.
- <sup>86</sup> Karich, A.; Kluge, M.; Ullrich, R.; Hofrichter, M. Benzene oxygenation and oxidation by the peroxygenase of *Agroclybe aegerita*. *AMB Express*. **2013**, *3* (5), 10-1186.

## Chapter 3

# **Persulfate-based UV/AOP for Potable Water Reuse: Impact of Chloramine, Chloride, pH, and Oxygen Levels on 1,4-dioxane Removal by UV/Persulfate**

*Submitted to Environmental Science & Technology*

Li, Wei, Samuel Patton, Kenneth P. Ishida, Jamie Gleason, Stephen P. Mezyk, Guadalupe Lara, Alex Numa and Haizhou Liu " Simultaneous UV Photolysis of Chloramine and Persulfate on 1,4-dioxane Removal in Reverse Osmosis Permeate for Potable Reuse." Submitted to Environmental science & Technology

### 3.1 Introduction

Potable water reuse provides a viable solution to water scarcity by treating municipal wastewater.<sup>1,2</sup> UV-based advanced oxidation processes (UV/AOPs) have become an integral part of the treatment train to degrade trace organic contaminants.<sup>3-9</sup> For example, 1,4-dioxane (1,4-D), a solvent widely used in production of adhesives, dyes, textiles and cosmetics, has been widely detected in wastewater and classified as a potential human carcinogen.<sup>10-13</sup> Because small and neutral trace organic contaminants including 1,4-D can pass through reverse osmosis (RO) membranes, UV/AOP typically takes place subsequently to membrane treatment to ultimately eliminate recalcitrant trace contaminants from RO permeate.

During the upstream membrane step, chloramine is added in the feed water to minimize membrane bio-fouling. Due to their small molecular sizes and neutral charge, chloramines easily pass through RO membranes and are carried over to downstream UV/AOP step and undergo photolysis.<sup>14</sup> In addition, an oxidant is added to the UV/AOP step to produce highly oxidative species. Hydrogen peroxide ( $\text{H}_2\text{O}_2$ ) is the default oxidant and produces hydroxyl radical ( $\text{HO}^\bullet$ ). Although possessing a high oxidative capacity,  $\text{HO}^\bullet$  is not selective and can be scavenged by carbonate and chloride and consequently adversely affects its efficiency.<sup>6,15,16</sup>

In recent years, persulfate ( $\text{S}_2\text{O}_8^{2-}$ ) becomes an alternative oxidant in UV/AOP.<sup>6,17,18</sup> The quantum yield of  $\text{SO}_4^{\bullet-}$  from  $\text{S}_2\text{O}_8^{2-}$  is higher than that of  $\text{HO}^\bullet$  from  $\text{H}_2\text{O}_2$  (0.7 vs. 0.5), while both  $\text{SO}_4^{\bullet-}$  and  $\text{HO}^\bullet$  have similar oxidizing power (2.5-3.1 V vs.

1.9-2.8 V).<sup>19-21</sup> Furthermore,  $\text{SO}_4^{\bullet-}$  is more selective towards electron-rich contaminants that typically observed in recycled water.<sup>6,22,23</sup> Therefore, UV/ $\text{S}_2\text{O}_8^{2-}$  can potentially reach a higher efficiency and a lower energy footprint than  $\text{H}_2\text{O}_2$ . Given the existence of *de facto* UV/ $\text{NH}_2\text{Cl}$  because of  $\text{NH}_2\text{Cl}$  as carry-over membrane anti-fouling agents and the future application of UV/ $\text{S}_2\text{O}_8^{2-}$ , it is important to understand the unique radical generation under photolysis of both  $\text{NH}_2\text{Cl}$  and  $\text{S}_2\text{O}_8^{2-}$ .

The mechanism on the simultaneous photolysis of  $\text{NH}_2\text{Cl}$  and  $\text{S}_2\text{O}_8^{2-}$  is not well developed.  $\text{NH}_2\text{Cl}$  has a high UV absorbance coefficient ( $371 \text{ M}^{-1}\text{cm}^{-1}$ ) and a quantum yield similar to  $\text{H}_2\text{O}_2$ .<sup>4,24, -26</sup>  $\text{NH}_2\text{Cl}$  can also act as a self-scavenger that decreases its radical yield upon UV irradiation.<sup>14</sup> However, most prior studies examined chloramine photolysis in solution conditions unrelated to potable reuse.<sup>4,8,24-30</sup> Our recent study showed that photolysis of  $\text{NH}_2\text{Cl}$  in RO permeate produce  $\text{HO}^{\bullet}$  and  $\text{Cl}_2^{\bullet-}$  that promote 1,4-D degradation. Furthermore,  $\text{SO}_4^{\bullet-}$  produced from  $\text{S}_2\text{O}_8^{2-}$  photolysis can react with  $\text{NH}_2\text{Cl}$  to generate secondary radicals, but the extent of chain reactions in RO permeate with the dual oxidants remains unknown.

The objectives of this study were to quantify the formation of reactive radicals during the simultaneous photolysis of  $\text{NH}_2\text{Cl}$  and  $\text{S}_2\text{O}_8^{2-}$ , examine the impact of oxidant dosage, pH, chloride and dissolved  $\text{O}_2$  on the degradation of 1,4-D, and develop a kinetic model to predict the radical yield and transformation of with both oxidants.

### 3.2 Materials and Methods

All solutions were prepared from reagent-grade chemicals with deionized water (DI) (resistivity  $<18.2\text{M}\Omega$ , Millipore System). A fresh 50 mM  $\text{NH}_2\text{Cl}$  stock solution was prepared daily by slowly titrating  $\text{NaOCl}$  with  $(\text{NH}_4)_2\text{SO}_4$  at 1:1.2 molar ratio and buffered with 4 mM borate at pH 8.8.<sup>31</sup> The prepared  $\text{NH}_2\text{Cl}$  solution was equilibrated for 3 hours in the dark and its concentration was verified using permanganate.<sup>32</sup> An equal-molar chloride residue always co-existed with  $\text{NH}_2\text{Cl}$  due to chloramine equilibrium chemistry. A 100-mM persulfate stock solution was prepared daily using  $\text{Na}_2\text{S}_2\text{O}_8$ . Most experiments were conducted using  $\text{N}_2$ -purged DI water to minimize dissolved  $\text{O}_2$ . In some experiments, DI water was purged with ambient air for 20 minutes to create an air-saturated solution. The solution pH was adjusted to a targeted value between 5 to 8 with phosphate buffer, which also maintained the ionic strength constant at 50 mM. Chloride concentration was adjusted between 0.2 and 2 mM.

To start a UV experiment, solutions of  $\text{NH}_2\text{Cl}$  ranging between 0 and 6 mM and  $\text{S}_2\text{O}_8^{2-}$  between 2 and 4 mM were mixed with 250  $\mu\text{M}$  of 1,4-D. In addition, 10  $\mu\text{M}$  benzoic acid (BA) and 20  $\mu\text{M}$  nitrobenzene (NB) were added as radical probe compounds. The solution was quickly mixed, transferred to multiple 8-mL quartz tubes with no headspace, and placed in a carousel UV reactor (ACE Glass) equipped with a low-pressure monochromatic ( $\lambda=254\text{ nm}$ ) mercury lamp (Philips TUV6T5, 6W).

Samples were withdrawn from the UV reactor at pre-determined time intervals.  $\text{NH}_2\text{Cl}$  concentration was measured immediately using the DPD colorimetric method.<sup>32</sup>

The presence of  $S_2O_8^{2-}$  in the sample had no interference with the measurement.  $S_2O_8^{2-}$  concentration was measured using KI titration by a Horiba UV spectrofluorometer after  $NH_2Cl$  was removed by purging the solution with air.<sup>33</sup> To quantify the generation of nitrogen species during  $NH_2Cl$  photolysis, total nitrogen (TN) was measured by a TOC analyzer with nitrogen detector (OI Analytical, Inc.); ammonium, nitrite and nitrate were measured using colorimetric methods with phenate, sulfanilamide and nicotinamide adenine dinucleotide phosphate, respectively;<sup>32</sup> gaseous nitrogen formation was calculated based on the loss of TN; the remaining fraction of nitrogen was accounted for as organic nitrogen. Chloride was measured by a Dionex-1000 ion chromatography equipped with a conductivity detector.

The steady-state radical concentrations were quantified based on the competitive kinetics of probe compounds. Using the observed first-order decay rates of the probe compounds (*i.e.* nitrobenzene (NB), benzoate(BA) and 1,4-dioxane (1,4-D), the steady-state concentrations of  $HO^\bullet$ ,  $SO_4^{\bullet-}$  and  $Cl_2^{\bullet-}$  were calculated. The steady-state concentration of  $HO^\bullet$  was calculated using NB, because NB predominantly reacted with  $HO^\bullet$ . First, the *pseudo* first-order decay rate of NB ( $k_{obs}$ ) was obtained from experimental measurement.  $[HO^\bullet]_{ss}$  was calculated based on Equation 1:

$$k_{obs} = -\ln \left( \frac{[NB]_t}{[NB]_0} \right) = k_{HO-NB} [HO^\bullet]_{ss} t \quad (\text{Eq. 1})$$

$$[HO^\bullet]_{ss} = \frac{k_{NB}}{k_{HO-NB}}$$

$[NB]_t$  is the concentration of nitrobenzene at a given reaction time  $t$ ;  $[NB]_0$  is the initial concentration of nitrobenzene (20  $\mu\text{M}$ );  $k_{HO-NB}$  is the second-order rate constant between  $HO^\bullet$  and NB, which is known as  $6.0 \times 10^9 \text{ M}^{-1} \text{ s}^{-1}$ .<sup>34</sup>  $k_{NB}$  is the experimentally obtained *pseudo* first-order decay rate of NB.

Second, based on the branching ratio calculation, the reaction between  $Cl_2^{\bullet-}$  and BA was negligible (Equation 2):

$$\%_{BA-Cl_2^{\bullet-}} = \frac{k_{BA-Cl_2^{\bullet-}}[BA]}{k_{BA-Cl_2^{\bullet-}}[BA] + k_{1,4-D-Cl_2^{\bullet-}}[1,4-D] + k_{H_2O-Cl_2^{\bullet-}} + k_{NH_2Cl-Cl_2^{\bullet-}}[NH_2Cl]} = < 1\% \quad (\text{Eq. 2})$$

$\%_{BA-Cl_2^{\bullet-}}$  is defined as the branching ratio of BA with  $Cl_2^{\bullet-}$ .  $k_{BA-Cl_2^{\bullet-}}$ ,  $k_{1,4-D-Cl_2^{\bullet-}}$ , and  $k_{NH_2Cl-Cl_2^{\bullet-}}$  are the second-order rate constants between  $Cl_2^{\bullet-}$  and benzoate,  $Cl_2^{\bullet-}$  and 1,4-D, and  $Cl_2^{\bullet-}$  and  $NH_2Cl$ , respectively, which are known as  $k_{BA-Cl_2^{\bullet-}} = 2.0 \times 10^6 \text{ M}^{-1} \text{ s}^{-1}$ ,<sup>35</sup>  $k_{1,4-D-Cl_2^{\bullet-}} = 3.3 \times 10^6 \text{ M}^{-1} \text{ s}^{-1}$ ,<sup>36</sup> and  $k_{NH_2Cl-Cl_2^{\bullet-}} = 10^6 \text{ M}^{-1} \text{ s}^{-1}$ . The rate constant for  $NH_2Cl$  and  $Cl_2^{\bullet-}$  is obtained from this study, which is discussed in Text S4.  $k_{H_2O-Cl_2^{\bullet-}}$  is the first-order rate constant between  $Cl_2^{\bullet-}$  and  $H_2O$ , which is  $1.3 \times 10^3 \text{ s}^{-1}$ .<sup>37</sup>

Because BA reacts with  $HO^\bullet$ ,  $SO_4^{\bullet-}$  and  $NH_2^\bullet$ , the *pseudo* first-order decay rate of BA was calculated based on Equation 3:

$$-\ln \frac{[BA]_t}{[BA]_0} = (k_{BA-HO^\bullet}[BA][HO^\bullet]_{ss} + k_{BA-SO_4^{\bullet-}}[BA][SO_4^{\bullet-}]_{ss} + k_{BA-NH_2^\bullet}[BA][NH_2^\bullet]_{ss})t \quad (\text{Eq. 3})$$

and the steady-state concentration of  $SO_4^{\bullet-}$  was obtained by solving the above equation:

$$[SO_4^{\bullet-}]_{ss} = \frac{k_{BA-HO^\bullet}[BA][HO^\bullet]_{ss} - k_{BA-NH_2^\bullet}[NH_2^\bullet]_{ss}}{k_{BA-SO_4^{\bullet-}}}$$

Here,  $[BA]_t$  is the concentration of BA at a given reaction time  $t$ ;  $[BA]_0$  is the initial concentration of BA (10  $\mu\text{M}$ );  $k_{HO\cdot-BA}$  is the second-order rate constant between  $HO\cdot$  and BA ( $6.0 \times 10^9 \text{ M}^{-1}\text{s}^{-1}$ ),  $k_{BA-SO_4^{\cdot-}}$  is the second-order rate constant between  $SO_4^{\cdot-}$  and BA ( $1.2 \times 10^9 \text{ M}^{-1}\text{s}^{-1}$ ),<sup>38</sup> and  $k_{BA-NH_2\cdot}$  is second-order rate constant between  $NH_2\cdot$  and BA ( $3.0 \times 10^6 \text{ M}^{-1}\text{s}^{-1}$ ).<sup>39</sup>  $k_{BA}$  is the experimentally obtained pseudo first-order decay rate of BA.  $[NH_2\cdot]_{ss}$  was obtained from the kinetic model (All reactions of the model are listed in **Appendix B-2**).

Finally,  $[Cl_2^{\cdot-}]_{ss}$  was calculated based on Equation 4.  $NH_2\cdot$  was not included in the equation because it has negligible reactivity with 1,4-D.<sup>40</sup>

$$-\ln \left( \frac{[1,4-D]_t}{[1,4-D]_0} \right) = (k_{HO\cdot-1,4-D}[HO\cdot]_{ss} + k_{SO_4^{\cdot-}-1,4-D}[SO_4^{\cdot-}]_{ss} + k_{Cl_2^{\cdot-}-1,4-D}[Cl_2^{\cdot-}]_{ss})t \quad (\text{Eq. 4})$$

$$[SO_4^{\cdot-}]_{ss} = \frac{k_{1,4-D} - k_{HO\cdot-1,4-D}[HO\cdot]_{ss} - k_{Cl_2^{\cdot-}-1,4-D}[Cl_2^{\cdot-}]_{ss}}{k_{SO_4^{\cdot-}-1,4-D}}$$

Here  $[1,4-D]_t$  is the concentration of 1,4-D at a given reaction time  $t$ ;  $[1,4-D]_0$  is the initial concentration of 1,4-D (250  $\mu\text{M}$ );  $k_{HO\cdot-1,4-D}$  is the second-order rate constant between  $HO\cdot$  and 1,4-D ( $3.1 \times 10^9 \text{ M}^{-1}\text{s}^{-1}$ ),<sup>41</sup>  $k_{SO_4^{\cdot-}-1,4-D}$  is the second-order rate constant between  $SO_4^{\cdot-}$  and 1,4-D ( $4.1 \times 10^7 \text{ M}^{-1}\text{s}^{-1}$ ),<sup>42</sup> and  $k_{Cl_2^{\cdot-}-1,4-D}$  is the second-order rate constant between  $Cl_2^{\cdot-}$  and 1,4-D ( $3.3 \times 10^6 \text{ M}^{-1}\text{s}^{-1}$ ).<sup>36</sup>  $k_{1,4-D}$  is the experimentally observed *pseudo* first-order rate constant of 1,4-D.

The concentrations of 1,4-D, BA and NB were measured by an Agilent 1200 liquid chromatography equipped with a diode array detector and a Zorbax Eclipse SB-C18

column (4.6×150mm, 5-μm particle size). A kinetics model was developed using the Kintecus software (all reactions of the model are listed in **Appendix B-2**).<sup>43</sup> The model development and optimization can be found in Text S4 and prior literature.<sup>18, 44</sup>

### 3.3 Results and Discussion

#### 3.3.1 Impact of $\text{NH}_2\text{Cl}$ dosage on $\text{UV}/\text{S}_2\text{O}_8^{2-}$

The effect of  $\text{NH}_2\text{Cl}$  on 1,4-D degradation by UV photolysis of  $\text{S}_2\text{O}_8^{2-}$  was investigated. The concentrations of  $\text{S}_2\text{O}_8^{2-}$  and 1,4-D were fixed at 2 mM and 0.25 mM, respectively. The UV fluence-normalized rate of 1,4-D degradation increased from  $7.5 \times 10^{-4}$  to  $9.7 \times 10^{-4} \text{ cm}^2 \cdot \text{mJ}^{-1}$  when the  $\text{NH}_2\text{Cl}$  dosage increased from 0 to 0.2 mM; however, the rate decreased to  $5.3 \times 10^{-4} \text{ cm}^2 \cdot \text{mJ}^{-1}$  when the  $\text{NH}_2\text{Cl}$  dosage was increased further to 4 mM (**Figure 11**). Analysis with probe compounds showed that  $\text{HO}^\bullet$  contributed the most to 1,4-D degradation, followed by  $\text{SO}_4^{\bullet-}$  and  $\text{Cl}_2^{\bullet-}$  (**Figure 11A**). The contribution of  $\text{HO}^\bullet$  reached a maximum at the optimal  $\text{NH}_2\text{Cl}$  dosage of 0.2 mM –corresponding to a  $\text{NH}_2\text{Cl}$ -to- $\text{S}_2\text{O}_8^{2-}$  molar ratio of 0.1:1, and decreased by 27% when  $\text{NH}_2\text{Cl}$  dosage increased to 4 mM. The contribution of  $\text{SO}_4^{\bullet-}$  to 1,4-D degradation dropped significantly to negligible when the  $\text{NH}_2\text{Cl}$ -to- $\text{S}_2\text{O}_8^{2-}$  ratio increased beyond 0.1, accompanied by a substantial increase in the contribution of  $\text{Cl}_2^{\bullet-}$  to 1,4-D removal (**Figure 11A**).

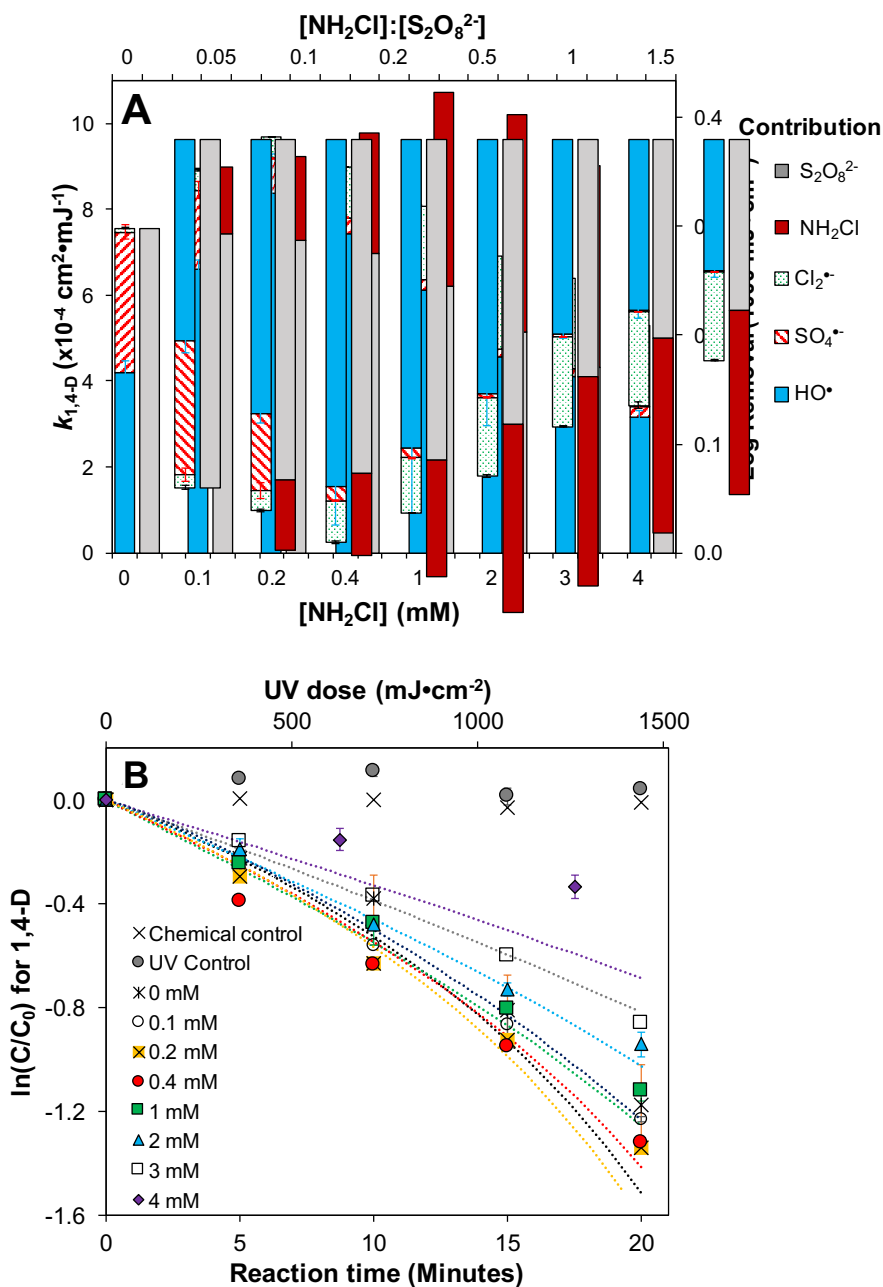


**Figure 11** Effect of  $\text{NH}_2\text{Cl}$  dose on 1,4-dioxane degradation. (A) UV fluence normalized rate of 1,4-dioxane,  $\text{S}_2\text{O}_8^{2-}$  and  $\text{NH}_2\text{Cl}$ ; (B) first order decay of 1,4-dioxane.  $[\text{S}_2\text{O}_8^{2-}] = 2 \text{ mM}$ ,  $[\text{NH}_2\text{Cl}] = 0-4 \text{ mM}$ ,  $[1,4\text{-dioxane}] = 0.25 \text{ mM}$ ,  $[\text{benzoic acid}] = 10 \mu\text{M}$ ,  $[\text{nitrobenzene}] = 20 \mu\text{M}$ ,  $\text{pH} = 5.8$ , UV dose =  $2760 \text{ mJ cm}^{-2}$ . Dash lines represent the modeled results.

As the concentration of  $\text{NH}_2\text{Cl}$  increased from 0 to 4 mM, photons were preferentially absorbed by  $\text{NH}_2\text{Cl}$  compared to  $\text{S}_2\text{O}_8^{2-}$ , which was supported by an increase in the photolysis rate of  $\text{NH}_2\text{Cl}$  and a decrease in the photolysis rate of  $\text{S}_2\text{O}_8^{2-}$  (**Figure 12A**). The percentage of light absorbed by  $\text{NH}_2\text{Cl}$  (solid gray bar) and  $\text{S}_2\text{O}_8^{2-}$  (red bar) in the mixed system was calculated (**Appendix B-4**) and shown in **Figure 11**. For instance, in the presence of 0.1 mM  $\text{NH}_2\text{Cl}$ ,  $\text{S}_2\text{O}_8^{2-}$  absorbed 98% of light as if no monochloramine were present, and only absorbed 51% of light when mixing with 4 mM  $\text{NH}_2\text{Cl}$ . Thus, the contribution of  $\text{S}_2\text{O}_8^{2-}$  to 1,4-D decreased by 2%. Meanwhile,  $\text{NH}_2\text{Cl}$  photolysis produced less reactive- $\text{Cl}^\bullet$  and  $\text{NH}_2^\bullet$  (Reaction 1 in **Scheme 7**, all subsequent reactions are referred to those in **Scheme 7**) as the primary radical.<sup>14</sup> As a result, the rate of 1,4-D degradation was compromised. In contrast, an increase in  $\text{S}_2\text{O}_8^{2-}$  dosage in the presence of a constant  $\text{NH}_2\text{Cl}$  level always promoted radical generation (**Figure 12B**).

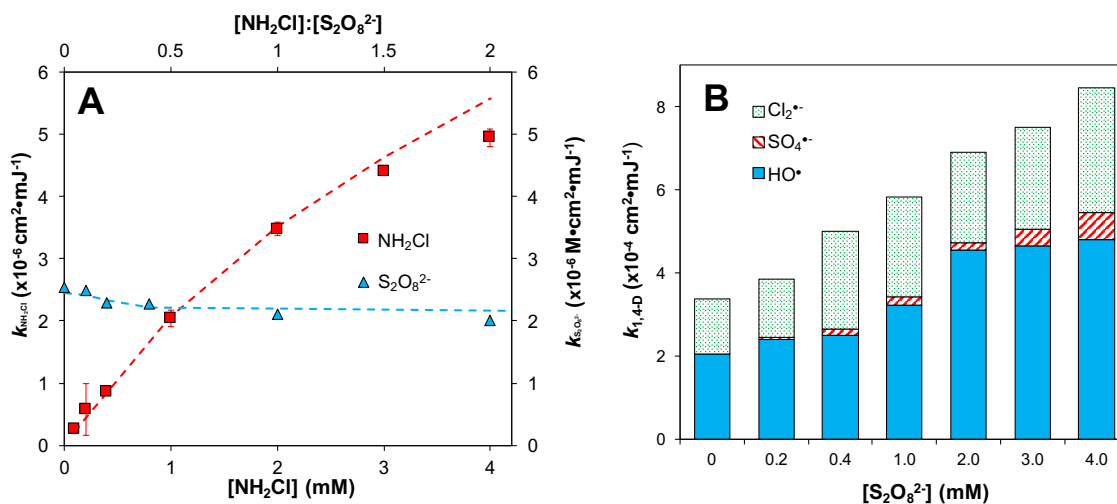


**Figure 12** Impact of oxidant dosage on 1,4-D degradation. (A) correlation between 1,4-D degradation rates and oxidants photolysis rates (B) effect of  $\text{S}_2\text{O}_8^{2-}$  dosage on 1,4-D degradation.  $[\text{S}_2\text{O}_8^{2-}] = 0 - 4$  mM,  $[\text{NH}_2\text{Cl}] = 2$  mM,  $[\text{1,4-dioxane}] = 0.25$  mM,  $[\text{benzoic acid}] = 10$   $\mu\text{M}$ ,  $[\text{nitrobenzene}] = 20$   $\mu\text{M}$ ,  $\text{pH} = 5.8$ , UV dose =  $2760$   $\text{mJ cm}^{-2}$ .

In addition, the experimentally observed 1,4-D degradation rate with both oxidants was always 10% to 40% lower than the theoretically additive value as if both oxidants existed separately (**Figure 11**, calculation provided in **Appendix B-5**). Furthermore, the degradation rate of 1,4-D was positively correlated with the photolysis rate of  $S_2O_8^{2-}$ , but inversely correlated with that of  $NH_2Cl$  (**Figure 13A**). These trends strongly suggested that in the mixed oxidant system,  $NH_2Cl$  rather than  $S_2O_8^{2-}$  had a stronger scavenging effect on reactive radicals.

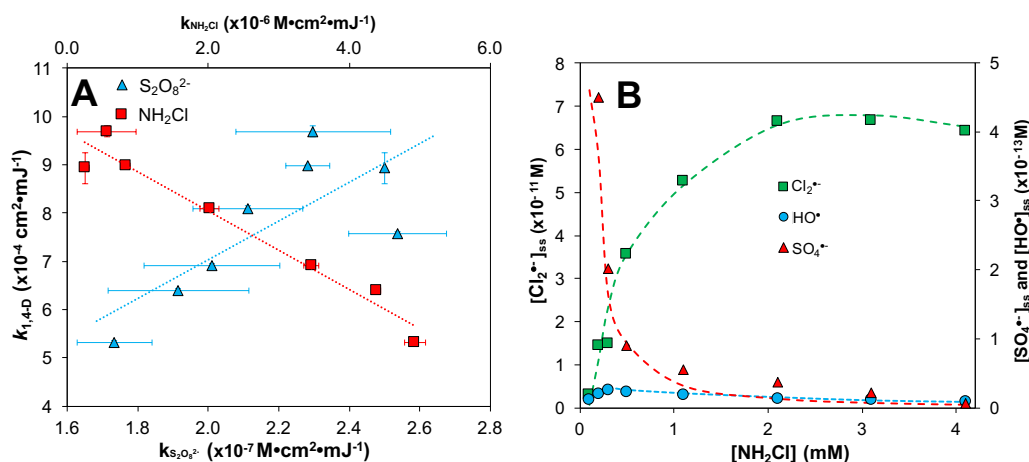


**Figure 13.** Effect of  $NH_2Cl$  dosage on the treatability of 1,4-dioxane by UV/  $S_2O_8^{2-}$  and  $NH_2Cl$ . (A) correlation between 1,4-D degradation rates and oxidants photolysis rates; (B) steady-state radical concentration.  $[S_2O_8^{2-}] = 2$  mM,  $[NH_2Cl] = 0-4$  mM,  $[1,4-dioxane] = 0.25$  mM,  $[benzoic\ acid] = 10$   $\mu M$ ,  $[nitrobenzene] = 20$   $\mu M$ ,  $pH = 5.8$ . UV dose =  $2760$   $mJ \cdot cm^{-2}$ . Dash lines represent the modeled results.

### 3.3.2 Radical distribution in UV photolysis of $S_2O_8^{2-}$ and $NH_2Cl$

Impacts of  $NH_2Cl$  on the radical generation and scavenging pathways in UV/ $S_2O_8^{2-}$  were elucidated in **Scheme 7**. Direct photolysis of  $S_2O_8^{2-}$  and  $NH_2Cl$  generated  $SO_4^{\bullet-}$ ,  $Cl^{\bullet}$  and  $NH_2^{\bullet}$  (Reactions 1-2 in **Scheme 7**). The co-existence of chloride with  $NH_2Cl$  leads to



$\text{Cl}_2^{\bullet-}$  could also be scavenged by  $\text{NH}_2\text{Cl}$  (Reaction 10). However, more  $\text{Cl}_2^{\bullet-}$  was produced with increasing  $\text{NH}_2\text{Cl}$  dosage, thus  $[\text{Cl}_2^{\bullet-}]_{\text{ss}}$  reached a plateau after  $\text{NH}_2\text{Cl}$  reached 2 mM (**Figure 13B**). 1,4-D is more reactive with  $\text{HO}^{\bullet}$  and  $\text{SO}_4^{\bullet-}$  than with  $\text{Cl}_2^{\bullet-}$ . Therefore, the overall degradation rate of 1,4-D slowed down significantly.

In addition, the co-existence of chloride with  $\text{NH}_2\text{Cl}$  acted as a scavenger to transform  $\text{SO}_4^{\bullet-}$  to  $\text{Cl}_2^{\bullet-}$  (Reaction 3-4). To eliminate the confounding effect by chloride, the initial  $\text{NH}_2\text{Cl}$  dosage was varied but chloride fixed at 4 mM. Results showed that the 1,4-D degradation rate decreased by 43% with increasing  $\text{NH}_2\text{Cl}$  concentrations (**Figure 14**). This trend further confirmed that indeed scavenging reactions with  $\text{NH}_2\text{Cl}$  (Reactions 8-10) decreased the radical yields.

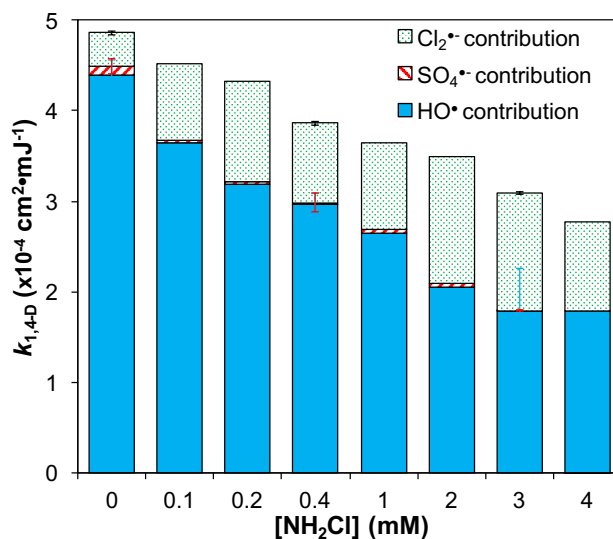


**Figure 14.** Effect of  $\text{NH}_2\text{Cl}$  dosage on 1,4-dioxane degradation by  $\text{UV}/\text{S}_2\text{O}_8^{2-}$  and  $\text{NH}_2\text{Cl}$  at a fixed chloride concentration.  $[\text{S}_2\text{O}_8^{2-}] = 2 \text{ mM}$ ,  $[\text{NH}_2\text{Cl}] = 0\text{-}4 \text{ mM}$ ,  $[\text{Cl}^-] = 4 \text{ mM}$ ,  $[\text{1,4-dioxane}] = 0.25 \text{ mM}$ ,  $[\text{benzoic acid}] = 10 \text{ }\mu\text{M}$ ,  $[\text{nitrobenzene}] = 20 \text{ }\mu\text{M}$ ,  $\text{pH} = 5.8$ ,  $\text{UV dose} = 2760 \text{ mJ cm}^{-2}$ .

### 3.3.3 Products from photolysis of $S_2O_8^{2-}$ and $NH_2Cl$

The major products of  $NH_2Cl$  photolysis were  $NH_4^+$ , nitrate, gaseous nitrogen and organic nitrogen (**Figure 15**).  $NH_4^+$  production mainly resulted from the oxidation of  $NH_2Cl$  by  $NH_2^\bullet$  (Reaction 11) and the eventual oxidation to form gaseous nitrogen (Reaction 12).  $NHCl^\bullet$  formed via  $HO^\bullet$ ,  $Cl^\bullet$ ,  $SO_4^{\bullet-}$  and  $Cl_2^{\bullet-}$  reacting with  $NH_2Cl$  (Reactions 8-10).  $NHCl^\bullet$  can also combine to produce  $N_2$  gas and  $Cl^-$  (Reaction 13). A small amount of  $NO_3^-$  was produced throughout the experiment, possibly due to the reaction between  $NH_2Cl$  and nitrite or  $H_2O$ .<sup>26,46</sup> Organic nitrogen was likely formed through the interaction of  $NH_2^\bullet$  and  $NHCl^\bullet$  with 1,4-D, benzoate, nitrobenzene and their degradation products. However, differentiating the organic nitrogen products was not the aim of this study, further investigation maybe required to examine the mechanism of organic nitrogen formation.

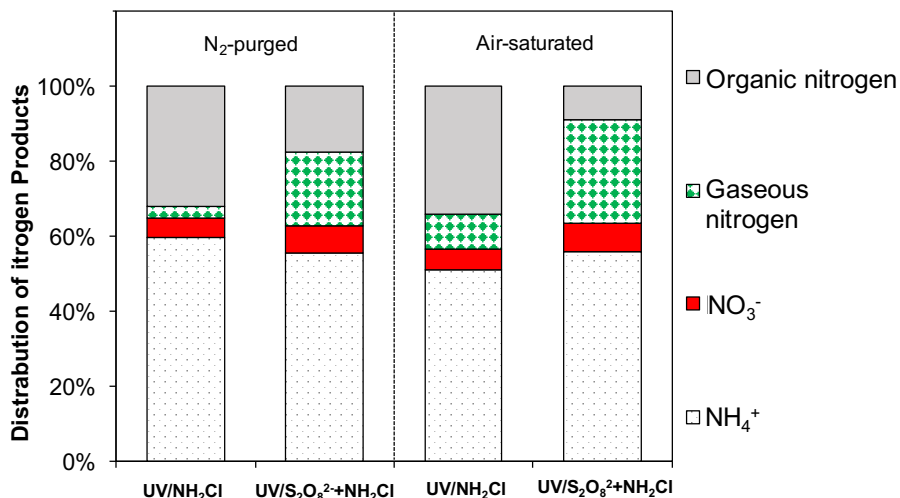


**Figure 15.** Impact of persulfate dosage and oxygen on  $NH_2Cl$  product distribution.  $[S_2O_8^{2-}] = 0-2$  mM,  $[NH_2Cl] = 2$  mM,  $[1,4\text{-dioxane}] = 250$   $\mu$ M,  $[\text{benzoic acid}] = 10$   $\mu$ M,  $[\text{nitrobenzene}] = 20$   $\mu$ M,  $pH = 5.8$ , UV dose =  $2760$   $\text{mJ}\cdot\text{cm}^{-2}$ .

In the absence of  $S_2O_8^{2-}$ , approximately 55% of  $NH_2Cl$  was converted to  $NH_4^+$ , 30% to organic nitrogen, 3% to gaseous nitrogen and 5% to nitrate, respectively (**Figure 15**). In contrast, in the presence of  $S_2O_8^{2-}$ ,  $NH_2Cl$  photolysis generated more gaseous nitrogen, but less organic nitrogen species.  $SO_4^{\bullet-}$  directly oxidizes  $NH_2Cl$  (Reaction 9), yielding more  $N_2$  (Reaction 13). This is consistent with the observation that gaseous nitrogen formation almost doubled with the inclusion of  $S_2O_8^{2-}$  (**Figure 15**).  $O_2$  reacts with  $NH_4^+$  forming intermediate products including hydroxylamine ( $NH_2OH$ ), nitrous acid ( $HNO_2$ ), nitric oxide ( $NO$ ) and nitroxyl ( $HNO$ ), which are further oxidized to  $N_2$ .<sup>47</sup> The results suggest that  $O_2$  and  $S_2O_8^{2-}$  aid in the production of more highly oxidized nitrogen species while  $SO_4^{2-}$ , with a 2:1 stoichiometry, was the only sulfur species observed from  $S_2O_8^{2-}$  photolysis (**Figure 16**).

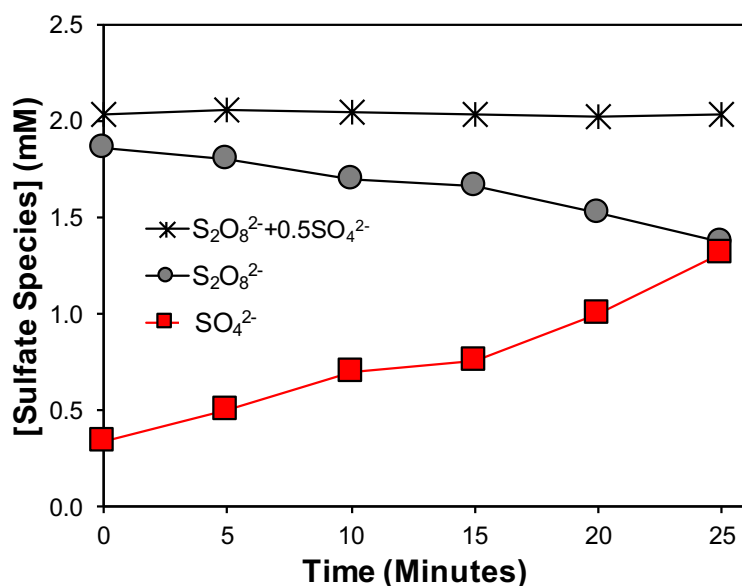


**Figure 16** Persulfate photolysis products.  $[S_2O_8^{2-}] = 2$  mM,  $[1,4\text{-dioxane}] = 0.25$  mM,  $[\text{benzoic acid}] = 10$   $\mu\text{M}$ ,  $[\text{nitrobenzene}] = 20$   $\mu\text{M}$ . UV dose =  $3450$   $\text{mJ cm}^{-2}$ .

### 3.3.4 Impact of total oxidant dosage on 1,4-dioxane degradation

The effect of total oxidant dosage in UV/S<sub>2</sub>O<sub>8</sub><sup>2-</sup>/NH<sub>2</sub>Cl on 1,4-D degradation was examined at two NH<sub>2</sub>Cl-to-S<sub>2</sub>O<sub>8</sub><sup>2-</sup> molar ratios, *i.e.*, 0.1:1 and 1:1. The 0.1:1-ratio generally achieved 33 to 240% more 1,4-D removal compared to the 1:1 ratio (**Figure 17A**). [SO<sub>4</sub><sup>•-</sup>]<sub>ss</sub> was approximately 5 times higher at the 0.1:1 ratio (**Figure 17B**), and [HO<sup>•</sup>]<sub>ss</sub> was 70 to 300% higher when the dosage exceeded 4 mM (**Figure 17B**). At the optimal ratio of 0.1:1, when the total oxidant (*i.e.*, S<sub>2</sub>O<sub>8</sub><sup>2-</sup> and NH<sub>2</sub>Cl) dosage exceeded 6 mM, major scavenging by S<sub>2</sub>O<sub>8</sub><sup>2-</sup> reduced the [HO<sup>•</sup>]<sub>ss</sub> by 15% (Reaction 14, **Figure 17B**), thus 1,4-D degradation rate also dropped by 15%. In contrast, at the NH<sub>2</sub>Cl-to-S<sub>2</sub>O<sub>8</sub><sup>2-</sup> ratio of 1:1, the rate exhibited a bell-shape curve with the maximal rate observed at 4 mM (**Figure 17A**). At this oxidant ratio, more SO<sub>4</sub><sup>•-</sup> was transformed to Cl<sub>2</sub><sup>•-</sup> which was less reactive with 1,4-D. Despite the conversion of the Cl<sub>2</sub><sup>•-</sup> to HO<sup>•</sup> (Reactions 3-7), the 1:1-ratio generally resulted in higher [Cl<sub>2</sub><sup>•-</sup>]<sub>ss</sub> concentration and lower [SO<sub>4</sub><sup>•-</sup>]<sub>ss</sub> compared to 0.1:1-ratio (**Figure 17B**). When the total dosage exceeded 6 mM, more than 60% of HO<sup>•</sup> was scavenged by NH<sub>2</sub>Cl (**Appendix B-5**), which resulted in a 30% decrease of [HO<sup>•</sup>]<sub>ss</sub> (**Figure 17B**). Additionally, the [Cl<sub>2</sub><sup>•-</sup>]<sub>ss</sub> increased by 200% and contributed significantly to 1,4-D degradation, but the overall rates still decreased.

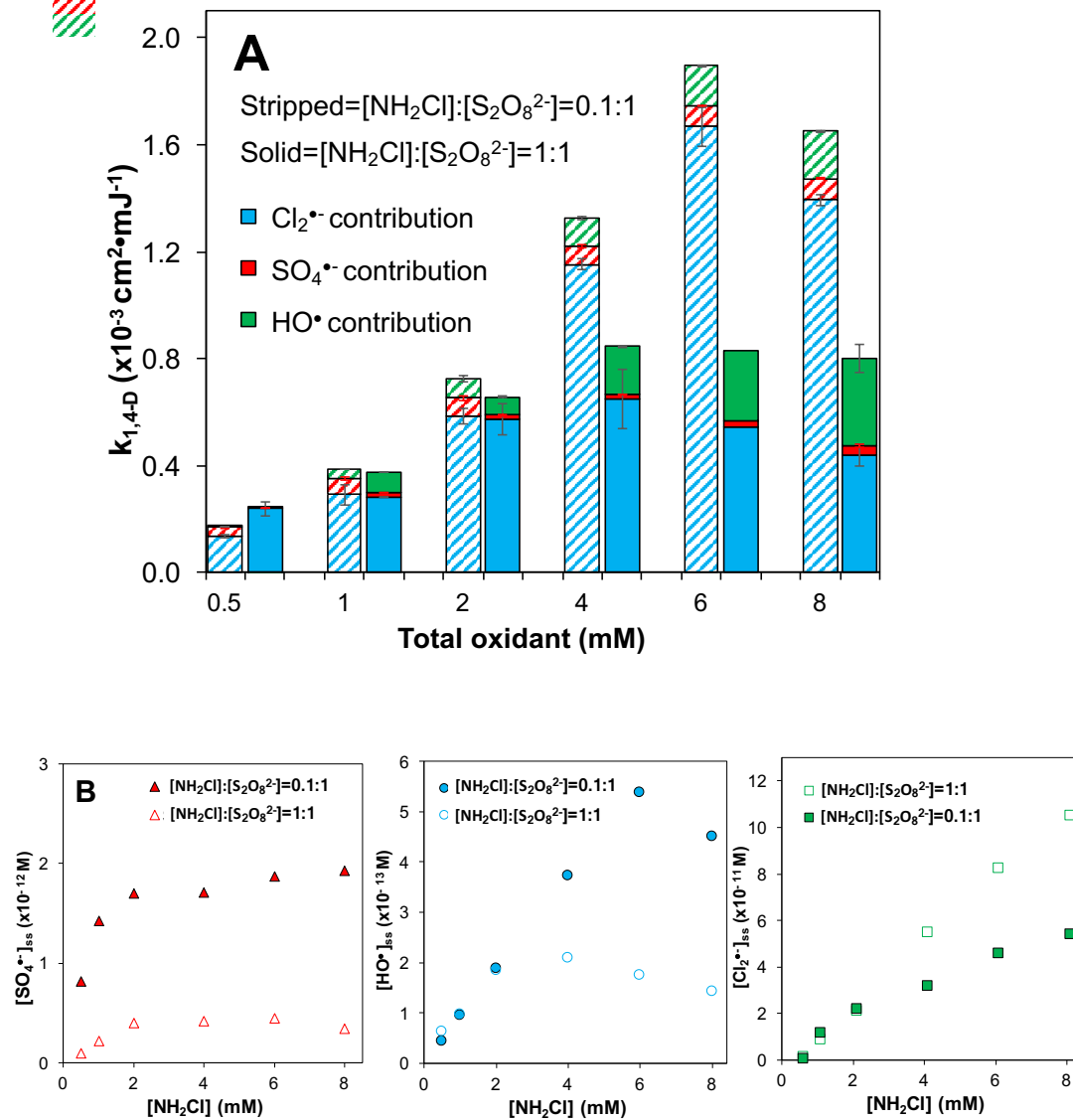


**Figure 17.** Impact of total oxidant dosage on the treatment of 1,4-dioxane by UV/  $\text{S}_2\text{O}_8^{2-}$  and  $\text{NH}_2\text{Cl}$ . (A) Effect of total oxidant dosage on 1,4-dioxane degradation rates; (B) Steady-state radical concentration.  $[\text{1,4-dioxane}] = 250 \mu\text{M}$ ,  $[\text{benzoic acid}] = 10 \mu\text{M}$ ,  $[\text{nitrobenzene}] = 20 \mu\text{M}$ ,  $\text{pH} = 5.8$ . UV dose =  $2760 \text{ mJ cm}^{-2}$ .

### 3.3.5 Impact of chloride

An increase of chloride concentration from 0.2 to 2 mM slowed 1,4-D degradation by 28%, and preferentially reduced the contribution from HO<sup>•</sup> (**Figure 18A**). There was a 40% and 80% reduction in [HO<sup>•</sup>]<sub>ss</sub> and [SO<sub>4</sub><sup>•-</sup>]<sub>ss</sub>, respectively, whereas [Cl<sub>2</sub><sup>•-</sup>]<sub>ss</sub> increased by 240% (**Figure 18B**) that resulted from the chloride-assisted conversion of HO<sup>•</sup> and SO<sub>4</sub><sup>•-</sup> to Cl<sub>2</sub><sup>•-</sup> (Reaction 3-4). Up to 87% of OH<sup>•</sup> and 97% of SO<sub>4</sub><sup>•-</sup> were scavenged by the 2 mM chloride (**Appendix B-5**); however, the ClOH<sup>•</sup> quickly dissociated and generated HO<sup>•</sup> (Reactions 5-7). The presence of 2 mM chloride accelerated the reaction between HO<sup>•</sup> and Cl<sup>-</sup> by 200% (Reaction 15) and also accelerated the reaction of HClOH<sup>•</sup> with Cl<sup>-</sup> (Reaction 16). Approximately 9% of HClOH<sup>•</sup> was scavenged by 2 mM chloride forming Cl<sub>2</sub><sup>•-</sup> (**Appendix B-7**). These two reserve reactions led to elevated [Cl<sub>2</sub><sup>•-</sup>]<sub>ss</sub> and reduced [HO<sup>•</sup>]<sub>ss</sub>.

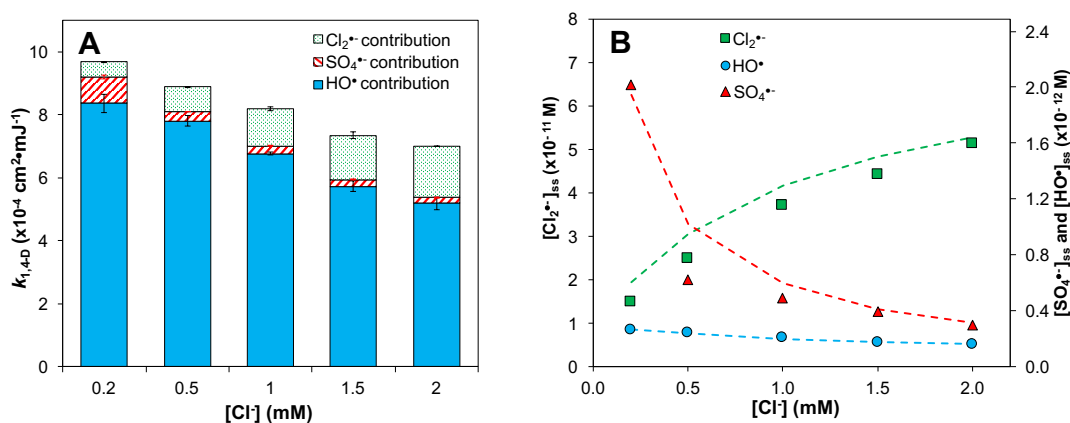


**Figure 18.** Impact of chloride on 1,4-dioxane treatment by UV/S<sub>2</sub>O<sub>8</sub><sup>2-</sup> and NH<sub>2</sub>Cl. (A) Impact of chloride on 1,4-dioxane degradation rate and radical contribution; (B) steady-state concentrations of radicals. [S<sub>2</sub>O<sub>8</sub><sup>2-</sup>]=2 mM, [NH<sub>2</sub>Cl]=0.2 mM, [Cl<sup>-</sup>]=0.2-2 mM, [1,4-dioxane]= 250 μM, [benzoic acid]=10 μM, [nitrobenzene]=20 μM. UV dose = 2760 mJ cm<sup>-2</sup>. Dash lines represent the modeled results.

### 3.3.6 Impact of dissolved oxygen

1,4-D degradation rates in both UV/S<sub>2</sub>O<sub>8</sub><sup>2-</sup> and UV/S<sub>2</sub>O<sub>8</sub><sup>2-</sup>/NH<sub>2</sub>Cl were modestly higher in air-saturated solution compared to N<sub>2</sub>-purged solution (**Figure 19**). Dissolved O<sub>2</sub> is important to the oxidation of 1,4-D.<sup>48</sup> After reaction with radicals, 1,4-D is transformed into a dioxane radical, which reacts with O<sub>2</sub> to form peroxy radical.<sup>49</sup> Peroxy radical is strong and has rate constants ranging between 10<sup>6</sup>–10<sup>8</sup> with various organics.<sup>50,51</sup> The peroxy radical could potentially react with 1,4-D and accelerate the degradation process. Furthermore, in the presence of NH<sub>2</sub>Cl, NH<sub>2</sub><sup>•</sup> predominantly reacted with NH<sub>2</sub>Cl instead of O<sub>2</sub> to produce non-reactive NHCl<sup>•</sup> (Reaction 11 vs. 17).<sup>52</sup> Therefore, in the absence of O<sub>2</sub>, the scavenging of NH<sub>2</sub>Cl by NH<sub>2</sub><sup>•</sup> to produce non-reactive radicals lowers the radical yield of NH<sub>2</sub>Cl photolysis, and decreased the 1,4-D degradation rate.

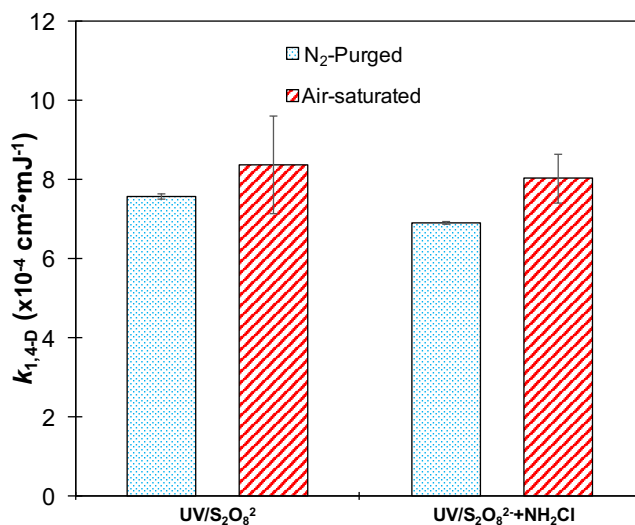


**Figure 19** Impact of oxygen on 1,4-D treatability by UV/S<sub>2</sub>O<sub>8</sub><sup>2-</sup> and NH<sub>2</sub>Cl. (A) 1,4-dioxane degradation rates; (B) NH<sub>2</sub>Cl photolysis rates. [S<sub>2</sub>O<sub>8</sub><sup>2-</sup>]=2 mM, [NH<sub>2</sub>Cl]=2 mM, [1,4-dioxane]= 250 μM, [benzoic acid]=10 μM, [nitrobenzene]=20 μM. UV dose = 2760 mJ cm<sup>-2</sup>.

### 3.3.7 Impact of pH on the photolysis of $S_2O_8^{2-}$ and $NH_2Cl$

RO permeate is typically acidic (pH=5.5-5.8) due to the application of the scale inhibitors to the feedwater. However, it is important to understand the effect of a wider range of pH on the performance of UV/AOP (**Figure 20A**). The higher pH at 8 enhanced the treatment efficiency. The increase of 1,4-D degradation kinetics from pH 5 to 8 was accompanied by an increase of  $[HO^\bullet]_{ss}$  and  $[SO_4^{\bullet-}]_{ss}$  (**Figure 20B**). The enhancement observed at higher pH (e.g. pH 7 and 8) was likely due to the stability of  $NH_2Cl$ .  $NH_2Cl$  disproportionates into  $NHCl_2$  at pH 5 via an acid catalyzed reaction, which is further converted to trichloramine ( $NCl_3$ ) under acidic conditions.<sup>53,54</sup> Dark control experiments showed that approximately 36% and 11% of  $NH_2Cl$  decayed into  $NHCl_2$  after 20 minutes at pH 5 and 6, respectively (**Figure 21**). Furthermore, the disproportionation of  $NH_2Cl$  also generates  $NH_4^+$  that scavenges  $Cl^\bullet$  (Reaction 18).<sup>26,55</sup>

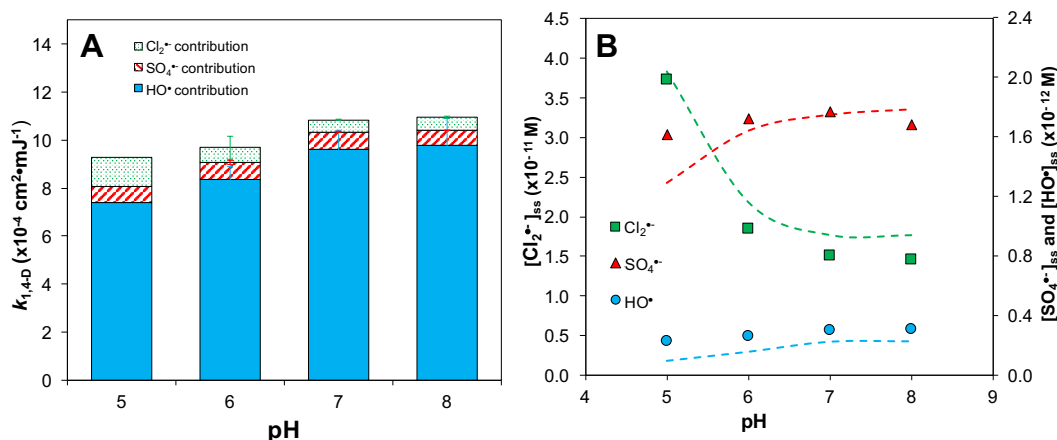


**Figure 20** Impact of pH on 1,4-dioxane treatability by UV/ $S_2O_8^{2-}$  and  $NH_2Cl$ . (A) Impact of pH on 1,4-dioxane degradation rate and radical contribution; (B) steady-state concentration of radicals.  $[S_2O_8^{2-}] = 2$  mM,  $[NH_2Cl] = 0.2$  mM,  $[1,4\text{-dioxane}] = 250$   $\mu$ M,  $[\text{benzoic acid}] = 10$   $\mu$ M,  $[\text{nitrobenzene}] = 20$   $\mu$ M. UV dose =  $2760$   $\text{mJ cm}^{-2}$ . Dash lines represent the modeled results.

To test the hypothesis that  $\text{NH}_4^+$  could scavenge reactive chlorine species, additional  $\text{UV}/\text{S}_2\text{O}_8^{2-}$  experiments were conducted by varying the  $\text{NH}_4^+$  concentration between 0 and 6 mM with a constant chloride concentration of 4 mM. The presence of  $\text{NH}_4^+$  decreased 1,4-D degradation by 30% (**Figure 22**). Collectively, the disproportionation of  $\text{NH}_2\text{Cl}$  and scavenging of  $\text{Cl}^\bullet$  and  $\text{Cl}_2^{\bullet-}$  by  $\text{NH}_4^+$  (Reactions 18-19) resulted in approximately 10% decrease of photolysis rate at pH 5 compared to pH 8.

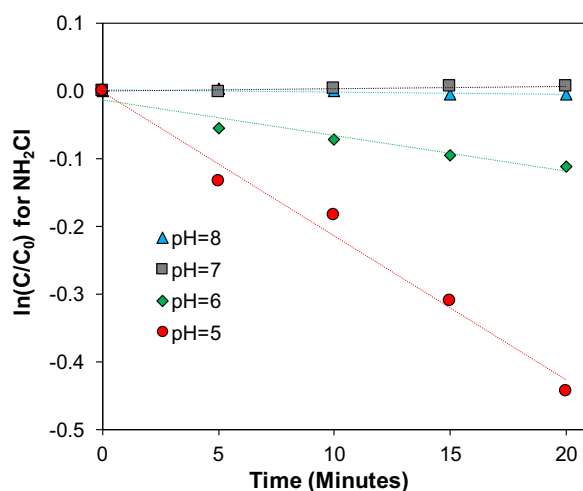


**Figure 21.** Effect of pH on 1,4-dioxane degradation without UV. [1,4-dioxane]= 250  $\mu\text{M}$

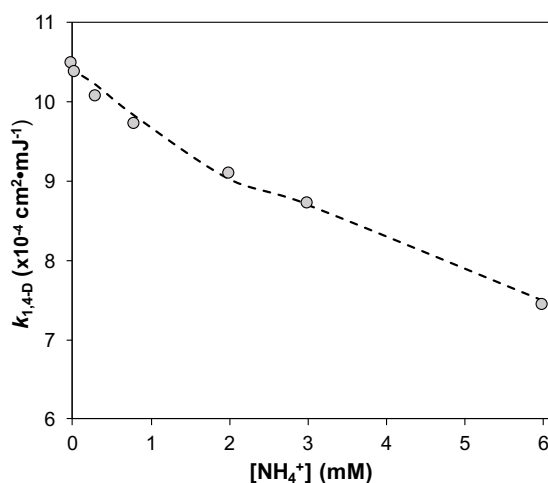


**Figure 22.** Effect of  $\text{NH}_4^+$  on 1,4-dioxane degradation rates.  $[\text{S}_2\text{O}_8^{2-}] = 2 \text{ mM}$ ,  $[\text{Cl}^-] = 4 \text{ mM}$ ,  $[\text{NH}_4^+] = 0\text{-}6 \text{ mM}$ ,  $[\text{1,4-dioxane}] = 0.25 \text{ mM}$ ,  $[\text{benzoic acid}] = 10 \mu\text{M}$ ,  $[\text{nitrobenzene}] = 20 \mu\text{M}$ . pH=6, UV dose =  $2760 \text{ mJ cm}^{-2}$ . Dash line represents modeled results.

### 3.4 Environmental Implications

The study demonstrated the application of an alternative oxidant,  $S_2O_8^{2-}$  in UV/AOP for 1,4-D removal for indirect potable reuse. The findings suggest that UV/ $S_2O_8^{2-}$  is an efficient UV/AOP technology that may help the water utility to comply with ever strengthening regulations. Specifically, UV/ $S_2O_8^{2-}$  can be operated efficiently in the presence of chloramine, a disinfectant that is widely used in recycled water treatment trains. When the  $NH_2Cl$ -to- $S_2O_8^{2-}$  molar ratio is carefully controlled at 0.1:1, UV/ $S_2O_8^{2-}$  performance is enhanced. However, beyond this optimal ratio, the performance is hindered because high  $NH_2Cl$  dosage has a photon filtering effect and significantly scavenges radicals, which decreases the yields of  $HO^\bullet$  and  $Cl_2^{\bullet-}$ . In addition, UV/ $S_2O_8^{2-}$  decreases the formation of undesired  $NH_2Cl$  decay products,  $NH_4^+$  and organic nitrogen, and promoted gaseous nitrogen production. Although, the concentration of chloride is relatively low in RO permeate, the presence of chloride may slow down 1,4-D degradation through the transformation of reactive  $HO^\bullet$  and  $SO_4^{\bullet-}$  to less reactive  $Cl_2^{\bullet-}$  that reacts with 1,4-D. This study also suggests that elevated pH could enhanced treatment efficiency. Results from this study elucidate the fundamental mechanisms of radical generation during the unique photolysis of dual oxidants, quantify the effects of inadvertent presence of  $NH_2Cl$  on the application of  $S_2O_8^{2-}$  in water reuse, and assist in the development of more efficient UV/AOP technologies.

### **3.5 Acknowledgements**

This work was supported by grants to H.L. from the U.S. National Science Foundation (CHE-1611306), and to W.L and S.P. from the U.S. National Science Foundation Graduate Research Fellowship and UC Riverside IGERT Water Sense Fellowship. We thank undergraduate students Guadalupe Lara from La Verne University and Alex Numa from UC Riverside for participation in this project.

## Reference:

---

- <sup>1</sup> National Research Council of the National Academies. *Water reuse: potential for expanding the nation's water supply through reuse of municipal wastewater*. The national Academies Press. Washington DC. 2012.
- <sup>2</sup> Sedlak, D. L. *Water 4.0: the past, present, and future of the world's most vital resource*. Yale University Press. New Haven, MA. 2014.
- <sup>3</sup> Bahnmüller, S.; Loi, C.; Linge, K.; von Gunten, U.; Canonica, S. Degradation rates of benzotriazoles and benzothiazoles under UV-C irradiation and the advanced oxidation process UV/H<sub>2</sub>O<sub>2</sub>. *Water Research*. **2015**, 74, 143-154.
- <sup>4</sup> Watts, M. J.; Linden, K. G. Chlorine photolysis and subsequent OH radical production during UV treatment of chlorinated water. *Water Research*. **2007**, 41 (13), 2871-2878.
- <sup>5</sup> An, D.; Westerhoff, P.; Zheng, M.; Wu, M.; Yang, Y.; Chiu, C. A. UV-activated persulfate oxidation and regeneration of NOM-Saturated granular activated carbon. *Water Research*. **2015**, 73, 304-310.
- <sup>6</sup> Yang, Y.; Pignatello, J. J.; Ma, J.; Mitch, W. A. Effect of matrix components on UV/H<sub>2</sub>O<sub>2</sub> and UV/S<sub>2</sub>O<sub>8</sub><sup>2-</sup> advanced oxidation processes for trace organic degradation in reverse osmosis brines from municipal wastewater reuse facilities. *Water Research*. **2016**, 89, 192-200.
- <sup>7</sup> Remucal, C. K.; Manley, D. Emerging investigators series: the efficacy of chlorine photolysis as an advanced oxidation process for drinking water treatment. *Environmental Science: Water Research & Technology*. **2016**, 2 (4), 565-579.
- <sup>8</sup> Soltermann, F.; Widler, T.; Canonica, S.; von Gunten, U. Photolysis of inorganic chloramine and efficiency of trichloramine abatement by UV treatment of swimming pool water. *Water Research*. **2014**, 56, 280-291.
- <sup>9</sup> Von Sonntag, C. Advanced oxidation processes: mechanistic aspects. *Water Science and Technology*. **2008**, 58 (5), 1015-1021.
- <sup>10</sup> Mohr, T. K.; Stickney, J. A.; DiGuseppi, W. H. *Environmental investigation and remediation: 1, 4-dioxane and other solvent stabilizers*. CRC Press. 2016.
- <sup>11</sup> Ozaki, H.; Li, H. Rejection of organic compounds by ultra-low pressure reverse osmosis membrane. *Water Research*. **2002**, 36 (1), 123-130.
- <sup>12</sup> Zenker, M. J.; Borden, R. C; Barlaz, M. A. Occurrence and treatment of 1,4-dioxane in aqueous environments. *Environmental Engineering Science*. **2003**, 20 (5), 423-432.

- 
- <sup>13</sup> International Agency for Research on Cancer. *IARC Monographs on the Evaluation of the Carcinogenic Risk of Chemicals to Humans*, Vol 71. 1999; pp 589-602.
- <sup>14</sup> Patton, S.; Li, W.; Couch, K.; Mezyk, S.; Ishida, K.; Liu, H. The impact of the UV photolysis of monochloramine on 1,4-dioxane removal: implications on potable water reuse. *Environmental Science & Technology Letters*. **2017**, 4 (1), 26-30.
- <sup>15</sup> Grebel, J.; Pignatello, J.; Mitch, W. Effect of halide ions and carbonates on organic contaminant degradation by hydroxyl radical-based advanced oxidation processes in saline waters. *Environmental Science & Technology*. **2010**, 44 (17), 6822-6828.
- <sup>16</sup> Lutze, H. V.; Kerlin, N.; Schmidt, T. C. Sulfate radical-based water treatment in the presence of chloride: formation of chlorate, inter-conversion of sulfate radicals into hydroxyl radicals and influence of bicarbonate. *Environmental Science & Technology*. **2015**, 72, 349-360.
- <sup>17</sup> Mark, G.; Schuchmann, M. N.; Schuchmann, H. P.; Von Sonntag, C. The photolysis of potassium peroxodisulphate in aqueous solution in the presence of tert-butanol: a simple actinometer for 254 nm radiation. *Journal of Photochemistry and Photobiology A: Chemistry*. **1990**, 55 (2), 157-168.
- <sup>18</sup> Li, W.; Jain, T.; Ishida, K.; Liu, H. A mechanistic understanding of the degradation of trace organic contaminants by UV/hydrogen peroxide, UV/persulfate and UV/free chlorine for water reuse. *Environmental Science: Water Research & Technology*. **2017**, 3 (1), 128-138.
- <sup>19</sup> Minisci, F.; Citterio, A.; Giordano, C. Electron-transfer processes: peroxydisulfate, a useful and versatile reagent in organic chemistry. *Accounts of Chemical Research*. **1983**, 16 (1), 27-32.
- <sup>20</sup> Neta, P.; Madhavan, V.; Zemel, H.; Fessenden, R. W. Rate constants and mechanism of reaction of sulfate radical anion with aromatic compounds. *Journal of the American Chemical Society*. **1977**, 99 (1), 163-164.
- <sup>21</sup> Peyton, G. R. The free-radical chemistry of persulfate-based total organic carbon analyzers. *Marine Chemistry*. **1993**, 41 (1-3), 91-103.
- <sup>22</sup> Fang, G. D.; Dionysiou, D. D.; Wang, Y.; Al-Abed, S. R.; Zhou, D. M. Sulfate radical-based degradation of polychlorinated biphenyls: effects of chloride ion and reaction kinetics. *Journal of Hazardous Materials*. **2012**, 227, 394-401.
- <sup>23</sup> Qian, Y.; Guo, X.; Zhang, Y.; Peng, Y.; Sun, P.; Huang, C. H.; Niu, J.; Zhou, X.; Crittenden, J. C. Perfluorooctanoic Acid Degradation Using UV-Persulfate Process: Modeling of the Degradation and Chlorate Formation. *Environmental Science & Technology*. **2015**, 50 (2), 772-781.

- 
- <sup>24</sup> De Laat, J.; Boudiaf, N.; Dossier-Berne, F. Effect of dissolved oxygen on the photodecomposition of monochloramine and dichloramine in aqueous solution by UV irradiation at 253.7 nm. *Water Research*. **2010**, *44* (10), 3261-3269.
- <sup>25</sup> Cooper, W. J.; Jones, A. C.; Whitehead, R. F.; Zika, R. G. Sunlight-induced photochemical decay of oxidants in natural waters: Implications in ballast water treatment. *Environmental Science & Technology*. **2007**, *41* (10), 3728-3733.
- <sup>26</sup> Li, J.; Blatchley, E. R. UV photodegradation of inorganic chloramines. *Environmental Science & Technology*. **2008**, *43* (1), 60-65.
- <sup>27</sup> Hansen, K. M. S.; Zortea, R.; Piketty, A.; Vega, S. R.; Andersen, H. R. Photolytic removal of DBPs by medium pressure UV in swimming pool water. *Science of the Total Environment*. **2013**, *443*, 850-856.
- <sup>28</sup> Yang, Y.; Pignatello, J. J.; Ma, J.; Mitch, W. A. Comparison of halide impacts on the efficiency of contaminant degradation by sulfate and hydroxyl radical-based advanced oxidation processes (AOPs). *Environmental Science & Technology*. **2014**, *48* (4), 2344-2351.
- <sup>29</sup> Zhang, R.; Sun, P.; Boyer, T. H.; Zhao, L.; Huang, C. H. Degradation of pharmaceuticals and metabolite in synthetic human urine by UV, UV/H<sub>2</sub>O<sub>2</sub>, and UV/PDS. *Environmental Science & Technology*. **2015**, *49* (5), 3056-3066.
- <sup>30</sup> Yang, Q.; Choi, H.; Chen, Y.; Dionysiou, D. Heterogeneous activation of peroxymonosulfate by supported cobalt catalysts for the degradation of 2,4-dichlorophenol in water: the effect of support cobalt precursor and UV radiation. *Applied Catalyst B: Environmental*. **2008**, *77* (3), 300-307.
- <sup>31</sup> Choi, J.; Valentine, R. L. Formation of N-nitrosodimethylamine (NDMA) from reaction of monochloramine: a new disinfection by-product. *Water Research*. **2002**, *36* (4), 817-824.
- <sup>32</sup> American Public Health Association (APHA), *Standard Methods for the Examination of Water and Wastewater 18<sup>th</sup> ed.*, American Public Health Association: Washington, DC, USA, 1992.
- <sup>33</sup> Liang, C.; Huang, C. F.; Mohanty, N.; Kurakalva, R. M. A rapid spectrophotometric determination of persulfate anion in ISCO. *Chemosphere*. **2008**, *73* (9), 1540-1543.
- <sup>34</sup> Neta, P.; Dorfman, L. M. Pulse radiolysis studies. XIII. Rate constants for the reaction of hydroxyl radicals with aromatic compound in aqueous solutions. **1968**. Ohio State Univ., Columbus.
- <sup>35</sup> Hasegawa, K.; Neta, P. Rate constants and mechanisms of reaction of chloride (Cl<sub>2</sub><sup>-</sup>)

- 
- radicals. *The Journal of Physical Chemistry*. **1978**, 82 (8), 854-857.
- <sup>36</sup> Patton, S.; Li, W.; Couch, K.; Mezyk, S.; Ishida, K.; Liu, H. The impact of the UV photolysis of monochloramine on 1,4-dioxane removal: implications on potable water reuse. *Environmental Science & Technology Letters*. **2017**, 4 (1), 26-30.
- <sup>37</sup> McElroy, W. J. A laser photolysis study of the reaction of  $\text{SO}_4^-$  with  $\text{Cl}^-$  and the subsequent decay of  $\text{Cl}_2^-$  in aqueous solution. *Journal of Physical Chemistry*. **1990**, 94 (6), 2435-2441.
- <sup>38</sup> Neta, P.; Madhavan, V.; Zemel, H.; Fessenden, R. W. Rate constants and mechanism of reaction of  $\text{SO}_4^-$  with aromatic compounds. [Pulse radiolysis study]. *Journal of American Chemical Society*. **1977**, 99 (1).
- <sup>39</sup> Neta, P.; Maruthamuthu, P.; Carton, P. M.; Fessenden, R. W. Formation and reactivity of the amino radical. *The Journal of Physical Chemistry*. **1978**, 82 (17), 1875-1878.
- <sup>40</sup> Patton, S.; Li, W.; Couch, K.; Mezyk, S.; Ishida, K.; Liu, H. The impact of the UV photolysis of monochloramine on 1,4-dioxane removal: implications on potable water reuse. *Environmental Science & Technology Letters*. **2017**, 4 (1), 26-30.
- <sup>41</sup> Eibenberger, J. Pulse radiolytic investigations concerning the formation and the oxidation of organic radicals in aqueous solutions. *INIS*. **1980**, 15 (08) 95.
- <sup>42</sup> Huie, R. E.; Clifton, C. L.; Kafafi, S. A. Rate constants for hydrogen abstraction reactions of the sulfate radical,  $\text{SO}_4^-$ : Experimental and theoretical results for cyclic ethers. *The Journal of Physical Chemistry*. **1991**, 95 (23), 9336-9340.
- <sup>43</sup> Lanni, J. C., Kintecus, Windows version 4.55. [www.kintecus.com](http://www.kintecus.com). **2012**.
- <sup>44</sup> Li, W.; Orozco, R.; Camargos, N.; Liu, H. Mechanisms on the Impacts of Alkalinity, pH, and Chloride on Persulfate-Based Groundwater Remediation. *Environmental Science & Technology*. **2017**, 51 (7), 3948-3959.
- <sup>45</sup> Eibenberger, J. Pulse radiolytic investigations concerning the formation and the oxidation of organic radicals in aqueous solutions. *INIS*. **1980**, 15 (08) 95.
- <sup>46</sup> Vikesland, P. J.; Ozekin, K.; Valentine, R. L. Effect of natural organic matter on monochloramine decomposition: pathway elucidation through the use of mass and redox balances. *Environmental Science & Technology*. **1998**, 32 (10), 1409-1416.
- <sup>47</sup> Zawadzki, J. The mechanism of ammonia oxidation and certain analogous reactions. *Discussions of the Faraday Society*. **1950**, 8, 140-152.

- 
- <sup>48</sup> Stefan, M. I.; Bolton, J. R. Mechanism of the degradation of 1, 4-dioxane in dilute aqueous solution using the UV/hydrogen peroxide process. *Environmental Science & Technology*. **1998**, *32* (11), 1588-1595.
- <sup>49</sup> Maurino, V.; Calza, P.; Minero, C.; Pelizzetti, E.; Vincenti, M. Light-assisted 1, 4-dioxane degradation. *Chemosphere*. **1997**, *35* (11), 2675-2688.
- <sup>50</sup> Neta, P.; Huie, R. E.; Maruthamuthu, P.; Steenzen, S. Solvent effects in the reactions of peroxy radicals with organic reductants: evidence for proton-transfer-mediated electron transfer. *The Journal of Physical Chemistry*. **1989**, *93* (22), 7654-7659.
- <sup>51</sup> Ross, A. B.; Mallard, W. G.; Helman, W. P.; Buxton, G. V.; Huie, R. E.; Neta, P. NDRL-NIST solution kinetics database. *National Institute of Standards and Technology (NIST)*, 1998.
- <sup>52</sup> Neta, P.; Maruthamuthu, P.; Carton, P. M.; Fessenden, R. W. Formation and reactivity of the amino radical. *The Journal of Physical Chemistry*. **1978**, *82* (17), 1875-1878.
- <sup>53</sup> Vikesland, P. J.; Ozekin, K.; Valentine, R. L. Monochloramine decay in model and distribution system waters. *Water Research*. **2001**, *35* (7), 1766-1776.
- <sup>54</sup> Schmalz, C.; Frimmel, F. H.; Zwiener, C. Trichloramine in swimming pools—formation and mass transfer. *Water Research*. **2011**, *45* (8), 2681-2690.
- <sup>55</sup> Zhang, X.; Li, W.; Blatchley, E. R.; Wang, X.; Ren, P. UV/chlorine process for ammonia removal and disinfection by-product reduction: comparison with chlorination. *Water Research*. **2015**, *68*, 804-811.

## **Chapter 4**

# **Modeling Approach for A Mechanistic Understanding of the Degradation of Trace Organic Contaminants by UV/Hydrogen Peroxide, UV/Persulfate and UV/Free Chlorine for Water Reuse**

**Previously Published in *Environmental Science: Water Research  
& Technology***

Li, Wei, Tushar Jain, Kenneth Ishida and Haizhou Liu

## 4.1 Introduction

Water scarcity is one of the most challenging global issues. The availability of high-quality fresh water sources continues to decrease due to population growth, urbanization and climate change.<sup>1-2</sup> To address water scarcity, potable water reuse – a viable means to increase drinking water supplies from untraditional sources including treated wastewater – has been proposed and employed in the recent decade.<sup>3-5</sup> It is estimated that approximately 12 billion gallons of municipal wastewater effluent is discharged to the ocean in the U.S. everyday; this is equivalent to 27% of the total U.S. public water supply.<sup>2</sup> Reclamation of these effluent discharges would directly augment available drinking water resources. Currently, only approximately 10% of the effluent is reused in the U.S.<sup>2</sup>

Conventionally treated wastewater effluent contains a variety of trace organic contaminants including pesticides, pharmaceuticals and personal care products.<sup>6-9</sup> Ultraviolet-based advanced oxidation processes (UV/AOPs) have been increasingly required as part of the treatment train process to remove these contaminants. During UV treatment, an oxidant is photolyzed to generate short-lived radicals. Hydrogen peroxide (H<sub>2</sub>O<sub>2</sub>) is the most widely used oxidant to generate reactive hydroxyl radicals (HO•) (Reaction 1):



Recently, UV/persulfate (S<sub>2</sub>O<sub>8</sub><sup>2-</sup>) has been proposed and sulfate radicals (SO<sub>4</sub>•<sup>-</sup>) are generated as the radical initiation step (Reaction 2):



$\text{SO}_4^{\bullet-}$  has a similar oxidizing power ( $E_{\text{SO}_4^{\bullet-}/\text{SO}_4^{2-}}^0 = 2.5\text{--}3.1$  V) compared to  $\text{HO}^{\bullet}$  ( $E_{\text{HO}^{\bullet}/\text{H}_2\text{O}}^0 = 1.9\text{--}2.7$  V), but possesses higher reaction rate constants with electron-rich contaminants.<sup>10</sup> This feature has made  $\text{SO}_4^{\bullet-}$  an efficient oxidant for groundwater remediation.<sup>11-12</sup> Furthermore,  $\text{S}_2\text{O}_8^{2-}$  has a 40% higher quantum yield ( $\Phi=0.7$ , Reaction 2)<sup>13</sup> compared to  $\text{H}_2\text{O}_2$  under UV irradiation at 254 nm ( $\Phi=0.5$ , Reaction 1),<sup>14</sup> thus generating more radicals than  $\text{H}_2\text{O}_2$ .

In addition, UV/chlorine (denoted as UV/HOCl) has become more popular in recent years.<sup>15-18</sup> Chlorine is the most commonly used disinfectant and can be combined with a UV source as an AOP system.<sup>19-20</sup> HOCl in solution exists as hypochlorous acid (HOCl) or hypochlorite ion ( $\text{OCl}^-$ ) with a  $\text{pK}_a$  of 7.6. Photolysis of chlorine can simultaneously produce  $\text{HO}^{\bullet}$  and chlorine atom ( $\text{Cl}^{\bullet}$ ):



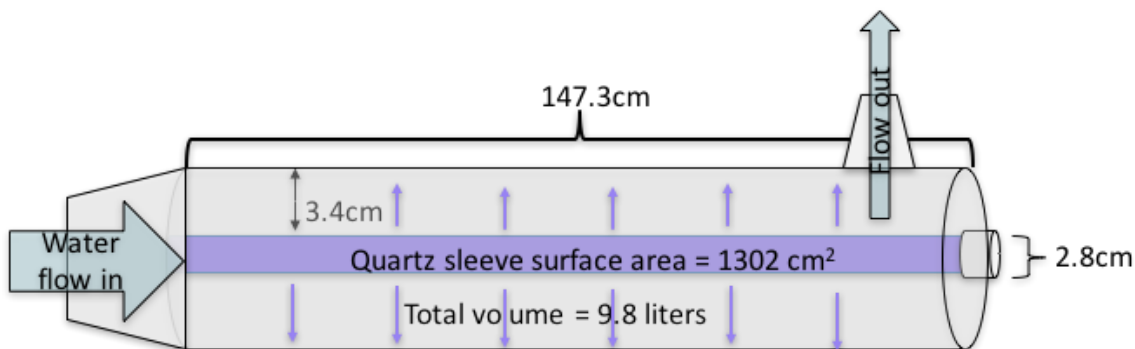
The redox potential of  $\text{Cl}^{\bullet}$  is comparable to that of  $\text{HO}^{\bullet}$  and  $\text{SO}_4^{\bullet-}$  ( $E_{\text{Cl}^{\bullet}/\text{Cl}^-}^0 = 2.41$  V).<sup>21</sup>  $\text{O}^{\bullet-}$  can further react with  $\text{H}_2\text{O}$  to generate  $\text{HO}^{\bullet}$ .<sup>22</sup> The quantum yield of HOCl is 40% higher than that of  $\text{OCl}^-$  ( $\Phi=0.7$  in Reaction 3 vs.  $\Phi=0.5$  in Reaction 4).<sup>20,23</sup>

A better understanding of the detailed mechanisms of radical distribution and transformation in UV/AOPs associated with contaminant removal are needed. Hundreds of radical reactions can impact the reaction pathways. While it is impossible to directly measure each radical under different chemical conditions, the application of a kinetic model can provide valuable insight into the radical pathways and predict the performance of AOPs. Prior studies have developed a variety of models including the steady-state radical model,<sup>24-31</sup> AdOx model,<sup>32</sup> probe model<sup>33</sup> and computational fluid dynamic model.<sup>34-36</sup> Although prior models had good estimations, there lacks a comprehensive model that can predict different UV/AOP performances in chemical conditions relevant to potable water reuse.

Ultimately, the efficiency of UV/AOPs on contaminant removal depends on the yields of reactive radicals (*e.g.*, HO<sup>•</sup>, SO<sub>4</sub><sup>•-</sup>, and Cl<sup>•</sup>), their reactivities with specific contaminants, and the solution chemical conditions that can impact the distribution and transformation of radicals. Solution chemical conditions including pH, bicarbonate, chloride and bromide can transform HO<sup>•</sup>, SO<sub>4</sub><sup>•-</sup>, and Cl<sup>•</sup> into secondary radicals such as carbonate radical (CO<sub>3</sub><sup>•-</sup>) and reactive halide radicals (*e.g.*, Cl<sub>2</sub><sup>•-</sup>, ClOH<sup>•-</sup> and Br<sup>•</sup>). These secondary radicals can exhibit distinct reactivities with trace organic contaminants compared to primary radicals, and consequently impact the rate of contaminant degradation.  
22,37

The objective of this work was to develop a kinetic model in order to investigate radical generation mechanisms in three UV/AOP systems, *i.e.*, UV/H<sub>2</sub>O<sub>2</sub>, UV/S<sub>2</sub>O<sub>8</sub><sup>2-</sup> and

UV/HOCl. The kinetic model was further employed to predict the degradation of trace contaminants in complex chemical conditions relevant to potable water reuse. Selective experiments were also conducted and together with the validated model to elucidate the impact of individual chemical parameters including pH, chloride and organic carbon on UV/AOP performance for water reuse. The versatile kinetic model provides a useful tool to compare the performances of different UV/AOP systems for treating a variety of contaminants of concern in a complex environment. It ultimately provides water utilities with a better direction for the design of UV/AOPs based on varying water chemical conditions.



**Scheme 8** A diagram of the single UV flow-through reactor (Trojan Technologies, London, ON). The kinetics modeling is based on the configuration of this reactor.

## 4.2 Materials and Methods

### 4.2.1 Modeling of radical reactions in UV/AOPs

The photolysis rate ( $r_p$ ) of  $\text{H}_2\text{O}_2$ ,  $\text{S}_2\text{O}_8^{2-}$  and HOCl with monochromatic low-pressure high-output (LPHO) mercury vapor UV lamp ( $\lambda=254\text{nm}$ ) was calculated as:

$$r_p = -2 \times \Phi \times I_0 \times f_{\text{oxidant}} \times f_{\text{solution}} \quad (\text{E1})$$

where  $\Phi$  is the primary quantum yield of the oxidant (mole/Einstein),  $I_0$  is volume-normalized surface irradiance from the UV reactor (Einsteins $\cdot\text{L}^{-1}\cdot\text{s}^{-1}$ ) that was calculated as  $1.27 \times 10^{-5}$  Einstein $\cdot\text{L}^{-1}\cdot\text{s}^{-1}$  based on a single UV flow-through reactor (Trojan Technologies, London, ON) (Detailed information is provided in **Appendix C-1** and **Scheme 8**),  $f_{\text{oxidant}}$  is the fraction of incident light absorbed by the oxidant and  $f_{\text{solution}}$  is the fraction absorbed by the total solution.

$$f_{\text{oxidant}} = \frac{\varepsilon_p c_p}{\sum \varepsilon_i c_i} \quad (\text{E2})$$

$$f_{\text{solution}} = 1 - 10^{-(\alpha + \sum \varepsilon_i c_i)l} \quad (\text{E3})$$

$\alpha$  is the absorption coefficient of the solution at the wavelength of 254 nm,  $\varepsilon_p$  and  $c_p$  are the molar extinction coefficient and the concentration of the oxidant, respectively ( $\text{M}^{-1}\cdot\text{cm}^{-1}$  and M),  $\varepsilon_i$  and  $c_i$  are the molar extinction coefficient and concentration of solution constituents, including natural organic matter (NOM) and contaminants, and  $l$  is the effective light path of the reactor (cm). A total of 221 elemental reactions were incorporated in the model (**Appendix C-2**). Major radical reactions are listed in **Table 8**. The kinetic model was built on the platform of Kintecus 4.55 software.<sup>38</sup>

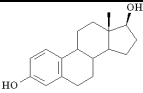
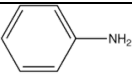
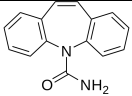
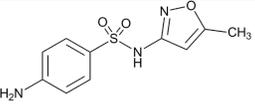
**Table 8** Major radical chain reactions that impact the distribution of radicals in UV/AOPs.

No.	Reaction	Rate Constant	Reference
1	$H_2O_2 \xrightarrow{hv} 2HO\cdot$	$1.0 \times 10^{-3} \text{ s}^{-1}$	This study
2	$S_2O_8^{2-} \xrightarrow{hv} 2SO_4^{\cdot-}$	$1.4 \times 10^{-3} \text{ s}^{-1}$	This study
3	$HOCl \xrightarrow{hv} HO\cdot + Cl\cdot$	$3.9 \times 10^{-3} \text{ s}^{-1}$	This study
4	$OCl^- \xrightarrow{hv} O^{\cdot-} + Cl\cdot$	$3.2 \times 10^{-3} \text{ s}^{-1}$	This study
5	$SO_4^{\cdot-} + H_2O \rightarrow HSO_4^- + HO\cdot$	$6.6 \times 10^2 \text{ s}^{-1}$	39
6	$SO_4^{\cdot-} + Cl^- \rightarrow SO_4^{2-} + Cl\cdot$	$3.0 \times 10^8 \text{ M}^{-1} \text{ s}^{-1}$	40
7	$Cl\cdot + H_2O \rightarrow ClOH^{\cdot-} + H^+$	$2.5 \times 10^5 \text{ s}^{-1}$	21
8	$Cl\cdot + Cl^- \rightarrow Cl_2^{\cdot-}$	$8.5 \times 10^9 \text{ M}^{-1} \text{ s}^{-1}$	41
9	$Cl_2^{\cdot-} + OH^- \rightarrow Cl^- + ClOH^{\cdot-}$	$4.5 \times 10^7 \text{ M}^{-1} \text{ s}^{-1}$	42
10	$ClOH^{\cdot-} \rightarrow HO\cdot + Cl^-$	$6.1 \times 10^9 \text{ s}^{-1}$	21
11	$HOCl + HO\cdot \rightarrow ClO\cdot + H_2O$	$2.0 \times 10^9 \text{ M}^{-1} \text{ s}^{-1}$	43
12	$HCO_3^- + HO\cdot \rightarrow CO_3^{\cdot-} + H_2O$	$8.6 \times 10^6 \text{ M}^{-1} \text{ s}^{-1}$	22
13	$HCO_3^- + SO_4^{\cdot-} \rightarrow CO_3^{\cdot-} + SO_4^{2-} + H^+$	$9.1 \times 10^6 \text{ M}^{-1} \text{ s}^{-1}$	44
14	$HCO_3^- + Cl\cdot \rightarrow CO_3^{\cdot-} + Cl^- + H^+$	$2.2 \times 10^8 \text{ M}^{-1} \text{ s}^{-1}$	78
15	$HO\cdot + Br^- \rightarrow BrOH^{\cdot-}$	$1.1 \times 10^{10} \text{ M}^{-1} \text{ s}^{-1}$	43
16	$SO_4^{\cdot-} + Br^- \rightarrow Br\cdot + SO_4^{2-}$	$3.5 \times 10^9 \text{ M}^{-1} \text{ s}^{-1}$	78
17	$Cl\cdot + Br^- \leftrightarrow ClBr^{\cdot-}$	$1.2 \times 10^{10} \text{ M}^{-1} \text{ s}^{-1}$	43
18	$ClBr^{\cdot-} \rightarrow Cl^- + Br\cdot$	$6.1 \times 10^4 \text{ s}^{-1}$	45
19	$BrOH^{\cdot-} \rightarrow HO\cdot + Br^-$	$3.3 \times 10^7 \text{ s}^{-1}$	46
20	$HO\cdot + Cl^- \rightarrow ClOH^{\cdot-}$	$4.3 \times 10^9 \text{ M}^{-1} \text{ s}^{-1}$	21
21	$Cl_2^{\cdot-} + HCO_3^- \rightarrow CO_3^{\cdot-} + 2Cl^- + H^+$	$8.0 \times 10^7 \text{ M}^{-1} \text{ s}^{-1}$	43
22	$S_2O_8^{2-} + Cl\cdot \rightarrow S_2O_8^{\cdot-} + Cl^-$	$8.8 \times 10^6 \text{ M}^{-1} \text{ s}^{-1}$	47

#### 4.2.2 Modeling of contaminant removal

Six representative trace organic contaminants were selected in this study due to their wide presence in wastewater effluent (**Table 9**). 1,4-dioxane is a widely used industrial solvent<sup>48</sup> with a drinking water notification level of 1 µg/L.<sup>49</sup> Phenol is a typical transformation product from aromatic contaminants.<sup>50 - 51</sup> 17β-estradiol is a natural estrogenic hormone.<sup>52</sup> Anilines, sulfamethoxazole and carbamazepine are frequently prescribed pharmaceuticals found in wastewater.<sup>53-55</sup>

**Table 9** Compound structure and their quantum yield, extinction coefficient and direct photolysis rate

Compound Name	Structure	Direct Photolysis Rate (s <sup>-1</sup> )	Reference
17b-estradiol		Negligible	56
1,4-dioxane		Negligible	57
Phenol		2.1 × 10 <sup>-4</sup> *	58
Aniline		Negligible	59
Carbamazepine		4.6 × 10 <sup>-4</sup> *	60
Sulfamethoxazole		1.1 × 10 <sup>-4</sup> *	61
Natural Organic Matter (NOM)		1.8 × 10 <sup>-10</sup> *	62

Based on the kinetic model, the overall degradation rate of each contaminant ( $k$ ) was a summation of direct photolysis rate ( $k_d$ ), indirect photolysis rate ( $k_i$ ) and the direct chemical reaction rate with an oxidant ( $k_o$ ):

$$k = k_d + k_i + k_o \quad (\text{E4})$$

$k_d$  is the direct photolysis rate for the test chemicals exposed to UV radiation based on equations E1–E3.  $k_i$  is controlled by reactions between the contaminant and each individual reactive radical:

$$\begin{aligned} k_i = \sum k_{R^{\bullet}} [R^{\bullet}]_{ss} = & k_{HO^{\bullet}} [HO^{\bullet}]_{ss} + k_{SO_4^{\bullet-}} [SO_4^{\bullet-}]_{ss} + k_{Cl^{\bullet}} [Cl^{\bullet}]_{ss} + k_{Cl_2^{\bullet-}} [Cl_2^{\bullet-}]_{ss} + \\ & k_{CO_3^{\bullet-}} [CO_3^{\bullet-}]_{ss} + k_{Br^{\bullet}} [Br^{\bullet}]_{ss} + k_{Br_2^{\bullet-}} [Br_2^{\bullet-}]_{ss} + k_{BrCl^{\bullet-}} [BrCl^{\bullet-}]_{ss} + \\ & k_{BrOH^{\bullet-}} [BrOH^{\bullet-}]_{ss} + k_{ClOH^{\bullet-}} [ClOH^{\bullet-}]_{ss} \end{aligned} \quad (\text{E5})$$

$[R^{\bullet}]_{ss}$  is the steady-state concentration of each individual radical  $R^{\bullet}$ . It is determined by the photolysis rate of an oxidant ( $r_p$ ) and the consumption rate of scavenging reactions:

$$[R^{\bullet}]_{ss} = - \frac{r_p}{\sum k_{R^{\bullet},s} [scavenger]_i} \quad (\text{E6})$$

$[scavenger]_i$  is the concentration of scavengers, *e.g.*,  $Cl^-$ ,  $HCO_3^-$ ,  $Br^-$ , and NOM.  $k_{R^{\bullet}}$  is the second-order rate constant of a reaction between a contaminant and  $R^{\bullet}$  (**Table 10**).  $k_{R^{\bullet},s}$  is the rate constant of a reaction between  $R^{\bullet}$  and a scavenger. These values were obtained from radiolysis literature or estimated based on prior literature.<sup>63</sup> When the rate constants were estimated (**Table 10**), the reaction rates were averaged by using the highest possible rate constants and the lowest possible rate constants, and the uncertainty was represented

as error bars. Although the transformation products of contaminants can react with radicals, those reactions were not considered in the kinetic model due to their lower concentrations and resultant smaller branching ratios in competitive kinetics.

**Table 10** Rate constants of reactions between selected organic contaminants and radicals

Contaminant	HO• (M <sup>-1</sup> s <sup>-1</sup> )	SO <sub>4</sub> <sup>-•</sup> (M <sup>-1</sup> s <sup>-1</sup> )	Cl• (M <sup>-1</sup> s <sup>-1</sup> )	Cl <sub>2</sub> <sup>-•</sup> (M <sup>-1</sup> s <sup>-1</sup> )	ClOH• (M <sup>-1</sup> s <sup>-1</sup> )
17β-estradiol	1.4×10 <sup>10</sup>	1.2×10 <sup>9</sup>	1.3–1.6×10 <sup>10</sup> *	2.0–2.4×10 <sup>7</sup> *	2.0–2.4×10 <sup>7</sup> *
Phenol	6.6×10 <sup>9</sup>	8.8×10 <sup>9</sup>	2.5×10 <sup>10</sup>	3.2×10 <sup>8</sup>	5.0–6.0×10 <sup>6</sup> *
Aniline	8.6×10 <sup>9</sup>	9.0×10 <sup>9</sup>	4.0×10 <sup>10</sup>	3.4–4.1×10 <sup>8</sup>	3.4–4.1×10 <sup>8</sup>
Sulfamethoxazole	4.9×10 <sup>9</sup>	1.3×10 <sup>10</sup>	4.4–5.4×10 <sup>9</sup> *	4.0–4.8×10 <sup>8</sup> *	4.0–4.8×10 <sup>8</sup> *
1,4-dioxane	3.1×10 <sup>9</sup>	4.1×10 <sup>7</sup>	2.8–3.4×10 <sup>9</sup> *	1.0×10 <sup>5-6</sup> *	1.0×10 <sup>5-6</sup> *
Carbamazepine	2.1×10 <sup>9</sup>	8.8×10 <sup>9</sup>	1.8–3.7×10 <sup>9</sup> *	2.1–2.5×10 <sup>6</sup> *	2.1–2.5×10 <sup>6</sup> *
Contaminant	CO <sub>3</sub> <sup>-•</sup> (M <sup>-1</sup> s <sup>-1</sup> )	Br• (M <sup>-1</sup> s <sup>-1</sup> )	Br <sub>2</sub> <sup>-•</sup> (M <sup>-1</sup> s <sup>-1</sup> )	ClBr• (M <sup>-1</sup> s <sup>-1</sup> )	
17β-estradiol	2.2×10 <sup>7</sup>	1.3–1.6×10 <sup>9</sup> *	2.0–2.4×10 <sup>7</sup> *	2.0–2.4×10 <sup>7</sup> *	
Phenol	4.9×10 <sup>6</sup>	5.9–7.3×10 <sup>8</sup> *	6.0×10 <sup>6</sup>	5.0–6.0×10 <sup>6</sup> *	
Aniline	5.4×10 <sup>8</sup>	7.7–9.5×10 <sup>8</sup> *	2.1×10 <sup>8</sup>	3.4–4.1×10 <sup>8</sup>	
Sulfamethoxazole	4.4×10 <sup>8</sup>	4.4–5.4×10 <sup>8</sup> *	4.0–4.8×10 <sup>8</sup> *	4.0–4.8×10 <sup>8</sup> *	
1,4-dioxane	1.0×10 <sup>2-6</sup> *	1.2×10 <sup>6</sup>	1.0×10 <sup>5-6</sup> *	1.0×10 <sup>5-6</sup> *	
Carbamazepine	2.3×10 <sup>6</sup>	7.9–9.7×10 <sup>9</sup> *	2.1–2.5×10 <sup>6</sup> *	2.1–2.5×10 <sup>6</sup> *	

\* Rates constants are estimated base on the known reactivity of radicals with other similar compounds

$k_o$  was only considered important during chlorine oxidation of aniline and carbamazepine in UV/HOCl.<sup>64</sup> In those cases,  $k_o$  was calculated as  $k_{HOCl}[HOCl]$ , where  $k_{HOCl}$  is the second-order rate constant between the contaminant and chlorine, and  $[HOCl]$  is the concentration of hypochlorous acid. Rate in Eq. 4 are normalized by UV irradiance and expressed in units of cm<sup>2</sup>·mW<sup>-1</sup>·s<sup>-1</sup>. Reactions with OCl<sup>-</sup> were not considered because OCl<sup>-</sup> was not the major free chlorine species at pH 5.8 (pK<sub>a</sub>=7.53).

In water reuse UV/AOP is typically applied after reverse osmosis (RO) membrane treatment. Therefore, the solution chemistry of UV/AOP is characteristic of RO permeate. Three important water chemical parameters associated with RO permeate were examined: pH, chloride, and carbonate. Trace levels of bromide and NOM were also present (**Table 11**). The ranges of concentrations were selected based on a water reuse facility in Southern California and would be applicable to UV/AOP coupled with RO in typical treatment train step utilized for potable water reuse. Concentrations of trace organic contaminants in wastewater effluent are in the range of nM and  $\mu\text{M}$ .<sup>50,65-68</sup> In this study the initial concentrations of contaminants were set at 50 nM.<sup>69</sup>

**Table 11** Chemical compositions for selected water matrix.

<b>Chemical Parameter</b>	<b>RO Permeate *</b>	<b>Typical Range</b>	<b>Unit</b>
Chloride	80	10 – 280	$\mu\text{M}$
Inorganic Carbon	200	40 – 400	$\mu\text{M}$
Bromide	0.2	0 – 2.0	$\mu\text{M}$
TOC	0.15	0.15	mg C/L
pH	5.8	5 – 7	--
Trace Organic Contaminant	50	50	nM

\*RO permeate water quality chosen in this study, based on data from wastewater reuse treatment facility in Southern California. Typical nitrate ( $\text{NO}_3^-$ ) concentration in RO permeate ranges from 10 to 20  $\mu\text{M}$ . The absorption coefficient at 254nm and the quantum yield for  $\text{HO}^\bullet$  are low,<sup>70-71</sup> therefore, the contribution of  $\text{NO}_3^-$  is not considered in the model.

### ***4.2.3 Experimental investigation of UV/AOP performance***

All chemicals used were ACS reagent grade and used without further purification. 1,4-dioxane degradation by UV/H<sub>2</sub>O<sub>2</sub>, UV/S<sub>2</sub>O<sub>8</sub><sup>2-</sup> and UV/HOCl was conducted using a carousel photochemical reactor (ACE Glass Inc.) equipped with a 6-W monochromatic UV lamp with a wavelength of 254 nm. A solution containing 2 mM of oxidant (H<sub>2</sub>O<sub>2</sub>, S<sub>2</sub>O<sub>8</sub><sup>2-</sup>, or HOCl) and 250 μM 1,4-dioxane in synthetic RO permeate (**Table 11**) was prepared. A combination of 10 μM benzoic acid, 20 μM nitrobenzene and 20 μM N,N-dimethylaniline was added as probe compounds for HO•, SO<sub>4</sub>•-, Cl•, Cl<sub>2</sub>•- and CO<sub>3</sub>•-. (detailed calculation on steady-state concentrations of radicals was described in **Appendix C-3**). To start a UV experiment, the reaction solution was transferred to multiple 8-mL quartz tubes without headspace and placed on the UV carousel reactor. At targeted time intervals, samples from sacrificial quartz tubes were withdrawn from the reactor. The concentration of the oxidant was measured using standard colorimetric method.<sup>72-73</sup> The samples were further quenched with methanol and analyzed for concentrations of trace organic contaminants and probe compounds using an Agilent-1200 liquid chromatography system equipped with a diode array detector and a Zorbax Eclipse SB-C18 column (4.6×150 mm, 5-μm particle size).

## **4.3 Results and Discussion**

### ***4.3.1 Degradation of contaminants in RO permeate by three UV/AOPs***

The modeling predicted UV photolysis rates of oxidants in the order of HOCl > S<sub>2</sub>O<sub>8</sub><sup>2-</sup> > H<sub>2</sub>O<sub>2</sub> (Reactions 1–4 in **Table 8**, all reactions henceforth refer to **Table 8**). The

photolysis rates of HOCl and  $S_2O_8^{2-}$  were approximately 300% and 40% higher than that of  $H_2O_2$ , respectively (**Figure 23**). The degradation rates ( $k$ ) of the selected organic contaminants varied by more than one order of magnitude among UV/ $H_2O_2$ , UV/ $S_2O_8^{2-}$ , and UV/HOCl (**Figure 24**).

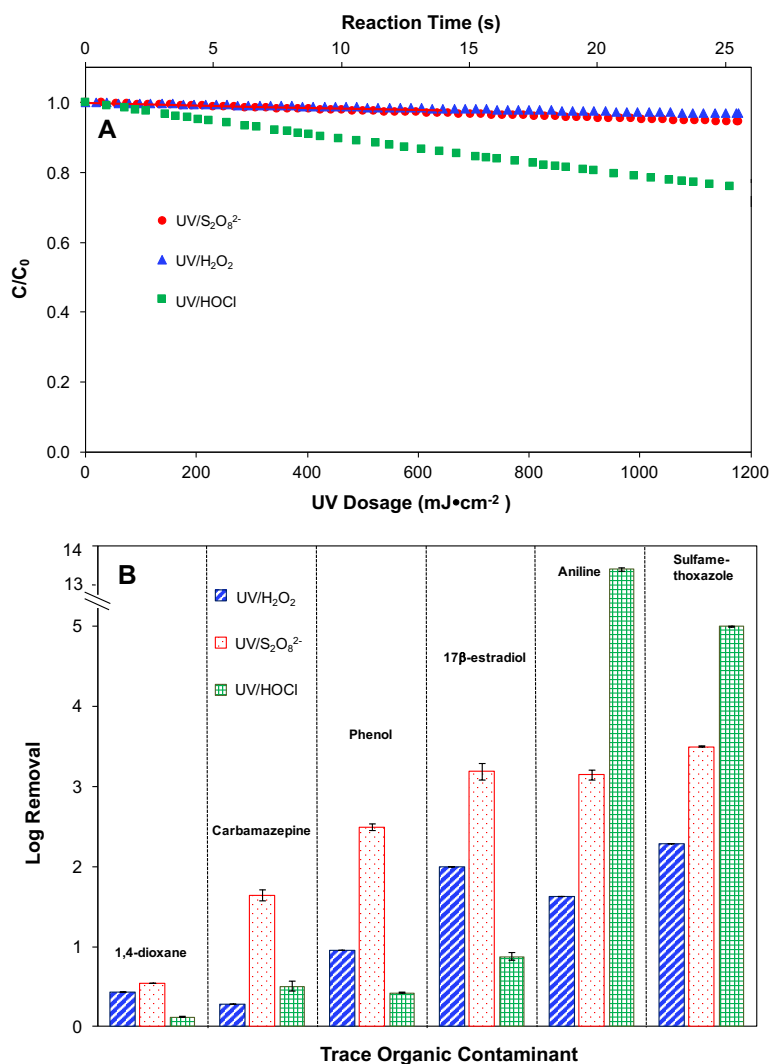


**Figure 23** Comparison of UV/ $H_2O_2$ , UV/ $S_2O_8^{2-}$  and UV/HOCl treatment based on the kinetic model. (A) Consumption of  $H_2O_2$ ,  $S_2O_8^{2-}$  and HOCl by UV irradiance. (B) Log removal of organic contaminants. [Oxidant]=88  $\mu M$ , [contaminant]=50 nM, [Cl $^-$ ]=80  $\mu M$ , [inorganic carbon]=200  $\mu M$ , [Br $^-$ ]=0.2  $\mu M$ , TOC=0.15 mg C/L, pH=8, UV irradiance=45.3 mW/cm $^2$ , UV dosage=1178 mJ/cm $^2$  in 26 seconds.

In UV/H<sub>2</sub>O<sub>2</sub>, the irradiance-normalized rates ranged from  $5.6 \times 10^{-4}$  to  $4.5 \times 10^{-3}$  cm<sup>2</sup>·mW<sup>-1</sup>·s<sup>-1</sup>. HO<sup>•</sup> contributed the most to the contaminant degradation with the exception that CO<sub>3</sub><sup>•-</sup> was important for aniline and sulfamethoxazole degradation. Direct photolysis was only important for sulfamethoxazole, which was also reported previously.<sup>74</sup>

In UV/S<sub>2</sub>O<sub>8</sub><sup>2-</sup>, the degradation rates ranged from  $1.1 \times 10^{-3}$  to  $6.8 \times 10^{-3}$  cm<sup>2</sup>·mW<sup>-1</sup>·s<sup>-1</sup>, *i.e.*, 24%–470% higher than those in UV/H<sub>2</sub>O<sub>2</sub>. Both HO<sup>•</sup> and SO<sub>4</sub><sup>•-</sup> are important for contaminant degradation. The contribution by Br<sup>•</sup> was also significant for carbamazepine, phenol, 17β-estradiol and aniline.

In UV/HOCl, the degradation rates ranged from  $2.3 \times 10^{-4}$  to  $2.6 \times 10^{-2}$  cm<sup>2</sup>·mW<sup>-1</sup>·s<sup>-1</sup>, *i.e.*, 56%–73% lower than those in UV/H<sub>2</sub>O<sub>2</sub> (**Figure 24**), mainly due to a lower yield of HO<sup>•</sup> in RO permeate chemical conditions in UV/HOCl. The exceptions were for carbamazepine, aniline and sulfamethoxazole wherein the contribution by Br<sup>•</sup>, CO<sub>3</sub><sup>•-</sup>, and HOCl chemical oxidation were also important. The log removal varied from 0.1 to 13.5 with a UV dosage of 1178 mJ/cm<sup>2</sup> (**Figure 23B**). Generally, higher log removal could be achieved in UV/S<sub>2</sub>O<sub>8</sub><sup>2-</sup>, followed by UV/H<sub>2</sub>O<sub>2</sub>, and then UV/HOCl except for aniline and sulfamethoxazole, which achieved better log removal in UV/HOCl.

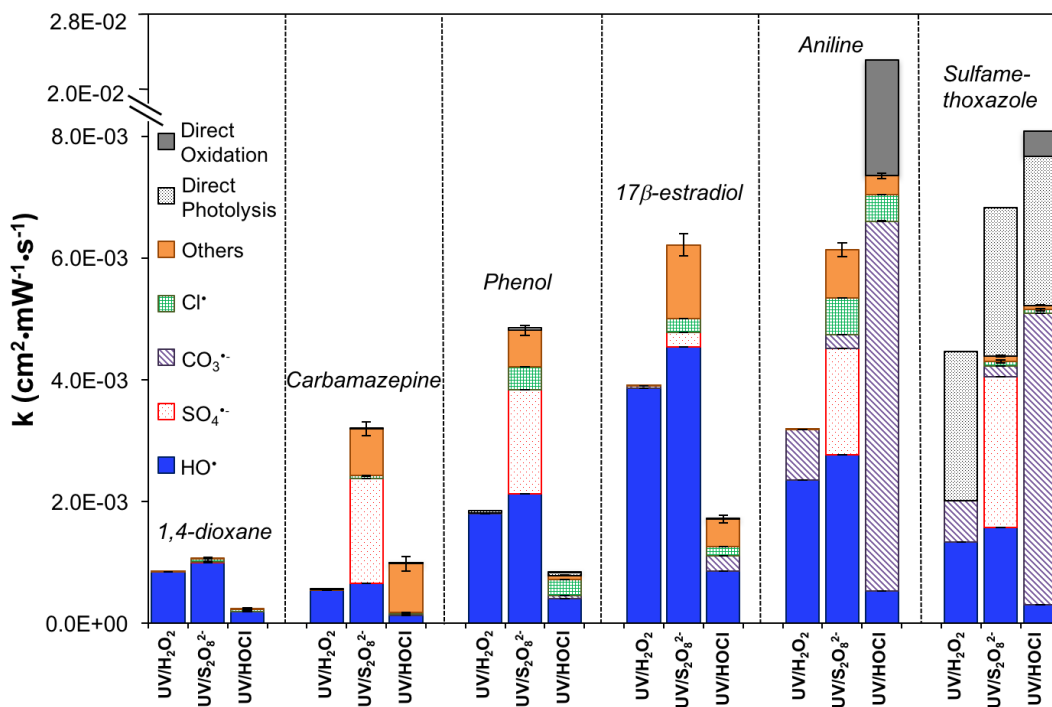


**Figure 24** The comparison of three UV/AOP systems on the degradation of six selected trace organic contaminants based on the kinetic model. [Oxidant]=88  $\mu\text{M}$ , [contaminant]=50 nM,  $[\text{Cl}^-]=80 \mu\text{M}$ , [inorganic carbon] = 0.2 mM,  $[\text{Br}^-]=0.2 \mu\text{M}$ , TOC=0.15 mg C/L, pH=5.8, UV irradiance=45  $\text{mW}/\text{cm}^2$ .



#### 4.3.2.1 Contribution of HO•

HO• is one of the most reactive radicals. It reacts non-selectively with organics at the near diffusion-limited rate constants of approximately  $10^{10} \text{ M}^{-1}\text{s}^{-1}$ .<sup>63,75</sup> It reacted with the six select contaminants with rate constants between  $2.1 \times 10^9$  and  $1.4 \times 10^{10} \text{ M}^{-1}\text{s}^{-1}$  (**Table 10**). In UV/H<sub>2</sub>O<sub>2</sub>, HO• was the major radical ( $[\text{HO}\cdot]_{\text{ss}}=1.2 \times 10^{-11} \text{ M}$ , **Table 12**) and contributed significantly to contaminant degradation (**Figure 24**). More HO• was generated in UV/S<sub>2</sub>O<sub>8</sub><sup>2-</sup> compared to UV/H<sub>2</sub>O<sub>2</sub> with a steady-state concentration 65% higher than that of SO<sub>4</sub><sup>•-</sup> (**Table 12**). The higher radical yield in UV/S<sub>2</sub>O<sub>8</sub><sup>2-</sup> was mainly due to the higher photolysis rate of S<sub>2</sub>O<sub>8</sub><sup>2-</sup> compared to H<sub>2</sub>O<sub>2</sub> (Reactions 1–2, **Table 8**). The contribution to contaminant degradation by HO• was 20% higher in UV/S<sub>2</sub>O<sub>8</sub><sup>2-</sup> than that in UV/H<sub>2</sub>O<sub>2</sub> (**Figure 24**). HO• was generated from SO<sub>4</sub><sup>•-</sup> via two pathways: hydrolysis of SO<sub>4</sub><sup>•-</sup> (Reaction 5) and Cl<sup>-</sup> scavenging effects on SO<sub>4</sub><sup>•-</sup> to produce Cl• (Reactions 6–10). In contrast, the contribution of HO• was significantly less in UV/HOCl (**Figure 24**). This was mainly due to a strong scavenging effect of HOCl on HO• (Reaction 11).

#### 4.3.2.2 Contribution of SO<sub>4</sub><sup>•-</sup>

SO<sub>4</sub><sup>•-</sup> generated in UV/S<sub>2</sub>O<sub>8</sub><sup>2-</sup> is reactive with compounds containing electron-donating functional groups including olefinic bonds, amine and hydroxyl groups.<sup>76-78</sup> Therefore, carbamazepine, phenol, aniline and sulfamethoxazole were reactive with SO<sub>4</sub><sup>•-</sup> ( $k_{\text{SO}_4\cdot^-} \sim k_{\text{HO}\cdot} \sim 10^9 \text{ M}^{-1}\text{s}^{-1}$ ), whereas 1,4-dioxane and 17β-estradiol exhibited much slower reactivity with SO<sub>4</sub><sup>•-</sup> than with HO• (*i.e.*,  $k_{\text{SO}_4\cdot^-} \leq 10\% \times k_{\text{HO}\cdot}$ ). As a result, these four

contaminants exhibited enhanced degradation rates in UV/S<sub>2</sub>O<sub>8</sub><sup>2-</sup> compared to UV/H<sub>2</sub>O<sub>2</sub> (Figure 24).

#### 4.3.2.3 Contribution of CO<sub>3</sub><sup>•-</sup>

CO<sub>3</sub><sup>•-</sup> was a major radical that formed in all three UV/AOPs (Table 12). CO<sub>3</sub><sup>•-</sup> was generated via the transformation of HO<sup>•</sup>, SO<sub>4</sub><sup>•-</sup> and Cl<sup>•</sup> in the presence of bicarbonate (Reactions 12–14). The effect was strongest in UV/HOCl, because HCO<sub>3</sub><sup>-</sup> reacts with Cl<sup>•</sup> 25 times faster than reacting with HO<sup>•</sup> or SO<sub>4</sub><sup>•-</sup>. However, CO<sub>3</sub><sup>•-</sup> reacts selectively towards compounds with amine and sulfur groups.<sup>79, 80</sup> Amine-containing aniline and sulfamethoxazole react faster with CO<sub>3</sub><sup>•-</sup> ( $k_{\text{CO}_3^{\bullet-}} > 10^8 \text{ M}^{-1}\text{s}^{-1}$ , Table 10), and their degradation was significantly enhanced in UV/HOCl in addition to direct photolysis and direct oxidation by HOCl (Figure 24).

#### 4.3.2.4 Contribution of reactive halide radicals

Two groups of halide radicals were generated by UV/AOP in the presence of Cl<sup>•</sup> and Br<sup>•</sup>: reactive chlorine species (RCS) and reactive bromine species (RBS). RCS including Cl<sup>•</sup>, Cl<sub>2</sub><sup>•-</sup> and ClOH<sup>•-</sup> can react with contaminants with rate constants as high as 10<sup>9</sup> M<sup>-1</sup>s<sup>-1</sup> (Table 10), but their steady-state concentrations were orders of magnitude lower than those of HO<sup>•</sup>, SO<sub>4</sub><sup>•-</sup>, and CO<sub>3</sub><sup>•-</sup> (Table 12). As a result, contributions from RCS to contaminant degradation were limited. RBS include Br<sup>•</sup>, Br<sub>2</sub><sup>•-</sup>, BrOH<sup>•-</sup>, and ClBr<sup>•-</sup>, but only Br<sup>•</sup> is considered reactive with contaminants.<sup>63</sup> Br<sup>•</sup> reacted with HO<sup>•</sup>, SO<sub>4</sub><sup>•-</sup>, and Cl<sup>•</sup> to

produce  $\text{BrOH}^\cdot$ ,  $\text{Br}^\cdot$ , and  $\text{ClBr}^\cdot$ , respectively (Reactions 15–19).  $\text{Br}^\cdot$  reacts with organic contaminants in similar mechanisms to  $\text{HO}^\cdot$  with reaction rate constants of  $10^9$ – $10^{10}$

$\text{M}^{-1}\text{s}^{-1}$ .<sup>63,81</sup>

**Table 12** The steady-state concentrations of radicals in three UV/AOPs. The calculation was based on typical RO permeate chemical matrix with 88  $\mu\text{M}$  of oxidant and 1178  $\text{mJ}/\text{cm}^2$  of UV irradiation.

Radical	Quasi Steady-State Concentration, $[\text{R}^\cdot]_{\text{ss}}$ (M)		
	UV/ $\text{H}_2\text{O}_2$	UV/ $\text{S}_2\text{O}_8^{2-}$	UV/ $\text{HOCl}$
$\text{HO}^\cdot$	$1.2 \times 10^{-11}$	$1.5 \times 10^{-11}$	$2.6 \times 10^{-12}$
$\text{SO}_4^{\cdot-}$	--	$8.8 \times 10^{-12}$	--
$\text{CO}_3^{\cdot-}$	$7.0 \times 10^{-11}$	$1.9 \times 10^{-11}$	$5.1 \times 10^{-10}$
$\text{Cl}^\cdot$	$5.2 \times 10^{-17}$	$6.8 \times 10^{-13}$	$4.9 \times 10^{-13}$
$\text{Cl}_2^{\cdot-}$	$5.4 \times 10^{-16}$	$7.0 \times 10^{-12}$	$5.5 \times 10^{-12}$
$\text{ClOH}^{\cdot-}$	$7.0 \times 10^{-16}$	$8.5 \times 10^{-16}$	$1.8 \times 10^{-16}$
$\text{Br}^\cdot$	$9.2 \times 10^{-15}$	$3.8 \times 10^{-11}$	$1.4 \times 10^{-11}$
$\text{Br}_2^{\cdot-}$	$1.3 \times 10^{-15}$	$4.5 \times 10^{-12}$	$1.8 \times 10^{-12}$
$\text{ClBr}^\cdot$	$1.3 \times 10^{-15}$	$4.8 \times 10^{-12}$	$2.0 \times 10^{-12}$
$\text{BrOH}^{\cdot-}$	$7.3 \times 10^{-16}$	$8.3 \times 10^{-16}$	$1.7 \times 10^{-16}$

#### 4.3.4 Model validation

1,4-dioxane and phenol degradation by UV/AOP were examined by bench-scale experiments. The kinetic model predictions matched well with the experimental data (Figure 25 and Figure 26). Approximately 0.5 to 1.0 log of removal was achieved for 1,4-dioxane and phenol, respectively. In UV/ $\text{S}_2\text{O}_8^{2-}$ , both  $\text{SO}_4^{\cdot-}$  and  $\text{HO}^\cdot$  contributed to

1,4-dioxane degradation, but only  $\text{SO}_4^{\cdot-}$  was important for phenol degradation. In UV/ $\text{H}_2\text{O}_2$ ,  $\text{HO}^{\cdot}$  was the major reactive radical. In UV/ $\text{HOCl}$ , because of the natural co-existence of chloride in free chlorine solution, chlorine dimer  $\text{Cl}_2^{\cdot-}$  was produced and contributed significantly to 1,4-dioxane degradation, whereas for phenol, direct oxidation by  $\text{HOCl}$  was predominant (**Figure 25D**). The experimental data validated the kinetic model.

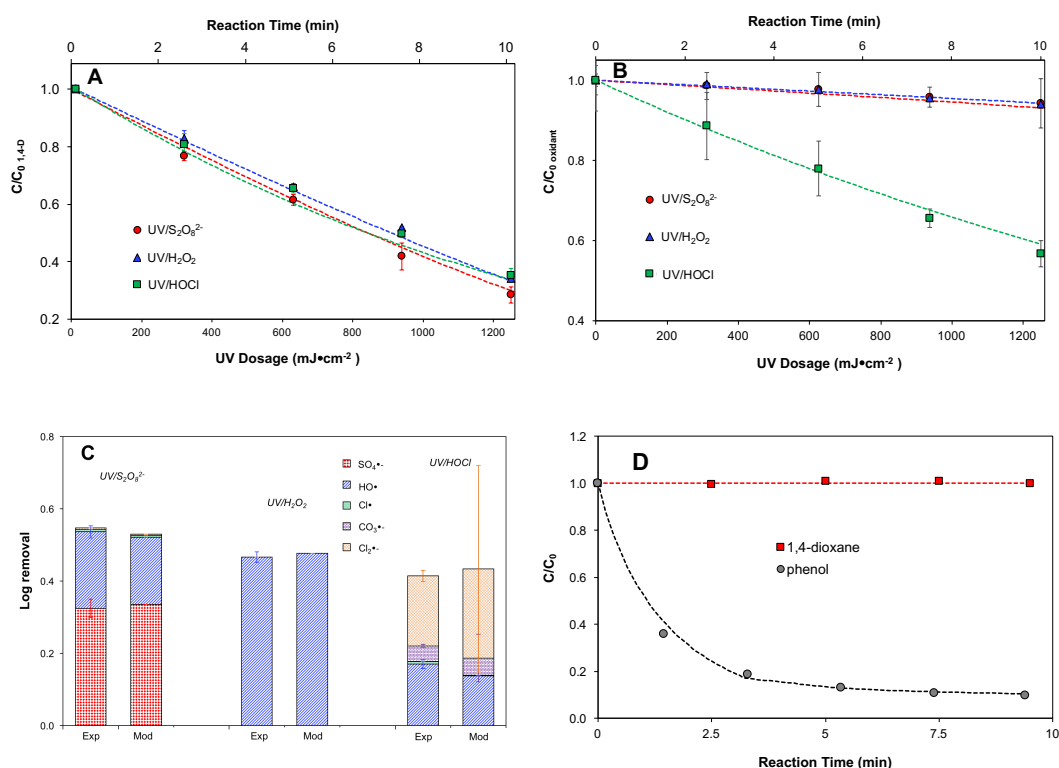


**Figure 25** 1,4-dioxane removal by UV/ $\text{H}_2\text{O}_2$ , UV/ $\text{S}_2\text{O}_8^{2-}$  and UV/ $\text{HOCl}$ . (A) First order decay of 1,4-dioxane. (B) First-order decay of  $\text{H}_2\text{O}_2$ ,  $\text{S}_2\text{O}_8^{2-}$  and  $\text{HOCl}$  by UV irradiance. (C) contribution of radicals to 1,4-dioxane decay. (D) Direct oxidation of 1,4-dioxane and phenol by  $\text{HOCl}$ . [Oxidant]=2 mM, [1,4-dioxane]=250  $\mu\text{M}$ ,  $[\text{Cl}^-]$ =80  $\mu\text{M}$ , [inorganic carbon]=200  $\mu\text{M}$ ,  $[\text{Br}^-]$ =0.2  $\mu\text{M}$ , TOC=0.15 mg C/L, pH=5.8, UV irradiance= 45.3  $\text{mW}/\text{cm}^2$ , UV dosage=1178  $\text{mJ}/\text{cm}^2$  in 26 seconds. Dash lines are modeled results.

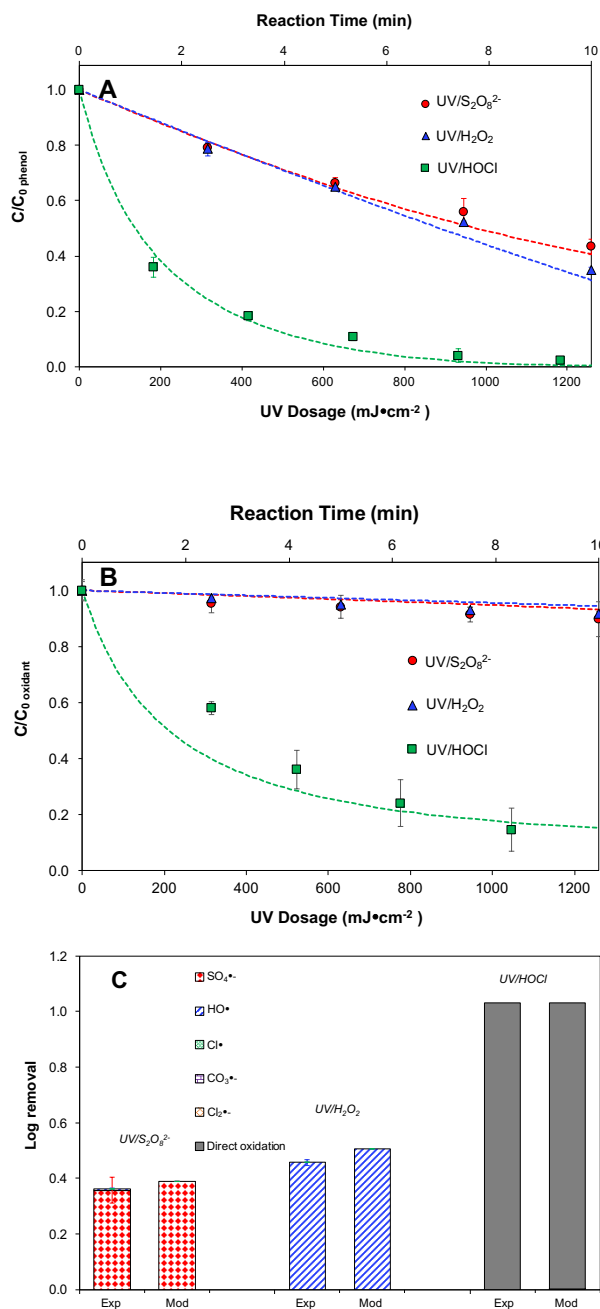


**Figure 26** Phenol removal by UV/H<sub>2</sub>O<sub>2</sub>, UV/S<sub>2</sub>O<sub>8</sub><sup>2-</sup> and UV/HOCl. (A) First order decay of phenol. (B) First order decay of H<sub>2</sub>O<sub>2</sub>, S<sub>2</sub>O<sub>8</sub><sup>2-</sup> and HOCl by UV irradiance. (C) Contribution of radicals to phenol decay. [Oxidant]=2 mM, [phenol]=250 μM, [Cl<sup>-</sup>]=80 μM, [inorganic carbon]=200 μM, [Br<sup>-</sup>]=0.2 μM, TOC=0.15 mg C/L, pH=5.8, UV irradiance= 45.3 mW/cm<sup>2</sup>, UV dosage=1178 mJ/cm<sup>2</sup> in 26 seconds. Dash lines are modeled results.

### ***4.3.5 Impact of water chemical conditions on UV/AOP performance***

#### ***4.3.5.1 Impact of pH***

The kinetic modeling results showed that UV/S<sub>2</sub>O<sub>8</sub><sup>2-</sup> was the most sensitive to pH (**Figure 27A**). [HO•]<sub>ss</sub> decreased by 50% as pH increased from 5 to 7, while the [CO<sub>3</sub><sup>•-</sup>]<sub>ss</sub> increased by 800% with the same pH increase (**Figure 27B**). As pH was increased, HCO<sub>3</sub><sup>-</sup> became the predominant carbonate species (pK<sub>a</sub>=6.35). This resulted in a faster transformation of Cl• to CO<sub>3</sub><sup>•-</sup> compared to the formation of HO• via Cl• (Reaction 14 vs. Reactions 7–10). [SO<sub>4</sub><sup>•-</sup>]<sub>ss</sub> was not sensitive to pH because the scavenging effect of SO<sub>4</sub><sup>•-</sup> by HCO<sub>3</sub><sup>-</sup> was negligible compared to the scavenging effect of Cl• (Reaction 6 vs. Reaction 13 in **Table 8**). Therefore, a reduction of contaminant degradation with increasing pH was observed in UV/S<sub>2</sub>O<sub>8</sub><sup>2-</sup> due to the decrease of [HO•]<sub>ss</sub> (**Figure 27A**).

UV/H<sub>2</sub>O<sub>2</sub> was not sensitive to pH between 5 and 7 in RO permeate chemical conditions (**Figure 28A**). As the major radical, [HO•]<sub>ss</sub> was insensitive to pH (**Figure 28B**). HO• was predominantly scavenged by Cl• to generate ClOH• (Reaction 20), but the dissociation of ClOH• produced HO• (Reaction 10). Therefore, the rate of contaminant degradation remained more or less constant with pH changes (**Figure 28A**).

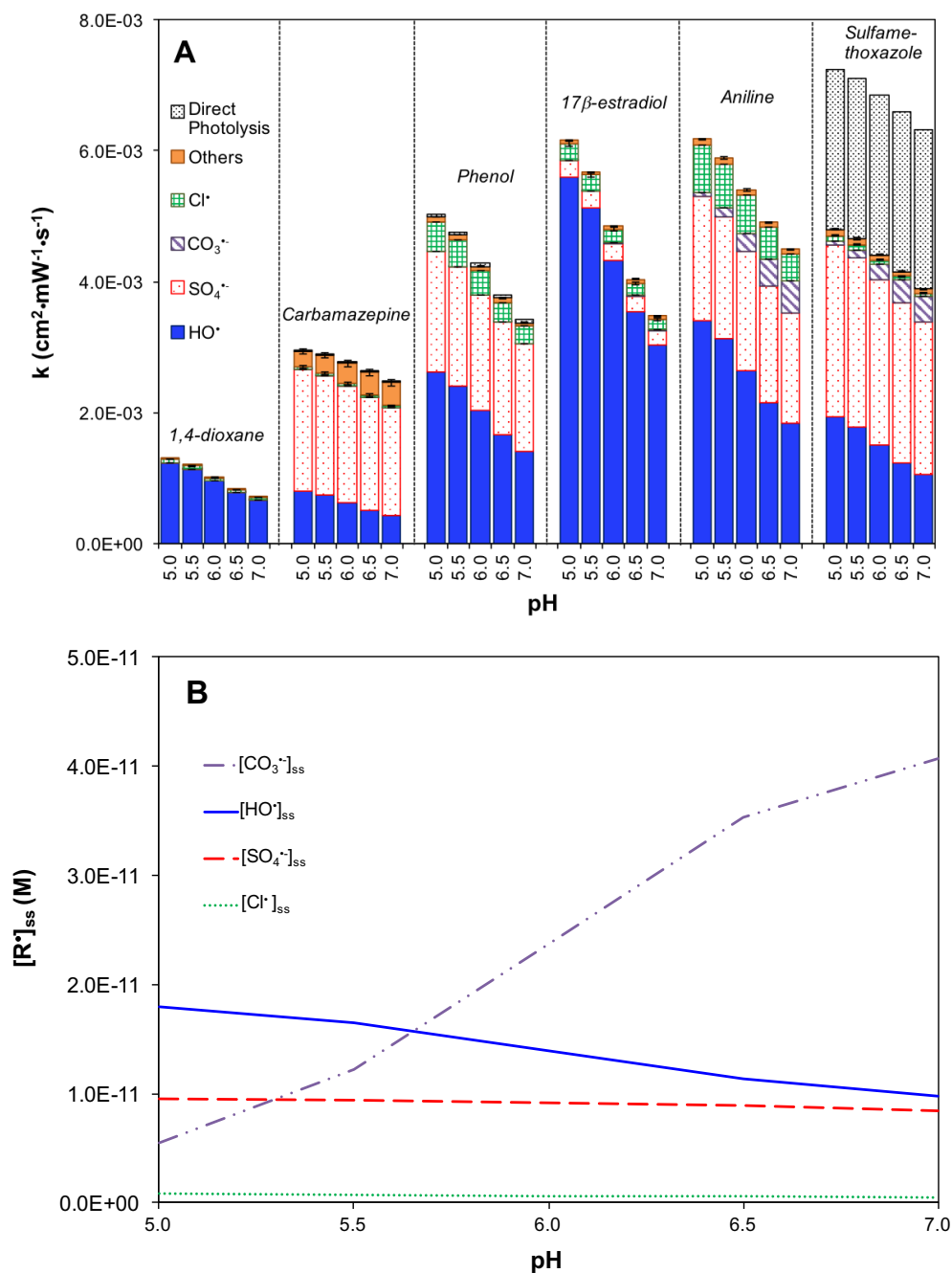


**Figure 27** The effect of pH on the treatment efficiency of UV/S<sub>2</sub>O<sub>8</sub><sup>2-</sup> based on the kinetic model. (A) first-order degradation rates of organic contaminants in treatment and (B) radical distribution. [S<sub>2</sub>O<sub>8</sub><sup>2-</sup>]=88 μM, [trace organic contaminant]=50 nM, [Cl<sup>-</sup>]=80 μM, [inorganic carbon]=0.2 mM, [Br<sup>-</sup>]=0.2 μM, TOC=0.15 mg C/L, UV irradiance=45 mW/cm<sup>2</sup>.

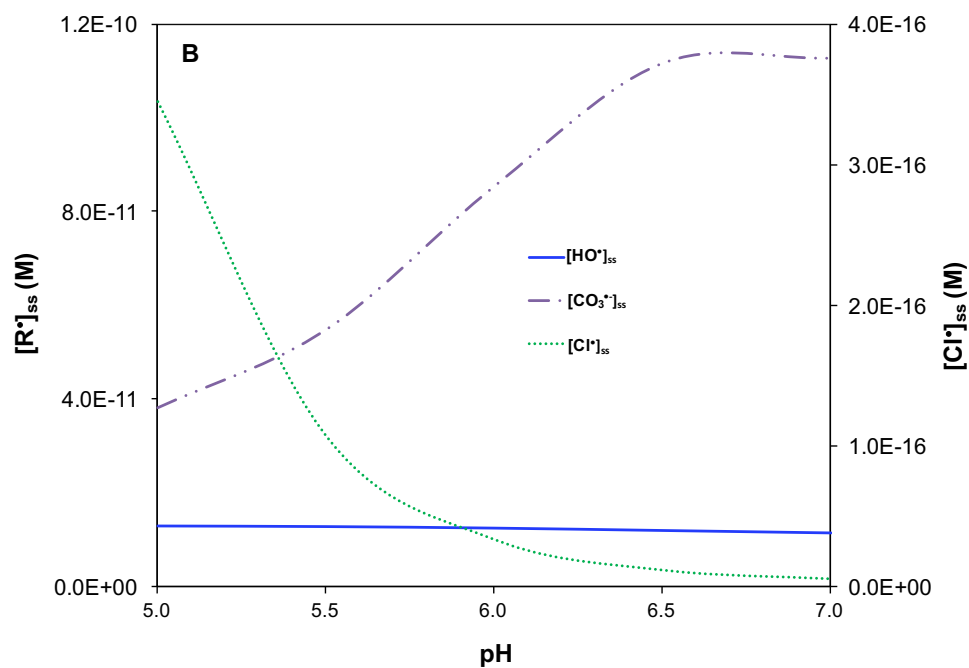
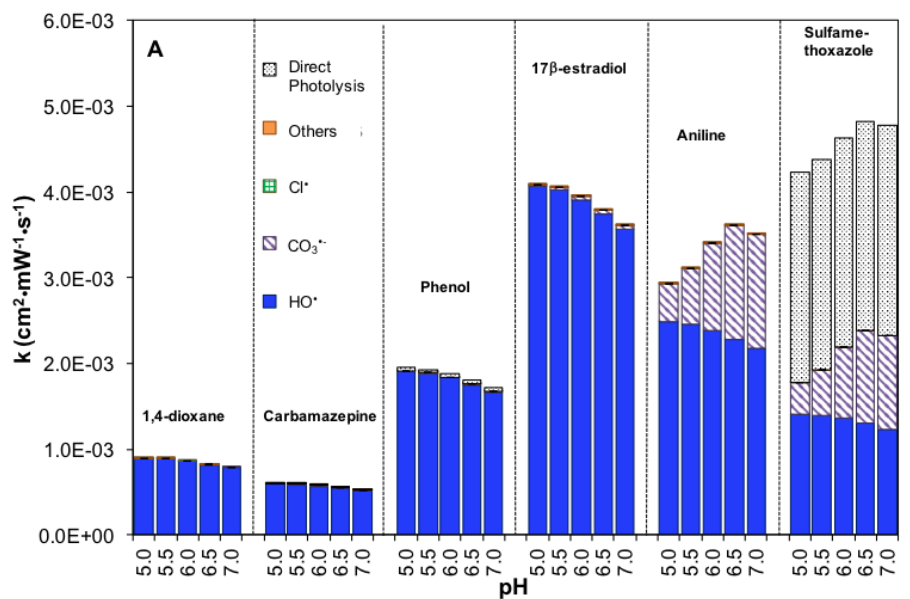


**Figure 28** Effect of pH on the treatment efficiency of UV/H<sub>2</sub>O<sub>2</sub> based on the kinetic model. (A) First-order degradation rates of organic contaminants in treatment. (B) Radical distribution. [H<sub>2</sub>O<sub>2</sub>]=88 μM, [trace organic contaminant]=50 nM, [Cl<sup>-</sup>]=0.08 mM, [inorganic carbon]=0.2 mM, [Br<sup>-</sup>]=0.2 μM, TOC=0.15 mg C/L, UV irradiance=45 mW/cm<sup>2</sup>.

UV/HOCl was modestly sensitive to pH (**Figure 29A**). The steady-state concentrations of HO<sup>•</sup>, Cl<sup>•</sup> and Br<sup>•</sup> decreased with increasing pH, mainly due to the scavenging effects of HCO<sub>3</sub><sup>-</sup> (**Figure 29B**). [HO<sup>•</sup>]<sub>ss</sub> decreased faster than [Cl<sup>•</sup>]<sub>ss</sub> and [Br<sup>•</sup>]<sub>ss</sub> because of a stronger scavenging effects of HCO<sub>3</sub><sup>-</sup> on HO<sup>•</sup> (Reaction 12 and Reaction 21). These scavenging effects resulted in a dramatic increase of [CO<sub>3</sub><sup>•-</sup>]<sub>ss</sub> (**Figure 29B**). Overall, the rate of contaminant decay decreased by 43% as pH increased from 5 to 7, except for aniline and sulfamethoxazole that were very reactive with CO<sub>3</sub><sup>•-</sup> (**Figure 29A**). The increase in pH also led to the conversion of HOCl to OCl<sup>-</sup> (pK=7.6), resulting in a decrease of direct oxidation of aniline by HOCl.

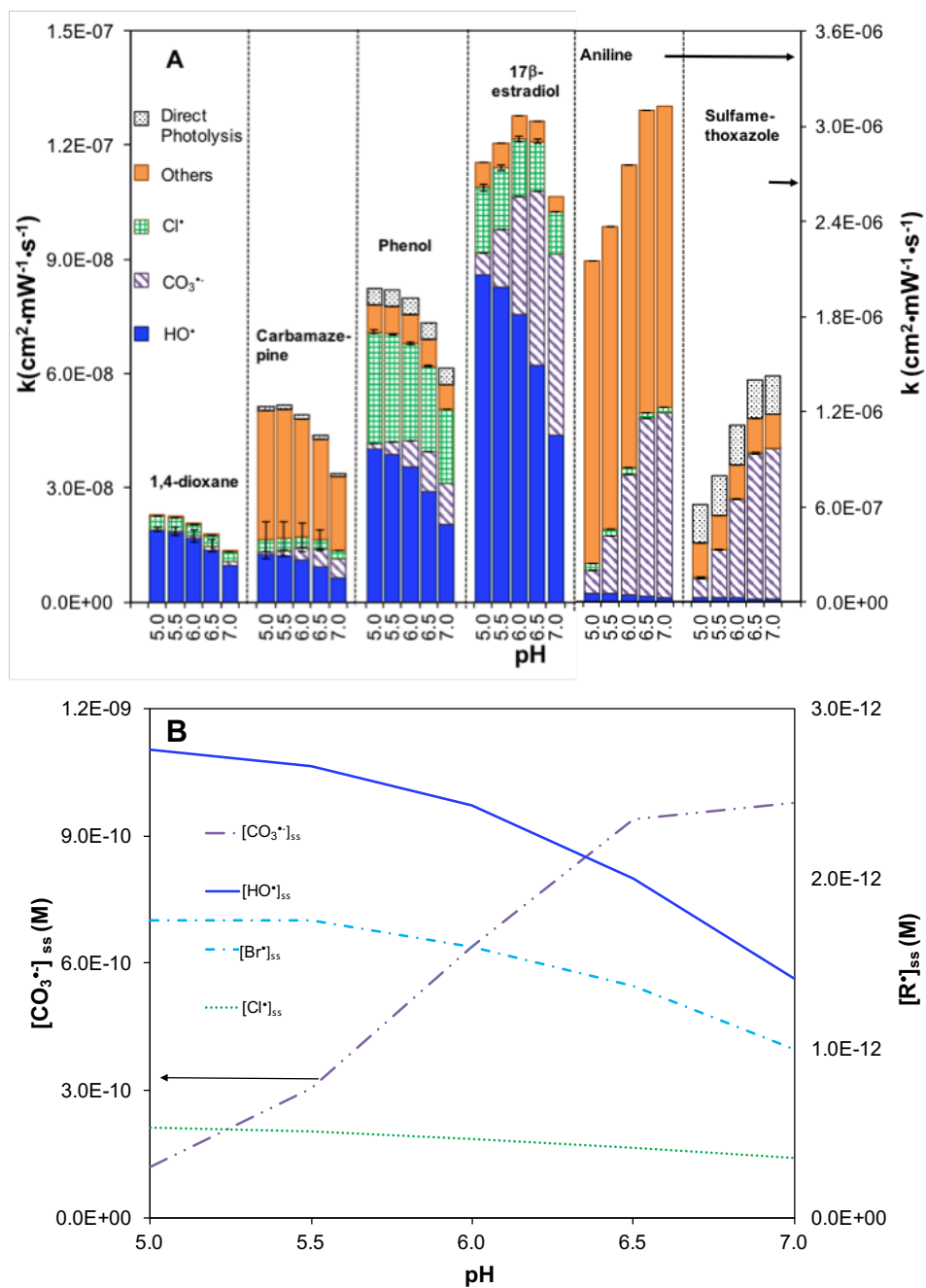


**Figure 29** Effect of pH on the treatment efficiency of UV/HOCl based on the kinetic model. (A) First-order degradation rates of organic contaminants in treatment. (B) Radical distribution. [HOCl]=88  $\mu$ M, [trace organic contaminant]=50 nM, [Cl<sup>-</sup>]=0.08 mM, [inorganic carbon]=0.2 mM, [Br<sup>-</sup>]=0.2  $\mu$ M, TOC=0.15 mg C/L, UV irradiance=45 mW/cm<sup>2</sup>.

#### 4.3.5.2 Impact of chloride

UV/S<sub>2</sub>O<sub>8</sub><sup>2-</sup> was most sensitive to chloride among the three UV/AOPs (**Figure 30A**). When Cl<sup>-</sup> concentration was increased from 10 to 280 μM, [SO<sub>4</sub><sup>•-</sup>]<sub>ss</sub> decreased by 94% due to the scavenging effect of Cl<sup>-</sup>, [HO<sup>•</sup>]<sub>ss</sub> remained stable and [CO<sub>3</sub><sup>•-</sup>]<sub>ss</sub> increased by 140% (**Figure 30A**). HO<sup>•</sup> initially increased with increasing chloride concentration due to the hydrolysis of Cl<sup>•</sup> (Reactions 7 and 10) and generation of more HO<sup>•</sup>. However, when the Cl<sup>-</sup> concentration was increased above 30 μM, Cl<sub>2</sub><sup>•-</sup> formation and its transformation to CO<sub>3</sub><sup>•-</sup> became the major pathway (Reactions 8 and 21). The rates of contaminant degradation generally decreased with increasing Cl<sup>-</sup> concentrations (**Figure 30A**).

UV/H<sub>2</sub>O<sub>2</sub> was not sensitive to chloride (**Figure 31A**). Both [HO<sup>•</sup>]<sub>ss</sub> and [CO<sub>3</sub><sup>•-</sup>]<sub>ss</sub> remained stable with changing Cl<sup>-</sup> concentration (**Figure 31B**). Although chloride can scavenge HO<sup>•</sup> (Reaction 20), the dissociation of ClOH<sup>•-</sup> quickly regenerated HO<sup>•</sup>, dampening the effects of chloride (Reactions 8-10). Because the formation of CO<sub>3</sub><sup>•-</sup> was mainly via HO<sup>•</sup> (Reaction 12), [CO<sub>3</sub><sup>•-</sup>]<sub>ss</sub> also remained stable.

In UV/HOCl, the change of Cl<sup>-</sup> concentration did not strongly affect [HO<sup>•</sup>]<sub>ss</sub>, however, decreased [Cl<sup>•</sup>]<sub>ss</sub> by 27% and increased [CO<sub>3</sub><sup>•-</sup>]<sub>ss</sub> by 400% (**Figure 32B**). This is caused by the conversion of Cl<sup>•</sup> to CO<sub>3</sub><sup>•-</sup> (Reaction 14). Consequently, this resulted in an enhanced degradation of 17β-estradiol, aniline and sulfamethoxazole (**Figure 32A**).

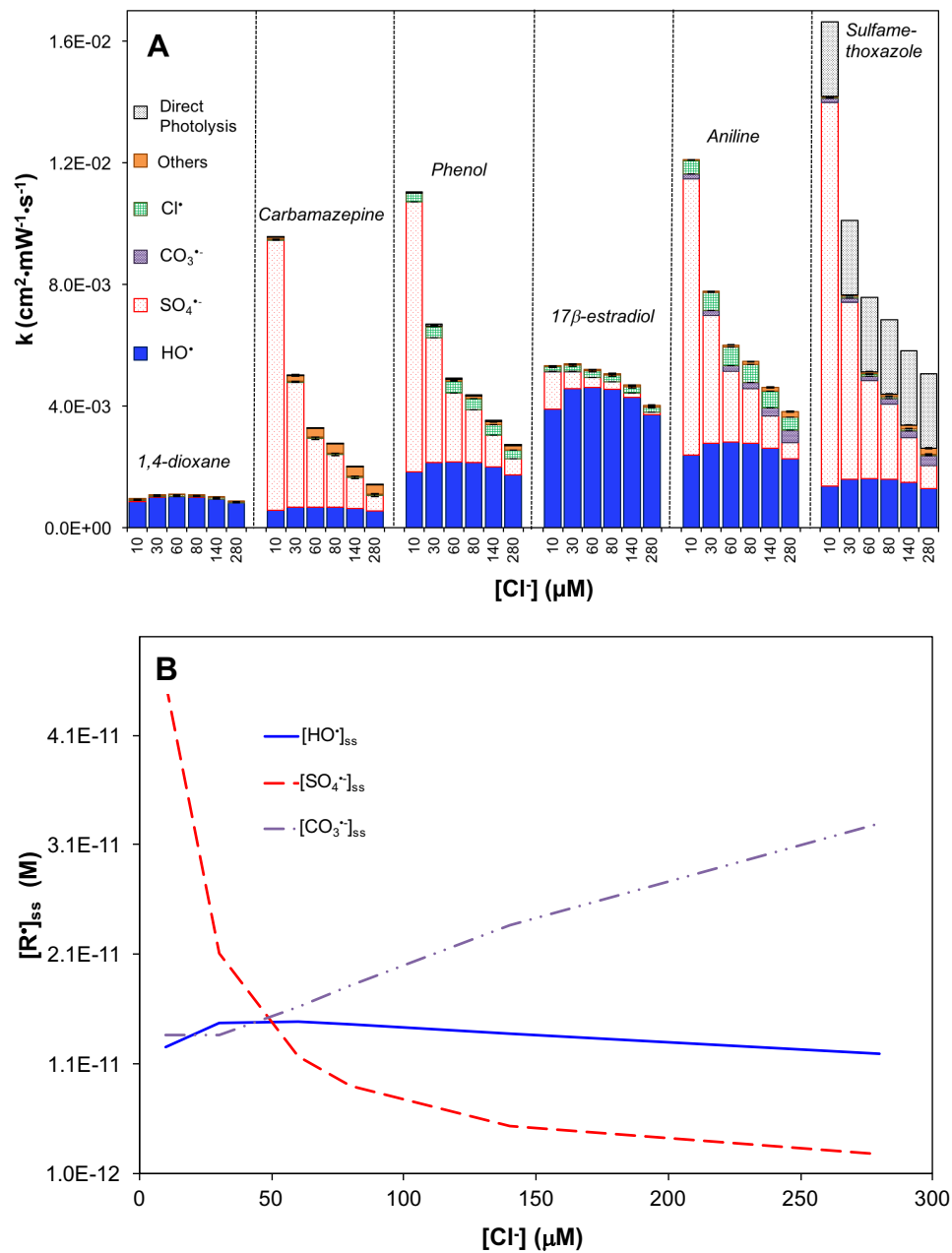


**Figure 30** The effect of chloride on the treatment efficiency of UV/S<sub>2</sub>O<sub>8</sub><sup>2-</sup> based on the kinetic model. (A) first-order degradation rates of organic contaminants in treatment and (B) radical distribution. [S<sub>2</sub>O<sub>8</sub><sup>2-</sup>]=88  $\mu\text{M}$ , [trace organic contaminant]=50 nM, pH=5.8, [inorganic carbon]=0.2 mM, [Br]=0.2  $\mu\text{M}$ , TOC=0.15 mg C/L, UV irradiance=45 mW/cm<sup>2</sup>.

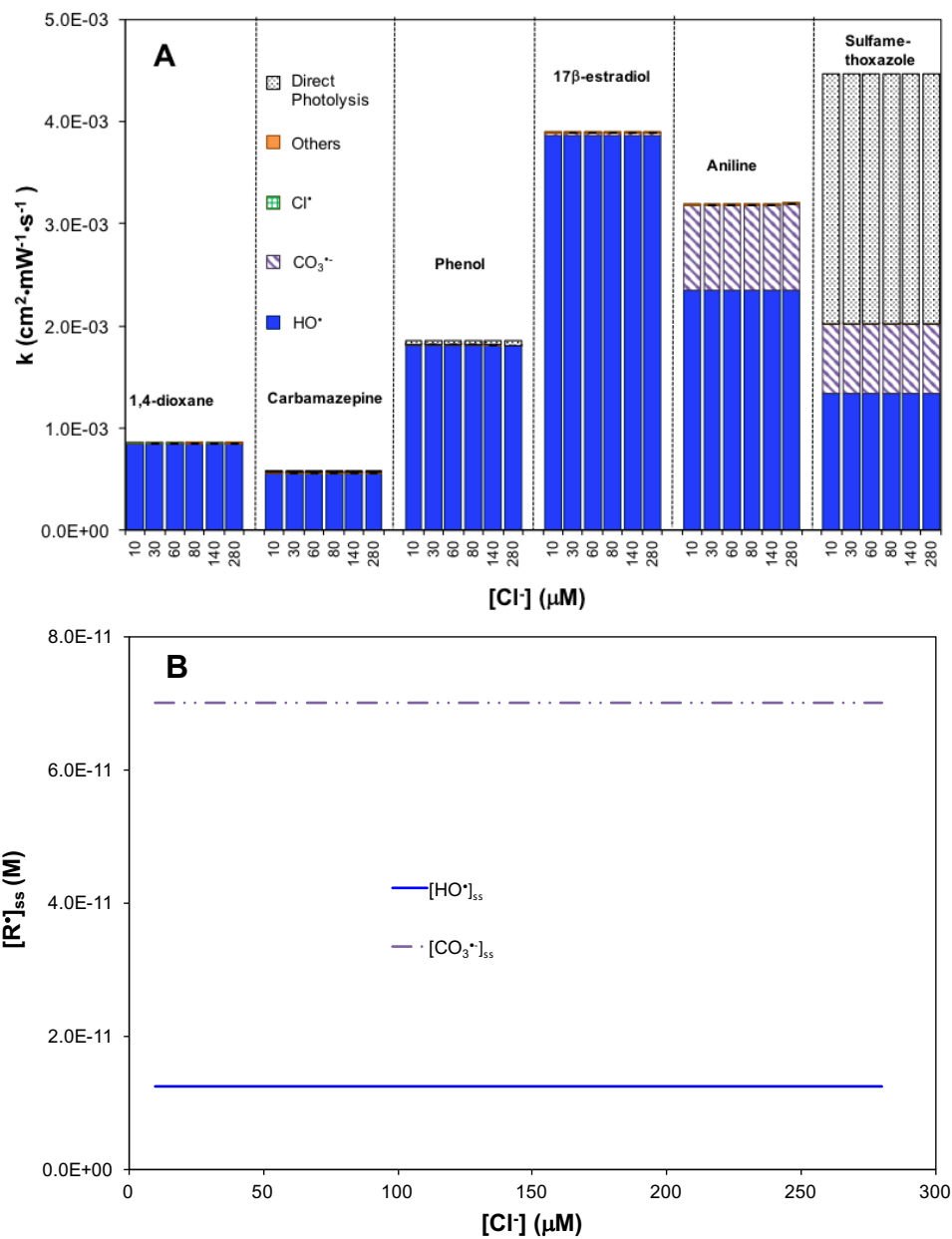


**Figure 31** Effect of chloride on the treatment efficiency of UV/H<sub>2</sub>O<sub>2</sub> based on the kinetic model. (A) First-order degradation rates of organic contaminants in treatment. (B) Radical distribution. [H<sub>2</sub>O<sub>2</sub>]=88  $\mu\text{M}$ , [trace organic contaminant]=50 nM, pH=5.8, [inorganic carbon]=0.2 mM, [Br<sup>-</sup>]=0.2  $\mu\text{M}$ , TOC=0.15 mg C/L, UV irradiance=45 mW/cm<sup>2</sup>.

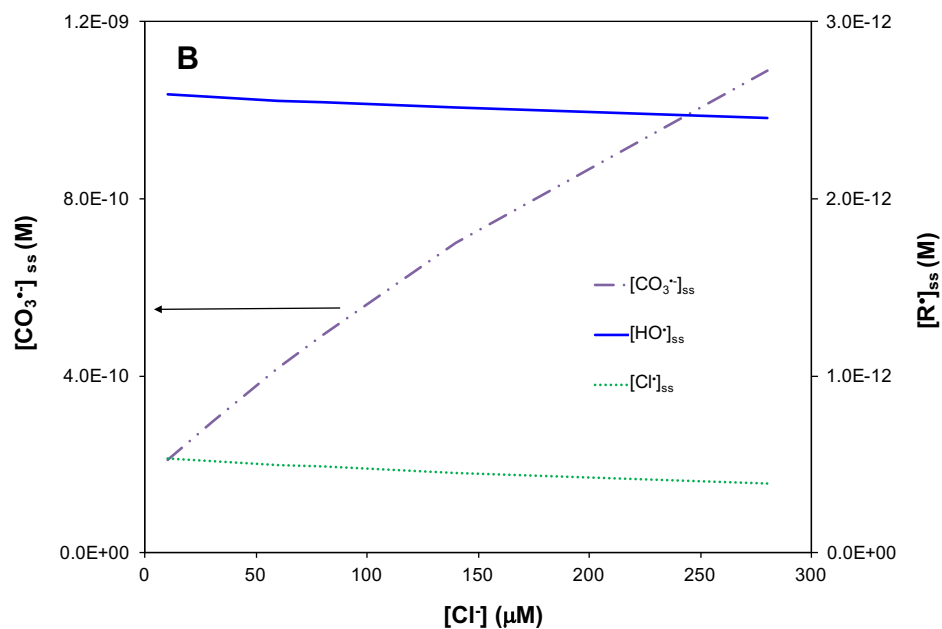
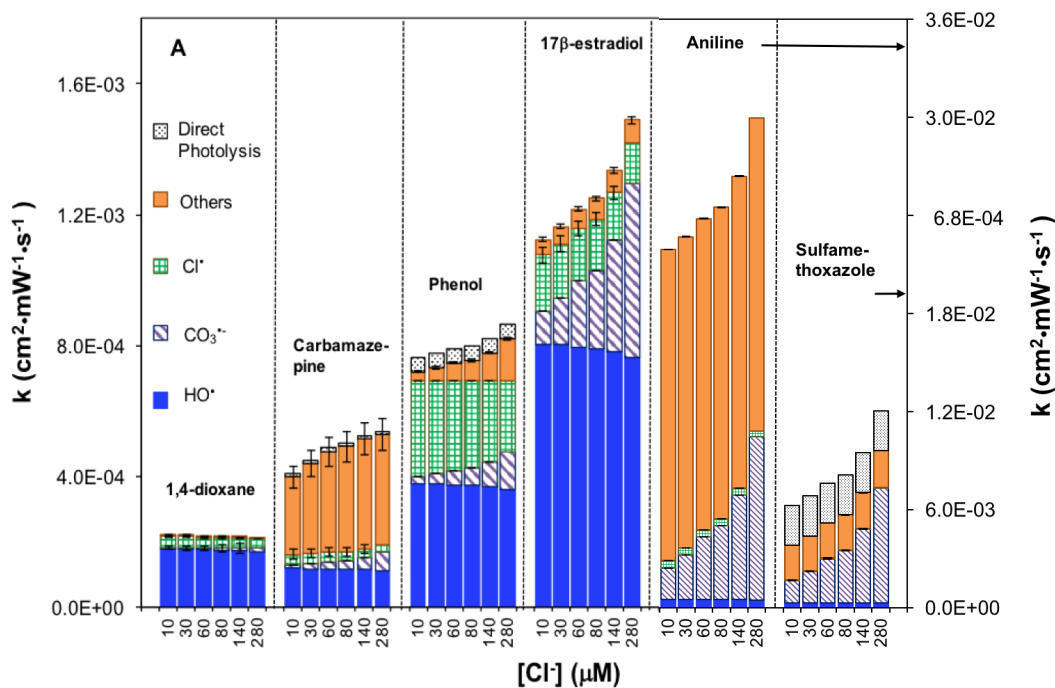


**Figure 32** Effect of chloride on the treatment efficiency of UV/HOCl based on the kinetic model. (A) First-order degradation rates of organic contaminants in treatment. (B) Radical distribution.  $[\text{HOCl}] = 88 \mu\text{M}$ ,  $[\text{trace organic contaminant}] = 50 \text{ nM}$ ,  $\text{pH} = 5.8$ ,  $[\text{inorganic carbon}] = 0.2 \text{ mM}$ ,  $[\text{Br}^-] = 0.2 \mu\text{M}$ ,  $\text{TOC} = 0.15 \text{ mg C/L}$ ,  $\text{UV irradiance} = 45 \text{ mW/cm}^2$ .

#### 4.3.5.3 Impact of inorganic carbon

UV/S<sub>2</sub>O<sub>8</sub><sup>2-</sup> was most sensitive to inorganic carbon (TOTCO<sub>3</sub>) (**Figure 33A**). When TOTCO<sub>3</sub> increased from 40 to 400 μM, [SO<sub>4</sub><sup>•-</sup>]<sub>ss</sub> decreased by 5%, [HO<sup>•</sup>]<sub>ss</sub> decreased by 33% and [CO<sub>3</sub><sup>•-</sup>]<sub>ss</sub> increased by 600% (**Figure 33B**). The reduction of [HO<sup>•</sup>]<sub>ss</sub> was due to the scavenging effect of HCO<sub>3</sub><sup>-</sup> on Cl<sup>•</sup> (Reaction 14), which subsequently suppresses HO<sup>•</sup> formation via ClOH<sup>•-</sup> pathway (Reactions 8–10). Consequently, the rates of contaminant degradation decreased with increasing TOTCO<sub>3</sub> (**Figure 33A**).

In contrast, UV/H<sub>2</sub>O<sub>2</sub> was not sensitive to inorganic carbon (**Figure 34A**). [HO<sup>•</sup>]<sub>ss</sub> remained stable with changing TOTCO<sub>3</sub> concentration (**Figure 34B**). Although HO<sup>•</sup> could be scavenged by Cl<sup>•</sup> (Reaction 20), it was quickly regenerated (Reaction 10). The scavenging effects of HCO<sub>3</sub><sup>-</sup> mainly suppressed Cl<sup>•</sup> and Cl<sub>2</sub><sup>•-</sup> (Reactions 14 and 21) and increased [CO<sub>3</sub><sup>•-</sup>]<sub>ss</sub> by 9 times (**Figure 34B**). The predicted contaminant degradation rates were not sensitive to TOTCO<sub>3</sub> except for aniline and sulfamethoxazole in which rates were enhanced due to the increase of [CO<sub>3</sub><sup>•-</sup>]<sub>ss</sub> (**Figure 34A**).

Similarly, UV/HOCl was not sensitive to TOTCO<sub>3</sub> with respect to [HO<sup>•</sup>]<sub>ss</sub> and [Cl<sup>•</sup>]<sub>ss</sub> (**Figure 35A**). When TOTCO<sub>3</sub> increased from 40 to 400 μM, both [HO<sup>•</sup>]<sub>ss</sub> and [Cl<sup>•</sup>]<sub>ss</sub> remained relatively constant; however, [CO<sub>3</sub><sup>•-</sup>]<sub>ss</sub> increased dramatically due to the scavenging effect of HCO<sub>3</sub><sup>-</sup> (**Figure 35B**). Therefore, contaminants that are reactive with [CO<sub>3</sub><sup>•-</sup>]<sub>ss</sub> exhibited an enhanced removal with increasing inorganic carbon concentration (**Figure 35A**).

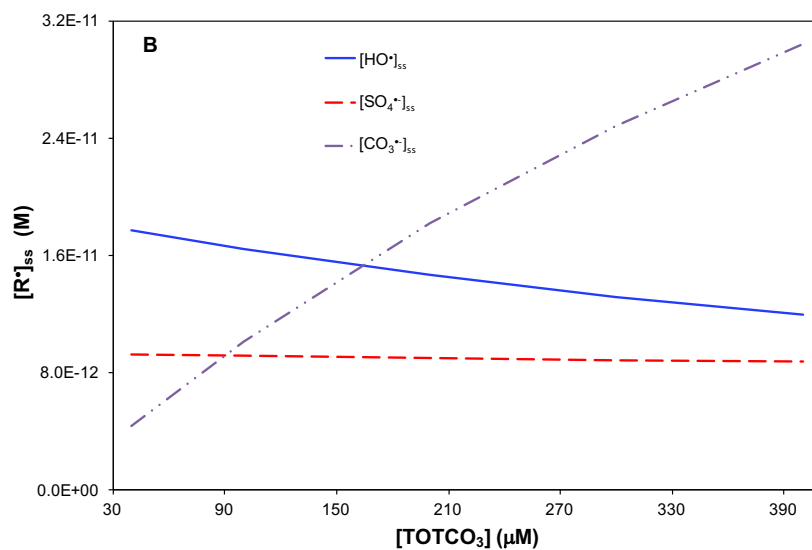
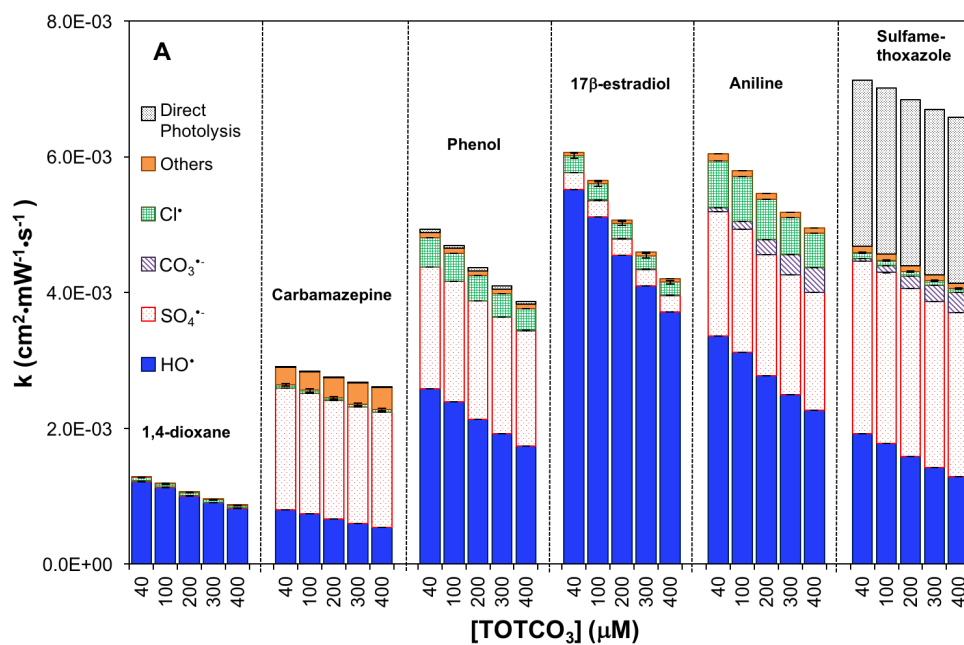


**Figure 33** Effect of inorganic carbon on the treatment efficiency of  $\text{UV}/\text{S}_2\text{O}_8^{2-}$  based on the kinetic model. (A) First-order degradation rates of organic contaminants in treatment. (B) Radical distribution.  $[\text{S}_2\text{O}_8^{2-}] = 88 \mu\text{M}$ ,  $[\text{trace organic contaminant}] = 50 \text{ nM}$ ,  $\text{pH} = 5.8$ ,  $[\text{Cl}^-] = 80 \mu\text{M}$ ,  $[\text{Br}^-] = 0.2 \mu\text{M}$ ,  $\text{TOC} = 0.15 \text{ mg C/L}$ ,  $\text{UV irradiance} = 45 \text{ mW/cm}^2$ .

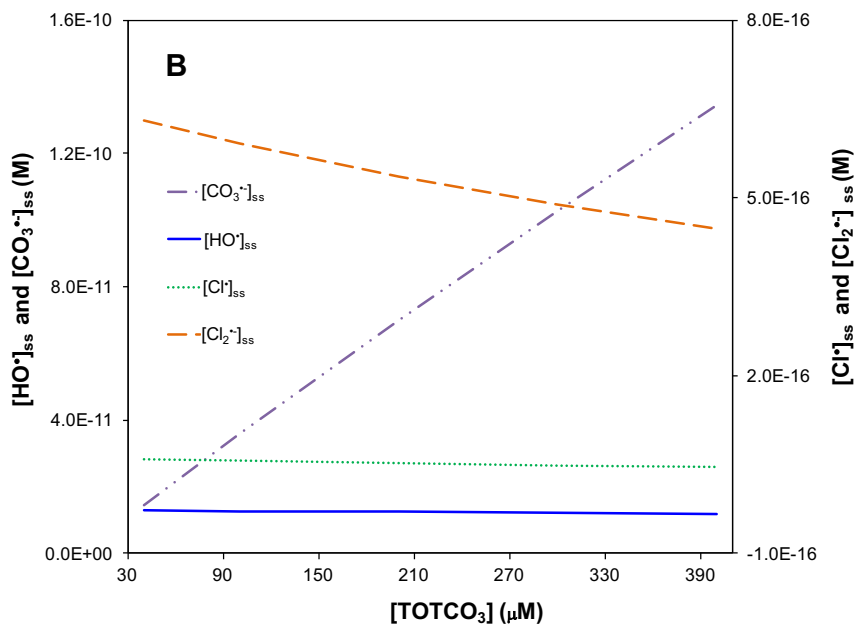
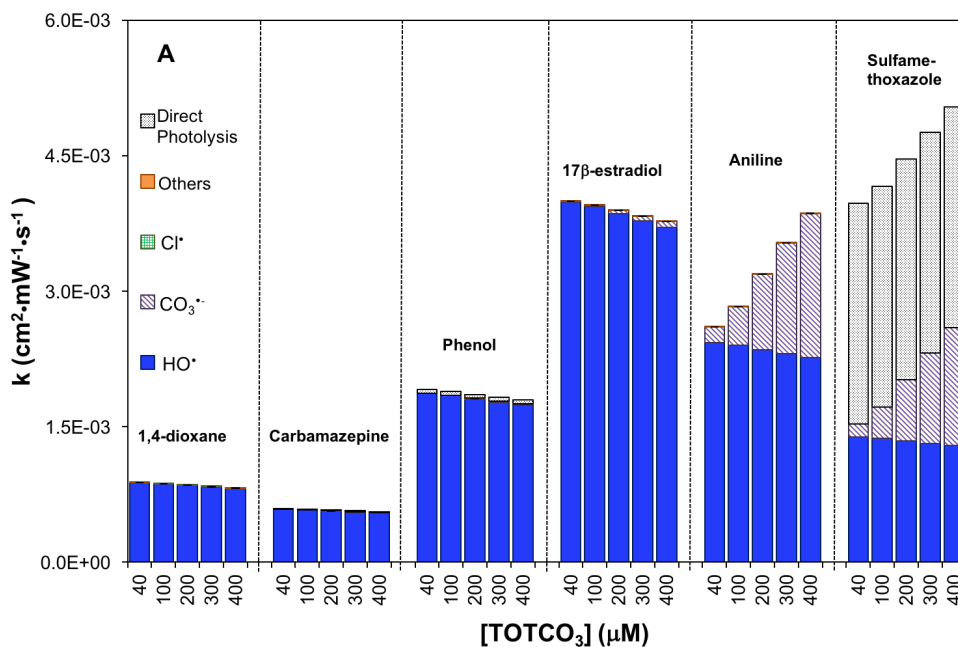


**Figure 34** Effect of inorganic carbon on the treatment efficiency of UV/H<sub>2</sub>O<sub>2</sub> based on the kinetic model. (A) First-order degradation rates of organic contaminants in treatment. (B) Radical distribution. [H<sub>2</sub>O<sub>2</sub>]=88 μM, [trace organic contaminant]=50 nM, pH=5.8, [Cl<sup>-</sup>]=80 μM, [Br<sup>-</sup>]=0.2 μM, TOC=0.15 mg C/L, UV irradiance=45 mW/cm<sup>2</sup>.

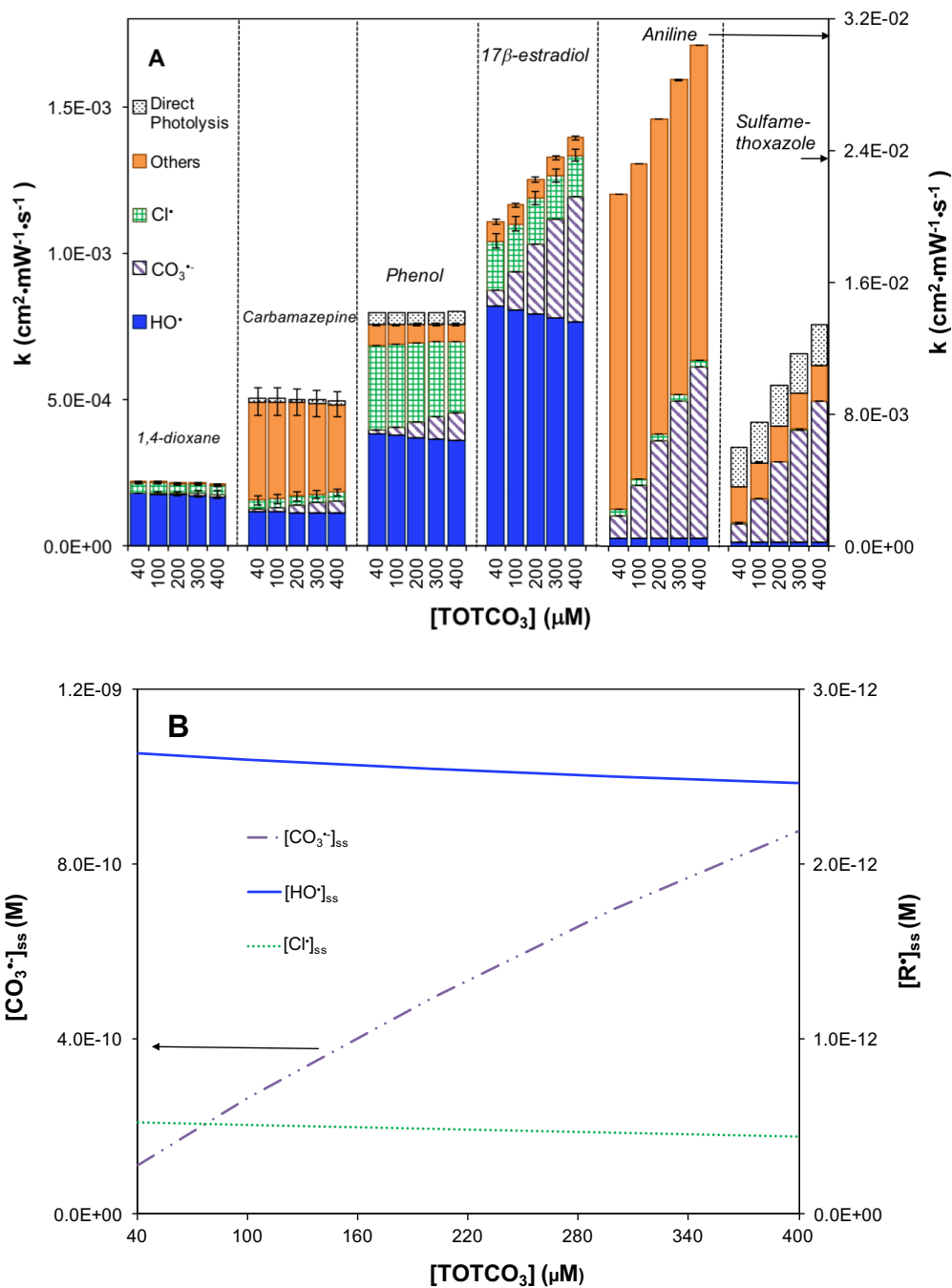


**Figure 35** The effect of inorganic carbon on the treatment efficiency of UV/HOCl based on the kinetic model. (A) first-order degradation rates of organic contaminants in treatment and (B) radical distribution. [HOCl]=88 μM, [trace organic contaminant]=50 nM, pH=5.8, [Cl<sup>-</sup>]=80 μM, [Br<sup>-</sup>]=0.2 μM, TOC=0.15 mg C/L, UV irradiance=45 mW/cm<sup>2</sup>.

## 4.4 Engineering Implications

In chemical conditions typical for potable water reuse, the kinetic modeling prediction and experimental observation showed that treatment efficiency followed the order of UV/persulfate > UV/hydrogen peroxide > UV/chlorine. This is mainly because  $S_2O_8^{2-}$  photolyzes faster than  $H_2O_2$  and generates higher levels of both  $SO_4^{\bullet-}$  and  $HO^{\bullet}$ . Because  $SO_4^{\bullet-}$  is more selective than  $HO^{\bullet}$  to react with electron-rich compounds, UV/ $S_2O_8^{2-}$  could potentially treat organic contaminants more efficiently than UV/ $H_2O_2$ , despite that the industrial implementation in water reuse is still in its infancy. While the application of UV/ $S_2O_8^{2-}$  can increase  $SO_4^{2-}$  concentration in treated water (<10 mg/L), this level is not likely to adversely affect drinking water quality, considering the US EPA guideline standard of 250 mg/L for  $SO_4^{2-}$ .<sup>82</sup> However, UV/ $S_2O_8^{2-}$  is more sensitive to pH, chloride, and inorganic carbon than the other two UV/AOPs. This sensitivity can impact its treatment efficiency, depending on the reactivities of radicals with individual contaminants.

UV/ $H_2O_2$  exhibited higher treatment efficiency than UV/HOCl for some groups of contaminants. The performance of UV/ $H_2O_2$  is limited by the rate of  $H_2O_2$  photolysis, the strong scavenging effect of  $H_2O_2$  on various radicals and a requirement to remove  $H_2O_2$  residual in drinking water. However, UV/ $H_2O_2$  is not as sensitive to changes of chemical parameters including pH, chloride, and bicarbonate as the other two UV/AOPs.

UV/HOCl is unique to the other AOPs in that it favors the generation of  $CO_3^{\bullet-}$  in water reuse chemical conditions. For compounds possessing high reactivity with  $CO_3^{\bullet-}$  (e.g., amine-containing contaminants), UV/HOCl can be very effective. For compounds that are inert to  $CO_3^{\bullet-}$ , UV/HOCl is less effective than UV/ $H_2O_2$  and UV/ $S_2O_8^{2-}$ . However, as a widely used disinfectant, HOCl is commonly employed in water treatment. The system can be easily upgraded to an AOP by with the addition of a UV source with less capital cost compared to other UV/AOPs.

The water chemical conditions and the targeted contaminants should be considered in the design of a UV/AOP for water reuse. For source waters containing low levels of  $\text{Cl}^-$  and  $\text{HCO}_3^-$ , UV/ $\text{S}_2\text{O}_8^{2-}$  and UV/ $\text{H}_2\text{O}_2$  work effectively. If the targeted contaminant contains amine functional groups, UV/HOCl is likely to be favored. In addition, pre-treatment steps should be carried out to minimize the presence of natural organic matter (NOM) prior to UV/AOP because NOM can significantly decrease the UV transmittance and scavenge major radicals.<sup>83-84</sup>

#### 4.5 Conclusions

The performances of UV/ $\text{S}_2\text{O}_8^{2-}$ , UV/ $\text{H}_2\text{O}_2$  and UV/HOCl were evaluated and compared using both comprehensive kinetic modeling and experimental investigation. The degradation of 1,4-dioxane, carbamazepine, phenol, 17 $\beta$ -estradiol, aniline, and sulfamethoxazole were examined in this study. The impacts of chemical conditions relevant to potable water reuse that included pH, chloride, and inorganic carbon were examined. UV/ $\text{S}_2\text{O}_8^{2-}$  was predicted to be the most efficient UV/AOP when applied to RO permeate, despite that its performance is most sensitive to pH,  $\text{Cl}^-$ , and  $\text{HCO}_3^-$ .  $\text{SO}_4^{\bullet-}$  is likely to be transformed through a  $\text{Cl}^-$  pathway to generate  $\text{HO}^\bullet$ . However, the presence of  $\text{HCO}_3^-$  also transforms  $\text{SO}_4^{\bullet-}$  and  $\text{Cl}^\bullet$  to less reactive  $\text{CO}_3^{\bullet-}$ .  $\text{HO}^\bullet$  is affected less by  $\text{Cl}^-$  and  $\text{HCO}_3^-$  because the formation of  $\text{ClOH}^{\bullet-}$  quickly regenerates  $\text{HO}^\bullet$ . An increase of pH can compromise the performance of UV/ $\text{S}_2\text{O}_8^{2-}$ , while pH changes have a negligible effect on UV/ $\text{H}_2\text{O}_2$  and UV/HOCl. The presence of  $\text{Cl}^-$  and  $\text{HCO}_3^-$  transforms  $\text{SO}_4^{\bullet-}$  to less reactive radicals and reduces the effectiveness of UV/ $\text{S}_2\text{O}_8^{2-}$ , whereas UV/ $\text{H}_2\text{O}_2$  and UV/HOCl are less sensitive to  $\text{Cl}^-$  and  $\text{HCO}_3^-$ . The kinetic model provides a fundamental tool to examine

the mechanisms of radical photochemistry to aid in the design of UV/AOP systems and to predict the performance under different chemical conditions.

#### **4.6 Acknowledgments**

This research was partially supported by grants to H.L. from National Science Foundation (CHE-1611306) and the UC Riverside Faculty Initiation Research Fund, and to W.L. from the National Science Foundation Graduate Research Fellowship and IGERT Water Sense Fellowship. We thank William Mitch at Stanford University and Steve Mezyk at California State University Long Beach for helping with the modeling input parameters.

## Reference:

---

- <sup>1</sup> Gosling S. Arnell N., The implications of climate policy for avoided impacts on water scarcity. *Procedia Environmental Sciences*. **2011**, 6, 112-121.
- <sup>2</sup> National Research Council (US), Committee on the Assessment of Water Reuse as an Approach for Meeting Future Water Supply Needs, *Water Reuse: Potential for expanding the nation's water supply through reuse of municipal wastewater*, National Academies Press: 2012.
- <sup>3</sup> Bixio, D.; Thoeye, C.; De Koning, J.; Joksimovic, D.; Savic, D.; Wintgens, T.; Melin, T. Wastewater reuse in Europe. *Desalination*. **2006**, 187 (1-3), 89-101.
- <sup>4</sup> I. Hespanhol, I.; Prost, A. M. E. WHO guidelines and national standards for reuse and water quality. *Water Research*. **1994**, 28 (1), 119-124.
- <sup>5</sup> Del Pino, M. P.; Durham, B.; Wastewater reuse through dual-membrane processes: opportunities for sustainable water resources. *Desalination*. **1999**, 124 (1), 271-277.
- <sup>6</sup> Kolpin, D.W.; Furlong, E.T.; Meyer, M.T.; Thurman, E.M.; Zaugg, S.D.; Barber, L.B.; Buxton, H.T. Pharmaceuticals, hormones, and other organic wastewater contaminants in US streams, 1999–2000: a national reconnaissance. *Environmental Science & Technology*. **2002**, 36, 1202–1211.
- <sup>7</sup> Kunkel U.; Radke M. Reactive tracer test to evaluate the fate of pharmaceuticals in rivers. *Environmental Science & Technology*. **2011**, 45 (15), 6296–6303.
- <sup>8</sup> Fono L.; Kolodziej E.; Sedlak D. Attenuation of wastewater-derived contaminants in an effluent-dominated river. *Environmental Science & Technology*. **2006**, 40 (23), 7257-7262.
- <sup>9</sup> Westerhoff, P.; Yoon, Y.; Snyder, S.; Wert, E.; Fate of endocrine-disruptor, pharmaceutical, and personal care product chemicals during simulated drinking water treatment processes. *Environmental Science & Technology*. **2005**, 39 (17), 6649-6663.
- <sup>10</sup> Yang, Q.; Choi, H.; Chen, Y.; Dionysiou, D. Heterogeneous activation of peroxymonosulfate by supported cobalt catalysts for the degradation of 2,4-dichlorophenol in water: the effect of support cobalt precursor and UV radiation. *Applied Catalysis B: Environmental*. **2008**, 77, 300–307.
- <sup>11</sup> Liu, H.; Bruton, T. A.; Doyle, F. M.; Sedlak, D. L. In situ chemical oxidation of contaminated groundwater by persulfate: decomposition by Fe (III)-and Mn (IV)-containing oxides and aquifer materials. *Environmental Science & Technology*. **2014**, 48 (17), 10330-10336.

- 
- <sup>12</sup> Liu, H.; Bruton, T.; Li, W.; Van Buren, J.; Prasse, C.; Doyle, F. A.; Sedlak, D. L. Oxidation of benzene by persulfate in the presence of Fe(III)- and Mn(IV)-containing oxides: stoichiometric efficiency and transformation products. *Environmental Science & Technology*. **2016**, *50* (2), 890-898.
- <sup>13</sup> Mark, G.; Schuchmann, M. N.; Schuchmann, H. P.; Von Sonntag, C. The photolysis of potassium peroxodisulphate in aqueous solution in the presence of tert-butanol: a simple actinometer for 254 nm radiation. *Journal of Photochemistry and Photobiology A: Chemistry*. **1990**, *55* (2), 157-168.
- <sup>14</sup> Baxendale, J. H.; Wilson, J. A. The photolysis of hydrogen peroxide at high light intensities. *Transactions of the Faraday Society*. **1957**, *53*, 344-356.
- <sup>15</sup> Fang, J.; Fu, Y.; Shang, C. The roles of reactive species in micropollutant degradation in the UV/free chlorine system. *Environmental Science & Technology*. **2014**, *48* (3), 1859-1868.
- <sup>16</sup> Qin, L.; Lin, Y.; Xu, B.; Hu, C.; Tian, F.; Zhang, T.; Zhu, W.; Huang, H.; Gao, N. Kinetic models and pathways of ronidazole degradation by chlorination, UV irradiation and UV/chlorine processes. *Water Research*. **2014**, *65*, 271-281.
- <sup>17</sup> Remucal, C. K.; Manley, D. Emerging investigators series: the efficacy of chlorine photolysis as an advanced oxidation process for drinking water treatment. *Environmental Science: Water Research & Technology*. **2016**, *2* (4), 565-579.
- <sup>18</sup> Sichel, C.; Garcia, C.; Andre, K.; Feasibility studies: UV/chlorine advanced oxidation treatment for the removal of emerging contaminants. *Water Research*. **2011**, *45* (19), 6371-6380.
- <sup>19</sup> Jin, J.; El-Din, M.G.; Bolton, J.R. Assessment of the UV/ chlorine process as an advanced oxidation process. *Water Research*. **2011**, *45* (4), 1890-1896.
- <sup>20</sup> Watts M.; Linden K. Chlorine photolysis and subsequent OH radical production during UV treatment of chlorinated water. *Water Research*. **2007**, *41* (13), 2871-2878.
- <sup>21</sup> Jayson, G. G.; Parsons, B. J.; Swallow, A. J. Some simple, highly reactive, inorganic chlorine derivatives in aqueous solution. Their formation using pulses of radiation and their role in the mechanism of the Fricke dosimeter. *Journal of the Chemical Society, Faraday Transactions 1: Physical Chemistry in Condensed Phases*. **1973**, *69*, 1597-1607.
- <sup>22</sup> Buxton, G. V.; Greenstock, C. L.; Helman, W.P.; Ross, A. B. Critical review of rate constants for reactions of hydrated electrons, hydrogen atoms and hydroxyl radicals ( $\cdot\text{OH}/\text{O}^-$  in aqueous solution. *Journal of Physical and Chemical Reference Data*. **1988**, *17* (2), 513-886.

- 
- <sup>23</sup> Nowell, L.H.; Hoigné, J. Photolysis of aqueous chlorine at sunlight and ultraviolet wavelengths—I. Degradation rates. *Water Research*. **1992**, *26* (5), 593-598.
- <sup>24</sup> Glaze, W. H.; Lay, Y.; Kang, J. W. Advanced oxidation processes. A kinetic model for the oxidation of 1, 2-dibromo-3-chloropropane in water by the combination of hydrogen peroxide and UV radiation. *Industrial & Engineering Chemistry Research*. **1995**, *34* (7), 2314-2323.
- <sup>25</sup> Weir, B. A.; Sundstrom, D. W. Destruction of trichloroethylene by UV light-catalyzed oxidation with hydrogen peroxide. *Chemosphere*. **1993**, *27* (7), 1279-1291.
- <sup>26</sup> De Latt, J. D.; Dore, M. Degradation of chloroethanes in dilute aqueous solution by H<sub>2</sub>O<sub>2</sub>/UV. *Water Research*. **1994**, *28* (12), 2507-2519.
- <sup>27</sup> Hong, A.; Zappi, M. E.; Kuo, C. H.; Hill, D. Modeling kinetics of illuminated and dark advanced oxidation processes. *Journal of Environmental Engineering*. **1996**, *122* (1), 58-62.
- <sup>28</sup> Schwarzenbach, R. P.; Gschwend, P. M.; Imboden, D. M. Photochemical transformation reactions. *Environmental Organic Chemistry*. **1993**, 436-484.
- <sup>29</sup> Pereira, V. J.; Weinberg, H. S.; Linden, K. G.; Singer, P. C. UV degradation kinetics and modeling of pharmaceutical compounds in laboratory grade and surface water via direct and indirect photolysis at 254 nm. *Environmental Science & Technology*. **2007**, *41* (5), 1682-1688.
- <sup>30</sup> Sharpless, C. M.; Linden, K. G. Experimental and model comparisons of low-and medium-pressure Hg lamps for the direct and H<sub>2</sub>O<sub>2</sub> assisted UV photodegradation of N-nitrosodimethylamine in simulated drinking water. *Environmental Science & Technology*. **2003**, *37* (9), 1933-1940.
- <sup>31</sup> Stefan, M. I.; Hoy, A. R.; Bolton, J. R. Kinetics and mechanism of the degradation and mineralization of acetone in dilute aqueous solution sensitized by the UV photolysis of hydrogen peroxide. *Environmental Science & Technology*. **1996**, *30* (7), 2382-2390.
- <sup>32</sup> Crittenden, J. C.; Hu, S.; Hand, D. W.; Green, S. A. A kinetic model for H<sub>2</sub>O<sub>2</sub>/UV process in a completely mixed batch reactor. *Water Research*. **1999**, *33* (10), 2315-2328.
- <sup>33</sup> Rosenfeldt, E. J.; Linden, K. G. The ROH, UV concept to characterize and the model UV/H<sub>2</sub>O<sub>2</sub> process in natural waters. *Environmental Science & Technology*. **2007**, *41* (7), 2548-2553.
- <sup>34</sup> Pareek, V. K.; Cox, S. J.; Brungs, M. P.; Young, B.; Adesina, A. A. Computational fluid dynamic (CFD) simulation of a pilot-scale annular bubble column photocatalytic reactor. *Chemical Engineering Science*. **2003**, *58* (3), 859-865.

- 
- <sup>35</sup> Alpert, S. M.; Knappe, D. R.; Ducoste, J. J. Modeling the UV/hydrogen peroxide advanced oxidation process using computational fluid dynamics. *Water Research*. **2010**, *44* (6), 1797-1808.
- <sup>36</sup> James, S. C.; Boriah, V. Modeling algae growth in an open-channel raceway. *Journal of Computational Biology*. **2010**, *17* (7), 895-906.
- <sup>37</sup> Yuan R.; Wang Z.; Hu Y.; Wang B.; Gao S. Probing the radical chemistry in UV/persulfate-based saline wastewater treatment: Kinetics modeling and byproducts identification. *Chemosphere*. **2014**, *109*, 106-112.
- <sup>38</sup> J. C. Lanni, Kintecus, Windows version 4.55. www.kintecus.com. 2012.
- <sup>39</sup> Herrmann, H.; Reese, A.; Zellner R. Time-resolved UV/VIS diode array absorption spectroscopy of  $\text{SO}_x^-$  ( $x= 3, 4, 5$ ) radical anions in aqueous solution. *Journal of Molecular Structure*. **1995**, *348*, 183-186.
- <sup>40</sup> Das, T. N. Reactivity and role of  $\text{SO}_5^-$  radical in aqueous medium chain oxidation of sulfite to sulfate and atmospheric sulfuric acid generation. *The Journal of Physical Chemistry A*. **2001**, *105* (40), 9142-9155.
- <sup>41</sup> Yu, X. Y.; Barker J. R. Hydrogen peroxide photolysis in acidic aqueous solutions containing chloride ions. I. Chemical mechanism. *The Journal of Physical Chemistry A*. **2003**, *107* (9), 1313-1324.
- <sup>42</sup> Grigorev, A. E.; Makarov I. E.; Pikaev A. K. Formation of  $\text{Cl}_2^-$  in the bulk of solution during radiolysis of concentrated aqueous solutions of chlorides. *High Energy Chemistry*. **1987**, *21* (2), 99-102.
- <sup>43</sup> Matthew, B. M.; Anastasio. C. A chemical probe technique for the determination of reactive halogen species in aqueous solution: Part 1—bromide solutions. *Atmospheric Chemistry and Physics*. **2006**, *6* (9), 2423-2437.
- <sup>44</sup> Dogliotti, L.; Hayon, E.; Flash photolysis of persulfate ions in aqueous solutions. Study of the sulfate and ozonide radical anions. *The Journal of Physical Chemistry*. **1967**, *71* (8), 2511-2516.
- <sup>45</sup> Donati, A. Spectroscopic and kinetic investigation of halogen containing radicals in the tropospheric aqueous phase. (Doctoral dissertation). **2002**.
- <sup>46</sup> Zehavi, D.; Rabani, J. Oxidation of aqueous bromide ions by hydroxyl radicals. Pulse radiolytic investigation. *The Journal of Physical Chemistry*. **1972**, *76* (3), 312-319.

- 
- <sup>47</sup> Yu, X. Y.; Bao, Z. C.; Barker, J. R. Free Radical Reactions Involving Cl, Cl<sub>2</sub><sup>-</sup>, and SO<sub>4</sub><sup>-</sup> in the 248 nm Photolysis of Aqueous Solutions Containing S<sub>2</sub>O<sub>8</sub><sup>2-</sup> and Cl. *The Journal of Physical Chemistry A*. **2004**, *108* (2), 295-308.
- <sup>48</sup> Budavari, S.; O'Neil, M. J.; Smith, A.; Heckelman, P. E.; Kinneary, J. F. The Merck Index. An encyclopedia of chemicals, drugs and biologicals. Whitehouse Station, NJ. Merck Research Laboratories Division of Merck & Co.: 1996.
- <sup>49</sup> State Water Resources Control Board (SWRCB), *Policy for maintaining instream flows in Northern California coastal streams*, SWRCB Division of Water Rights, California Environmental Protection Agency, Sacramento, California, USA, 2010.
- <sup>50</sup> Kujawski, W.; Warszawski, A.; Ratajczak, W.; Porebski, T.; Capała, W.; Ostrowska, I. Removal of phenol from wastewater by different separation techniques. *Desalination*. **2004**, *163* (1-3), 287-296.
- <sup>51</sup> Pereira, C. C.; Habert, A. C.; Nobrega, R.; Borges, C. P. New insights in the removal of diluted volatile organic compounds from dilute aqueous solution by pervaporation process. *Journal of Membrane Science*. **1998**, *138* (2), 227-235.
- <sup>52</sup> De Mes, T.; Grietje Z.; Gatze L. Occurrence and fate of estrone, 17β-estradiol and 17α-ethynylestradiol in STPs for domestic wastewater. *Reviews in Environmental Science and Bio/Technology*. **2005**, *4* (4), 275-311.
- <sup>53</sup> Tixier, C.; Singer, H.P.; Oellers, S.; Muller, S.R. Occurrence and fate of carbamazepine, clofibric acid, diclofenac, ibuprofen, ketoprofen, and naproxen in surface waters. *Environmental Science & Technology*. **2003**, *37* (6), 1061-1068.
- <sup>54</sup> Zhang, T.; Li, B. Occurrence, transformation, and fate of antibiotics in municipal wastewater treatment plants Crit. Rev. *Environmental Science & Technology*. **2011**, *41* (11), 951– 998.
- <sup>55</sup> Wenk, J.; Canonica, S. Phenolic antioxidants inhibit the triplet-induced transformation of anilines and sulfonamide antibiotics in aqueous solution. *Environmental Science & Technology*. **2012**, *46* (10), 5455-5462.
- <sup>56</sup> Mendez, A. S.; Deconto, L.; Garcia, C. V. UV derivative spectrophotometric method for determination of estradiol valerate in tablets. *Química Nova*, **2010**, *33* (4), 981-983.
- <sup>57</sup> Stefan, M. I.; Bolton, J. R. Mechanism of the degradation of 1,4-dioxane in dilute aqueous solution using the UV/hydrogen peroxide process. *Environmental Science & Technology*. **1998**, *32* (11), 1588-1595.
- <sup>58</sup> Prah, S. Phenol. URL: <http://omlc.org/spectra/PhotochemCAD/html/072.html>. 2012.

- 
- <sup>59</sup> Tang, H.; Li, J.; Bie, Y.; Zhu, L.; Zou, J. Photochemical removal of aniline in aqueous solutions: switching from photocatalytic degradation to photo-enhanced polymerization recovery. *Journal of Hazardous materials*. **2010**, *175* (1), 977-984.
- <sup>60</sup> Pereira, V. J.; Linden, K. G.; Weinberg, H. S. Evaluation of UV irradiation for photolytic and oxidative degradation of pharmaceutical compounds in water. *Water Research*. **2007**, *41* (19), 4413-4423.
- <sup>61</sup> Zhang, R.; Sun, P.; Boyer, T. H.; Zhao, L.; Huang, C. H. Degradation of Pharmaceuticals and Metabolite in Synthetic Human Urine by UV, UV/H<sub>2</sub>O<sub>2</sub>, and UV/PDS. *Environmental Science & Technology*. **2015**, *49* (5), 3056-3066.
- <sup>62</sup> Jasper, J. T.; Sedlak, D. L. Phototransformation of wastewater-derived trace organic contaminants in open-water unit process treatment wetlands. *Environmental Science & Technology*. **2013**, *47* (19), 10781-10790.
- <sup>63</sup> NIST Standard Reference Database 40: NDRL/NIST Solutions Kinetics Database V. 3.0, Gaithersburg, MD.
- <sup>64</sup> Deborde, M.; von Gunten, U. R. S. Reactions of chlorine with inorganic and organic compounds during water treatment—kinetics and mechanisms: a critical review. *Water Research*. **2008**, *42* (1), 13-51.
- <sup>65</sup> Lindqvist, N.; Tuhkanen, T.; Kronberg, L. Occurrence of acidic pharmaceuticals in raw and treated sewages and in receiving waters. *Water Research*. **2005**, *39* (11), 2219-2228.
- <sup>66</sup> Heberer, T. Occurrence, fate, and removal of pharmaceutical residues in the aquatic environment: a review of recent research data. *Toxicology letters*. **2002**, *131* (1), 5-17.
- <sup>67</sup> Vieno, N. M.; Tuhkanen, T.; Kronberg, L. Seasonal variation in the occurrence of pharmaceuticals in effluents from a sewage treatment plant and in the recipient water. *Environmental Science & Technology*. **2005**, *39* (21), 8220-8226.
- <sup>68</sup> Zenker, M. J.; Borden, R. C.; Barlaz, M. A. Occurrence and treatment of 1, 4-dioxane in aqueous environments. *Environmental Engineering Science*. **2003**, *20* (5), 423-432.
- <sup>69</sup> Kimura, K.; Amy, G.; Drewes, J. E.; Heberer, T.; Kim, T. U.; Watanabe, Y. Rejection of organic micropollutants (disinfection by-products, endocrine disrupting compounds, and pharmaceutically active compounds) by NF/RO membranes. *Journal of Membrane Science*. **2003**, *227* (1), 113-121.
- <sup>70</sup> Jankowski, J. J.; Kieber, D. J.; Mopper, K. Nitrate and nitrite ultraviolet actinometers. *Photochemistry and Photobiology*. **1999**, *70* (3), 319-328.

- 
- <sup>71</sup> Ijpelaar, G. F. *Fluence monitoring in UV disinfection systems: development of a fluence meter*. American Water Works Association. IWA Publishing, London, UK: 2006.
- <sup>72</sup> Liang, C.; Huang, C. F.; Mohanty, N.; Kurakalva, R. M. A rapid spectrophotometric determination of persulfate anion in ISCO. *Chemosphere*. **2008**, *73* (9), 1540-1543.
- <sup>73</sup> American Public Health Association (APHA), *Standard Methods for the Examination of Water and Wastewater 18<sup>th</sup> ed.*, American Public Health Association: Washington, DC, USA, 1992.
- <sup>74</sup> Zhang, R.; Sun, P.; Boyer, T. H.; Zhao, L.; Huang, C. H. Degradation of Pharmaceuticals and Metabolite in Synthetic Human Urine by UV, UV/H<sub>2</sub>O<sub>2</sub>, and UV/PDS. *Environmental Science & Technology*. **2015**, *49* (5), 3056-3066.
- <sup>75</sup> Appiani, E.; Page, S. E.; McNeill, K. On the use of hydroxyl radical kinetics to assess the number-average molecular weight of dissolved organic matter. *Environmental Science & Technology*. **2014**, *48* (20), 11794-11802.
- <sup>76</sup> Minisci, F.; Citterio, A.; Giordano, C. Electron-transfer processes: peroxydisulfate, a useful and versatile reagent in organic chemistry. *Accounts of Chemical Research*. **1983**, *16* (1), 27-32.
- <sup>77</sup> Neta, P.; Madhavan, V.; Zemel, H.; Fessenden, R. W. Rate constants and mechanism of reaction of sulfate radical anion with aromatic compounds. *Journal of the American Chemical Society*. **1977**, *99* (1), 163-164.
- <sup>78</sup> Peyton, G. R. The free-radical chemistry of persulfate-based total organic carbon analyzers. *Marine Chemistry*. **1993**, *41* (1), 91-103.
- <sup>79</sup> Chen, S. N.; Hoffman, M. Z.; Parsons Jr. G. H. Reactivity of the carbonate radical toward aromatic compounds in aqueous solution. *The Journal of Physical Chemistry*. **1975**, *79* (18), 1911-1912.
- <sup>80</sup> Huang, J.; Mabury, S. A. Steady-state concentrations of carbonate radicals in field waters. *Environmental Toxicology and Chemistry*. **2000**, *19* (9), 2181-2188.
- <sup>81</sup> Grebel J.; Pignatello J.; Mitch W. Effect of halide ions and carbonates on organic contaminant degradation by hydroxyl radical-based advanced oxidation processes in saline waters. *Environmental Science & Technology*. **2010**, *44* (17), 6822-6828.
- <sup>82</sup> US Environmental Protection Agency (USEPA), *National Recommended Water Quality Criteria*, 2009.

- 
- <sup>83</sup> Sharpless, C. M.; Linden, K. G. UV photolysis of nitrate: effects of natural organic matter and dissolved inorganic carbon and implications for UV water disinfection. *Environmental Science & Technology*. **2001**, 35 (14), 2949-2955.
- <sup>84</sup> Rosario-Ortiz, F. L.; Wert, E. C.; Snyder, S. A. Evaluation of UV/H<sub>2</sub>O<sub>2</sub> treatment for the oxidation of pharmaceuticals in wastewater. *Water Research*. **2010**, 44 (5), 1440-1448.

## **Chapter 5**

# **Toxicity Assessment of Benzene and 1,4-dioxane Oxidation Byproducts**

**Submitted to *Environmental Science & Technology Letters***

Wei Li, Heidi Li, Elvis Genbo Xu, Daniel Schlenk and Haizhou  
Liu

## 5.1 Introduction

Water shortage has become a global crisis, and our drinking water resources are limited and facing ever-increasing contamination.<sup>1-4</sup> Remediation of contaminated groundwater and reuse of treated wastewater effluent are promising solutions to mitigate the water crisis. Advanced Oxidation Processes (AOPs) have been widely used for many contaminated groundwater sites and water recycle treatment trains.<sup>5-7</sup> Persulfate ( $S_2O_8^{2-}$ )-based AOPs for *in situ* Chemical Oxidation (ISCO) and potable water reuse have gained increasing attention in recent years due to its capacity to degrade a variety of organic contaminants such as contaminants of emerging concerns (CECs) including hydrocarbons,<sup>8</sup> pharmaceuticals and personal care products (PPCPs).<sup>9,10</sup> Enhancement for the removal efficiency of target contaminants by  $S_2O_8^{2-}$ -based AOPs has taken place,<sup>11-15</sup> however, the formation and kinetics of oxidative byproducts (OBPs) with potentially high toxicity is of increasing concern. The formation of toxic disinfection byproducts (DBPs) in other AOPs, such as halogenated DPBs in chlorination,<sup>16-21</sup> bromate in ozonation<sup>22-25</sup> and nitrogenous DBPs in chloramination<sup>26-30</sup> have been reported. It is likely that  $S_2O_8^{2-}$ -based AOPs may also produce toxic OBPs when the parent contaminants are not fully mineralized.<sup>31-33</sup> Therefore, it is important to monitor the formation of oxidation byproducts, assess their toxicity, and develop new advanced oxidative treatments with minimal toxic byproduct formation.

In this study, we used benzene and 1,4-dioxane as model contaminate as they are commonly found in contaminated groundwater and wastewater effluent. Benzene is a ubiquitous contaminant and its toxicity to humans and wildlife has been well studied.

Chronic benzene exposure progressively decreases bone marrow function and increases the possibility of bone marrow cancer<sup>34,35</sup>. Sources of benzene contamination of soil and groundwater mainly come from the petroleum industry, and benzene has been frequently detected in soil and groundwater<sup>36</sup>. Benzene can be effectively oxidized by sulfate radicals to produce phenol and other organic acids, which are more easily metabolized by soil microorganisms to produce CO<sub>2</sub>. 1,4-dioxane is listed as a class B carcinogen by the USEPA and the notification level is 1 ppb in California.<sup>37</sup> It is used as a surrogate for UV/AOPs efficiency validation.<sup>38</sup>

In this study, we compared the degradation of benzene by MnO<sub>4</sub><sup>-</sup>, goethite-activated S<sub>2</sub>O<sub>8</sub><sup>2-</sup> and H<sub>2</sub>O<sub>2</sub>, which were the most common AOPs used in *in situ* Chemical Oxidation. We chose goethite to activate S<sub>2</sub>O<sub>8</sub><sup>2-</sup> and H<sub>2</sub>O<sub>2</sub> because our previous studies showed that goethite exhibited the highest stoichiometric efficiency.<sup>39</sup> Products were identified during the treatment and toxicity of the oxidation byproducts and parent compounds were evaluated. In addition, we examined UV/H<sub>2</sub>O<sub>2</sub>, UV/S<sub>2</sub>O<sub>8</sub><sup>2-</sup> and UV/NH<sub>2</sub>Cl on 1,4-dioxane removal. UV/H<sub>2</sub>O<sub>2</sub> is the most common UV/AOP utilized in potable water reuse treatment, and UV/S<sub>2</sub>O<sub>8</sub><sup>2-</sup> and UV/NH<sub>2</sub>Cl are also becoming popular.<sup>40-42</sup> NH<sub>2</sub>Cl is frequently used as an antifoulant or disinfectant during advanced treatment trains, and it can also produce Cl<sup>•</sup> radical in photolysis. The objectives of this research are to (1) identify and compare the formation and distribution of oxidation byproducts during each AOP treatment, (2) Evaluate the toxicity of the transformation products, and compare their toxicity to the parent compounds using human cell-based bioassays.

## 5.2. Materials and Methods

### 5.2.1 ISCO treatments

All chemicals used in this study were reagent grade and obtained from ACROS Organics, Sigma Aldrich or Fisher Scientific. All chemicals were used as received without further purification. Goethite was synthesized by precipitating  $\text{Fe}(\text{NO}_3)_3$  with  $\text{NaOH}$ ,<sup>43</sup> and sieved to a uniformed size ( $38\ \mu\text{m} \sim 150\ \mu\text{m}$ ). All cell culture supplies and chemicals were obtained from Life Technologies or Fisher Scientific and stored in appropriate conditions as instructed. Benzene was prepared one day before its use and stored in a  $4^\circ\text{C}$  refrigerator. To avoid benzene evaporation, benzene was prepared daily for each experiment at final concentration (3 mM) in Milli-Q water that contained 50 mM borate buffer with minimal air space. The flask was inverted for three hours and left overnight for equilibrium to occur. Goethite was first introduced to 0.98-ml glass tubes at a final concentration of 50 g/L prior to the transfer of benzene solution. Crystal  $\text{K}_2\text{S}_2\text{O}_8$ ,  $\text{KMnO}_4$ , and liquid  $\text{H}_2\text{O}_2$  (30%) were added to the benzene solution directly at a final concentration of 150 mM. After complete mixing, the solution was quickly transferred to individual tubes. The final experimental solution consisted goethite (50g/L), 150 mM  $\text{K}_2\text{S}_2\text{O}_8$ ,  $\text{H}_2\text{O}_2$  or  $\text{MnO}_4^-$ , 3 mM benzene and 50 mM borate buffer. The solution was maintained at pH 8.  $\text{MnO}_4^-$  experiments did not include goethite. The tubes were then rotated and left in room temperature in the dark. One glass tube was removed for chemical analysis every five days.

### **5.2.2 UV/AOP treatments**

A  $\text{NH}_2\text{Cl}$  stock solution (50mM) was prepared daily by adding a  $\text{HOCl}$  stock solution to  $(\text{NH}_4)_2\text{SO}_4$  with a N:Cl molar ratio of 1.2:1 buffered at pH 8 using borate. The working solution contained 5 mM oxidants (*e.g.*  $\text{H}_2\text{O}_2$ ,  $\text{S}_2\text{O}_8^{2-}$ , and  $\text{NH}_2\text{Cl}$ ) and 1 mM 1,4-dioxane at pH 8. Prepared solutions were then transferred to multiple 8-mL quartz tubes and placed in a carousel in a UV chamber. The samples were illuminated with a low-pressure monochromatic UV lamp ( $\lambda=254$  nm) at an intensity of  $2.3 \text{ mW/cm}^2$  (Phillips TUV6T5) which was cooled by circulated water. Samples were collected every five minutes for chemical analysis.

### **5.2.3 Aldehyde preparation**

The oxidation product that exhibited aldehyde-like features was prepared by UV irradiation of 15 mM benzene with 3 mM  $\text{S}_2\text{O}_8^{2-}$  for two hours. The products were separated and concentrated by Solid Phase Extraction.<sup>44</sup> Following chromatography, the purified compound was then condensed to dryness by purging with  $\text{N}_2$ , followed by re-suspending in MQ water to a final concentration of 10 mM. The concentration of aldehyde-like compound was estimated by using DNPH derivatized glutaraldehyde followed by HPLC-UV analysis (**Figure 36**).<sup>45</sup>

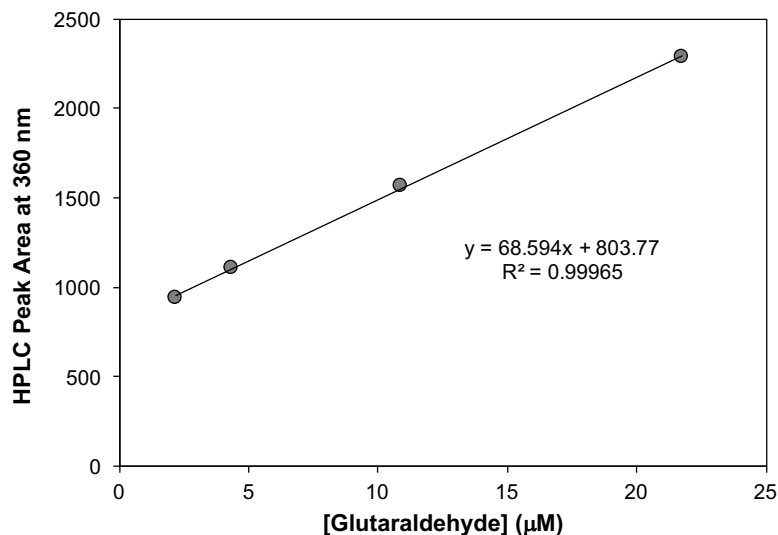


**Figure 36** Calibration curve of DNPH-derivatized glutaraldehyde.

#### 5.2.4 Analytical methods

Concentrations of  $\text{H}_2\text{O}_2$ ,  $\text{S}_2\text{O}_8^{2-}$ ,  $\text{MnO}_4^-$  and  $\text{NH}_2\text{Cl}$  were determined using potassium iodine (KI) and DPD titration, respectively.<sup>46</sup> Concentrations of benzene, 1,4-dioxane and EGD were directly measured with an Agilent 1200 high performance liquid chromatograph equipped with a diode array detector. A Zorbax Eclipse Deltabond column (4.6×200mm, 5.0-µm particle size). Concentrations of formaldehyde and glycolaldehyde were derivatized with 2,4-dinitrophenylhydrazine (DNPH) according to EPA Method 8315, and then analyzed by HPLC. The composition of mobile phase for benzene, phenol and aldehyde were 97% formic acid (10 mM) and 3% acetonitrile. The retention times were 7.3 minutes, 5.5 minutes and 3.5 minutes for benzene, phenol, and aldehyde, respectively. For 1,4-dioxane and ethylene glycol diformate, the composition of mobile phase was 92%  $\text{H}_2\text{O}$  and 8% acetonitrile. The retention time was 2.7 minutes and 1.9 minutes for 1,4-

Dioxane and Ethylene glycol diformate, respectively. For Formaldehyde and Glycolaldehyde, the mobile phase composition was 40% acetonitrile and 60% H<sub>2</sub>O. The retention time was 3.5 minutes and 5.6 minutes, respectively. The sample injection volume was 100 µL and the flow rate was set at 1.0 mL/min for a total of 6 min run time. Concentrations of glycolic acid, formic acid and methoxyacetic acid were quantified by Ion Chromatography (Dionex 1000, USA).

### ***5.2.5 Toxicity assays***

HCT-116 Human colorectal carcinoma cells were cultured at 37°C in a humidified 5% CO<sub>2</sub> incubator, and collected after the fourth passage for the toxicity assays.<sup>47</sup> HCT-116 Human colorectal carcinoma cells were cultured in polystyrene culture flasks (Corning T-75) with McCoy's 5A Medium including 10% dialyzed fetal bovine serum (FBS), 100ug/ml Penicillin/Streptomycin, and 5ug/ml Blasticidin. Cells were collected before reaching 80% confluence after the fourth passage and suspended with Opti-MEM Reduced Serum Assay Medium including 0.5% dialyzed fetal bovine serum (FBS), 1% 1 mM Sodium Pyruvate, 1% 0.1mM Non-essential amino acids (NEAA) and 1% of 100u/ml Penicillin/Streptomycin at a concentration of 5,5000 cells/ml. An aliquot of 90ul of the cell suspension was added into each well of the black, clear-bottom, 96-well assay plate (Corning 3603). The cells were incubated overnight prior to sample exposures.

For cytotoxicity measurements, an 10-µl aliquot of each concentration of the test compounds was dissolved in assay medium with 5% DMSO and transferred to the assay plate. The final compound concentration in the 100-µl assay volume ranged from 0 µM to

500  $\mu\text{M}$  over 8 concentrations. Three replicates were tested for each concentration. The plate was allowed to settle for 30 min at room temperature and then incubated at 37 °C, 5%  $\text{CO}_2$  for 16 hours. After 16 hours, 10- $\mu\text{l}$  of MTT reagent was added to the wells, which was incubated at 37 °C for 4 hours. The assay medium was then aspirated and 100- $\mu\text{l}$  of DMSO detergent was added. Cells were then again incubated for 3 hours at room temperature in the dark. Cytotoxicity was assessed by recording the absorbance at 570 nm using the EnVision microplate reader (Perkin Elmer, Shelton, CT). Percentage reduction in cell proliferation (relative cell density) was compared to that achieved in the growth medium controls. All the readings in the test compounds were corrected with reference to the background readings. Dose response curves were plotted using GraphPad Prism 7.0, and the EC50 of each compound was calculated using the Four-Parameter Logistic nonlinear regression function.

For genotoxicity, 20  $\mu\text{l}$  of LiveBLAzer™ - FRET B/G substrate mixture was added to each well after 16-hours of incubation. The substrate mixture was prepared in the absence of direct light. The plates were then incubated at room temperature for 2 hours, and fluorescence intensity was measured at 460 and 530 nm emission and with excitation at 405 nm. Readings for each well were normalized by the growth medium control. The ratio of emissions at 460nm/530 nm was calculated by Excel and dose response curves were plotted (GraphPad Prism 7.0) to compare to the positive control, Mitomycine.

The compounds used to treat the cells were prepared from known standards except that for the unsaturated aldehyde compound from benzene oxidation which was collected from HPLC eluent. For the mixture toxicity at different treatment times, the chemical

standards were combined based on the experimentally determined product compositions after treatment for 10 and 20 minutes (Table S1). After chemical exposure, fluorescence of the mixture was recorded using a Victor 2 plate reader (Perkin Elmer, Shelton, CT). Dose response curves were then plotted and the EC50s were calculated using GraphPad Prism 7. Both theoretical and experimentally observed genotoxicity Mitomycin equivalency quotients (MEQ) were calculated to determine the genotoxicity of 1,4-dioxane degradation during UV/AOP treatments.

#### ***5.2.4 Mitomycin Equivalency Quotient (MEQ) calculations***

First, the Relative Effect Potency (REP) values were calculated as:

$$\text{REP} = \text{EC}_{50(\text{mitomycin})} / \text{EC}_{50(i)}$$

where  $i$  is a specific oxidation product, the  $\text{EC}_{50(\text{mitomycin})} = 4.77 \mu\text{M}$ .

Second, the theoretical mitomycin EQ was calculated:

$$\text{MEQ}_{\text{theoretical}} = \sum (1000 \mu\text{M} \times \%_i \times \text{REP})$$

$\%_i$  is the oxidation products composition listed in **Figure 13**

Third, the experimentally observed MEQ was calculated as:

$$\text{MEQ}_{\text{observed}} = \text{EC}_{50(\text{mitomycin})} / \text{EC}_{50(\text{time 10 min or 20 min})}$$

$\text{EC}_{50(\text{time 10 min or 20 min})}$  was experimentally determined (**Figure 37**)

**Table 13** Products distribution during UV/AOPs treatment

Reaction Time	UV/S <sub>2</sub> O <sub>8</sub> <sup>2-</sup>			UV/H <sub>2</sub> O <sub>2</sub>		UV/NH <sub>2</sub> Cl	
	0 min	10 min	20 min	10 min	20 min	10 min	20 min
1,4-Dioxane	100%	20%	4%	51%	14%	84%	65%
Glycolaldehyde		26%	18%	24%	46%	8%	21%
Formaldehyde		4%	7%	5%	9%	1%	2%
Formic acid		13%	16%	17%	22%	0%	0%
Methoxylacetic acid		17%	28%	2%	5%	0%	0%
Glycolic acid		0%	0%	1%	4%	0%	0%
EGD		20%	27%	0%	0%	7%	12%

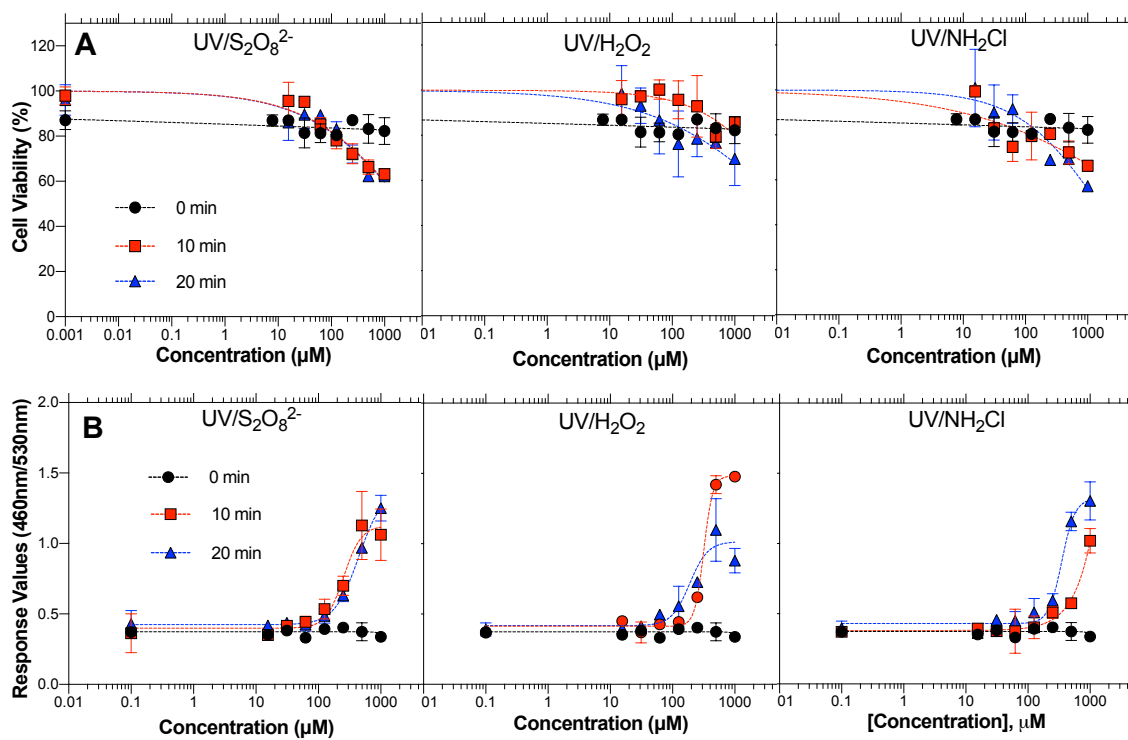


**Figure 37** (A) Cytotoxicity and (B) Genotoxicity evolution of 1,4-D during UV/AOPs treatment.

### 5.3. Results and Discussion

#### 5.3.1 Products distribution of benzene in treatments of $\text{MnO}_4^-$ , goethite-activated $\text{S}_2\text{O}_8^{2-}$ and $\text{H}_2\text{O}_2$

The rates of oxidant disappearance followed the order of  $\text{H}_2\text{O}_2 > \text{S}_2\text{O}_8^{2-} > \text{MnO}_4^-$  (**Figure 38A**), and benzene degradation followed the same order (**Figure 38B**). Approximately 80%, 90% and less than 5% of benzene was oxidized by  $\text{H}_2\text{O}_2$ ,  $\text{S}_2\text{O}_8^{2-}$ , and  $\text{MnO}_4^-$ , respectively.  $\text{H}_2\text{O}_2$  was quickly activated by goethite in the first three days; hence, benzene was also quickly oxidized. After three days, all  $\text{H}_2\text{O}_2$  was completely consumed and benzene degradation also stopped.  $\text{S}_2\text{O}_8^{2-}$  was very persistent and its concentration remained stable throughout 20 days of reaction. Benzene was slowly, but continuously degraded by activated  $\text{S}_2\text{O}_8^{2-}$ , and achieved better removal efficiency than  $\text{H}_2\text{O}_2$ .  $\text{MnO}_4^-$  was not consumed and only less than 5% of benzene disappeared, probably due to volatilization. Goethite-activated  $\text{H}_2\text{O}_2$  produced highly reactive  $\text{OH}^\bullet$ , that reacted with benzene at a diffusion-controlled rate ( $7.8 \times 10^9 \text{ M}^{-1}\text{s}^{-1}$ ).<sup>48</sup> However, iron oxide could also decompose  $\text{H}_2\text{O}_2$  without producing radicals.<sup>49</sup> In addition,  $\text{OH}^\bullet$  also oxidized  $\equiv\text{Fe}^{2+}$  to  $\equiv\text{Fe}^{3+}$ ,<sup>50</sup> making  $\text{H}_2\text{O}_2$  a less efficient process. In contrast,  $\text{S}_2\text{O}_8^{2-}$  has been reported to be more persistent, which may help achieve long term remediation goals.<sup>51</sup>  $\text{MnO}_4^-$  was unable to oxidize benzene, which was consistent with a previous study.<sup>52</sup>

The distribution of benzene oxidation products was shown in **Figure 38C** and **D**. Two major products, phenol and an unsaturated aldehyde were observed in  $\text{H}_2\text{O}_2$  and  $\text{S}_2\text{O}_8^{2-}$  treatments. The mechanism of benzene degradation to phenol and the unsaturated aldehyde

was proposed by a previous study and showed that in **Scheme 10**.<sup>43</sup> No products were observed in the treatment with  $\text{MnO}_4^-$ . In the  $\text{S}_2\text{O}_8^{2-}$  treatment, product formation reached a peak at day 3, and then were quickly oxidized by  $\text{SO}_4^{\bullet-}$ . At the peak, the phenol and aldehyde accounted for 60% and 15% of degraded benzene, respectively. Another 30% of undefined products were probably carboxylic acids, which were not the focus in this study. In  $\text{H}_2\text{O}_2$  treatment, product formation peaked after 1 day of reaction with 35% of phenol and 20% of aldehyde.

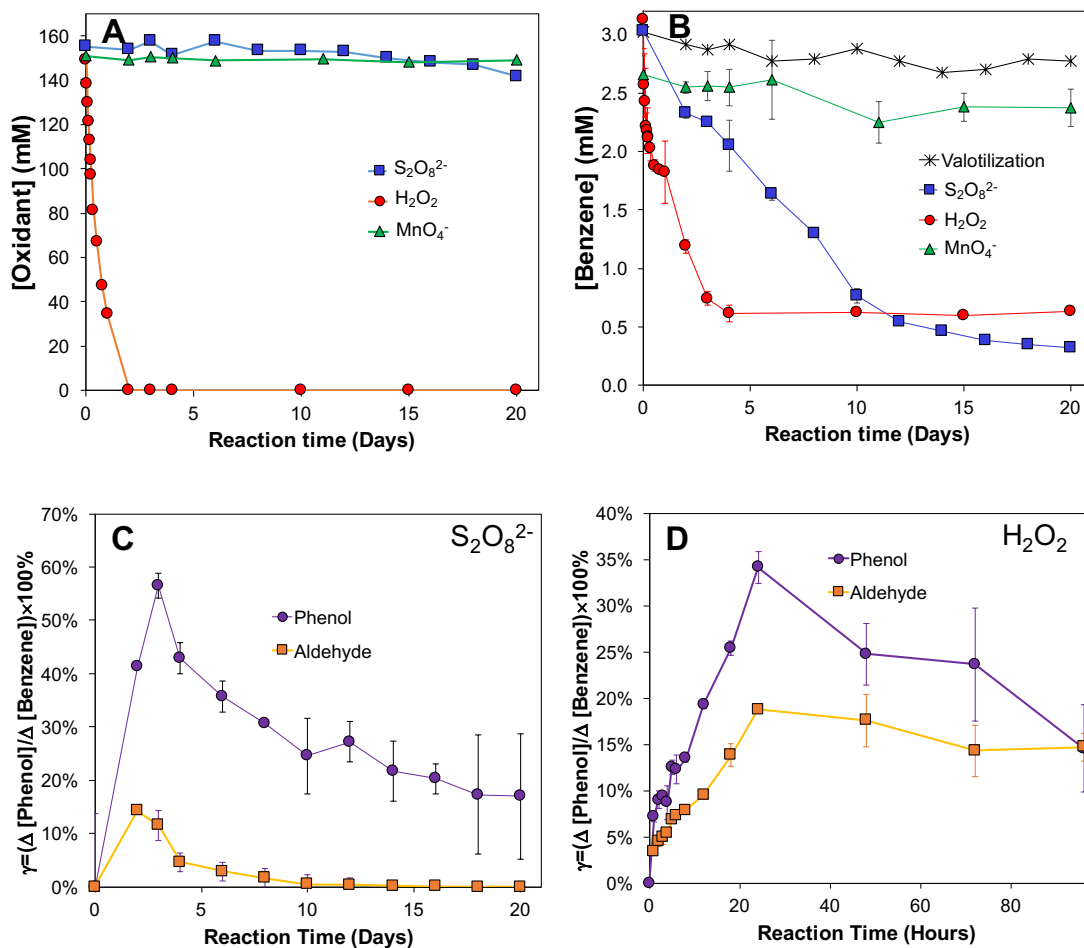
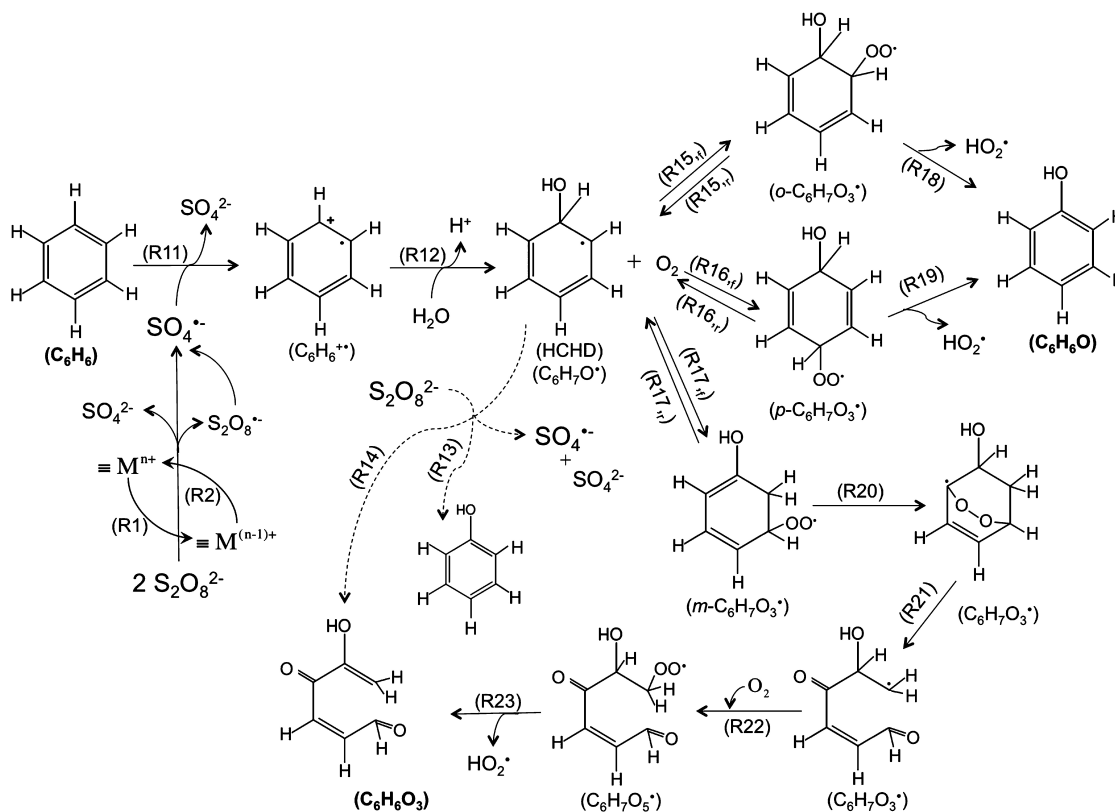


**Figure 38** Benzene degradation and products evolution in  $\text{S}_2\text{O}_8^{2-}$ ,  $\text{H}_2\text{O}_2$  and  $\text{MnO}_4^-$ . (A) benzene degradation; (B) products formation in goethite-activated  $\text{S}_2\text{O}_8^{2-}$ ; (C) products formation in goethite-activated  $\text{H}_2\text{O}_2$ . [Oxidants]=150mM, [Benzene]=3mM, pH=8.



**Scheme 10** Proposed benzene degradation pathway. Derived from Liu et. al. 2016.

### 5.3.2 Products distribution of 1,4-dioxane in UV/S<sub>2</sub>O<sub>8</sub><sup>2-</sup>, UV/H<sub>2</sub>O<sub>2</sub>, UV/NH<sub>2</sub>Cl

In general, UV/S<sub>2</sub>O<sub>8</sub><sup>2-</sup> had faster kinetics with respect to 1,4-dioxane removal than UV/H<sub>2</sub>O<sub>2</sub> and UV/NH<sub>2</sub>Cl (**Figure 39**). UV/S<sub>2</sub>O<sub>8</sub><sup>2-</sup> had a higher quantum yield than UV/H<sub>2</sub>O<sub>2</sub> (0.7 vs. 0.5), and produced a diverse set of radicals including both SO<sub>4</sub><sup>•-</sup> and HO<sup>•</sup>.<sup>53</sup> UV/NH<sub>2</sub>Cl produced less reactive Cl<sup>•</sup> and Cl<sub>2</sub><sup>•-</sup>, which both had slow kinetics with 1,4-dioxane transformation.<sup>54</sup> Furthermore, the NH<sub>2</sub>Cl itself was a strong scavenger and decreased radical yield.<sup>54</sup> Product distribution in three UV/AOPs showed similar product evolution pathways after 1,4-dioxane was oxidized (**Scheme 11**). The oxidation products

included ethylene glycol diformate (EGD), formaldehyde (FD), glycolaldehyde (GD), glycolic acid (GA), formic acid (FA), and methoxyacetic acid (MA), which were consistent with previous observations.<sup>55</sup> GA was not observed in UV/S<sub>2</sub>O<sub>8</sub><sup>2-</sup> treatments, and EGD was not observed in treatments with UV/H<sub>2</sub>O<sub>2</sub>. In UV/NH<sub>2</sub>Cl treatments, only aldehyde products were observed. Both UV/S<sub>2</sub>O<sub>8</sub><sup>2-</sup> and UV/H<sub>2</sub>O<sub>2</sub> promoted further oxidation of EGD, GD, and FD to FA, GA and MA, while UV/NH<sub>2</sub>Cl did not efficiently degrade aldehyde products.

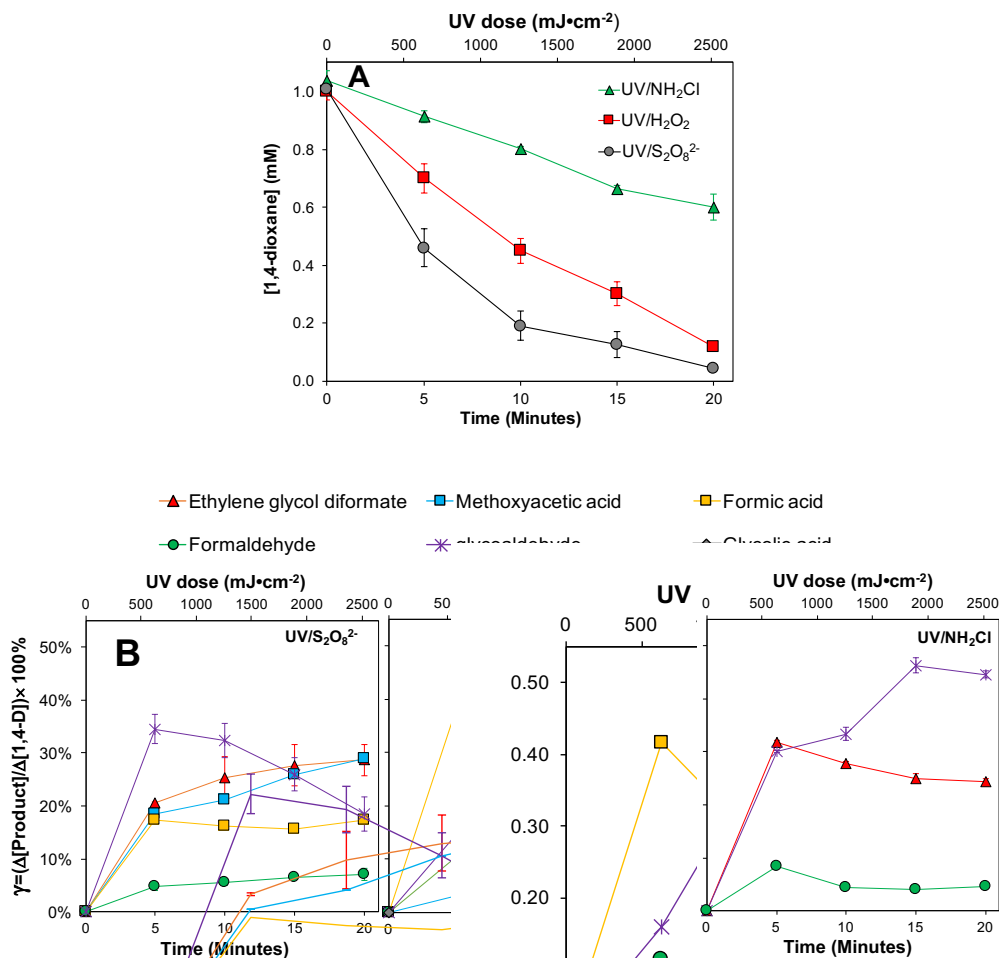
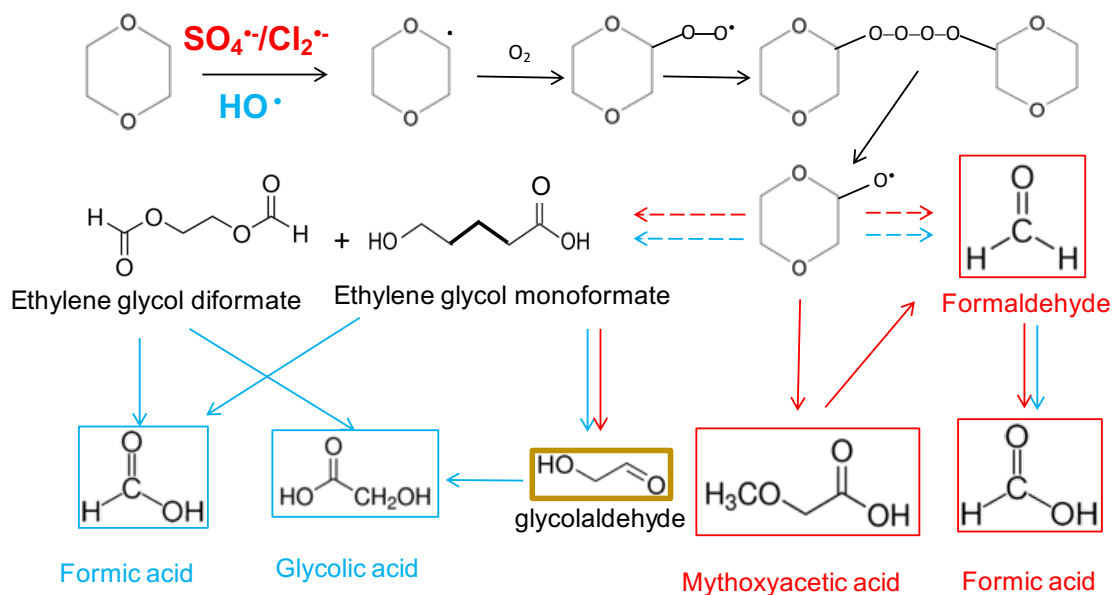


**Figure 39.** 1,4-D degradation and products evolution in UV/S<sub>2</sub>O<sub>8</sub><sup>2-</sup>, UV/H<sub>2</sub>O<sub>2</sub>, UV/NH<sub>2</sub>Cl. (A) 1,4-D degradation; (B) Product formation. [Oxidants]=5mM, [1,4-Dioxane]=1mM, pH=8.



**Scheme 11** Proposed 1,4-Dioxane degradation pathway in  $\text{UV}/\text{S}_2\text{O}_8^{2-}$ ,  $\text{UV}/\text{H}_2\text{O}_2$ , and  $\text{UV}/\text{NH}_2\text{Cl}$ .

### 5.3.3 Cytotoxicity and genotoxicity of benzene and its OBPs

The  $\text{EC}_{50}$  of benzene and its oxidation products was derived from the concentration response curve shown in **Figure 40A** and listed in **Table 15**. The cytotoxicity rank order was: aldehyde > phenol > benzene, with aldehyde being the most cytotoxic ( $\text{EC}_{50} = 26 \mu\text{M}$ ) followed by phenol ( $\text{EC}_{50} = 36 \mu\text{M}$ ) and benzene ( $\text{EC}_{50} = 292 \mu\text{M}$ ). Genotoxicity also followed the same order (**Figure 40B**). The  $\text{EC}_{50}$  determined was  $22 \mu\text{M}$  for aldehyde,  $694 \mu\text{M}$  for phenol, and non-determinable for benzene. Unsaturated aldehydes have been reported to be 100-300-fold more cytotoxic to human bronchial fibroblasts than saturated aldehydes.<sup>56</sup> Unsaturated aldehydes affect cell survival and thiol levels by inhibiting the DNA repair enzyme,  $\text{O}^6$ -methylguanine-DNA methyltransferase.<sup>56</sup> It may also impair cellular defense mechanisms such as DNA repair and detoxification, and make cells

susceptible to other toxic chemical.<sup>56</sup> In addition, unsaturated aldehydes are capable of inducing sister-chromatid-exchange and production of micronuclei, which are indicators of genotoxicity.<sup>57</sup> Phenol has been used as positive control substance for cytotoxicity assays in Balb/c 3T3 cells and showed linear cytotoxic responses.<sup>58,59</sup> Phenol induced cytotoxicity by generating phenoxyl radicals, that caused site-specific oxidative stress in the membrane phospholipids and decreased protein SH groups.<sup>60</sup> Phenol induced chromatid breaks and exchanges which resulted in DNA damage.<sup>61</sup> Benzene has also been reported to induce cytotoxicity and genotoxicity in bone marrow cells; however, the mechanism is still unclear.<sup>62</sup>

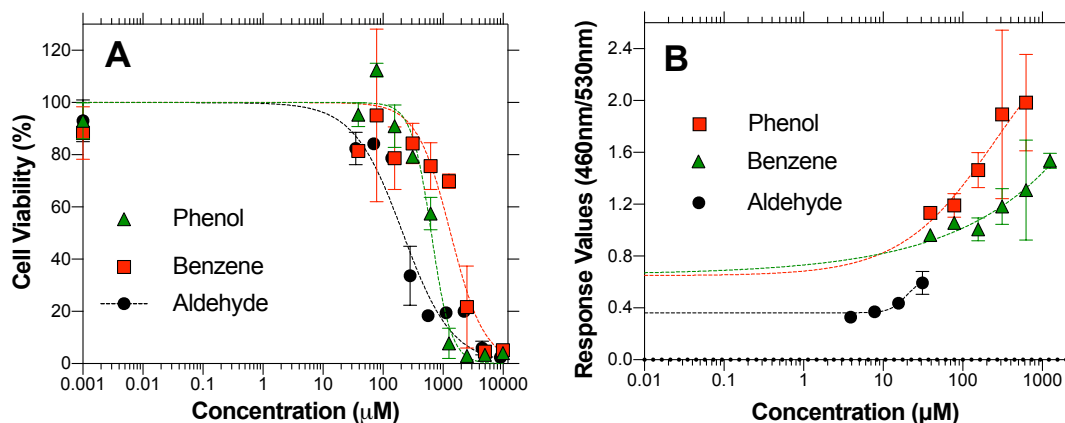


**Figure 40** (A) Cytotoxicity and (B) Genotoxicity concentration response curves of benzene, phenol, and aldehyde. Each value represents the mean of three replicates  $\pm$  standard deviation.

**Table 14.** EC<sub>50</sub> values of benzene and its degradation products in P53RE-bla HCT-116 cell line after 16h exposure.

<b>Toxic rank order</b>	<b>Benzene &amp; DPs</b>	<b>Cytotoxicity EC<sub>50</sub>(uM)</b>	<b>Genotoxicity EC<sub>50</sub>(uM)</b>
1	Aldehyde	26 ± 27%	20 ± 59%
2	Phenol	36 ± 13%	256 ± 81%
3	Benzene	202 ± 36%	-

#### 5.3.4 Cytotoxicity and genotoxicity of 1,4-dioxane and its OBPs

**Figure 41A** presents a concentration-response curve of cell viability for 1,4-Dioxane, FD and GD in HCT-116 cells. Other compounds that had negligible cytotoxicity were shown in **Figure 42**. The EC<sub>50</sub> concentrations were reported in **Table 15**, with GD being the most cytotoxic (EC<sub>50</sub>= 155 μM) followed by FD (EC<sub>50</sub>=613 μM). The rank order for cytotoxicity of 1,4-dioxane and its OPDs based on their LC<sub>50</sub> values was: GD > FD > FA > GA > 1,4-Dioxane > EGD ≈ MA. In general, aldehyde compounds (*i.e.*, GD and FD) exhibited high cytotoxicity except EDF. GD was highly cytotoxic to HK-2 cells and caused depletion of adenosine triphosphate (ATP), release of lactate dehydrogenase (LDH), and degradation of enzymes as well as selected phospholipids.<sup>63</sup> GD also induced growth inhibition and oxidative stress in human breast cancer cells.<sup>64</sup> FD is a known carcinogen and highly reactive with proteins and DNA.<sup>65</sup> FD-induced cytotoxicity inhibited mitochondrial respiration, decreased ATP depletion, and generated reactive oxygen species which contributed to oxidative stress and cell lysis in isolated rat hepatocytes.<sup>66</sup> EGD has two carbonyl groups; however, when applied to HCT-116 cells, cell viability was not reduced in the present study. Although studies on the toxicity of EGD have not been

reported, our data suggests EGD might be quickly metabolized to downstream products that are not cytotoxic.

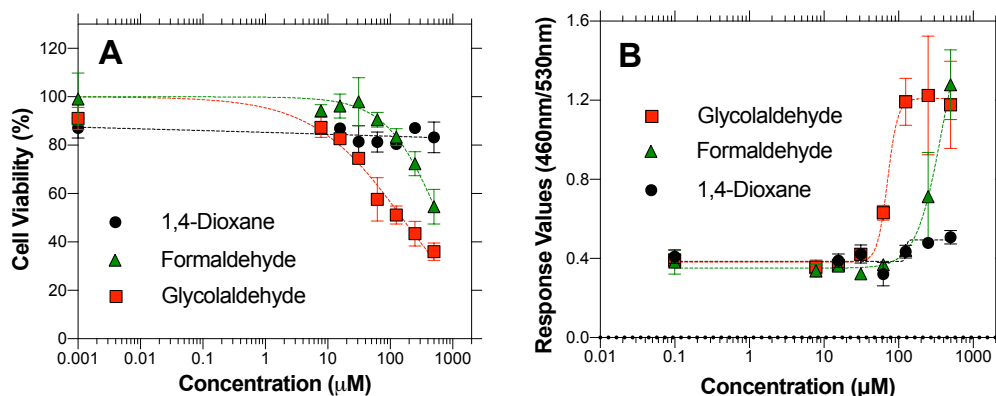


**Figure 41.** (A) Cytotoxicity and (B) Genotoxicity dose response curves of 1,4-dioxane, Formaldehyde, and glycolaldehyde. Each value represents the mean of three replicates  $\pm$  standard deviation.

**Table 15.** LC<sub>50</sub>, EC<sub>50</sub> and relative effect potency (REP) values of 1,4-dioxane and its degradation products in P53RE-bla HCT-116 cell line after 16h exposure.

Toxicity-level Ranking	Chemicals	Cytotoxicity EC <sub>50</sub> (uM)	Genotoxicity EC <sub>50</sub> (uM)	REP*
1	Glycolaldehyde	$(1.6 \pm 0.2) \times 10^2$	$(7.1 \pm 1.0) \times 10^1$	$6.7 \times 10^{-2}$
2	Formaldehyde	$(6.1 \pm 0.9) \times 10^2$	$(4.0 \pm 2.5) \times 10^2$	$1.2 \times 10^{-2}$
3	Formic acid	$(1.3 \pm 30) \times 10^{14}$	-	-
4	Glycolic acid	$(7.8 \pm 31) \times 10^{15}$	-	-
5	1,4-dioxane	$(1.1 \pm 5.2) \times 10^{29}$	$>(2.0 \pm 7.9) \times 10^4$	$2.4 \times 10^{-4}$

\* Relative genotoxicity effect potency values,  $REP = EC_{50}(\text{mitomycin}) / EC_{50}(i)$ , where  $i$  is a specific degradation product.

Aldehydes are highly reactive electrophilic molecules that damage DNA through formation of aldehyde-derived DNA adducts.<sup>67,68</sup> The genotoxicity assay using P53-GeneBLazer Assay indicated that aldehyde compounds were highly genotoxic (**Figure 41B**) compared to 1,4-dioxane and its carboxylic acid degradates (**Figure 42B**). The EC<sub>50</sub>

concentrations were 71  $\mu\text{M}$  for GD and 395  $\mu\text{M}$  for FD (**Table 15**). 1,4-dioxane showed relatively low genotoxicity with an  $\text{EC}_{50} > 20000 \mu\text{M}$ . GD has been reported to cause DNA-protein crosslinks and DNA single-strand breaks in human peripheral ononuclear blood cells.<sup>69</sup> Similarly, FD formed adducts with DNA and proteins,<sup>70</sup> and resulted in chromosome loss due to formaldehyde-induced defects in the mitotic apparatus.<sup>71</sup> In agreement with our observation, 1,4-dioxane produced negative genotoxicity responses in several in vitro assays.<sup>72,73</sup> A few studies reported that 1,4-dioxane elevated chromosomal breaks and DNA repairs in rats or mice with chonical injection of 1,4-dioxane.<sup>74,75</sup> Our results indicated that 1,4-dioxane is a weak geno-toxinant to human cells. In contrast, its aldehyde OBPs were extreamtly toxic to human cells.

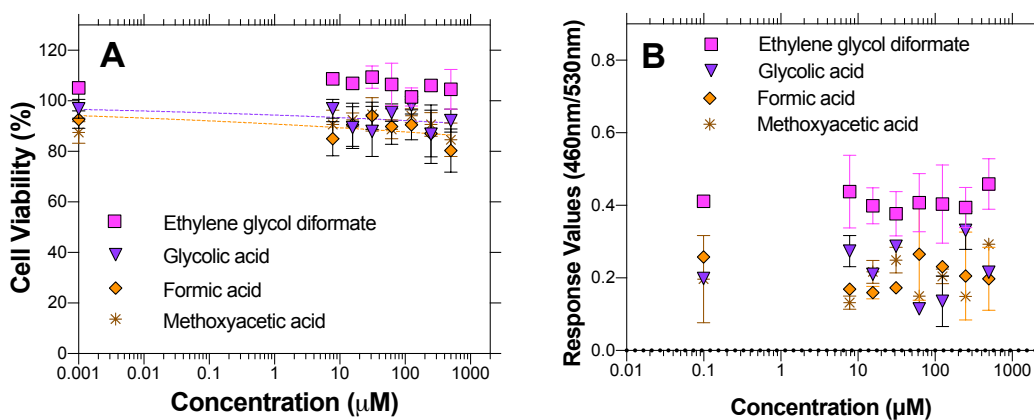


**Figure 42** (A) Cytotoxicity and (B) Genotoxicity dose response curves of Ethylenen glycol diformate, glycolic acid, formic acid and methoxyacetic acid. Each value represents the mean of three replicates  $\pm$  standard deviation.

### 5.3.5 Genotoxicity comparison among $\text{UV}/\text{S}_2\text{O}_8^{2-}$ , $\text{UV}/\text{H}_2\text{O}_2$ , and $\text{UV}/\text{NH}_2\text{Cl}$ treatments

The mitomycin equivalency quotient (MEQ) at the beginning (0 minute), middle (10 minutes), and end (20 minutes) of the UV treatment was compared for the three

UV/AOP treatments (**Figure 43**). At the beginning of the treatment, 1,4-dioxane was only chemical present in the system with a mitomycin EQ of  $2.4 \times 10^{-4}$ . After 10 minutes of UV irradiation, UV/S<sub>2</sub>O<sub>8</sub><sup>2-</sup>, UV/H<sub>2</sub>O<sub>2</sub>, and UV/NH<sub>2</sub>Cl treatments increased the mitomycin EQs from  $2.4 \times 10^{-4}$  to  $1.9 \times 10^{-2}$ ,  $1.6 \times 10^{-2}$ , and  $4.0 \times 10^{-3}$ , respectively (Figure 3). Glycolaldehyde was consistently the major contributor to the mitomycin EQs in the three AOP treatments (**Table 15** and **Figure 13**). After 20 min UV/S<sub>2</sub>O<sub>8</sub><sup>2-</sup> treatment, the mitomycin EQ was decreased from  $1.9 \times 10^{-2}$  to  $1.2 \times 10^{-2}$ , due to the oxidation of glycolaldehyde to non-toxic carboxylic acids (**Figure 13**). In contrast, UV/H<sub>2</sub>O<sub>2</sub>, and UV/NH<sub>2</sub>Cl treatments further increased the mitomycin EQs 2 to 3 folds after 20 minutes (Figure 3), which was consistent with the 2-3-fold increase of glycolaldehyde concentrations. The results suggest that UV/S<sub>2</sub>O<sub>8</sub><sup>2-</sup> can quickly oxidize 1,4-dioxane and further degrade its products; while UV/H<sub>2</sub>O<sub>2</sub> and UV/NH<sub>2</sub>Cl degraded 1,4-dioxane at slower rates, resulting in an accumulation of toxic glycolaldehyde during the treatment. In comparison with UV/H<sub>2</sub>O<sub>2</sub>, UV/NH<sub>2</sub>Cl exhibited lower TEQ because UV/NH<sub>2</sub>Cl was inefficient to degrade 1,4-Dioxane, as evidenced by the large portion of 1,4-dioxane remaining after 20-minutes of treatment.

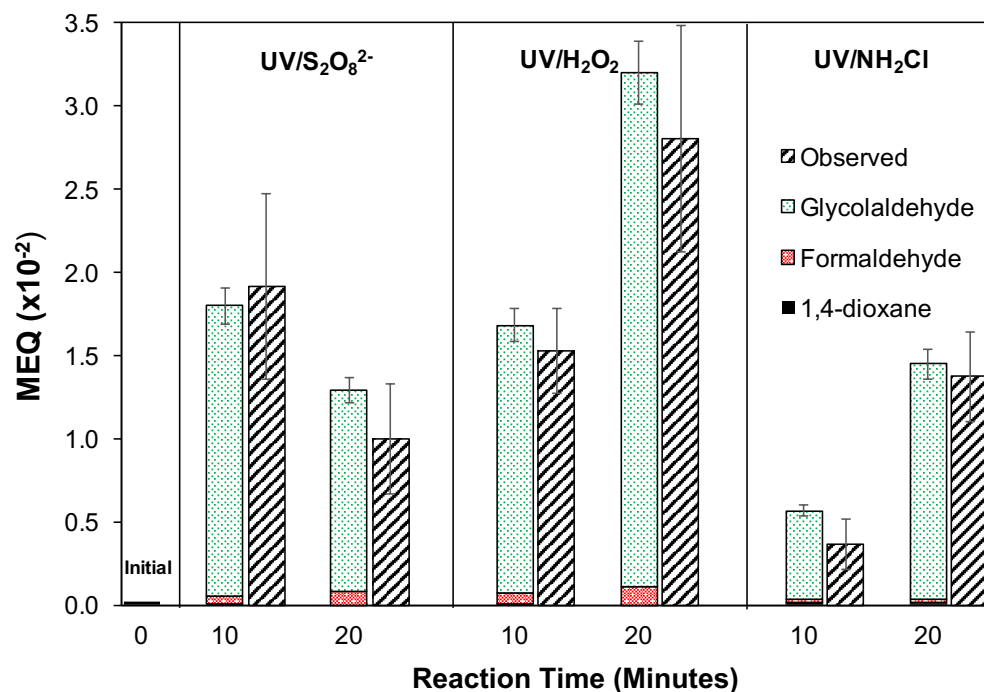


**Figure 43.** Mitomycin Equivalent of genotoxicity evolution during UV/AOPs treatment. Observed Mitomycin Equivalent was the calculated based on experimentally obtained EC<sub>50</sub> (Details please refer to Text S5). Error bars represent SQRT. UV/S<sub>2</sub>O<sub>8</sub><sup>2-</sup>: two-way ANOVA test showed no difference between calculated and observed MEQ (P=0.677); and a significant difference between MEQ at time 0, 10 and 20 (P=0.014). UV/H<sub>2</sub>O<sub>2</sub>: calculated vs. Observed (P=0.254); time factor (P=0.0043). UV/NH<sub>2</sub>Cl: calculated vs. Observed (P=0.250); time factor (P=0.005).

#### 5.4 Engineering Implications

AOPs are usually implemented in ISCO and water reuse treatment processes due to their ability to degrade contaminants. However, our study brought up the concerns of the formation of more toxic OBPs during AOP treatments while treating toxic contaminants in groundwater or recycled wastewater. Oxidizing benzene by mineral-activated S<sub>2</sub>O<sub>8</sub><sup>2-</sup> and H<sub>2</sub>O<sub>2</sub> generated more toxic phenol and an unsaturated aldehyde. In the case of 1,4-dioxane degradation by UV/S<sub>2</sub>O<sub>8</sub><sup>2-</sup>, UV/H<sub>2</sub>O<sub>2</sub>, and UV/NH<sub>2</sub>Cl, the oxidation

generates glycolaldehyde and formaldehyde that are 100 times more toxic than 1,4-dioxane. For many aromatic compounds, the initial oxidation steps usually leads to the formation of aldehydes as intermediates with high geno- and cyto- toxicity. Despite the low-level existence of OBPs in highly treated water, the risk of long term exposure warrants great attention. Our results also demonstrate that  $S_2O_8^{2-}$  is a much more stable oxidant than  $H_2O_2$  when applied to ISCO treatment, and can completely remove parent compound and oxidation products with extended treatment. UV/  $S_2O_8^{2-}$  is also superior to UV/ $H_2O_2$  and UV/ $NH_2Cl$  in terms of minimizing the formation of more toxic OBPs. For instance, UV/ $S_2O_8^{2-}$  showed a better efficiency in degrading both 1,4-dioxane and its OBPs to nontoxic derivatives than UV/ $H_2O_2$ , and UV/ $NH_2Cl$ .

## **5.5 Acknowledgments**

This research was partially supported by grants to H.L. from National Science Foundation (CHE-1611306) and the UC Riverside Faculty Initiation Research Fund, and to W.L. from the National Science Foundation Graduate Research Fellowship, IGERT Water Sense Fellowship, and One Health Fellowship. We thank Shane Snyder at University of Arizona for providing the HTC-116 cell lines.

## Reference:

---

- <sup>1</sup> Bove, F. J.; Fulcomer, M. C.; Klotz, J. B.; Esmart, J.; Dufficy, E. M.; Savrin, J. E. Public drinking water contamination and birth outcomes. *American Journal of Epidemiology*. **1995**, *141* (9), 850-862.
- <sup>2</sup> Suja, F.; Pramanik, B. K.; Zain, S. M. Contamination, bioaccumulation and toxic effects of perfluorinated chemicals (PFCs) in the water environment: a review paper. *Water Science and Technology*. **2009**, *60*(6), 1533-1544.
- <sup>3</sup> Wright, J.; Gundry, S.; Conroy, R. Household drinking water in developing countries: a systematic review of microbiological contamination between source and point-of-use. *Tropical Medicine & International Health*. **2004**, *9* (1), 106-117.
- <sup>4</sup> Pye, V. I.; Patrick, R. Ground water contamination in the United States. *Science*. **1983**, *221* (4612), 713-718.
- <sup>5</sup> Cronk, G. Case study comparison of multiple activation methods for sodium persulfate ISCO treatment. In *Sixth International Conference on Remediation of Chlorinated and Recalcitrant Compounds*. **2008**, 200.
- <sup>6</sup> Brown, R.; Robinson, D. D.; Sethi, D.; Block, P. Second generation persulfate ISCO. In *Second International Conference on Oxidation and Reduction Technologies for In-Situ Treatment of Soil and Groundwater*. **2002**, 17.
- <sup>7</sup> Ortiz, M.; Raluy, R. G.; Serra, L. Life cycle assessment of water treatment technologies: wastewater and water-reuse in a small town. *Desalination*. **2007**, *204* (1-3), 121-131.
- <sup>8</sup> Huling, Scott G.; Bruce E. Pivetz. *In-situ chemical oxidation*. No. EPA/600/R-06/072. USEPA, Washington DC Office of Water, 2006.
- <sup>9</sup> Sra, K. S.; Thomson, N. R.; Barker, J. F. Persistence of persulfate in uncontaminated aquifer materials. *Environmental Science & Technology*. **2010**, *44* (8), 3098-3104.
- <sup>10</sup> Liang, S. H.; Kao, C. M.; Kuo, Y. C.; Chen, K. F.; Yang, B. M. *In situ* oxidation of petroleum-hydrocarbon contaminated groundwater using passive ISCO system. *Water Research*. **2011**, *45* (8), 2496-2506.
- <sup>11</sup> Westerhoff, P.; Moon, H.; Minakata, D.; Crittenden, J. Oxidation of organics in retentates from reverse osmosis wastewater reuse facilities. *Water Research*. **2009**, *43* (16), 3992-3998.
- <sup>12</sup> Watts, R. J.; Teel, A. L. Treatment of contaminated soils and groundwater using ISCO. *Practice Periodical of Hazardous, Toxic, and Radioactive Waste Management*. **2006**, *10* (1), 2-9.

- 
- <sup>13</sup> Wols, B. A.; Hofman-Caris, C. H. M. Review of photochemical reaction constants of organic micropollutants required for UV advanced oxidation processes in water. *Water Research*. **2012**, *46* (9), 2815-2827.
- <sup>14</sup> Lester, Y.; Ferrer, I.; Thurman, E. M.; Linden, K. G. Demonstrating sucralose as a monitor of full-scale UV/AOP treatment of trace organic compounds. *Journal of hazardous materials*. **2014**, *280*, 104-110.
- <sup>15</sup> Pereira, V. J.; Linden, K. G.; Weinberg, H. S. Evaluation of UV irradiation for photolytic and oxidative degradation of pharmaceutical compounds in water. *Water Research*. **2007**, *41* (19), 4413-4423.
- <sup>16</sup> Grünwald, A.; Šťastný, B.; Slavíčková, K.; Slavíček, M. Formation of haloforms during chlorination of natural waters. *Acta Polytechnica*. **2002**, *42* (2).
- <sup>17</sup> Bellar, T. A.; Lichtenberg, J. J.; Kroner, R. C. The occurrence of organohalides in chlorinated drinking waters. *Journal (American Water Works Association)*. **1974**, 703-706.
- <sup>18</sup> Richardson, S. D.; Postigo, C. *Drinking water disinfection by-products*. In Emerging organic contaminants and human health. Springer Berlin Heidelberg. 2011, pp. 93-137.
- <sup>19</sup> Richardson, S. D.; Simmons, J. E.; Rice, G. *Peer reviewed: disinfection byproducts: the next generation*. 2002.
- <sup>20</sup> Boorman, G. A. Drinking water disinfection byproducts: review and approach to toxicity evaluation. *Environmental Health Perspectives*. **1999**, *107* (Suppl 1), 207.
- <sup>21</sup> Richardson, S. D.; Plewa, M. J.; Wagner, E. D.; Schoeny, R.; DeMarini, D. M. Occurrence, genotoxicity, and carcinogenicity of regulated and emerging disinfection by-products in drinking water: a review and roadmap for research. *Mutation Research/Reviews in Mutation Research*. **2007**, *636* (1), 178-242.
- <sup>22</sup> Von Gunten, U.; Hoigné, J. Bromate formation during ozonation of bromide-containing waters: interaction of ozone and hydroxyl radical reactions. *Environmental Science & Technology*. **1994**, *28* (7), 1234-1242.
- <sup>23</sup> Krasner, S. W.; Glaze, W. H.; Weinberg, H. S.; Daniel, P. A.; Najm, I. N. Formation and control of bromate during ozonation of waters containing bromide. *Journal/American Water Works Association*. **1993**, *85* (1), 73-81.
- <sup>24</sup> Haag, W. R.; Hoigne, J. Ozonation of bromide-containing waters: kinetics of formation of hypobromous acid and bromate. *Environmental Science & Technology*. **1983**, *17* (5), 261-267.

- 
- <sup>25</sup> Pinkernell, U.; von Gunten, U. Bromate minimization during ozonation: mechanistic considerations. *Environmental Science & Technology*. **2001**, *35* (12), 2525-2531.
- <sup>26</sup> Choi, J.; Valentine, R. L. Formation of N-nitrosodimethylamine (NDMA) from reaction of monochloramine: a new disinfection by-product. *Water Research*. **2002**, *36* (4), 817-824.
- <sup>27</sup> Le Roux, J.; Gallard, H.; Croué, J. P. Chloramination of nitrogenous contaminants (pharmaceuticals and pesticides): NDMA and halogenated DBPs formation. *Water Research*. **2011**, *45* (10), 3164-3174.
- <sup>28</sup> Cornwell, D. A.; Brown, R. A.; Krasner, S. W. Evaluating Polymers to Avoid Polymer-Induced N-Nitrosodimethylamine Formation. *Journal-American Water Works Association*. **2017**, *109* (6), E197-E214.
- <sup>29</sup> McCurry, D. L.; Krasner, S. W.; Von Gunten, U.; Mitch, W. A. Determinants of disinfectant pretreatment efficacy for nitrosamine control in chloraminated drinking water. *Water Research*. **2015**, *84*, 161-170.
- <sup>30</sup> Krasner, S. W.; Mitch, W. A.; Westerhoff, P.; Dotson, A. Formation and control of emerging C-and N-DBPs in drinking water. *Journal-American Water Works Association*. **2012**, *104*(11), E582-E595.
- <sup>31</sup> Oliveira, A.; Maniero, M. G.; Guimaraes, J. R. Lomefloxacin degradation: antimicrobial activity, toxicity and byproducts. *Journal of Advanced Oxidation Technologies*. **2015**, *18* (2), 211-220.
- <sup>32</sup> Fernández-Alba, A. R.; Hernando, D.; Agüera, A.; Cáceres, J.; Malato, S. Toxicity assays: a way for evaluating AOPs efficiency. *Water Research*. **2002**, *36* (17), 4255-4262.
- <sup>33</sup> de Luna, L. A.; da Silva, T. H.; Nogueira, R. F. P.; Kummrow, F.; Umbuzeiro, G. A. Aquatic toxicity of dyes before and after photo-Fenton treatment. *Journal of Hazardous Materials*. **2014**, *276*, 332-338.
- <sup>34</sup> Synder R.; Kocsis JJ.; Drew, R. Current concept of chronic benzene toxicity. *CRC Critical Review in Toxicology*. **1975**, *3*, (3) 265-288.
- <sup>35</sup> Snyder R. The benzene problem in historical perspective. *Fundamental and Applied Toxicology*. **1984**, *4* (5), 692-699.
- <sup>36</sup> Uzochukwu G.; Schimmel, K.; Chang, S.-Y.; Kabadi, V.; Luster-Teasley, S.; Reddy, G. Nzewi, E. *Proceedings of the 2007 National Conference on Environmental Science and Technology*. Springer-Verlag, New York: 2009.

- 
- <sup>37</sup> Simonich, S. M.; Sun, P.; Casteel, K.; Dyer, S.; Wernery, D.; Garber, K., ... Federle, T. Probabilistic analysis of risks to us drinking water intakes from 1, 4-dioxane in domestic wastewater treatment plant effluents. *Integrated Environmental Assessment and Management*. **2013**, *9* (4), 554-559.
- <sup>38</sup> Patel, M. UV/AOP A Key Part of the Groundwater Replenishment System. *Proceedings of the Water Environment Federation*. **2011**, (13), 3516-3525.
- <sup>39</sup> Li, W.; Orozco, R.; Camargos, N.; Liu, H. Mechanisms on the Impacts of Alkalinity, pH, and Chloride on Persulfate-Based Groundwater Remediation. *Environmental Science & Technology*. **2017**, *51* (7), 3948-3959.
- <sup>40</sup> Ballester, N. A.; Malley, J. P. Sequential disinfection of adenovirus type 2 with UV-chlorine-chloramine. *Journal (American Water Works Association)*. **2004**, *96* (10), 97-103.
- <sup>41</sup> Lyon, B. A.; Dotson, A. D.; Linden, K. G; Weinberg, H. S. The effect of inorganic precursors on disinfection byproduct formation during UV-chlorine/chloramine drinking water treatment. *Water Research*. **2012**, *46* (15), 4653-4664.
- <sup>42</sup> Yang, C.; Xu, Y. R.; Teo, K. C.; Goh, N. K.; Chia, L. S.; Xie, R. J. Destruction of organic pollutants in reusable wastewater using advanced oxidation technology. *Chemosphere*. **2005**, *59* (3), 441-445.
- <sup>43</sup> Schwertmann, U.; Cambier, P.; Murad, E. Properties of goethite of varying crystallinity. *Clays and Clay Minerals*. **1985**, *33* (5), 369-378.
- <sup>44</sup> Liu, H.; Bruton, T. A.; Li, W.; Buren, J. V.; Prasse, C.; Doyle, F. M.; Sedlak, D. L. Oxidation of benzene by persulfate in the presence of Fe (III)-and Mn (IV)-containing oxides: stoichiometric efficiency and transformation products. *Environmental Science & Technology*. **2016** *50* (2), 890-898.
- <sup>45</sup> US Environmental Protection Agency. Method 8315A. Determination of carbonyl compounds by high performance liquid chromatography.
- <sup>46</sup> Rice, E.; Baird, R.; Eaton, A.; Cleceri, L. *Standard Methods for the Examination of Water and Wastewater 22nd Edition*; 2012.
- <sup>47</sup> Escher, B. I.; Allinson, M.; Altenburger, R.; Bain, P. A.; Balaguer, P.; Busch, W., Crago, J; Denslo, N. D.; Dopp, E.; Hilscherova, K.; Humpage, A. R.;...Humpage, A. R. Benchmarking organic micropollutants in wastewater, recycled water and drinking water with in vitro bioassays. *Environmental Science & Technology*. **2013**, *48* (3), 1940-1956.

- 
- <sup>48</sup> Gordon, S.; Schmidt, K. H.; Hart, E. J. A pulse radiolysis study of aqueous benzene solutions. *The Journal of Physical Chemistry*. **1977**, *81* (2), 104-109.
- <sup>49</sup> Pham, A. L. T., Doyle, F. M., & Sedlak, D. L. (2012). Kinetics and efficiency of H<sub>2</sub>O<sub>2</sub> activation by iron-containing minerals and aquifer materials. *Water research*, *46*(19), 6454-6462.
- <sup>50</sup> Lin, S. S.; Gurol, M. D. Catalytic decomposition of hydrogen peroxide on iron oxide: kinetics, mechanism, and implications. *Environmental Science & Technology*. **1998**, *32* (10), 1417-1423.
- <sup>51</sup> Sra, K. S.; Thomson, N. R.; Barker, J. F. Persistence of persulfate in uncontaminated aquifer materials. *Environmental Science & Technology*. **2010**, *44* (8), 3098-3104.
- <sup>52</sup> Brown, G. S.; Barton, L. L.; Thomson, B. M. Permanganate oxidation of sorbed polycyclic aromatic hydrocarbons. *Waste Management*. **2003**, *23* (8), 737-740.
- <sup>53</sup> Li, W.; Jain, T.; Ishida, K.; Liu, H. A mechanistic understanding of the degradation of trace organic contaminants by UV/hydrogen peroxide, UV/persulfate and UV/free chlorine for water reuse. *Environmental Science: Water Research & Technology*. **2017**, *3* (1), 128-138.
- <sup>54</sup> Patton, S.; Li, W.; Couch, K. D.; Mezyk, S. P.; Ishida, K. P.; Liu, H. Impact of the Ultraviolet Photolysis of Monochloramine on 1, 4-Dioxane Removal: New Insights into Potable Water Reuse. *Environmental Science & Technology Letters*. **2016**, *4* (1), 26-30.
- <sup>55</sup> Maurer, T.; Hass, H.; Barnes, I.; Becker, K. H. Kinetic and product study of the atmospheric photooxidation of 1, 4-dioxane and its main reaction product ethylene glycol diformate. *The Journal of Physical Chemistry A*. **1999**, *103* (26), 5032-5039.
- <sup>56</sup> Krokan, H.; Grafstrom, R. C.; Sundqvist, K.; Esterbauer, H.; Harris, C. C. Cytotoxicity, thiol depletion and inhibition of O<sup>6</sup>-methylguanine-DNA methyltransferase by various aldehydes in cultured human bronchial fibroblasts. *Carcinogenesis*. **1985**, *6* (12), 1755-1759.
- <sup>57</sup> Dittberner, U.; Eisenbrand, G.; Zankl, H. Genotoxic effects of the  $\alpha$ ,  $\beta$ -unsaturated aldehydes 2-trans-butenal, 2-trans-hexenal and 2-trans, 6-cis- $\alpha$ -methylacrolein. *Mutation Research/Environmental Mutagenesis and Related Subjects*. **1995**, *335* (3), 259-265.
- <sup>58</sup> Hanks, C. T.; Diehl, M. L.; Craig, R. G.; Makinen, P. K.; Pashley, D. H. Characterization of the "in vitro pulp chamber" using the cytotoxicity of phenol. *Journal of Oral Pathology & Medicine*. **1989**, *18* (2), 97-107.
- <sup>59</sup> Spangberg, L. Kinetic and quantitative evaluation of material cytotoxicity in vitro. *Oral Surgery, Oral Medicine, Oral Pathology*. **1973**, *35* (3), 389-401.

- 
- <sup>60</sup> Shvedova, A. A.; Kommineni, C.; Jeffries, B. A.; Castranova, V.; Tyurina, Y. Y.; Tyurin, V. A., ... Kagan, V. E. Redox cycling of phenol induces oxidative stress in human epidermal keratinocytes. *Journal of Investigative Dermatology*. **2000**, *114* (2), 354-364.
- <sup>61</sup> Stich, H. F.; Rosin, M. P.; Wu, C. H.; Powrie, W. D. The action of transition metals on the genotoxicity of simple phenols, phenolic acids and cinnamic acids. *Cancer Letters*. **1981**, *14* (3), 251-260.
- <sup>62</sup> Recio, L.; Bauer, A.; Faiola, B. Use of genetically modified mouse models to assess pathways of benzene-induced bone marrow cytotoxicity and genotoxicity. *Chemico-biological interactions*. **2005**, *153*, 159-164.
- <sup>63</sup> Poldelski, V.; Johnson, A.; Wright, S.; Rosa, V. D.; Zager, R. A. Ethylene glycol-mediated tubular injury: Identification of critical metabolites and injury pathways. *American Journal of Kidney Diseases*. **2001**, *38* (2), 339-348.
- <sup>64</sup> Al-Enezi, K. S.; Alkhalaf, M.; Benov, L. T. Glycolaldehyde induces growth inhibition and oxidative stress in human breast cancer cells. *Free Radical Biology and Medicine*. **2006**, *40* (7), 1144-1151.
- <sup>65</sup> Shaham, J.; Bomstein, Y.; Meltzer, A.; Kaufman, Z.; Palma, E.; Ribak, J. DNA-protein crosslinks, a biomarker of exposure to formaldehyde—in vitro and in vivo studies. *Carcinogenesis*. **1996**, *17* (1), 121-126.
- <sup>66</sup> Teng, S.; Beard, K.; Pourahmad, J.; Moridani, M.; Easson, E.; Poon, R.; O'Brien, P. J. The formaldehyde metabolic detoxification enzyme systems and molecular cytotoxic mechanism in isolated rat hepatocytes. *Chemico-biological Interactions*. **2001**, *130*, 285-296.
- <sup>67</sup> Vasiliou, V.; Pappa, A.; Petersen, D. R. Role of aldehyde dehydrogenases in endogenous and xenobiotic metabolism. *Chemico-biological Interactions*. **2000**, *129* (1), 1-19.
- <sup>68</sup> Voulgaridou, G. P.; Anestopoulos, I.; Franco, R.; Panayiotidis, M. I.; Pappa, A. DNA damage induced by endogenous aldehydes: current state of knowledge. *Mutation Research/Fundamental and Molecular Mechanisms of Mutagenesis*. **2011**, *711* (1), 13-27.
- <sup>69</sup> Hengstler, J. G.; Fuchs, J.; Gebhard, S.; Oesch, F. Glycolaldehyde causes DNA-protein crosslinks: a new aspect of ethylene oxide genotoxicity. *Mutation Research/Fundamental and Molecular Mechanisms of Mutagenesis*. **1994**, *304* (2), 229-234.

- 
- <sup>70</sup> Shaham, J.; Bomstein, Y.; Meltzer, A.; Kaufman, Z.; Palma, E.; Ribak, J. DNA-protein crosslinks, a biomarker of exposure to formaldehyde—in vitro and in vivo studies. *Carcinogenesis*. **1996**, *17* (1), 121-126.
- <sup>71</sup> Orsiere, T.; Sari-Minodier, I.; Iarmarcovai, G.; Botta, A. Genotoxic risk assessment of pathology and anatomy laboratory workers exposed to formaldehyde by use of personal air sampling and analysis of DNA damage in peripheral lymphocytes. *Mutation Research/Genetic Toxicology and Environmental Mutagenesis*. **2006**, *605* (1), 30-41.
- <sup>72</sup> Morita, T.; Hayashi, M. 1, 4-Dioxane is not mutagenic in five in vitro assays and mouse peripheral blood micronucleus assay, but is in mouse liver micronucleus assay. *Environmental and Molecular Mutagenesis*. **1998**, *32* (3), 269-280.
- <sup>73</sup> Goldsworthy, T. L.; Monticello, T. M.; Morgan, K. T.; Bermudez, E.; Wilson, D. M.; Jäckh, R.; Butterworth, B. E. Examination of potential mechanisms of carcinogenicity of 1, 4-dioxane in rat nasal epithelial cells and hepatocytes. *Archives of Toxicology*. **1991**, *65* (1), 1-9.
- <sup>74</sup> Stott, W. T.; Quast, J. F.; Watanabe, P. G. Differentiation of the mechanisms of oncogenicity of 1, 4-dioxane and 1, 3-hexachlorobutadiene in the rat. *Toxicology and Applied Pharmacology*. **1981**, *60* (2), 287-300.
- <sup>75</sup> Roy, S. K.; Thilagar, A. K.; Eastmond, D. A. Chromosome breakage is primarily responsible for the micronuclei induced by 1, 4-dioxane in the bone marrow and liver of young CD-1 mice. *Mutation Research/Genetic Toxicology and Environmental Mutagenesis*. **2005**, *586* (1), 28-37.

# **Chapter 6**

## **Summary and Conclusions**

Activated  $S_2O_8^{2-}$  has recently gained popularity in ISCO applications. Alternatively,  $S_2O_8^{2-}$  would be applied in advanced treatment train for portable water reuse. However, the underlying activation mechanism is not fully understood. Hence, the goal of this dissertation was to investigate and better understand the kinetics and mechanism of  $S_2O_8^{2-}$ -based AOPs in ISCO and UV/AOP applications. To that end, we explored how common chemical constituents, such as carbonate, chloride, and pH can impact benzene degradation by mineral-activated  $S_2O_8^{2-}$  when applied to ISCO (Chapter 2); how the presence of  $NH_2Cl$ , chloride, pH and oxygen levels impacted 1,4-dioxane removal when  $S_2O_8^{2-}$  was used as oxidant in UV/AOPs for treating RO permeate (Chapter 3); How to develop a kinetic model to predict the large scale UV/AOP treatment efficiency and elucidate underlying chemical mechanism (Chapter 4); and what oxidation byproducts could be formed during the  $S_2O_8^{2-}$ -based AOPs, and how the toxicity potency of the degradation products were compared to the parent compounds (Chapter 5).

### **6.1 Persulfate-Based ISCO for Groundwater Remediation: Impacts of Alkalinity, pH and Chloride**

In Chapter 2, we examined the impacts of alkalinity, pH and chloride on benzene degradation by heterogeneously activated  $S_2O_8^{2-}$ .  $S_2O_8^{2-}$  was activated by ferrihydrite, goethite and pyrolusite to generate  $SO_4^{\bullet-}$ . Benzene was used as a model aquifer contaminant. A comprehensive kinetic model was established to elucidate the mechanisms of radical generation, mineral surface complexation and radical distribution. A few key findings were derived from this study.

First, the surface area-normalized rates of  $S_2O_8^{2-}$  decomposition and benzene degradation followed the order of pyrolusite > goethite > ferrihydrite. The  $S_2O_8^{2-}$  decomposition was mainly due to Fenton-like reactions involving oxidized and reduced surfaces sites of metal oxides reacting with  $S_2O_8^{2-}$ . Benzene degradation was primary due to  $SO_4^{\bullet-}$ . However,  $SO_4^{\bullet-}$  was also scavenged by reactive mineral surface complexes such as ferrihydrite, which lowers the radical yield.

Second, an increase of alkalinity from 0 to 10 meq/L decreased the rates of  $S_2O_8^{2-}$  decomposition and benzene degradation. Carbonate species, especially  $CO_3^{2-}$  are strong chelating agents that form carbonano-complexes with mineral surfaces and decreases the reactivity of the surfaces. The presence of alkalinity also transformed reactive  $SO_4^{\bullet-}$  and  $HO^{\bullet}$  to non-reactive  $CO_3^{\bullet-}$ , which hindered benzene degradation.

Third, an increase in pH from 8 to 12 generally accelerated  $S_2O_8^{2-}$  decomposition and benzene degradation due to enhanced formation of reactive surface hydroxo complexes. However, a further pH increase from 12 to 13 decreased the reaction rate because the concentrations of reactive hydroxo surface complex decreased by 10 times from pH 12 to 13 due to hydroxo surface equilibrium.

Forth, a change in the chloride level up to 5 mM had a negligible effect on the reaction kinetics because chloride did not strongly impact mineral surface complexes. Although, the presence of chloride accelerated the transformation of  $SO_4^{\bullet-}$  to  $CO_3^{\bullet-}$ , it also prevented the formation of carbonato complexes, hence, the overall rates of  $S_2O_8^{2-}$  decomposition and benzene degradation were not affected.

Finally, both phenol and aldehyde were identified as the major transformation products of benzene degradation. The yields of phenol and aldehyde were positively correlated with the branching ratio of  $\text{SO}_4^{\cdot-}$  reacting with benzene, but inversely correlated with that of  $\text{HO}^{\cdot}$  or  $\text{CO}_3^{\cdot-}$ , indicating that  $\text{SO}_4^{\cdot-}$  preferentially oxidized benzene via pathways involving fewer hydroxylation steps compared to  $\text{HO}^{\cdot}$  or  $\text{CO}_3^{\cdot-}$ .

This study demonstrated that  $\text{S}_2\text{O}_8^{2-}$ -based ISCO is applicable to groundwater remediation with elevated salinity, however, the remediation efforts need to pay special attention to native alkalinity and pH levels. These factors can alter the redox reactivity in the aquifer and the effectiveness on persulfate activation. Results also suggest that aquifers with abundant goethite can increase the persistence of persulfate and increase remediation efficiency. Although aquifer minerals with higher abundance of ferrihydrite and pyrolusite can accelerate persulfate decomposition, these minerals tend to have lower stoichiometric efficiency of radical yields.

## **6.2 $\text{S}_2\text{O}_8^{2-}$ -Based AOPs for Potable Water Reuse**

In Chapter 3, we studied the application of  $\text{S}_2\text{O}_8^{2-}$  as an alternative oxidant to replace  $\text{H}_2\text{O}_2$  in UV/AOPs for treating 1,4-dioxane, a contaminant that readily passes through RO membranes. The impact of antifouling agent,  $\text{NH}_2\text{Cl}$ , chloride, pH and oxygen were examined. The results presented in Chapter 3 contain four key findings.

First, the results suggested that  $\text{NH}_2\text{Cl}$ -to- $\text{S}_2\text{O}_8^{2-}$  molar ratio of 0.1 exhibited the highest treatment efficiency. Beyond this ratio,  $\text{NH}_2\text{Cl}$  has a photon filtering effect that competed with  $\text{S}_2\text{O}_8^{2-}$  for UV light.  $\text{NH}_2\text{Cl}$  photolysis rate increased with increasing dosage,

while  $S_2O_8^{2-}$  photolysis was suppressed. Although,  $NH_2Cl$  was quickly photolyzed, it produced less reactive  $Cl^\bullet$  and  $NH_2^\bullet$ . Furthermore, high  $NH_2Cl$  dosage significantly scavenged  $HO^\bullet$ ,  $SO_4^{\bullet-}$ , and  $Cl_2^{\bullet-}$  radicals and decreased 1,4-dioxane degradation rate.

Second, at the optimal ratio, the degradation rate of 1,4-dioxane increased linearly with the increasing total oxidant dose up to 6 mM. When the total oxidant dosage exceeded 6 mM, major scavenging by  $S_2O_8^{2-}$  reduced the  $[HO^\bullet]_{ss}$ , thus 1,4-dioxane degradation rate also reduced. In contrast, at 1:1-ratio, 1,4-dioxane degradation rate was 33 to 240% lower compared to that at 0.1:1 ratio, and the optimal condition was observed at 4 mM. At 1:1-ratio, the high  $NH_2Cl$  dosage decreased the yield of  $HO^\bullet$  and  $SO_4^{\bullet-}$ .

Third, the major products of  $NH_2Cl$  photolysis were  $NH_4^+$ , nitrate, gaseous nitrogen and organic nitrogen, and products of  $S_2O_8^{2-}$  photolysis was sulfate ( $SO_4^{2-}$ ), with a 2:1 stoichiometry. In addition,  $UV/S_2O_8^{2-}$  promoted gaseous nitrogen formation and decreases the formation of undesired  $NH_2Cl$  decay products,  $NH_4^+$  and organic nitrogen.

Fourth, the presence of chloride hindered 1,4-dioxane degradation rate in  $UV/S_2O_8^{2-}$  due to the transformation of reactive  $HO^\bullet$  and  $SO_4^{\bullet-}$  to less reactive  $Cl_2^{\bullet-}$ . Furthermore, the simultaneous photolysis of  $NH_2Cl$  and  $S_2O_8^{2-}$  was sensitive to the solution pH, due to a disproportionation of  $NH_2Cl$  into less photo-reactive dichloramine ( $NHCl_2$ ) and radical scavenger  $NH_4^+$  at pH lower than 6. Presence of dissolved  $O_2$  also promoted 1,4-dioxane degradation by participating in the 1,4-dioxane and  $NH_4^+$  oxidation steps.

Results from this study suggested that the presence of  $NH_2Cl$  can be beneficial to  $UV/S_2O_8^{2-}$  to remove 1,4-dioxane, however, the treatment efficiency depends on a careful

control of an optimal  $\text{NH}_2\text{Cl}$  dosage and a minimal chloride residue. Results from this study assist in the development of more efficient UV/AOP technologies for potable water reuse.

### **6.3 Modeling Approach for Simulating and Comparing Full Scale UV/ $\text{H}_2\text{O}_2$ , UV/ $\text{S}_2\text{O}_8^{2-}$ , and UV/HOCl**

In chapter 4, we developed a kinetic model using open source software, Kintecus, to compare the treatment efficiency of UV/ $\text{H}_2\text{O}_2$ , UV/ $\text{S}_2\text{O}_8^{2-}$ , and UV/HOCl on the degradation of six representative trace organic contaminants namely 1,4-dioxane, carbamazepine, phenol,  $17\beta$ -estradiol, aniline, and sulfamethoxazole. The fundamental mechanisms of radical generation, radical distribution, and contaminant degradation in three UV/AOPs were investigated. The impacts of RO permeate chemical constituents including pH, chloride and inorganic carbon were examined. The analysis of the results in Chapter 4 revealed four key findings.

First, results showed that the treatment efficiency of contaminants generally followed the order of UV/ $\text{S}_2\text{O}_8^{2-}$  > UV/ $\text{H}_2\text{O}_2$  > UV/HOCl, because  $\text{S}_2\text{O}_8^{2-}$  photolyzed faster than  $\text{H}_2\text{O}_2$  and generated higher levels of both  $\text{SO}_4^{\cdot-}$  and  $\text{HO}^{\cdot}$ . In UV/ $\text{S}_2\text{O}_8^{2-}$  treatment, both  $\text{SO}_4^{\cdot-}$  and  $\text{HO}^{\cdot}$  were important for contaminant degradation. In UV/ $\text{H}_2\text{O}_2$  treatment,  $\text{HO}^{\cdot}$  contributed the most to the contaminant degradation with the exception that  $\text{CO}_3^{\cdot-}$  was important for aniline and sulfamethoxazole degradation. Interestingly,  $\text{CO}_3^{\cdot-}$  was predominate in UV/HOCl due to fast kinetics of the reaction between chloride and carbonates.

Second, the model results suggested that UV/S<sub>2</sub>O<sub>8</sub><sup>2-</sup> was most sensitive to pH, UV/HOCl was modestly sensitive to pH, and UV/H<sub>2</sub>O<sub>2</sub> was insensitive to pH. This was because at pH 7, HCO<sub>3</sub><sup>-</sup> was the dominant carbonate species. In UV/S<sub>2</sub>O<sub>8</sub><sup>2-</sup> and UV/HOCl treatments, both SO<sub>4</sub><sup>•-</sup> and Cl<sup>•</sup> could be quickly transformed into CO<sub>3</sub><sup>•-</sup> by HCO<sub>3</sub><sup>-</sup> at pH 7, which had lower reactivity with contaminants. While in UV/H<sub>2</sub>O<sub>2</sub> treatment, HO<sup>•</sup> equilibrated with chloride and not significantly impacted by HCO<sub>3</sub><sup>-</sup> with increasing pH.

Third, the sensitivity to chloride follows the following order: UV/S<sub>2</sub>O<sub>8</sub><sup>2-</sup> > UV/HOCl > UV/H<sub>2</sub>O<sub>2</sub>. In UV/S<sub>2</sub>O<sub>8</sub><sup>2-</sup>, the presence of chloride accelerated the transformation of SO<sub>4</sub><sup>•-</sup> to Cl<sup>•</sup>, which quickly reacting with HCO<sub>3</sub><sup>-</sup> to generate CO<sub>3</sub><sup>•-</sup>. The same mechanism was also observed in UV/HOCl. However, UV/H<sub>2</sub>O<sub>2</sub> was not sensitive to chloride because it reacted with chloride to generate ClOH<sup>•-</sup>, but the dissociation of ClOH<sup>•-</sup> quickly regenerated HO<sup>•</sup>.

Forth, carbonates also exhibited higher influence in treatments of UV/S<sub>2</sub>O<sub>8</sub><sup>2-</sup> and UV/HOCl than in UV/H<sub>2</sub>O<sub>2</sub>, mainly because both SO<sub>4</sub><sup>•-</sup> and Cl<sup>•</sup> reacted quickly with carbonates to form non-reactive CO<sub>3</sub><sup>•-</sup>. In contrast, UV/H<sub>2</sub>O<sub>2</sub> was not sensitive to carbonates because it reacted faster with chloride than with carbonates.

Overall in Chapter 4, the combined experimental and modeling approach provided fundamental chemistry understanding on different UV/AOPs and guidance on the design and optimization of UV/AOP systems for water reuse under diverse chemical conditions. Among three UV/AOPs, UV/S<sub>2</sub>O<sub>8</sub><sup>2-</sup> demonstrated the highest treatment performance. However, it was more sensitive to pH, chloride, and inorganic carbon than the other two

UV/AOPs. UV/H<sub>2</sub>O<sub>2</sub> exhibited higher treatment efficiency than UV/HOCl for some groups of contaminants, but its performance is limited by the rate of H<sub>2</sub>O<sub>2</sub> photolysis. UV/HOCl is unique to the other AOPs in that it favors the generation of CO<sub>3</sub><sup>•-</sup>, and very effective in degrading amine-containing contaminants.

#### **6.4 Toxicity Assessment of Benzene and 1,4-dioxane Oxidation Byproducts**

In chapter 5, the formation and distribution of oxidation byproducts of benzene and 1,4-dioxane during various AOPs were compared. The cytotoxicity and genotoxicity of the individual byproducts and the toxicity evolution of 1,4-dioxane during the AOP treatments were evaluated using HCT-116 Human colorectal carcinoma cells. Three key findings were observed in this study.

First, results showed that benzene was transformed to phenol and unsaturated aldehyde products in both goethite-activated S<sub>2</sub>O<sub>8</sub><sup>2-</sup> and H<sub>2</sub>O<sub>2</sub> treatments, and no products were observed in MnO<sub>4</sub><sup>-</sup> treatment because benzene was not oxidized by MnO<sub>4</sub><sup>-</sup> in the experimental period examined in this study (*e.g.* 14 days). 1,4-dioxane was transformed to six major intermediates after UV/S<sub>2</sub>O<sub>8</sub><sup>2-</sup> and UV/H<sub>2</sub>O<sub>2</sub> treatments including ethylene glycol diformate, formaldehyde, glycolaldehyde, glycolic acid, formic acid, and methoxyacetic acid. Only aldehyde products were observed in UV/NH<sub>2</sub>Cl treatment.

Second, both genotoxicity and cytotoxicity studies indicated that aldehyde byproducts were way more toxic than benzene or 1,4-dioxane. Aldehyde and phenol from benzene oxidation was 10 times more toxic than benzene. Similarly, formaldehyde and glycolaldehyde were a few folds more toxic than 1,4-dioxane. The rank order for

cytotoxicity of benzene and its oxidation byproducts based on their LC50 values was: aldehyde > phenol > benzene. The rank order for 1,4-dioxane and OBPs was: GD > FD > FA > GA > 1,4-Dioxane > EGD  $\approx$  MA. Unsaturated aldehyde, phenol, GD and FD induced strong genotoxicity, whereas benzene and 1,4-dioxane exhibited weak genotoxicity.

Third, 1,4-dioxane oxidation increased total toxicity during the three UV/AOPs, mainly because of the formation of glycolaldehyde. Fortunately, UV/S<sub>2</sub>O<sub>8</sub><sup>2-</sup> could further reduce the toxicity with extended treatment time due to the transformation of toxic aldehydes to less toxic organic acids.

This study suggests UV/AOP treatments could produce OBPs with higher geno- and cyto- toxicity than their parent compounds, which calls for new treatment strategies to minimize the formation of more toxic oxidation byproducts when applying AOP treatments to remove CECs. For many aromatic compounds, the initial oxidation steps usually lead to the formation of aldehydes as intermediates with high geno- and cyto- toxicity. Despite the low-level existence of OBPs in highly treated water, the risk of long term exposure warrants great attention. Our results also suggested that there would be strategies for minimizing the formation of more toxic OBPs. For instance, S<sub>2</sub>O<sub>8</sub><sup>2-</sup>-based AOP can significantly decrease the formation of toxic byproducts with extend treatment time. In both ISCO and wastewater recycle scenario, UV/S<sub>2</sub>O<sub>8</sub><sup>2-</sup> showed a better efficiency in degrading benzene, 1,4-dioxane and their OBPs than other AOPs.

# **Appendix A**

## **Supplemental Information for Chapter 2**

### Appendix A-1 Surface site concentration of ferrihydrite, goethite and pyrolusite.

The surface site concentrations were calculated based on prior literature values of surface density and the surface area of each mineral measured in this study. Based on prior literature, the surface density of ferrihydrite, goethite and pyrolusite was  $2.0 \times 10^{-1}$  mole site/mole Fe(III),  $1.6 \times 10^{-2}$  mole site/mole Fe(III) and  $8.7 \times 10^{-2}$  mole site /mole Mn(IV), respectively.<sup>1-3</sup> These literature values were reported for minerals with a particular surface area. The surface area of each mineral used in this study was directly measured and listed in Table S1. Accordingly, the actual surface site concentrations of each mineral in this study was calculated based on the prior literature values and adjusted with the experimentally measured surface area.

The surface site concentration of ferrihydrite was calculated as:

$$C_{\text{surface sites}} = \frac{100 \text{ g ferrihydrite}}{L} \times \frac{180 \text{ m}^2}{\text{g}} \times \frac{\text{g}}{600 \text{ m}^2} \times \frac{1 \text{ mole}}{88.9 \text{ g}} \times \frac{2.0 \times 10^{-1} \text{ mole sites}}{\text{mole ferrihydrite}}$$
$$= 6.7 \times 10^{-2} \text{ M sites}$$

The surface site concentration of goethite was calculated as:

$$C_{\text{surface sites}} = \frac{100 \text{ g goethite}}{L} \times \frac{1 \text{ mole}}{88.9 \text{ g}} \times \frac{21 \text{ m}^2}{\text{g}} \times \frac{\text{g}}{79 \text{ m}^2} \times \frac{1.6 \times 10^{-2} \text{ mole sites}}{\text{mole goethite}}$$
$$= 4.8 \times 10^{-3} \text{ M sites}$$

The surface site concentration of pyrolusite was calculated as:

$$C_{\text{surface sites}} = \frac{100 \text{ g pyrolusite}}{L} \times \frac{1 \text{ mole}}{86.9 \text{ g}} \times \frac{1.1 \times 10^{-1} \text{ m}^2}{\text{g}} \times \frac{\text{g}}{188 \text{ m}^2} \times \frac{8.7 \times 10^{-2} \text{ mole sites}}{\text{mole pyrolusite}}$$
$$= 5.9 \times 10^{-5} \text{ M sites}$$

## **Appendix A- 2 High performance liquid chromatography and its operating conditions.**

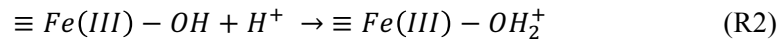
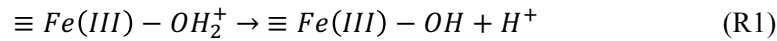
Chromatographic separation of benzene and its products was achieved using an Agilent 1200 high performance liquid chromatography equipped with a Diode array detector. A Zorbax Eclipse XDB-C18 column (4.6×50mm, 1.8 µm particle size) equipped with a guard column (Eclipse XDB-C18, 4.6×12.5mm) was used. 10 mM formic acid and pure acetonitrile were used as eluents. The composition of eluents was optimized and changed with elution time for better peak separations. Specifically, between 0 and 4.5 minutes of elution, the eluent was 97% formic acid and 3% acetonitrile. Between 4.5 and 7 minutes, the eluent was 30% formic acid and 70% acetonitrile. Between 7 and 10 minutes, the eluent was 97% formic acid and 3% acetonitrile. The sample injection volume was 100µL and the flow rate was set at 1.0 mL/min. The calibration curves of benzene and phenol were first established under the conditions described above and the concentration of benzene and phenol were quantified based on the peak areas recorded.

### **Appendix A-3 Details on the comprehensive kinetic modeling**

The kinetic model on persulfate decomposition and benzene degradation was built on the platform of Kintecus 4.55 software. A total of 77 and 56 elemental reactions were established to model persulfate decomposition and benzene degradation in the presence of Fe(III) oxide and Mn(IV) oxide, respectively. All reactions incorporated in the kinetic model were summarized in Table S2. Of 77 reactions for Fe(III) oxides, 67 rate constants were directly obtained from radiolysis literature. For the rest of the reactions with unknown rate constants, four reactions involving homogeneous persulfate activation by soluble Fe(III) were optimized using experimental data from persulfate activation by soluble Fe(III), and rate constants of six reactions involving heterogeneous persulfate activation by ferrihydrite and goethite were optimized using experimental data at different alkalinity, pH, and chloride levels. Of 56 reactions involving Mn(IV) oxide, 53 rate constants were directly obtained from radiolysis literature. The remaining three unknown rate constants involving heterogeneous persulfate activation by pyrolusite was also model-derived based on the experimental data. Soluble Mn(IV) activation of persulfate was not considered due to the extremely low solubility of pyrolusite.

Specifically, among reactions with known rate constants, rate constants of eight reactions for each mineral involving hydroxo and carbonato surface complexation were derived based on the published values of equilibrium constants (Reactions 25-40 in Table 1 of the main text and Reactions 46-53 and 60-67 in Table S2 of the SI).

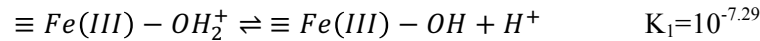
Using ferrihydrite as an example, three hydroxo surface complexes exist at the pH ranging between 8 and 13:  $\equiv\text{Fe(III)-OH}_2^+$ ,  $\equiv\text{Fe(III)-OH}^0$  and  $\equiv\text{Fe(III)-O}^-$  ( $\text{pK}_1=7.29$ ;  $\text{pK}_2=8.93$ ).<sup>1</sup> The first step of protonation/deprotonation between  $\equiv\text{Fe(III)-OH}_2^+$  and  $\equiv\text{Fe(III)-OH}^0$  involves the forward reaction (R1) and the reverse reaction (R2) as follows:



The rate constant of the reverse reaction ( $k_2$ ) was fixed at  $1 \times 10^{11} \text{ M}^{-1} \text{ s}^{-1}$  (*i.e.*, the maximal diffusion-limited rate constant for a second-order reaction). The choice of a very large value of rate constants ensured an instantaneous equilibrium of metal hydroxo surface complexes. The rate constant of the forward reaction ( $k_1$ ) was calculated as:

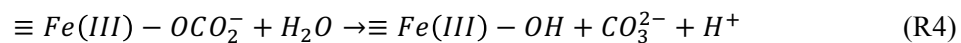
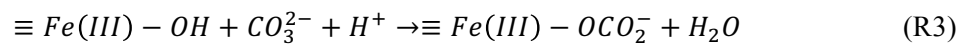
$$k_1 = K_1 \times k_2$$

$K_1$  is the equilibrium constant between  $\equiv\text{Fe(III)-OH}_2^+$  and  $\equiv\text{Fe(III)-OH}^0$  for the following equilibrium reaction:



The ratio of  $k_1$  to  $k_2$  is always equal to the known equilibrium constant  $K_1$ .

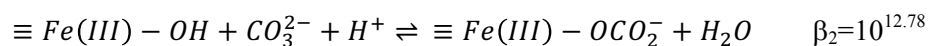
Similar approaches were applied to the kinetic modeling of surface carbonato complexation reactions. Using ferrihydrite as an example, surface carbonato complexes are generated via  $\equiv\text{Fe(III)-OH}^0$  in the presence of carbonate:



The rate constant of the forward reaction ( $k_3$ ) was set at  $1 \times 10^{15} \text{ M}^{-2} \text{ s}^{-1}$ , *i.e.*, the maximal diffusion-limited rate constant for a third-order reaction. The choice of a very large value of rate constants ensured an instantaneous equilibrium of metal hydroxo surface complexes. and the rate constant of the reverse reaction ( $k_4$ ) was calculated as:

$$k_4 = \frac{k_3}{\beta_2}$$

$\beta_2$  ( $\log \beta_2 = 12.78$ )<sup>4</sup> is the equilibrium constant between  $\equiv \text{Fe(III)-OH}$  and  $\equiv \text{Fe(III)-OCO}_2^-$  for the following equilibrium:



The ratio of  $k_3$  to  $k_4$  is always equal to the known equilibrium constant  $\beta_2$ .

Using this approach, the equilibria of all metal surface hydroxo and carbonato complexes were established in the Kintecus software platform as a series of fast forward and reverse reactions (Reactions 25-40 in Table 1 of the main text and Reactions 46-53 and 60-67 in Table S2 of the SI).

In addition, rate constants of four reactions (Reactions 2, 7, 22 and 42 in Table S2) involving homogeneous persulfate decomposition by soluble Fe(III) were optimized using the experimental data of persulfate activation by soluble Fe(III).

Rate constants of six reactions involving heterogeneous persulfate decomposition by ferrihydrite and goethite and rate constants of three reactions involving persulfate decomposition by pyrolusite were optimized using experimental data at different alkalinity, pH and chloride levels (Reactions 1-6 and 14-16 in Table 1 of the main text and Reactions

54-59 and 68-70 in Table S2 of the SI). Using ferrihydrite as an example, firstly, persulfate activation by the surface hydroxo complexes of  $\equiv\text{Fe(III)-O}^-$  (Reaction 3-4 in Table 1) and  $\text{SO}_4^{\bullet-}$  scavenging reaction by  $\equiv\text{Fe(III)-O}^-$  (Reaction 15 in Table 1) were fitted using the experimental dataset at pH 12 and 13 (Figure 3A-3B). Because the pK value of  $\equiv\text{Fe(III)-OH}/\equiv\text{Fe(III)-O}^-$  deprotonation is 8.93,<sup>1</sup>  $\equiv\text{Fe(III)-O}^-$  is the predominant hydroxo surface complex at pH 12 and 13, and Reactions 1-2 and 14 involving the surface complexes of  $\text{Fe(III)-OH}$  were negligible at pH 12 and 13. Accordingly, Reactions 1-2 and 14 were not considered during this first step of modeling.

The best model fitting of the rate constants for Reactions 3-4 and 15 were achieved by applying Powell non-restricted algorithms to minimize the root mean squares (RMS) between the model prediction and experimental observation based on the kinetics of persulfate decomposition and benzene degradation. Following that, two sets of rate constants were obtained at pH 12 and 13. The average values of the rate constants with standard deviations were calculated based on the fitting results at these two pHs.

Secondly, the rate constants of Reactions 1-2 and 14 in Table 1 were modelled using nine sets of experimental data, including experiments conducted at pH 8 and 10 (two sets of data shown in Figures 3A and 3B), three alkalinity levels (three sets of data shown in Figures 2A and 2B) and four chloride levels (four sets of data shown in Figures S4A and S4B). The rate constants of Reactions 1-2 and 14 were modelled independently for nine times, using one set of data each time. The average values of the rate constants with standard deviations were calculated from these nine sets of data accordingly.

Same procedures were applied to model the rate constants of persulfate activation by surface complexes of goethite (Reactions 54-59 in Table S2), which were fitted using the experimental data set at different levels of pH (dataset from Figure 3C-3D), alkalinity (dataset from Figure 2C-D), and chloride (dataset from Figure S4C-4D). Persulfate activation by the surface complexes of pyrolusite (Reaction 5-6 in Table 1, also shown as Reactions 68-69 in Table S2) and  $\text{SO}_4^{\bullet-}$  scavenging reaction by surface complex of pyrolusite (Reaction 16 in Table 1, also shown as Reaction 70 in Table S2) were fitted using the experimental data set at different levels of pH (dataset from Figure 3E-3F), alkalinity (dataset from Figure 2E-F) and chloride (dataset from Figure S4E-4F).

Finally, the uncertainty analysis for the predicted steady-state concentrations of surface complexes was conducted using Kintecus software, which calculated the average values and standard deviations of each predicted parameter. Specifically, the modelled rate constants were randomized within the predicted rate constants  $\pm$  standard deviations. The model ran one hundred simulations with varied rate constants using Gaussian distributed random numbers to calculate the confidence band at 95% confidence level.

#### Appendix A-4 Calculations on the contribution of each reaction to the total persulfate decomposition and the radical contribution to benzene degradation

Persulfate decomposition was contributed by Fenton-like reactions, surface reactions and radical reactions. Taking goethite as an example, the rate of persulfate decomposition by goethite was calculated as follows:

$$\begin{aligned}
 -\frac{d[S_2O_8^{2-}]}{dt} &= k_{obs}[S_2O_8^{2-}] \\
 &= (k_1 + k_2[Fe^{3+}]_{ss} + k_3[Fe^{2+}]_{ss} + k_{54}[\equiv Fe(III) - OH]_{ss} + k_{55}[\equiv Fe(II) - OH]_{ss} + \\
 &\quad k_{56}[\equiv Fe(III) - O^-]_{ss} + k_{57}[\equiv Fe(II) - O^-]_{ss} + k_{20}[HO\cdot]_{ss} + \\
 &\quad k_{21}[SO_4^{\cdot-}]_{ss} + k_{22}[CO_3^{\cdot-}]_{ss} + k_{71}[Cl\cdot]_{ss}) [S_2O_8^{2-}]
 \end{aligned}$$

Where  $k_{obs}$  is the observed first-order rate constant of persulfate decomposition obtained from the experiments. All other  $k_i$  values (except for  $k_j$ ) are the second-order rate constants corresponding to the reactions listed in **Appendix A-5**, where  $i$  stands for the number of reaction in **Appendix A-5**. For example,  $k_j$  is the first-order rate constant for Reaction 1 in **Appendix A-5**,  $k_2$  is the second-order rate constant for Reaction 2 in **Appendix A-5**. The same calculation was applied to ferrihydrite and pyrolusite. Reaction 2 and 3 were not included for pyrolusite because Mn(IV) and Mn(III) species were not soluble.

The percentile contribution of each reaction to the total rate of persulfate decomposition was calculated as the branching ratio of each reaction to the overall observed first-order rate constant.

The rate of benzene degradation was calculated as:

$$\begin{aligned}
-\frac{d[\textit{benzene}]}{dt} &= k_{\textit{obs-benzene}}[\textit{benzene}] \\
&= (k_{39}[\textit{SO}_4^{\cdot-}]_{ss} + k_{40}[\textit{HO}^{\cdot}]_{ss} + k_{41}[\textit{CO}_3^{\cdot-}]_{ss} + k_{88}[\textit{Cl}^{\cdot}]_{ss})[\textit{benzene}]
\end{aligned}$$

Where  $k_{\textit{obs-benzene}}$  is the observed first-order rate constant of benzene degradation obtained from the experiments. All other  $k_i$  values are the second-order rate constants corresponding to the reactions listed in **Appendix A-5**, where  $i$  stands for the number of reaction in **Appendix A-5**. For example,  $k_{39}$  is the first-order rate constant for Reaction 39 in **Appendix A-5**.

The percentile contribution of  $\textit{SO}_4^{\cdot-}$  to benzene degradation was calculated as:

$$\%_{\textit{SO}_4^{\cdot-}} = \frac{k_{39}[\textit{SO}_4^{\cdot-}]_{ss}}{k_{\textit{obs-benzene}}} \times 100\%$$

Similar calculations were conducted to quantify the contributions of  $\textit{HO}^{\cdot}$ ,  $\textit{Cl}^{\cdot}$  and  $\textit{CO}_3^{\cdot-}$  to benzene degradation.

**Appendix A-5 Table of reactions and their rate constants used in the kinetic model.**

No.	Reaction	Rate Constant (M <sup>-1</sup> s <sup>-1</sup> )	Reference *
Homogeneous Reactions			
1	$S_2O_8^{2-} \rightarrow 2SO_4^{\cdot-}$ (25 °C)	$1.7 \times 10^{-8}$	5 <sup>a</sup>
2	$S_2O_8^{2-} + Fe^{3+} \rightarrow S_2O_8^{\cdot-} + Fe^{2+}$	$(6.6 \pm 1.2) \times 10^{-2}$	
3	$S_2O_8^{2-} + Fe^{2+} \rightarrow SO_4^{\cdot-} + SO_4^{2-} + Fe^{3+}$	$2.7 \times 10^1$	6
4	$4Fe^{2+} + O_2 + 4H^+ \rightarrow 4Fe^{3+} + 2H_2O$	$7.2 \times 10^3$	7 <sup>a,d</sup>
5	$Fe^{2+} + SO_4^{\cdot-} \rightarrow SO_4^{2-} + Fe^{3+}$	$9.9 \times 10^8$	8
6	$Fe^{2+} + HO^{\cdot} \rightarrow OH^- + Fe^{3+}$	$3.5 \times 10^8$	9
7	$Fe^{2+} + CO_3^{\cdot-} \rightarrow CO_3^{2-} + Fe^{3+}$	$(4.7 \pm 0.8) \times 10^5$	
8	$Fe^{2+} + HCO_3^- \rightarrow FeHCO_3^+$	$9.3 \times 10^6$	10
9	$FeHCO_3^+ \rightarrow Fe^{2+} + HCO_3^-$	$1.0 \times 10^5$	10 <sup>a</sup>
10	$Fe^{2+} + CO_3^{2-} \rightarrow FeCO_3$	$1.0 \times 10^9$	10
11	$FeCO_3 \rightarrow Fe^{2+} + CO_3^{2-}$	$4.7 \times 10^4$	10 <sup>a</sup>
12	$Fe^{2+} + 2CO_3^{2-} \rightarrow Fe(CO_3)_2^{2-}$	$1.2 \times 10^{11}$	10 <sup>b</sup>
13	$Fe(CO_3)_2^{2-} \rightarrow Fe^{2+} + 2CO_3^{2-}$	$1.0 \times 10^5$	10 <sup>a</sup>
14	$Fe^{2+} + CO_3^{2-} + OH^- \rightarrow Fe(CO_3)(OH)^-$	$7.9 \times 10^{13}$	10 <sup>b</sup>
15	$Fe(CO_3)(OH)^- \rightarrow Fe^{2+} + CO_3^{2-} + OH^-$	$1.0 \times 10^5$	10 <sup>a</sup>
16	$Fe^{3+} + SO_4^{2-} \rightarrow FeSO_4^+$	$3.9 \times 10^7$	11
17	$FeSO_4^+ \rightarrow Fe^{3+} + SO_4^{2-}$	$1.0 \times 10^5$	11 <sup>a</sup>
18	$Fe^{2+} + SO_4^{2-} \rightarrow FeSO_4^0$	$2.3 \times 10^6$	11
19	$FeSO_4^0 \rightarrow Fe^{2+} + SO_4^{2-}$	$1.0 \times 10^5$	11 <sup>a</sup>
20	$S_2O_8^{2-} + HO^{\cdot} \rightarrow S_2O_8^{\cdot-} + OH^-$	$1.4 \times 10^7$	12
21	$S_2O_8^{2-} + SO_4^{\cdot-} \rightarrow S_2O_8^{\cdot-} + SO_4^{2-}$	$6.5 \times 10^5$	13
22	$S_2O_8^{2-} + CO_3^{\cdot-} \rightarrow S_2O_8^{\cdot-} + CO_3^{2-}$	$(1.6 \pm 0.2) \times 10^3$	
23	$SO_4^{\cdot-} + H_2O \rightarrow HSO_4^- + HO^{\cdot}$	$1.2 \times 10^1$	14
24	$SO_4^{\cdot-} + OH^- \rightarrow SO_4^{2-} + HO^{\cdot}$	$7.0 \times 10^7$	15

25	$HO\cdot + OH^- \rightarrow O^{\cdot-} + H_2O$	$1.3 \times 10^{10}$	16
26	$O^{\cdot-} + H_2O \rightarrow HO\cdot + OH^-$	$3.3 \times 10^3$	16
27	$O^{\cdot-} + O_2 \rightarrow O_3^{\cdot-}$	$3.6 \times 10^9$	16
28	$O_3^{\cdot-} \rightarrow O_2 + O^{\cdot-}$	$2.6 \times 10^3$	17 <sup>a</sup>
29	$H_2CO_3 \rightarrow HCO_3^- + H^+$	$2.5 \times 10^4$	18 <sup>a</sup>
30	$HCO_3^- + H^+ \rightarrow H_2CO_3$	$5.0 \times 10^{10}$	18
31	$HCO_3^- \rightarrow CO_3^{2-} + H^+$	$2.5 \times 10^0$	19 <sup>a</sup>
32	$HCO_3^- + HO\cdot \rightarrow CO_3^{\cdot-} + H_2O$	$8.6 \times 10^6$	16
33	$HCO_3^- + Cl\cdot \rightarrow CO_3^{\cdot-} + HCl$	$2.2 \times 10^8$	20
34	$HCO_3^- + Cl_2^{\cdot-} \rightarrow 2 Cl^- + H^+ + CO_3^{\cdot-}$	$8.0 \times 10^7$	18
35	$HCO_3^- + SO_4^{\cdot-} \rightarrow CO_3^{\cdot-} + SO_4^{2-} + H^+$	$9.1 \times 10^6$	21
36	$CO_3^{2-} + H^+ \rightarrow HCO_3^-$	$5.0 \times 10^{10}$	18
37	$CO_3^{2-} + HO\cdot \rightarrow CO_3^{\cdot-} + OH^-$	$3.9 \times 10^8$	16
38	$CO_3^{2-} + SO_4^{\cdot-} \rightarrow CO_3^{\cdot-} + SO_4^{2-}$	$2.5 \times 10^6$	22
39	$C_6H_6 + SO_4^{\cdot-} \rightarrow C_6H_6^+ + SO_4^{2-}$	$3.0 \times 10^9$	23
40	$C_6H_6 + HO\cdot \rightarrow C_6H_7O\cdot$	$7.8 \times 10^9$	24
41	$C_6H_6 + CO_3^{\cdot-} + H_2O \rightarrow C_6H_7O\cdot + HCO_3^-$	$5.0 \times 10^4$	25
42	$C_6H_6^+ + H_2O \rightarrow C_6H_7O\cdot + H^+$	$(3.2 \pm 0.6) \times 10^5$	25 <sup>a</sup>
43	$C_6H_7O\cdot + O_2 \rightarrow C_6H_7O_3$	$1.5 \times 10^9$	26
44	$C_6H_7O_3 \rightarrow C_6H_7O\cdot + O_2$	$8.0 \times 10^5$	25 <sup>a</sup>
45	$C_6H_7O_3 \rightarrow phenol$	$2.0 \times 10^4$	25 <sup>a</sup>
<b>Heterogeneous Reactions</b>			
46	$\equiv Fe(III) - OH_2 \rightleftharpoons Fe(III) - OH + H^+$	$4.0 \times 10^1$	27 <sup>a</sup>
47	$\equiv Fe(III) - OH + H^+ \rightleftharpoons Fe(III) - OH_2$	$5.0 \times 10^9$	27
48	$\equiv Fe(III) - OH \rightleftharpoons Fe(III) - O^- + H^+$	$4.0 \times 10^{-1}$	27 <sup>a</sup>
49	$\equiv Fe(III) - O^- + H^+ \rightleftharpoons Fe(III) - OH$	$5.0 \times 10^9$	27

50	$\equiv Fe(III) - OH + CO_3^{2-} + H^+ \rightarrow \equiv Fe(III) - OCO_2^- + H_2O$	$1.0 \times 10^{15}$	27 <sup>b</sup>
51	$\equiv Fe(III) - OHCO_2^- \rightarrow \equiv Fe(III) - OH + CO_3^{2-}$	$1.7 \times 10^2$	27 <sup>a</sup>
52	$\equiv Fe(III) - OH + CO_3^{2-} + 2H^+ \rightarrow \equiv Fe(III) - OCO_2H^0 + H_2O$	$1.0 \times 10^{20}$	27 <sup>c</sup>
53	$\equiv Fe(III) - OCO_2H^0 + H_2O \rightarrow \equiv Fe(III) - OH + CO_3^{2-} + 2H^+$	$5.0 \times 10^1$	27 <sup>a</sup>
54	$\equiv Fe(III) - OH + S_2O_8^{2-} \rightarrow \equiv Fe(II) - OH + S_2O_8^{\cdot-}$	$(1.9 \pm 0.3) \times 10^{-5}$	
55	$\equiv Fe(II) - OH + S_2O_8^{2-} \rightarrow \equiv Fe(III) - OH + SO_4^{\cdot-} + SO_4^{2-}$	$(2.8 \pm 0.3) \times 10^{-5}$	
56	$\equiv Fe(III) - O^- + S_2O_8^{2-} \rightarrow \equiv Fe(II) - O^- + S_2O_8^{\cdot-}$	$(1.2 \pm 0.3) \times 10^{-5}$	
57	$\equiv Fe(II) - O^- + S_2O_8^{2-} \rightarrow \equiv Fe(III) - O^- + SO_4^{\cdot-} + SO_4^{2-}$	$(2.8 \pm 0.5) \times 10^{-5}$	
58	$0.5S_2O_8^{\cdot-} + \equiv Fe(III) - OH \rightarrow SO_4^{\cdot-} + \equiv Fe(II) - OH$	$(4.0 \pm 0.9) \times 10^{-6}$	
59	$0.5S_2O_8^{\cdot-} + \equiv Fe(III) - O^- \rightarrow SO_4^{\cdot-} + \equiv Fe(II) - O^-$	$(1.8 \pm 0.2) \times 10^{-6}$	
60	$\equiv Mn(IV) - OH_2 \rightarrow \equiv Mn(IV) - OH + H^+$	$1.3 \times 10^9$	3 <sup>a</sup>
61	$\equiv Mn(IV) - OH + H^+ \rightarrow \equiv Mn(IV) - OH_2$	$5.0 \times 10^9$	3
62	$\equiv Mn(IV) - OH \rightarrow \equiv Mn(IV) - O^- + H^+$	$1.3 \times 10^7$	3 <sup>a</sup>
63	$\equiv Mn(IV) - O^- + H^+ \rightarrow \equiv Mn(IV) - OH$	$5.0 \times 10^9$	3
64	$\equiv Mn(IV) - OH + CO_3^{2-} + H^+ \rightarrow \equiv Mn(IV) - OCO_2^- + H_2O$	$1.0 \times 10^{15}$	28 <sup>b</sup>
65	$\equiv Mn(IV) - OCO_2^- + H_2O \rightarrow \equiv Mn(IV) - OH + CO_3^{2-} + H^+$	$7.1 \times 10^0$	28 <sup>a</sup>
66	$\equiv Mn(IV) - OH + CO_3^{2-} + 2H^+ \rightarrow \equiv Mn(IV) - OCO_2H^0 + H_2O$	$1.0 \times 10^{20}$	28 <sup>c</sup>
67	$\equiv Mn(IV) - OCO_2H^0 + H_2O \rightarrow \equiv Mn(IV) - OH + CO_3^{2-} + 2H^+$	$2.2 \times 10^{-3}$	28 <sup>a</sup>
68	$\equiv Mn(IV) - O^- + S_2O_8^{2-} \rightarrow \equiv Mn(III) - O^- + S_2O_8^{\cdot-}$	$(2.2 \pm 0.4) \times 10^{-3}$	
69	$\equiv Mn(III) - O^- + S_2O_8^{2-} \rightarrow \equiv Mn(IV) - O^- + SO_4^{\cdot-} + SO_4^{2-}$	$(4.9 \pm 1.3) \times 10^{-3}$	
70	$\equiv Mn(III) - O^- + SO_4^{\cdot-} \rightarrow \equiv Mn(IV) - O^- + SO_4^{2-}$	$(5.6 \pm 1.5) \times 10^{10}$	
71	$S_2O_8^{2-} + Cl^{\cdot} \rightarrow S_2O_8^{\cdot-} + Cl^-$	$8.8 \times 10^6$	29
72	$SO_4^{2-} + Cl^{\cdot} \rightarrow SO_4^{\cdot-} + Cl^-$	$2.5 \times 10^8$	30
73	$SO_4^{\cdot-} + Cl^- \rightarrow SO_4^{2-} + Cl^{\cdot}$	$6.6 \times 10^8$	31
74	$HO^{\cdot} + Cl^- \rightarrow ClOH^{\cdot-}$	$4.3 \times 10^9$	32
75	$ClOH^{\cdot-} \rightarrow Cl^- + HO^{\cdot}$	$6.1 \times 10^9$	32 <sup>a</sup>

76	$ClOH\cdot^- + Cl^- \rightarrow OH^- + Cl_2^-$	$1.0 \times 10^4$	33
77	$ClOH\cdot^- + H^+ \rightarrow Cl\cdot + H_2O$	$2.1 \times 10^{10}$	33
78	$Cl\cdot + H_2O \rightarrow ClOH\cdot^- + H^+$	$4.5 \times 10^3$	33
79	$Cl\cdot + OH^- \rightarrow ClOH\cdot^-$	$1.8 \times 10^{10}$	34
80	$Cl\cdot + Cl^- \rightarrow Cl_2^-$	$8.5 \times 10^9$	35
81	$Cl_2^- + OH^- \rightarrow Cl^- + ClOH\cdot^-$	$4.5 \times 10^7$	35
82	$Cl_2^- + H_2O \rightarrow Cl^- + HClOH\cdot$	$2.4 \times 10^0$	36
83	$HClOH\cdot \rightarrow H^+ + ClOH\cdot^-$	$1.0 \times 10^8$	36 <sup>a</sup>
84	$H^+ + Cl^- \rightarrow HCl$	$5.0 \times 10^{10}$	18
85	$HCl \rightarrow H^+ + Cl^-$	$8.6 \times 10^{16}$	18 <sup>a</sup>
86	$CO_3^{2-} + Cl\cdot \rightarrow CO_3^- + Cl^-$	$5.0 \times 10^8$	20
87	$CO_3^{2-} + Cl_2^- \rightarrow CO_3^- + 2 Cl^-$	$1.6 \times 10^8$	20
88	$C_6H_6 + Cl\cdot + H_2O \rightarrow C_6H_7O\cdot + HCl$	$6.0 \times 10^9$	37

\* Reaction rate constants without references were obtained in this study from the kinetic model. All rate constants on Fe(III) in this table are for goethite. Rate constants for ferrihydrite are listed in Table 1 of the main text.

<sup>a</sup> rate constants are in unit of  $s^{-1}$

<sup>b</sup> rate constants are in unit of  $M^{-2} s^{-1}$

<sup>c</sup> rate constants are in unit of  $M^{-3} s^{-1}$

<sup>d</sup> Reaction is a first-order reaction and independent of pH when  $pH > 8$ .

## Reference:

---

- <sup>1</sup> Dzombak, D. A.; Morel, F. M. *Surface complexation modeling: hydrous ferric oxide*. John Wiley & Sons: 1990.
- <sup>2</sup> Ali, M. A.; Dzombak, D. A. Competitive sorption of simple organic acids and sulfate on goethite. *Environmental Science & Technology*. **1996**, 30 (4), 1061-1071.
- <sup>3</sup> Wang, Z.; Lee, S. W.; Catalano, J. G.; Lezama-Pacheco, J. S.; Bargar, J. R.; Tebo, B. M.; Giammar, D. E. Adsorption of uranium (VI) to manganese oxides: X-ray absorption spectroscopy and surface complexation modeling. *Environmental Science & Technology*. **2012**, 47 (2), 850-858.
- <sup>4</sup> Appelo, C. A. J.; Van der Weiden, M. J. J.; Tournassat, C.; Charlet, L. Surface complexation of ferrous iron and carbonate on ferrihydrite and the mobilization of arsenic. *Environmental Science & Technology*. **2002**, 36 (14), 3096-3103.
- <sup>5</sup> Liu, H.; Bruton, T. A.; Doyle, F. M.; Sedlak, D. L. *In situ* chemical oxidation of contaminated groundwater by persulfate: decomposition by Fe (III) and Mn (IV) containing oxides and aquifer materials. *Environmental Science & Technology*. **2014**, 8 (17), 10330-10336.
- <sup>6</sup> Xu, X. R.; Li, X. Z. Degradation of azo dye Orange G in aqueous solutions by persulfate with ferrous ion. *Separation and Purification Technology*. **2010**, 72 (1), 105-111.
- <sup>7</sup> Morgan, B.; Lahav, O. The effect of pH on the kinetics of spontaneous Fe (II) oxidation by O<sub>2</sub> in aqueous solution—basic principles and a simple heuristic description. *Chemosphere*. **2007**, 68 (11), 2080-2084.
- <sup>8</sup> Heckel, E.; Henglein, A.; Beck, G. Pulsradiolytische Untersuchung des Radikalanions SO<sub>4</sub><sup>2-</sup>. *Berichte der Bunsengesellschaft für Physikalische Chemie*. **1966**, 70 (2), 149-154.
- <sup>9</sup> Rabani, J.; Zehavi, D. Pulse radiolytic investigation of O<sub>aq</sub>-radical ions. *The Journal of Physical Chemistry*. **1971**, 75 (11), 1738-1744.
- <sup>10</sup> King, D. W. Role of carbonate speciation on the oxidation rate of Fe (II) in aquatic systems. *Environmental Science & Technology*. **1998**, 32 (19), 2997-3003.
- <sup>11</sup> De Laat, J.; Le, G. T.; Legube, B. A comparative study of the effects of chloride, sulfate and nitrate ions on the rates of decomposition of H<sub>2</sub>O<sub>2</sub> and organic compounds by Fe (II)/H<sub>2</sub>O<sub>2</sub> and Fe (III)/H<sub>2</sub>O<sub>2</sub>. *Chemosphere*. **2004**, 55 (5), 715-723.

- 
- <sup>12</sup> Buxton, G. V.; Salmon, G. A.; Wood, N. D. A pulse radiolysis study of the chemistry of oxysulphur radicals in aqueous solution. *In Physico-Chemical Behaviour of Atmospheric Pollutants*. **1990**, 245-250.
- <sup>13</sup> Jiang, P. Y.; Katsumura, Y.; Domae, M.; Ishikawa, K.; Nagaishi, R.; Ishigure, K.; Yoshida, Y. Pulse radiolysis study of concentrated phosphoric acid solutions. *Journal of the Chemical Society. Faraday Transactions*. **1992**, 88 (22), 3319-3322.
- <sup>14</sup> Herrmann, H.; Reese, A.; Zellner, R. Time-resolved UV/VIS diode-array absorption spectroscopy of  $\text{SO}_x^-$  ( $x=3, 4, 5$ ) radical anions in aqueous solution. *Journal of Molecular Structure*. **1995**, 348, 183-186.
- <sup>15</sup> Peyton, G. R. The free-radical chemistry of persulfate-based total organic carbon analyzers. *Marine Chemistry*. **1993**, 41 (1-3), 91-103.
- <sup>16</sup> Buxton, G. V.; Greenstock, C. L.; Helman, W. P.; Ross, A. B. Critical review of rate constants for reactions of hydrated electrons, hydrogen atoms and hydroxyl radicals ( $\cdot\text{OH}/\text{O}^-$  in aqueous solution. *Journal of Physical and Chemical Reference Data*. **1988**, 17 (2), 513-886.
- <sup>17</sup> Elliot, A. J. A pulse radiolysis study of the temperature dependence of reactions involving H, OH and  $e^-_{\text{aq}}$  in aqueous solutions. *International Journal of Radiation Applications and Instrumentation. Part C. Radiation Physics and Chemistry*. **1989**, 34 (5), 753-758.
- <sup>18</sup> Yang, Y.; Pignatello, J. J.; Ma, J.; Mitch, W. A. Comparison of halide impacts on The efficiency of contaminant degradation by sulfate and hydroxyl radical-based advanced oxidation processes (AOPs). *Environmental Science & Technology*. **2014**, 48 (4), 2344-2351.
- <sup>19</sup> Matthew, B. M.; Anastasio, C. A chemical probe technique for the determination of reactive halogen species in aqueous solution: Part 1 - bromide solutions. *Atmospheric Chemistry and Physics*. **2006**, 6 (9), 2423-2437.
- <sup>20</sup> Mertens, R.; von Sonntag, C. Photolysis ( $\lambda= 354$  nm) of tetrachloroethene in aqueous solutions. *Journal of Photochemistry and Photobiology A: Chemistry*. **1995**, 85, (1), 1-9.
- <sup>21</sup> Dogliotti, L.; Hayon, E. Flash photolysis of persulfate ions in aqueous solutions. Study of the sulfate and ozonide radical anions. *The Journal of Physical Chemistry*. **1967**, 71 (8), 2511-2516.
- <sup>22</sup> Padmaja, S.; Neta, P.; Huie, R. E. Rate constants for some reactions of inorganic radicals with inorganic ions. Temperature and solvent dependence. *International Journal of Chemical Kinetics*. **1993**, 25 (6), 445-455.

- 
- <sup>23</sup> Neta, P.; Madhavan, V.; Zemel, H.; Fessenden, R. W. Rate constants and mechanism of reaction of sulfate radical anion with aromatic compounds. *Journal of the American Chemical Society*. **1977**, *99* (1), 163-164.
- <sup>24</sup> Gordon, S.; Schmidt, K. H.; Hart, E. J. A pulse radiolysis study of aqueous benzene solutions. *The Journal of Physical Chemistry*. **1977**, *81* (2), 104-109.
- <sup>25</sup> Lilie, J.; Henglein, A.; Hanrahan, R. J. Reactions of the carbonate radical anion with organic and inorganic solutes in aqueous solution. *176<sup>th</sup> Meeting Am. Chemistry Society Miami Beach, Fla.* **1978**.
- <sup>26</sup> Liu, H.; Bruton, T. A.; Li, W.; Van Buren, J.; Prasse, C.; Doyle, F. M.; Sedlak, D. L. Oxidation of benzene by persulfate in the presence of Fe (III)-and Mn (IV)-containing oxides: stoichiometric efficiency and transformation products. *Environmental Science & Technology*. **2016**, *50* (2), 890–898.
- <sup>27</sup> Villalobos, M.; Leckie, J. O. Surface complexation modeling and FTIR study of carbonate adsorption to goethite. *Journal of Colloid and Interface Science*. **2001**. 235 (1), 15-32.
- <sup>28</sup> Pokrovsky, O. S.; Schott, J. Surface chemistry and dissolution kinetics of divalent metal carbonates. *Environmental Science & Technology*. **2002**. 36 (3), 426-432.
- <sup>29</sup> Yu, X. Y.; Bao, Z. C.; Barker, J. R. Free radical reactions involving Cl, Cl<sub>2</sub><sup>-</sup>, and SO<sub>4</sub><sup>-</sup> in the 248 nm photolysis of aqueous solutions containing S<sub>2</sub>O<sub>8</sub><sup>2-</sup> and Cl. *The Journal of Physical Chemistry A*. **2004**, *108* (2), 295-308.
- <sup>30</sup> Das, T. Reactivity and role of SO<sub>5</sub><sup>-</sup> radical in aqueous medium chain oxidation of sulfite to sulfate and atmospheric sulfuric acid generation. *The Journal of Physical Chemistry A*. **2001**, *105* (40), 9142-9155.
- <sup>31</sup> McElroy, W. J. A laser photolysis study of the reaction of SO<sub>4</sub><sup>-</sup> with Cl<sup>-</sup> and the subsequent decay of Cl<sub>2</sub><sup>-</sup> in aqueous solution. *Journal of Physical Chemistry*, **1990**, *94* (6), 2435-2441.
- <sup>32</sup> Jayson, G.; Parsons, B.; Swallow, A. J. Some simple, highly reactive, inorganic chlorine derivatives in aqueous solution. Their formation using pulses of radiation and their role in the mechanism of the Fricke dosimeter. *Journal of the Chemical Society. Faraday Transaction 1: Physical Chemistry in Condensed Phases*. **1973**, (69), 1597- 1607.
- <sup>33</sup> Grigorev, A. E.; Makarov, I. E.; Pikaev, A. K. Formation of Cl<sub>2</sub><sup>-</sup> in the bulk solution during the radiolysis of concentrated aqueous-solutions of chlorides. *High Energy Chemistry*. **1987**, *21* (2), 99-102.

- 
- <sup>34</sup> Kläning, U. K.; Wolff, T. Laser flash photolysis of HClO, ClO<sup>-</sup>, HBrO, and BrO<sup>-</sup> in aqueous solution. Reactions of Cl<sup>-</sup> and Br<sup>-</sup> Atoms. *Berichte der Bunsengesellschaft für physikalische Chemie*. **1985**, *89* (3), 243-245.
- <sup>35</sup> Yu, X. Y.; Barker, J. R. Hydrogen peroxide photolysis in acidic aqueous solutions containing chloride ions. I. Chemical mechanism. *The Journal of Physical Chemistry A*. **2003**, *107* (9), 1313-1324.
- <sup>36</sup> McElroy, W. J. A laser photolysis study of the reaction of SO<sub>4</sub><sup>-</sup> with Cl<sup>-</sup> and the subsequent decay of Cl<sub>2</sub><sup>-</sup> in aqueous-solution. *Journal of Physics*. **1990**, *94* (6), 2435-2441.
- <sup>37</sup> Bunce, N. J.; Ingold, K. U.; Landers, J. P.; Lusztyk, J.; Scaiano, J. C. Kinetic study of the photochlorination of 2, 3-dimethylbutane and other alkanes in solution in the presence of benzene. First measurements of the absolute rate constants for hydrogen abstraction by the "free" chlorine atom and the chlorine atom-benzene. pi.-complex. Identification of these two species as the only hydrogen abstractors in these systems. *Journal of the American Chemical Society*. **1985**, *107* (19), 5464-5472.

# **Appendix B**

## **Supplemental Information for Chapter 3**

## Appendix B-1 Calculation of direct photolysis rates

The photolysis rate ( $r_p$ ) of  $S_2O_8^{2-}$  and  $NH_2Cl$  with monochromatic low-pressure mercury vapor UV lamp ( $\lambda=254nm$ ) was calculated as:

$$r_p = -\Phi \times I_0 \times f_{oxidant} \times f_{solution} \quad (\text{Eq. S1})$$

where  $\Phi$  is the primary quantum yield of the oxidant ( $\Phi_{S_2O_8^{2-}}=1.4$  mole/Einstein,  $\Phi_{NH_2Cl}=0.54$  mole/Einstein),<sup>1,2</sup>  $I_0$  is volume-normalized surface irradiance of the UV lamp (Einsteins $\cdot L^{-1}\cdot s^{-1}$ ) that was calculated as  $7.1 \times 10^{-6}$  Einstein $\cdot L^{-1}\cdot s^{-1}$ ,  $f_{oxidant}$  is the fraction of incident light absorbed by the oxidant and  $f_{solution}$  is the fraction absorbed by the total solution.

$$f_{oxidant} = \frac{\varepsilon_p c_p}{\sum \varepsilon_i c_i} \quad (\text{Eq.S2})$$

$$f_{solution} = 1 - 10^{-(\alpha + \sum \varepsilon_i c_i)l} \quad (\text{Eq. S3})$$

$\alpha$  is the absorption coefficient of the solution at the wavelength of 254 nm,  $\varepsilon_p$  and  $c_p$  are the molar extinction coefficient ( $M^{-1}\cdot cm^{-1}$ ) and the concentration (M) of the oxidant, respectively ( $\varepsilon_{S_2O_8^{2-}}=21.1 M^{-1}\cdot cm^{-1}$ ,  $\varepsilon_{NH_2Cl} = 371 M^{-1}\cdot cm^{-1}$ ),<sup>3,4</sup>  $\varepsilon_i$  and  $c_i$  are the molar extinction coefficient and concentration of solution constituents, and  $l$  is the effective light path of the reactor ( $l=0.49cm$ ).

## Appendix B-2 Table of Rate constants and elemental reactions for kinetics modeling

No.	Reaction	Rate Constant (M <sup>-1</sup> s <sup>-1</sup> )	Reference *
Photolysis of S <sub>2</sub> O <sub>8</sub> <sup>2-</sup> and relevant reactions			
1	$S_2O_8^{2-} \xrightarrow{h\nu} 2SO_4^{\cdot-}$	See Appendix B-1	Calculated
2	$S_2O_8^{2-} + OH^{\cdot} \rightarrow S_2O_8^{\cdot-}$	1.4×10 <sup>7</sup>	5
3	$S_2O_8^{2-} + SO_4^{\cdot-} \rightarrow S_2O_8^{\cdot-} + SO_4^{2-}$	6.6×10 <sup>5</sup>	6
4	$S_2O_8^{2-} + Cl^{\cdot} \rightarrow S_2O_8^{\cdot-} + Cl$	8.8×10 <sup>6</sup>	7
5	$S_2O_8^{2-} + Cl_2^{\cdot-} \rightarrow S_2O_8^{\cdot-} + 2Cl^-$	(6.0 ± 2.3)×10 <sup>5</sup>	Modelled
6	$S_2O_8^{2-} + S_2O_8^{\cdot-} \rightarrow product$	(4.0 ± 0.8)×10 <sup>-1</sup>	Modelled
7	$SO_5^{2-} + H^+ \rightarrow HSO_5^-$	5.0×10 <sup>10</sup>	3
8	$SO_5^{2-} + SO_4^{\cdot-} \rightarrow SO_5^- + SO_4^{2-}$	1.0×10 <sup>8</sup>	8
9	$HSO_5^- \rightarrow H^+ + SO_5^{2-}$	2.0×10 <sup>11</sup> a	3
10	$HSO_5^- + OH^{\cdot} \rightarrow H_2O + SO_5^{\cdot-}$	1.7×10 <sup>7</sup>	9
11	$HSO_4^{2-} \rightarrow H^+ + SO_4^{2-}$	6.3×10 <sup>8</sup> a	Calculated based on pka
12	$H^+ + SO_4^{2-} \rightarrow HSO_4^{\cdot-}$	5.0×10 <sup>10</sup>	Calculated based on pka
13	$SO_4^{\cdot-} + H_2O \rightarrow HSO_4^{2-} + OH^{\cdot}$	6.6×10 <sup>2</sup> a	10
14	$SO_4^{2-} + Cl^{\cdot} \rightarrow SO_4^{\cdot-} + Cl^-$	2.5×10 <sup>8</sup>	8
15	$SO_4^{\cdot-} + OH^- \rightarrow SO_4^{2-} + OH^{\cdot}$	7.0×10 <sup>7</sup>	11
16	$SO_4^{\cdot-} + Cl^- \rightarrow SO_4^{2-} + Cl^{\cdot}$	3.0×10 <sup>8</sup>	8
17	$SO_4^{\cdot-} + OH^{\cdot} \rightarrow HSO_5^-$	1.0×10 <sup>10</sup>	8
18	$SO_4^{\cdot-} + HSO_5^- \rightarrow SO_5^{\cdot-} + SO_4^{2-} + H^+$	1.0×10 <sup>6</sup>	8
19	$SO_4^{\cdot-} + S_2O_8^{2-} \rightarrow S_2O_8^{\cdot-} + SO_2 + O_2$	9.9×10 <sup>5</sup>	12
20	$SO_4^{\cdot-} + SO_5^{2-} \rightarrow S_2O_8^{2-} + 0.5O_2$	9.0×10 <sup>9</sup>	12
21	$SO_4^{\cdot-} + SO_4^{2-} \rightarrow S_2O_8^{2-}$	7.0×10 <sup>8</sup>	8
22	$SO_4^{\cdot-} + HO_2^{\cdot} \rightarrow HSO_4^{\cdot-} + O_2$	3.5×10 <sup>9</sup>	6
23	$SO_5^{\cdot-} + SO_5^{2-} \rightarrow S_2O_8^{2-} + O_2$	2.2×10 <sup>8</sup>	8
24	$SO_5^{\cdot-} + SO_5^{\cdot-} \rightarrow SO_4^{\cdot-} + SO_4^{\cdot-} + O_2$	2.1×10 <sup>8</sup>	8
25	$SO_5^{\cdot-} + HO_2^{\cdot} \rightarrow O_2 + HSO_5^-$	5.0×10 <sup>7</sup>	13
26	$H_2O \rightarrow H^+ + OH^-$	1.0×10 <sup>-3</sup> a	14
27	$H^+ + OH^- \rightarrow H_2O$	1.0×10 <sup>11</sup>	14
28	$H^+ + O_2^{\cdot-} \rightarrow HO_2^{\cdot}$	5.0×10 <sup>10</sup>	15
29	$OH^{\cdot} + OH^- \rightarrow O^{\cdot-} + H_2O$	1.2×10 <sup>10</sup>	16
30	$O^{\cdot-} + H_2O \rightarrow OH^{\cdot} + OH^-$	1.8×10 <sup>5</sup> a	16
31	$O^{\cdot-} + HO_2^{\cdot} \rightarrow O_2^{\cdot-} + OH^-$	4.0×10 <sup>8</sup>	16
32	$O^{\cdot-} + O_2 \rightarrow O_3^{\cdot-}$	3.6×10 <sup>9</sup>	16
34	$O_3^{\cdot-} \rightarrow O_2 + O^{\cdot-}$	2.6×10 <sup>3</sup> a	17
35	$OH^{\cdot} + O^{\cdot-} \rightarrow HO_2^{\cdot}$	1.0×10 <sup>10</sup>	16
36	$OH^{\cdot} + HO_2^{\cdot} \rightarrow HO_2^{\cdot} + OH^-$	7.5×10 <sup>9</sup>	18
37	$OH^{\cdot} + HO_2^{\cdot} \rightarrow H_2O + O_2$	6.6×10 <sup>9</sup>	19
38	$OH^{\cdot} + O_2^{\cdot-} \rightarrow OH^- + O_2$	7.0×10 <sup>9</sup>	20
39	$OH^{\cdot} + OH^{\cdot} \rightarrow H_2O_2$	5.5×10 <sup>9</sup>	17
40	$OH^{\cdot} + Cl^- \rightarrow ClOH^{\cdot-}$	4.3×10 <sup>9</sup>	21
41	$OH^{\cdot} + HSO_4^- \rightarrow H_2O + SO_4^{\cdot-}$	1.7×10 <sup>6</sup>	22
42	$HO_2^{\cdot} + HO_2^{\cdot} \rightarrow H_2O_2 + O_2$	8.3×10 <sup>5</sup>	23
43	$HO_2^{\cdot} + O_2^{\cdot-} \rightarrow HO_2^{\cdot} + O_2$	9.7×10 <sup>7</sup>	23

44	$HO_2 \cdot \rightarrow H^+ + O_2^{\cdot-}$ Photolysis of $NH_2Cl$ and relevant reactions	$1.6 \times 10^5$ <sup>a</sup>	23
45	$NH_2Cl \xrightarrow{h\nu} NH_2 \cdot + Cl \cdot$	See Text S3	Calculated
46	$NH_2Cl + OH \cdot \rightarrow NHCl \cdot + H_2O$	$5.1 \times 10^8$	24
47	$NH_2Cl + SO_4^{\cdot-} \rightarrow NHCl \cdot + HSO_4^-$	$(2.4 \pm 0.2) \times 10^7$	This study
48	$NH_2Cl + Cl \cdot \rightarrow NHCl \cdot + HCl$	$2.4 \times 10^7$	This study
49	$NH_2Cl + Cl_2^{\cdot-} \rightarrow NHCl \cdot + H^+ + 2Cl^-$	$(6.5 \pm 3.5) \times 10^6$	Modeled
50	$NH_2Cl + NH_2 \cdot \rightarrow NHCl \cdot + NH_3$	$(1.0 \pm 0.8) \times 10^5$	Modeled
51	$NH_2Cl + H \cdot \rightarrow NHCl \cdot + HCl$	$1.2 \times 10^9$	
52	$NH_2Cl + ClO \cdot \rightarrow NHCl \cdot + HOCl$	$1.0 \times 10^5$	
53	$NH_2Cl + H_2O \rightarrow HOCl + NH_3$	$2.8 \times 10^{-5}$ <sup>a</sup>	25
54	$HOCl + NH_3 \rightarrow NH_2Cl + H_2O$	$4.2 \times 10^6$	25
55	$NH_2Cl + NH_2Cl \rightarrow NHCl_2 + NH_3$	$k_d$ <sup>b</sup>	26
56	$NHCl_2 + NH_3 \rightarrow NH_2Cl + NH_2Cl$	$6.1 \times 10^4$	27
57	$NH_2Cl + NHCl_2 \rightarrow 3HCl + N_2$	$1.5 \times 10^{-2}$	26
58	$NH_4^+ \rightarrow NH_3 + H^+$	$4.2 \times 10^1$ <sup>a</sup>	Calculated based on pka
59	$NH_3 + H^+ \rightarrow NH_4^+$	$8.4 \times 10^{10}$	Calculated based on pka
60	$NH_3 + OH \cdot \rightarrow NH_2 \cdot + H_2O$	$9.7 \times 10^7$	28
61	$NH_3 + SO_4^{\cdot-} \rightarrow NH_2 \cdot + HSO_4^-$	$1.4 \times 10^7$	29
62	$NH_3 + Cl \cdot \rightarrow NH_2 \cdot + HCl$	$1.0 \times 10^7$	assumed
63	$NH_3 + Cl_2^{\cdot-} \rightarrow NH_2 \cdot + HCl + Cl^-$	$1.0 \times 10^7$	assumed
64	$NH_3 + O_2^{\cdot-} \rightarrow NH_2 \cdot + OH^-$	$3.0 \times 10^7$	30
65	$NH_4^+ + H \cdot \rightarrow product$	$4.0 \times 10^4$	31
66	$NH_4^+ + SO_4^{\cdot-} \rightarrow NH_2 \cdot + HSO_4^-$	$3.0 \times 10^5$	29
67	$NH_4^+ + Cl \cdot \rightarrow NH_2 \cdot + HCl$	$(1.3 \pm 0.5) \times 10^5$	modeled
68	$NH_4^+ + Cl_2^{\cdot-} \rightarrow NH_2 \cdot + HCl + Cl^-$	$(1.3 \pm 0.5) \times 10^5$	modeled
69	$NH_2 \cdot + H^+ \rightarrow NH_3^+$	$5.0 \times 10^9$	Calculated based on pka
70	$NH_3^+ \rightarrow NH_2 \cdot + H^+$	$1.0 \times 10^3$ <sup>a</sup>	Calculated based on pka
71	$NH_3^+ + NH_2Cl \rightarrow NH_3 + NHCl \cdot + H^+$	$1.0 \times 10^5$	assumed
72	$NH_2 \cdot + O_2 \rightarrow NH_2O_2$	$1.0 \times 10^7$	29
73	$NH_2 \cdot + NH_2 \cdot \rightarrow H_2NNH_2$	$2.2 \times 10^9$	32
74	$NH_2 \cdot + OH \cdot \rightarrow H_2NOH$	$9.5 \times 10^9$	32
75	$NH_2O_2 + O_2^{\cdot-} \rightarrow ONO_2^- + H_2O$	$2.3 \times 10^7$	32
76	$NH_2O_2 + O_2^{\cdot-} \rightarrow H_2NO_2^- + O_2$	$6.6 \times 10^8$	32
77	$NHCl \cdot + O_2 \rightarrow NHCl$	$1.0 \times 10^7$	assumed
78	$NHCl \cdot + NHCl \cdot \rightarrow N_2 + 2HCl$	$1.0 \times 10^9$	assumed
79	$NHCl_2 \xrightarrow{h\nu} NHCl \cdot + Cl \cdot$	See Text S3	Calculated
80	$NHCl_2 + OH \cdot \rightarrow NHCl \cdot + H_2O$	$8.0 \times 10^8$	This study
81	$NHCl_2 + SO_4^{\cdot-} \rightarrow NHCl \cdot + HSO_4^-$	$(1.0 \pm 0.2) \times 10^8$	This study
82	$NHCl_2 + Cl \cdot \rightarrow NHCl \cdot + HCl$	$(3.2 \pm 0.4) \times 10^7$	This study
83	$NHCl_2 + Cl_2^{\cdot-} \rightarrow NHCl \cdot + H^+ + 2Cl^-$	$(4.4 \pm 1.2) \times 10^6$	This study
84	$NHCl_2 + NH_2 \cdot \rightarrow NHCl \cdot + NH_3$	$1.0 \times 10^5$	assumed
85	$NHCl_2 + HOCl \rightarrow NHCl_2 + H_2O$	$3.5 \times 10^2$	26
86	$NHCl_2 + H_2O \rightarrow NHCl_2 + HOCl$	$6.4 \times 10^{-7}$	33
87	$NHCl_2 + H_2O \rightarrow NOH + 2HCl$	$1.7 \times 10^2$	26
88	$NOH + NHCl_2 \rightarrow N_2 + HOCl + HCl$	$2.8 \times 10^4$	26

89	$NOH + NH_2Cl \rightarrow N_2 + H_2O + HCl$	$8.3 \times 10^3$	26
	Reactive chlorine species reactions		
90	$ClOH^- \rightarrow Cl^- + OH^\cdot$	$6.1 \times 10^9$ <sup>a</sup>	21
91	$ClOH^- + Cl^- \rightarrow OH^- + Cl_2^-$	$1.0 \times 10^4$	34
92	$ClOH^- + H^+ \rightarrow Cl + H_2O$	$2.1 \times 10^{10}$	21
93	$Cl + H_2O \rightarrow ClOH^- + H^+$	$2.5 \times 10^5$ <sup>a</sup>	21
94	$Cl + OH^- \rightarrow ClOH^-$	$1.8 \times 10^{10}$	35
95	$Cl + Cl^- \rightarrow Cl_2^-$	$8.5 \times 10^9$	36
96	$Cl + Cl_2 \rightarrow Cl_3$	$5.3 \times 10^8$	37
97	$Cl + ClO^- \rightarrow ClO^\cdot + Cl^-$	$8.3 \times 10^9$	35
98	$Cl + Cl \rightarrow Cl_2$	$8.8 \times 10^7$	38
99	$Cl_2^- + Cl \rightarrow Cl_2 + Cl^-$	$2.1 \times 10^9$	36
100	$Cl_2^- + OH^- \rightarrow Cl^- + ClOH^-$	$4.5 \times 10^7$	34
101	$Cl_2^- \rightarrow Cl + Cl^-$	$6.0 \times 10^4$ <sup>a</sup>	36
102	$Cl_2^- + Cl_2^- \rightarrow 2 Cl^- + Cl_2$	$9.0 \times 10^8$	36
103	$Cl_2^- + H_2O \rightarrow Cl^- + HClOH^\cdot$	$1.3 \times 10^3$ <sup>a</sup>	37
104	$Cl_2^- + OH^\cdot \rightarrow HOCl + Cl^-$	$1.0 \times 10^9$	39
105	$Cl_2^- + HO_2^\cdot \rightarrow O_2 + H^+ + 2 Cl^-$	$3.0 \times 10^9$	40
106	$Cl_2^- + O_2^- \rightarrow O_2 + 2 Cl^-$	$2.0 \times 10^9$	41
107	$HClOH^\cdot \rightarrow H^+ + ClOH^-$	$1.0 \times 10^8$ <sup>a</sup>	37
108	$HClOH^\cdot \rightarrow Cl + H_2O$	$1.0 \times 10^2$ <sup>a</sup>	37
109	$HClOH^\cdot + Cl^- \rightarrow Cl_2^- + H_2O$	$5.0 \times 10^9$	37
110	$H^+ + Cl^- \rightarrow HCl$	$5.0 \times 10^{10}$	14
111	$HCl \rightarrow H^+ + Cl^-$	$8.6 \times 10^{16}$ <sup>a</sup>	14
112	$ClO^- + OH^\cdot \rightarrow ClO^\cdot + OH^-$	$8.8 \times 10^9$	42
113	$ClO^- + O_2^- + H_2O \rightarrow Cl + 2 OH^- + O_2$	$2.0 \times 10^8$	43
114	$ClO^\cdot + ClO^\cdot \rightarrow product$	$2.5 \times 10^9$	35
115	$Cl_2 + Cl^- \rightarrow Cl_3^-$	$2.0 \times 10^4$	44
116	$Cl_2 + O_2^- \rightarrow O_2 + Cl_2^-$	$1.0 \times 10^9$	43
117	$Cl_2 + HO_2^\cdot \rightarrow H^+ + O_2 + Cl_2^-$	$1.0 \times 10^9$	45
118	$Cl_2 + H_2O \rightarrow HOCl + Cl^- + H^+$	$2.2 \times 10^0$ <sup>a</sup>	46
119	$Cl_2OH^- \rightarrow HOCl + Cl^-$	$5.5 \times 10^9$ <sup>a</sup>	46
120	$Cl_3^- \rightarrow Cl_2 + Cl^-$	$1.1 \times 10^5$ <sup>a</sup>	44
121	$Cl_3^- + HO_2^\cdot \rightarrow Cl_2^- + HCl + O_2$	$1.0 \times 10^9$	45
122	$Cl_3^- + O_2^- \rightarrow Cl_2^- + Cl^- + O_2$	$3.8 \times 10^9$	43
	Phosphate relevant reactions		
123	$H_3PO_4 \rightarrow H_2PO_4^- + H^+$	$4.0 \times 10^8$ <sup>a</sup>	14
124	$H_2PO_4^- + H^+ \rightarrow H_3PO_4$	$5.0 \times 10^{10}$	14
125	$H_2PO_4^- \rightarrow HPO_4^{2-} + H^+$	$3.2 \times 10^3$ <sup>a</sup>	14
126	$HPO_4^{2-} + H^+ \rightarrow H_2PO_4^-$	$5.0 \times 10^{10}$	14
127	$HPO_4^{2-} \rightarrow PO_4^{3-} + H^+$	$2.5 \times 10^{-2}$ <sup>a</sup>	14
128	$PO_4^{3-} + H^+ \rightarrow HPO_4^{2-}$	$5.0 \times 10^{10}$	14
129	$H_3PO_4 + OH^\cdot \rightarrow H_2PO_4^- + H_2O$	$4.2 \times 10^4$	6
130	$H_2PO_4^- + OH^\cdot \rightarrow HPO_4^{2-} + H_2O$	$4.2 \times 10^4$	29
131	$HPO_4^{2-} + OH^\cdot \rightarrow HPO_4^{2-} + OH^-$	$1.5 \times 10^5$	29
132	$PO_4^{3-} + OH^\cdot \rightarrow product$	$1.0 \times 10^7$	47
133	$H_2PO_4^- + SO_4^- \rightarrow HPO_4^{2-} + HSO_4^-$	$7.0 \times 10^4$	29
134	$HPO_4^{2-} + SO_4^- \rightarrow HPO_4^{2-} + SO_4^{2-}$	$1.2 \times 10^6$	29

135	$HPO_4^- + Cl^- \rightarrow HPO_4^{2-} + Cl^-$	$1.0 \times 10^4$	29
136	$HPO_4^- + HPO_4^- \rightarrow P_2O_8^{4-} + 2H^+$	$4.5 \times 10^8$	47
137	$HPO_4^- + SO_4^{2-} \rightarrow \text{product}$	$1.0 \times 10^4$	48
Organics reactions			
138	$1,4 - D + OH^\cdot \rightarrow \text{product}$	$3.1 \times 10^9$	41
139	$1,4 - D + SO_4^{\cdot-} \rightarrow \text{product}$	$4.1 \times 10^7$	42
140	$1,4 - D + Cl^\cdot \rightarrow \text{product}$	$4.4 \times 10^6$	36
141	$1,4 - D + Cl_2^{\cdot-} \rightarrow \text{product}$	$3.3 \times 10^6$	36
142	$BA + OH^\cdot \rightarrow \text{product}$	$6.0 \times 10^9$	34
143	$BA + SO_4^{\cdot-} \rightarrow \text{product}$	$1.2 \times 10^9$	38
144	$BA + Cl^\cdot \rightarrow \text{product}$	$1.8 \times 10^{10}$	49
145	$BA + Cl_2^{\cdot-} \rightarrow \text{product}$	$2.0 \times 10^6$	35
146	$BA + ClO^\cdot \rightarrow \text{product}$	$3.0 \times 10^6$	50
147	$BA + O^{\cdot-} \rightarrow \text{product}$	$4.0 \times 10^7$	51
148	$BA + NH_2^\cdot \rightarrow \text{product}$	$4.0 \times 10^5$	39
149	$NB + OH^\cdot \rightarrow \text{product}$	$4.7 \times 10^9$	34
150	$NB + H^\cdot \rightarrow \text{product}$	$2.3 \times 10^9$	34

<sup>a</sup> rate constants are in unit of  $s^{-1}$

<sup>b</sup>  $k_d = k_{H^+}[H^+] + k_{H_3PO_4}[H_3PO_4] + k_{H_2PO_4^-}[H_2PO_4^{2-}]$ ,  $k_{H^+} = 7 \times 10^3 M^{-2}s^{-1}$ ,<sup>26</sup>  $k_{H_3PO_4} = 8.9 \times 10^2 M^{-2}s^{-1}$

<sup>1</sup>,<sup>52</sup>  $k_{H_2PO_4^-} = 3.9 \times 10^{-1} M^{-2}s^{-1}$ <sup>52</sup>

### **Appendix B-3 Details on the comprehensive kinetic modeling**

The kinetic model was built on the platform of Kintecus 4.55 software. A total of 150 elemental reactions were established to predict  $S_2O_8^{2-}$  and  $NH_2Cl$  photolysis rates and calculate steady-state concentrations of radical species. All reactions incorporated in the kinetic model were summarized in Table S1. Of 150 reactions, 130 rate constants were directly obtained from radiolysis literature, and 6 rate constants were optimized using data fitting into the model. First, the rate constants for Reactions 67-68 were optimized using the data sets from 1,4-D degradation by  $UV/S_2O_8^{2-}$  at different  $NH_4^+$  dosages. Then the rate constants for Reactions 5-6 and 49-50 were optimized using experimental data from 1,4-D degradation by  $UV/S_2O_8^{2-}$  at different  $NH_2Cl$  dosages. The best model fittings were achieved by applying Powell non-restricted algorithms to minimize the root mean squares (RMS) between the model prediction and experimental observation based on the kinetics of oxidant photolysis rates and 1,4-dioxane degradation rates. One rate constant was optimized at each concentration, and the average values of the rate constants with standard deviations were then calculated. The rate constants for Reactions 62-63, 71, 77-78, and 84 were assumed based on the reactivity of similar compounds. Rate constants for Reaction 47-48, 80-83 were obtained through Pulse-radiolysis studies (**Appendix B-5**). Finally, the modelled rate constants were randomized within the predicted rate constants  $\pm$  standard deviations, and calculated the confidence band at 95% confidence level.

#### Appendix B-4 Calculation of theoretical additive degradation rate of 1,4-D by UV/S<sub>2</sub>O<sub>8</sub><sup>2-</sup> and UV/NH<sub>2</sub>Cl

The theoretical additive degradation kinetics of 1,4-D by UV/S<sub>2</sub>O<sub>8</sub><sup>2-</sup> and UV/NH<sub>2</sub>Cl was calculated based on equation S4:

$$k_{1,4-D} = k_{S_2O_8^{2-}} \times f_{S_2O_8^{2-}} + k_{NH_2Cl} \times f_{NH_2Cl} \quad (\text{Eq. S4})$$

Where  $k_{1,4-D}$  is the total degradation rate of 1,4-D,  $k_{S_2O_8^{2-}}$  is the observed 1,4-D degradation rate by UV/S<sub>2</sub>O<sub>8</sub><sup>2-</sup> ( $[S_2O_8^{2-}] = 2\text{mM}$ ),  $f_{S_2O_8^{2-}}$  is the fraction of UV light absorbed by 2 mM S<sub>2</sub>O<sub>8</sub><sup>2-</sup> in the mix system,  $k_{NH_2Cl}$  is the rate of 1,4-D degradation by UV/NH<sub>2</sub>Cl at a specific concentration (0.1-4 mM), and  $f_{NH_2Cl}$  is the fraction of light absorbed by NH<sub>2</sub>Cl at the specific concentration (0.1-4 mM) in the mix system.

$f_{S_2O_8^{2-}}$  is calculated as:

$$f_{S_2O_8^{2-}} = \frac{\epsilon_{S_2O_8^{2-}} \times [S_2O_8^{2-}]}{\epsilon_{S_2O_8^{2-}} \times [S_2O_8^{2-}] + \epsilon_{NH_2Cl} \times [NH_2Cl]} \quad (\text{Eq. S5})$$

$\epsilon_{S_2O_8^{2-}}$  and  $\epsilon_{NH_2Cl}$  are the molar extinction coefficients of S<sub>2</sub>O<sub>8</sub><sup>2-</sup> and NH<sub>2</sub>Cl, respectively (M<sup>-1</sup>·cm<sup>-1</sup>).  $[S_2O_8^{2-}]$  and  $[NH_2Cl]$  are the concentrations of the S<sub>2</sub>O<sub>8</sub><sup>2-</sup> NH<sub>2</sub>Cl, respectively (M).

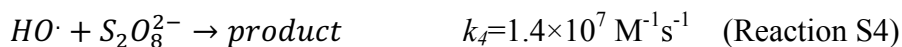
Similarly,  $f_{NH_2Cl}$  is calculated as:

$$f_{NH_2Cl} = \frac{\epsilon_{NH_2Cl} \times [NH_2Cl]}{\epsilon_{S_2O_8^{2-}} \times [S_2O_8^{2-}] + \epsilon_{NH_2Cl} \times [NH_2Cl]} \quad (\text{Eq. S6})$$

## Appendix B-5 Calculation of fate of each reactive radical species.

### B-5.1 Fate of HO<sup>•</sup> in UV/S<sub>2</sub>O<sub>8</sub><sup>2-</sup> and NH<sub>2</sub>Cl:

Once HO<sup>•</sup> was generated, it participated in the following four reactions:<sup>5,24,34</sup>



Under the experimental condition with 2 mM of S<sub>2</sub>O<sub>8</sub><sup>2-</sup>, 0-4 mM of NH<sub>2</sub>Cl and 250 μM of 1,4-dioxane, HO<sup>•</sup> branching ratio was calculated as:

$$\%_{HO^{\bullet}-Cl^{-}} = \frac{k_1[Cl^{-}]}{k_1[Cl^{-}] + k_2[NH_2Cl] + k_3[1,4D] + k_4[S_2O_8^{2-}]} \times 100\% = 1 - 81\% \quad (\text{Eq. S7})$$

$$\%_{HO^{\bullet}-NH_2Cl} = \frac{k_2[NH_2Cl]}{k_1[Cl^{-}] + k_2[NH_2Cl] + k_3[1,4D] + k_4[S_2O_8^{2-}]} \times 100\% = 0 - 14\% \quad (\text{Eq. S8})$$

$$\%_{HO^{\bullet}-1,4D} = \frac{k_3[1,4D]}{k_1[Cl^{-}] + k_2[NH_2Cl] + k_3[1,4D] + k_4[S_2O_8^{2-}]} \times 100\% = 5 - 96\% \quad (\text{Eq. S9})$$

$$\%_{HO^{\bullet}-S_2O_8^{2-}} = \frac{k_4[S_2O_8^{2-}]}{k_1[Cl^{-}] + k_2[NH_2Cl] + k_3[1,4D] + k_4[S_2O_8^{2-}]} \times 100\% = 0 - 4\% \quad (\text{Eq. S10})$$

Branching ratios of HO<sup>•</sup> with different species were summarized:

[NH <sub>2</sub> Cl] (mM)	0	0.1	0.2	0.4	1	2	3	4
%HO <sup>•</sup> -Cl <sup>-</sup>	1%	26%	40%	55%	70%	77%	79%	81%
%HO <sup>•</sup> -NH <sub>2</sub> Cl	0%	4%	7%	9%	12%	13%	14%	14%
%HO <sup>•</sup> -1,4-D	96%	67%	51%	35%	18%	10%	7%	5%
%HO <sup>•</sup> -S <sub>2</sub> O <sub>8</sub> <sup>2-</sup>	4%	2%	2%	1%	1%	0%	0%	0%

**B-5.2 Fate of  $SO_4^{\bullet-}$  in UV/ $S_2O_8^{2-}$  and  $NH_2Cl$ :**

Once  $SO_4^{\bullet-}$  was generated, five reactions could act as sinks for  $SO_4^{\bullet-}$ :<sup>37,36</sup>



The rate constant for  $SO_4^{\bullet-}$  with  $NH_2Cl$  was obtained from the model.

Under the experimental condition of 2 mM  $S_2O_8^{2-}$ , 250 mM 1,4-D and 0-4 mM  $NH_2Cl$ , the branching ratio of  $SO_4^{\bullet-}$  with each species in UV/ $S_2O_8^{2-}$ / $NH_2Cl$  were calculated:

$$\%_{SO_4^{\bullet-}-1,4D} = \frac{k_5[1,4D]}{k_5[1,4D]+k_6[S_2O_8^{2-}]+k_7+k_8[Cl^-]+k_9[NH_2Cl]} \times 100\% = 1 - 80\% \quad (\text{Eq. S11})$$

$$\%_{SO_4^{\bullet-}-S_2O_8^{2-}} = \frac{k_6[S_2O_8^{2-}]}{k_5[1,4D]+k_6[S_2O_8^{2-}]+k_7+k_8[Cl^-]+k_9[NH_2Cl]} \times 100\% = 0 - 10\% \quad (\text{Eq. S12})$$

$$\%_{SO_4^{\bullet-}-H_2O} = \frac{k_7}{k_5[1,4D]+k_6[S_2O_8^{2-}]+k_7+k_8[Cl^-]+k_9[NH_2Cl]} \times 100\% = 0 - 5\% \quad (\text{Eq. S13})$$

$$\%_{SO_4^{\bullet-}-Cl^-} = \frac{k_8[Cl^-]}{k_5[1,4D]+k_6[S_2O_8^{2-}]+k_7+k_8[Cl^-]+k_9[NH_2Cl]} \times 100\% = 5 - 91\% \quad (\text{Eq. S14})$$

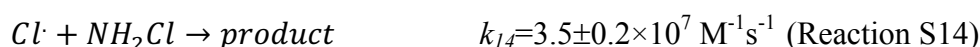
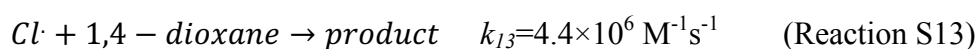
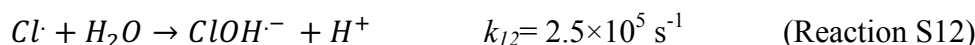
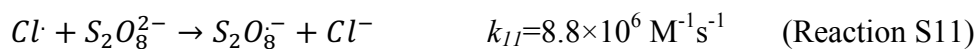
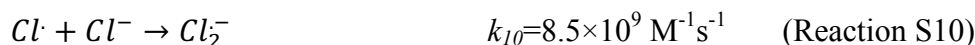
$$\%_{SO_4^{\bullet-}-NH_2Cl} = \frac{k_9[NH_2Cl]}{k_5[1,4D]+k_6[S_2O_8^{2-}]+k_7+k_8[Cl^-]+k_9[NH_2Cl]} \times 100\% = 0 - 8\% \quad (\text{Eq. S15})$$

Branching ratios of  $SO_4^{\bullet-}$  with different species were summarized:

[ $NH_2Cl$ ] (mM)	0	0.1	0.2	0.4	1	2	3	4
<b>%<math>SO_4^{\bullet-}</math>-1,4-D</b>	80%	23%	13%	7%	4%	2%	2%	1%
<b>%<math>SO_4^{\bullet-}</math>-<math>S_2O_8^{2-}</math></b>	10%	3%	2%	1%	0%	0%	0%	0%
<b>%<math>SO_4^{\bullet-}</math>-<math>H_2O</math></b>	5%	1%	1%	0%	0%	0%	0%	0%
<b>%<math>SO_4^{\bullet-}</math>-<math>Cl^-</math></b>	5%	68%	78%	85%	89%	91%	91%	91%
<b>%<math>SO_4^{\bullet-}</math>-<math>NH_2Cl</math></b>	0%	5%	6%	7%	7%	7%	7%	8%

### B-5.3 Fate of Cl<sup>•</sup> in UV/S<sub>2</sub>O<sub>8</sub><sup>2-</sup> and NH<sub>2</sub>Cl:

Cl<sup>•</sup> also has multiple sinks, including Cl<sup>-</sup>, S<sub>2</sub>O<sub>8</sub><sup>2-</sup>, H<sub>2</sub>O, 1,4-dioxane and NH<sub>2</sub>Cl:  
36,8,34,54



The rate of Cl<sup>•</sup> reacting NH<sub>2</sub>Cl was obtained from the model.

Under the experimental condition of 2 mM S<sub>2</sub>O<sub>8</sub><sup>2-</sup>, 250 mM 1,4-dioxane and 0-4 mM NH<sub>2</sub>Cl, the branching ratio of Cl<sup>•</sup> with each species was then calculated as:

$$\%_{Cl^{\bullet}-Cl^{-}} = \frac{k_{10}[Cl^{-}]}{k_{10}[Cl^{-}] + k_{11}[S_2O_8^{2-}] + k_{12} + k_{13}[1,4D] + k_{14}[NH_2Cl]} \times 100\% = 6 - 99\% \quad (\text{Eq. S16})$$

$$\%_{Cl^{\bullet}-S_2O_8^{2-}} = \frac{k_{11}[S_2O_8^{2-}]}{k_{10}[Cl^{-}] + k_{11}[S_2O_8^{2-}] + k_{12} + k_{13}[1,4D] + k_{14}[NH_2Cl]} \times 100\% = 0 - 6\% \quad (\text{Eq. S17})$$

$$\%_{Cl^{\bullet}-H_2O} = \frac{k_{12}}{k_{10}[Cl^{-}] + k_{11}[S_2O_8^{2-}] + k_{12} + k_{13}[1,4D] + k_{14}[NH_2Cl]} \times 100\% = 1 - 87\% \quad (\text{Eq. S18})$$

$$\%_{Cl^{\bullet}-1,4D} = \frac{k_{13}[1,4D]}{k_{10}[Cl^{-}] + k_{11}[S_2O_8^{2-}] + k_{12} + k_{13}[1,4D] + k_{14}[NH_2Cl]} \times 100\% = < 0.4\% \quad (\text{Eq. S19})$$

$$\%_{Cl^{\bullet}-NH_2Cl} = \frac{k_{14}[NH_2Cl]}{k_{10}[Cl^{-}] + k_{11}[S_2O_8^{2-}] + k_{12} + k_{13}[1,4D] + k_{14}[NH_2Cl]} \times 100 = < 1\% \quad (\text{Eq. S20})$$

Branching ratios of Cl<sup>•</sup> with different species were summarized:

[NH <sub>2</sub> Cl] (mM)	0	0.1	0.2	0.4	1	2	3	4
%Cl <sup>•</sup> -Cl <sup>-</sup>	6%	76%	86%	92%	97%	98%	99%	99%
%Cl <sup>•</sup> -S <sub>2</sub> O <sub>8</sub> <sup>2-</sup>	6%	2%	1%	0%	0%	0%	0%	0%
%Cl <sup>•</sup> -H <sub>2</sub> O	87%	22%	13%	7%	3%	1%	1%	1%
%Cl <sup>•</sup> -1,4-D	0%	0%	0%	0%	0%	0%	0%	0%
%Cl <sup>•</sup> -NH <sub>2</sub> Cl	0%	0%	0%	0%	0%	0%	0%	0%

**B-5.4 Fate of  $Cl_2^{\cdot-}$  in UV/ $S_2O_8^{2-}$  and  $NH_2Cl$ :**

$Cl_2^{\cdot-}$  also has multiple sinks, including  $NH_2Cl$ ,  $S_2O_8^{2-}$ ,  $H_2O$ , and 1,4-dioxane:



The rate constant of  $Cl_2^{\cdot-}$  with  $NH_2Cl$  was obtained from the model.

Under the experimental condition with 2 mM of  $S_2O_8^{2-}$ , 0-4 mM of  $NH_2Cl$  and 250  $\mu\text{M}$  of 1,4-dioxane,  $Cl_2^{\cdot-}$  branching ratio was calculated as:

$$\%Cl_2^{\cdot-}-NH_2Cl = \frac{k_{15}[NH_2Cl]}{k_{15}[NH_2Cl]+k_{16}[S_2O_8^{2-}]+k_{17}+k_{18}[1,4D]} \times 100\% = 0 - 86\% \quad (\text{Eq. S21})$$

$$\%Cl_2^{\cdot-}-S_2O_8^{2-} = \frac{k_{16}[S_2O_8^{2-}]}{k_{15}[NH_2Cl]+k_{16}[S_2O_8^{2-}]+k_{17}+k_{18}[1,4D]} \times 100\% = 5 - 36\% \quad (\text{Eq. S22})$$

$$\%Cl_2^{\cdot-}-H_2O = \frac{k_{17}}{k_{15}[NH_2Cl]+k_{16}[S_2O_8^{2-}]+k_{17}+k_{18}[1,4D]} \times 100\% = 6 - 39\% \quad (\text{Eq. S23})$$

$$\%Cl_2^{\cdot-}-1,4D = \frac{k_{18}[1,4D]}{k_{15}[NH_2Cl]+k_{16}[S_2O_8^{2-}]+k_{17}+k_{18}[1,4D]} \times 100\% = 3 - 25\% \quad (\text{Eq. S24})$$

Branching ratios of  $Cl_2^{\cdot-}$  with different species were summarized:

[ $NH_2Cl$ ] (mM)	0	0.1	0.2	0.4	1	2	3	4
$\%Cl_2^{\cdot-}-NH_2Cl$	0%	23%	35%	49%	68%	78%	82%	86%
$\%Cl_2^{\cdot-}-S_2O_8^{2-}$	36%	28%	23%	18%	12%	8%	7%	5%
$\%Cl_2^{\cdot-}-H_2O$	39%	30%	25%	20%	13%	9%	7%	6%
$\%Cl_2^{\cdot-}-1,4-D$	25%	19%	16%	13%	8%	5%	4%	3%

**Appendix B-6 Electron pulse radiolysis for determining second-order rate constants of  $\text{SO}_4^{\bullet-}$ ,  $\text{Cl}^{\bullet}$  and  $\text{Cl}_2^{\bullet-}$  with  $\text{NH}_2\text{Cl}$  and  $\text{NHCl}_2$ .**

Detailed radical generation and experimental procedures would be found in our previous publication.<sup>36</sup>

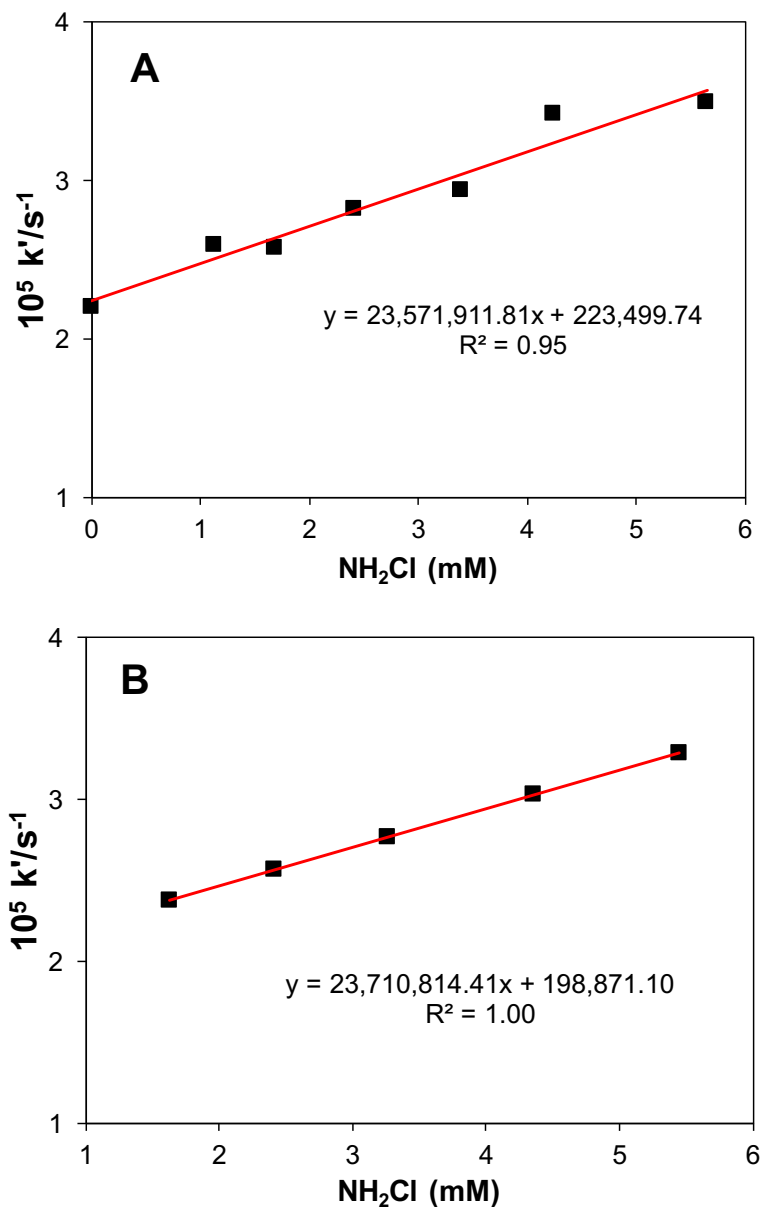


**Figure B1** Variation in  $\text{NH}_2\text{Cl}$  growth kinetics from data in Table S5 were used to determine second order rate constants for (A)  $\text{NH}_2\text{Cl}$  reaction with  $\text{SO}_4^{\bullet-}$  and (B)  $\text{NH}_2\text{Cl}$  reaction with  $\text{Cl}^{\bullet}$ . Based on the slope of the correlation, the second-order rate constants between  $\text{NH}_2\text{Cl}$  reaction with  $\text{SO}_4^{\bullet-}$ ,  $(2.4 \pm 0.2) \times 10^7 \text{ M}^{-1}\text{s}^{-1}$  and between  $\text{NH}_2\text{Cl}$  reaction with  $\text{Cl}^{\bullet}$ ,  $2.4 \times 10^7 \text{ M}^{-1}\text{s}^{-1}$ .

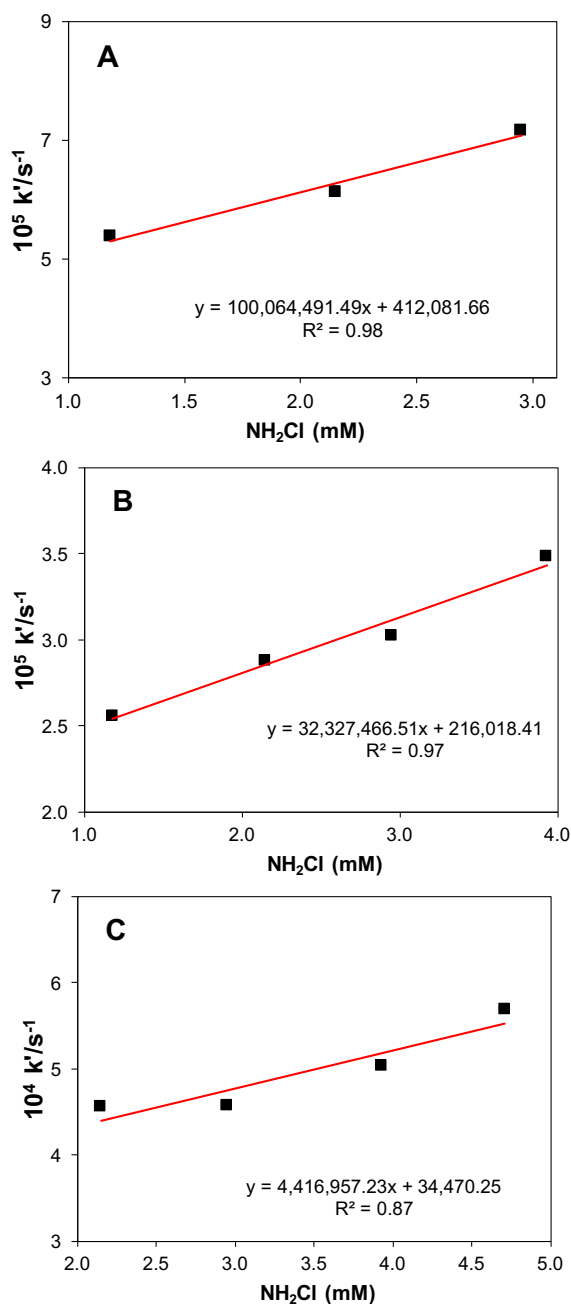
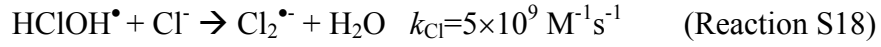


**Figure B2** Variation in  $\text{NH}_2\text{Cl}$  growth kinetics from top data used to determine second order rate constants for (A)  $\text{NHCl}_2$  reaction with  $\text{SO}_4^{\bullet-}$ ; (B)  $\text{NHCl}_2$  reaction with  $\text{Cl}^{\bullet}$ ; (C)  $\text{NHCl}_2$  reaction with  $\text{Cl}_2^{\bullet-}$ . Based on the slope of the correlation, the second-order rate constant between  $\text{NHCl}_2$  reaction with  $\text{SO}_4^{\bullet-} = (1.0 \pm 0.15) \times 10^8 \text{ M}^{-1}\text{s}^{-1}$ , the second-order rate constant between  $\text{NHCl}_2$  reaction with  $\text{Cl}^{\bullet} = (3.2 \pm 0.38) \times 10^7 \text{ M}^{-1}\text{s}^{-1}$ , the second-order rate constant between  $\text{NHCl}_2$  reaction with  $\text{Cl}_2^{\bullet-} = (4.4 \pm 1.2) \times 10^6 \text{ M}^{-1}\text{s}^{-1}$ .

### Appendix B-7 Calculation of HClOH• scavenging by chloride

HClOH• reacts with chloride through the following equation:



Therefore, HClOH• scavenging by chloride is calculated as:

$$\%_{\text{HClOH}\cdot-\text{Cl}^-} = \frac{k_{\text{Cl}^-}[\text{Cl}^-]}{k_{\text{HClOH}\cdot} + k_{\text{Cl}^-}[\text{Cl}^-]} \times 100\% = 9\%$$

$$[\text{ClOH}\cdot^-]_{\text{ss}} \text{ also decreased by } 9\%, \text{ because } [\text{ClOH}\cdot^-]_{\text{ss}} = \frac{k_{\text{HClOH}\cdot}[\text{HClOH}\cdot]_{\text{ss}}}{k_{\text{ClOH}\cdot^-}}$$

The branching ratio of HO• reacting with 2 mM chloride and 0.2 mM is calculated as:

*Branching ratio*<sub>HO•-Cl</sub>

$$= \frac{k_{\text{Cl}^-}[0.002\text{M}] + k_{\text{NH}_2\text{Cl}}[\text{NH}_2\text{Cl}] + k_{1,4\text{D}}[1,4\text{-dioxane}] + k_{\text{S}_2\text{O}_8^{2-}}[\text{S}_2\text{O}_8^{2-}]}{k_{\text{Cl}^-}[0.0002\text{M}] + k_{\text{NH}_2\text{Cl}}[\text{NH}_2\text{Cl}] + k_{1,4\text{D}}[1,4\text{-dioxane}] + k_{\text{S}_2\text{O}_8^{2-}}[\text{S}_2\text{O}_8^{2-}]} \times 100\% = 217\%$$

## Reference:

---

- <sup>1</sup> G. Mark; M. N. Schuchmann; H. P. Schuchmann; C. Von Sonntag. The photolysis of potassium peroxodisulphate in aqueous solution in the presence of tert-butanol: a simple actinometer for 254 nm radiation. *J. Photochem. Photobiol. B: Chem.* **1990**, *55*, 157-168.
- <sup>2</sup> De Laat, J.; Boudiaf, N.; Dossier-Berne, F. Effect of dissolved oxygen on the photodecomposition of monochloramine and dichloramine in aqueous solution by UV irradiation at 253.7 nm. *Water Research.* **2010**, *44* (10), 3261-3269.
- <sup>3</sup> Yang, Y.; Pignatello, J. J.; Ma, J.; Mitch, W. A. Comparison of halide impacts on the efficiency of contaminant degradation by sulfate and hydroxyl radical-based advanced oxidation processes (AOPs). *Environmental Science & Technology.* **2014** *48* (4), 2344-2351.
- <sup>4</sup> Li, J.; Blatchley Iii, E. R. UV photodegradation of inorganic chloramines. *Environmental Science & Technology.* **2008**, *43* (1), 60-65.
- <sup>5</sup> Buxton, George V.; G. Arthur Salmon; and Nicholas D. Wood. A pulse radiolysis study of the chemistry of oxysulphur radicals in aqueous solution. *Physico-Chemical Behaviour of Atmospheric Pollutants.* Springer Netherlands. **1990**. 245-250.
- <sup>6</sup> Jiang, P. Y.; Katsumura, Y.; Domae, M.; Ishikawa, K.; Nagaishi, R.; Ishigure, K.; Yoshida, Y. Pulse radiolysis study of concentrated phosphoric acid solutions. *Journal of the Chemical Society. Faraday Transactions.* **1992**, *88* (22), 3319-3322.
- <sup>7</sup> Yu, X. Y.; Bao, Z. C.; Barker, J. R. Free radical reactions involving Cl, Cl<sub>2</sub><sup>-</sup>, and SO<sub>4</sub><sup>-</sup> in the 248 nm photolysis of aqueous solutions containing S<sub>2</sub>O<sub>8</sub><sup>2-</sup> and Cl. *The Journal of Physical Chemistry A.* **2004**, *108* (2), 295-308.
- <sup>8</sup> Das, T. Reactivity and role of SO<sub>5</sub><sup>-</sup> radical in aqueous medium chain oxidation of sulfite to sulfate and atmospheric sulfuric acid generation. *The Journal of Physical Chemistry A.* **2001**, *105* (40), 9142-9155.
- <sup>9</sup> Maruthamuthu, P.; Neta, P. Radiolytic chain decomposition of peroxomonophosphoric and peroxomonosulfuric acids. *The Journal of Physical Chemistry.* **1977**, *81* (10), 937-940.
- <sup>10</sup> Herrmann, H.; Reese, A.; Zellner, R. Time-resolved UV/VIS diode-array absorption spectroscopy of SO<sub>x</sub><sup>-</sup> (x=3, 4, 5) radical anions in aqueous solution. *Journal of Molecular Structure.* **1995**, *348*, 183-186.

- 
- <sup>11</sup> Peyton, G. R. The free-radical chemistry of persulfate-based total organic carbon analyzers. *Marine Chemistry*. **1993**, *41* (1-3), 91-103.
- <sup>12</sup> Qian, Y.; Guo, X.; Zhang, Y.; Peng, Y.; Sun, P.; Huang, C. H.; Niu, J.; Zhou, X.; Crittenden, J. C. Perfluorooctanoic Acid Degradation Using UV–Persulfate Process: Modeling of the Degradation and Chlorate Formation. *Environmental Science & Technology*. **2015**, *50* (2), 772-781.
- <sup>13</sup> Yermakov, A. N.; Zhitomirsky, B. M.; Poskrebyshev, G. A.; Stoliarov, S. I. Kinetic Study of  $\text{SO}_5^-$  and  $\text{HO}_2$  Radicals Reactivity in Aqueous Phase Bisulfite Oxidation. *The Journal of Physical Chemistry*. **1995**, *99* (10), 3120-3127.
- <sup>14</sup> De Laat, J.; Boudiaf, N.; Dossier-Berne, F. Effect of dissolved oxygen on the photodecomposition of monochloramine and dichloramine in aqueous solution by UV irradiation at 253.7 nm. *Water Research*. **2010**, *44* (10), 3261-3269.
- <sup>15</sup> Ilan, Y.; Rabani, J. On some fundamental reactions in radiation chemistry: Nanosecond pulse radiolysis. *International Journal for Radiation Physics and Chemistry*. **1976**, *8* (5), 609-611.
- <sup>16</sup> Buxton, G. V.; Greenstock, C. L.; Helman, W. P.; Ross, A. B. Critical review of rate constants for reactions of hydrated electrons, hydrogen atoms and hydroxyl radicals ( $\text{OH}^\bullet/\text{O}^\bullet$  in aqueous solution. *Journal of Physical and Chemical Reference Data*. **1988**, *17* (2), 513-886.
- <sup>17</sup> Elliot, A. J. A pulse radiolysis study of the temperature dependence of reactions involving H, OH and  $e^-_{\text{aq}}$  in aqueous solutions. International Journal of Radiation Applications and Instrumentation. Part C. *Radiation Physics and Chemistry*. **1989**, *34* (5), 753-758.
- <sup>18</sup> Christensen, H.; Sehested, K.; Corfitzen, H. Reactions of hydroxyl radicals with hydrogen peroxide at ambient and elevated temperatures. *The Journal of Physical Chemistry*. **1982**, *86* (9), 1588-1590.
- <sup>19</sup> Sehested, K.; Rasmussen, O. L.; Fricke, H. Rate constants of OH with  $\text{HO}_2$ ,  $\text{O}_2^-$ , and  $\text{H}_2\text{O}_2^+$  from hydrogen peroxide formation in pulse-irradiated oxygenated water. *The Journal of Physical Chemistry*. **1968**, *72* (2), 626-631.
- <sup>20</sup> Beck, G. Elektrische leitfähigkeitsmessungen zum nachweis geladener zwischenprodukte der pulsradiolyse. *International Journal for Radiation Physics and Chemistry*. **1969**, *1* (3), 361-371.
- <sup>21</sup> Jayson, G.; Parsons, B.; Swallow, A. J. Some simple, highly reactive, inorganic chlorine derivatives in aqueous solution. Their formation using pulses of radiation and their role

- 
- in the mechanism of the Fricke dosimeter. *Journal of the Chemical Society. Faraday Transaction 1: Physical Chemistry in Condensed Phases*. **1973**, (69), 1597-1607.
- <sup>22</sup> Heckel, E.; Henglein, A.; Beck, G. Pulsradiolytische Untersuchung des Radikalanions  $\text{SO}_4^{2-}$ . *Berichte der Bunsengesellschaft für Physikalische Chemie*. **1966**, 70 (2), 149-154.
- <sup>23</sup> Bielski, B. H.; Cabelli, D. E.; Arudi, R. L.; Ross, A. B. Reactivity of  $\text{HO}_2/\text{O}_2^-$  radicals in aqueous solution. *Journal of Physical and Chemical Reference Data*. **1985**, 14 (4), 1041-1100.
- <sup>24</sup> Poskrebyshev, G. A.; Huie, R. E.; Neta, P. Radiolytic reactions of monochloramine in aqueous solutions. *The Journal of Physical Chemistry A*. **2003**, 107 (38), 7423-7428.
- <sup>25</sup> Jolley, R. L.; Brungs, W.A.; Cotruvo, J.A.; Cumming, R.B.; Mattice, J.S.; Jacobs V.A. *Water Chlorination: Environmental Impact and Health Effects, Vol. 4*. Ann Arbor Science, Ann Arbor, MI. 1981. pp. 49-62
- <sup>26</sup> Valentine, R. L.; Brandt, K. I.; Jafvert, C. T. A spectrophotometric study of the formation of an unidentified monochloramine decomposition product. *Water Research*. **1986**, 20 (8), 1067-1074.
- <sup>27</sup> Hand, V. C.; Margerum, D. W. Kinetics and mechanisms of the decomposition of dichloramine in aqueous solution. *Inorganic Chemistry*. **1983**, 22 (10), 1449-1456.
- <sup>28</sup> Hickel, B.; Sehested, K. Reaction of hydroxyl radicals with ammonia in liquid water at elevated temperatures. *International Journal of Radiation Applications and Instrumentation. Part C. Radiation Physics and Chemistry*. **1992**, 39 (4), 355-357.
- <sup>29</sup> Neta, P.; Maruthamuthu, P.; Carton, P. M.; Fessenden, R. W. Formation and reactivity of the amino radical. *The Journal of Physical Chemistry*. **1978**, 82 (17), 1875-1878.
- <sup>30</sup> Men'kin, V. B.; Makarov, I. E.; Pikaev, A. K. Pulse radiolysis study of reaction rates of OH and O-radicals with ammonia in aqueous solutions. *High Energy Chemistry (English Translation)*. **1989**, 22 (5), 333-336.
- <sup>31</sup> Scholes, G.; Simic, M. Reactivity of the hydrogen atoms produced in the radiolysis of aqueous systems. *The Journal of Physical Chemistry*. 1964, 68 (7), 1738-1743.
- <sup>32</sup> Pagsberg, P. B. Investigation of the  $\text{NH}_2$  radical produced by pulse radiolysis of ammonia in aqueous solution. *Aspects of Research at Risø*. **1972**, 5, 209.
- <sup>33</sup> Margerum, D. W.; Gray JR, E. T.; Huffman, R. P. *Chlorination and the formation of N-chloro compounds in water treatment*. F.E. Brinckman, J.M. Bellama (Eds.),

---

*Organometals and Organometalloids: Occurrence and Fate in the Environment.* ACS Books, Washington, DC. 1978. pp. 278-291

- <sup>34</sup> Grigorev, A. E.; Makarov, I. E.; Pikaev, A. K. Formation of  $\text{Cl}_2^-$  in the bulk solution during the radiolysis of concentrated aqueous-solutions of chlorides. *High Energy Chemistry*. **1987**, *21* (2), 99-102.
- <sup>35</sup> Klänig, U. K.; Wolff, T. Laser Flash Photolysis of  $\text{HClO}$ ,  $\text{ClO}^-$ ,  $\text{HBrO}$ , and  $\text{BrO}^-$  in Aqueous Solution. Reactions of  $\text{Cl}^\cdot$  and  $\text{Br}^\cdot$  Atoms. *Berichte der Bunsengesellschaft für physikalische Chemie*. **1985**, *89* (3), 243-245.
- <sup>36</sup> Yu, X. Y.; Barker, J. R. Hydrogen peroxide photolysis in acidic aqueous solutions containing chloride ions. I. Chemical mechanism. *The Journal of Physical Chemistry A*. **2003**, *107* (9), 1313-1324.
- <sup>37</sup> Bunce, N. J.; Ingold, K. U.; Landers, J. P.; Luszyk, J.; Scaiano, J. C. Kinetic study of the photochlorination of 2,3-dimethylbutane and other alkanes in solution in the presence of benzene. First measurements of the absolute rate constants for hydrogen abstraction by the "free" chlorine atom and the chlorine atom-benzene.  $\pi$ -complex. Identification of these two species as the only hydrogen abstractors in these systems. *Journal of the American Chemical Society*. **1985**, *107* (19), 5464-5472.
- <sup>38</sup> Wu, D.; Wong, D.; Di Bartolo, B. Evolution of  $\text{Cl}_2^-$  in aqueous NaCl solutions. *Journal of Photochemistry*. **1980**, *14* (4), 303-310.
- <sup>39</sup> Wagner, I.; Karthäuser, J.; Strehlow, H. On the decay of the dichloride anion  $\text{Cl}_2^-$  in aqueous solution. *Berichte der Bunsengesellschaft für Physikalische Chemie*. **1986**, *90* (10), 861-867.
- <sup>40</sup> Gogolev, A. Y.; Makarov, I. E.; Pikaev, A. K. Pulsed Radiolysis of Concentrated Hydrochloric-acid. *High Energy Chemistry*. **1984**, *18* (6), 390-395.
- <sup>41</sup> Zhestkova, T. P.; Pikaev, A. K. Destruction rate of  $\text{Cl}_2^-$  anion-radicals during pulse radiolysis of concentrated aqueous lithium chloride solutions. *Russian Chemical Bulletin*. **1974**, *23* (4), 877-878.
- <sup>42</sup> Buxton, G. V.; Subhani, M. S. Radiation chemistry and photochemistry of oxychlorine ions. Part 1.—Radiolysis of aqueous solutions of hypochlorite and chlorite ions. *Journal of the Chemical Society, Faraday Transactions 1: Physical Chemistry in Condensed Phases*. **1972**, *68*, 947-957.
- <sup>43</sup> Matthew, B. M.; Anastasio, C. A chemical probe technique for the determination of reactive halogen species in aqueous solution: Part 1 - bromide solutions. *Atmospheric Chemistry and Physics*. **2006**, *6* 2423-2437.

- 
- <sup>44</sup> Ershov, B. G. Kinetics, mechanism and intermediates of some radiation-induced reactions in aqueous solutions. *Usp. Khim.* **2004**, 73 (1), 107-120.
- <sup>45</sup> Bjergbakke, E.; Navaratnam, S.; Parsons, B.J. Reaction between HO<sub>2</sub><sup>•</sup> And chlorine in aqueous solution. *Journal of Chemical Society.* **1981**, 102, 5926-5928.
- <sup>46</sup> Wang, T. X.; Margerum, D. W. Kinetics of reversible chlorine hydrolysis: Temperature dependence and general-acid/ base-assisted mechanisms. *Inorganic Chemistry.* **1994**, 33 (6), 1050-1055.
- <sup>47</sup> Black, E. D.; Hayon, E. Pulse radiolysis of phosphate anions H<sub>2</sub>PO<sub>4</sub><sup>-</sup>, HPO<sub>4</sub><sup>2-</sup>, PO<sub>4</sub><sup>3-</sup>, and P<sub>2</sub>O<sub>7</sub><sup>4-</sup> in aqueous solutions. *The Journal of Physical Chemistry*, **1970**, 74 (17), 3199-3203.
- <sup>48</sup> Maruthamuthu, P.; Neta, P. Phosphate radicals. Spectra, acid-base equilibria, and reactions with inorganic compounds. *The Journal of Physical Chemistry.* **1978**, 82 (6), 710-713.
- <sup>49</sup> Remucal, C. K.; Manley, D. Emerging investigators series: the efficacy of chlorine photolysis as an advanced oxidation process for drinking water treatment. *Environmental Science: Water Research & Technology.* **2016**, 2(4), 565-579.
- <sup>50</sup> Alfassi, Z. B.; Huie, R. E.; Mosseri, S.; Neta, P. Kinetics of one-electron oxidation by the ClO radical. International Journal of Radiation Applications and Instrumentation. Part C. *Radiation Physics and Chemistry.* **1988**, 32 (1), 85-88.
- <sup>51</sup> Simic, M.; Hoffman, M. Z. Acid-base properties of the radicals produced in the pulse radiolysis of aqueous solutions of benzoic acid. *The Journal of Physical Chemistry.* **1972**, 76 (10), 1398-1404.
- <sup>52</sup> Valentine, R. L.; Jafvert, C. T.; Leung, S. W. Evaluation of a chloramine decomposition model incorporating general acid catalysis. *Water Research.* **1988**, 22 (9), 1147-1153.
- <sup>53</sup> Eibenberger, J. Pulse radiolytic investigations concerning the formation and the oxidation of organic radicals in aqueous solutions. *INIS.* **1980**. 15 (08) 95.
- <sup>54</sup> Nagarajan, V.; Fessenden, R. W. Flash photolysis of transient radicals. 1. X<sub>2</sub><sup>-</sup> with X= Cl, Br, I, and SCN. *The Journal of Physical Chemistry.* **1985**, 89 (11).

# **Appendix C**

## **Supplemental Information for Chapter 4**

### Appendix C-1 Calculation of photolysis rates

The photolysis rate ( $r_p$ ) of  $\text{H}_2\text{O}_2$ ,  $\text{S}_2\text{O}_8^{2-}$  and  $\text{HOCl}$  by low-pressure high-output (LPHO) mercury vapor UV lamp ( $\lambda=254\text{nm}$ ) was calculated based on the following equation:

$$r_p = -2 \times \Phi \times I_o \times f_{\text{oxidant}} \times f_{\text{solution}} \quad (1)$$

$\Phi$  is the extinction coefficient of the oxidation, *i.e.*,  $\Phi_{\text{H}_2\text{O}_2}=0.5$  (Baxendale and Wilson, 1957),  $\Phi_{\text{persulfate}}=0.7$  (Mark et al., 1990),  $\Phi_{\text{HOCl}}=0.7$  (Watts and Linden, 2007),  $\Phi_{\text{OCl}^-}=0.52$  (Nowell and Hoigne, 1992).  $I_o$  is volume-normalized UV irradiance from the flow-through UV reactor (Scheme S1).

$f_{\text{oxidant}}$  is the fraction of incident light absorbed by the oxidant.  $f_{\text{solution}}$  is the fraction of light absorbed by the total solution, which were calculated as:

$$f_{\text{oxidant}} = \frac{\varepsilon_p c_p}{\sum \varepsilon_i c_i} \quad (2)$$

$$f_{\text{solution}} = 1 - 10^{-(\alpha + \sum \varepsilon_i c_i)l} \quad (3)$$

$\varepsilon_p$  is the molar extinction coefficient of the oxidant ( $\text{M}^{-1}\cdot\text{cm}^{-1}$ ),  $c_p$  is the concentration of the oxidant (M).  $\varepsilon_i$  and  $c_i$  are the molar extinction coefficient and concentration for NOM and a particular contaminant selected.  $\alpha$  is the absorption coefficient of the solution at the wavelength of 254 nm and  $l$  is the path length of the reactor (cm). The direct photolysis rate for NOM and a particular contaminant is also calculated based on the same equations except  $f_{\text{contaminant}}$  is calculated based on the  $\varepsilon_i$  and  $c_i$  of the particular contaminant.

The volume-normalized surface irradiance from a flow-through UV reactor ( $I_o$ ) was calculated as follows:

$$I_0 = \frac{W_{UV} \times S_{UV}}{E_{254nm} \times V \times t} \quad (4)$$

The flow-through UV reactor was based on a configuration widely applied in water reuse facilities (Scheme S1). The hydraulic retention time of the UV reactor ( $t$ ) is 26 second. The energy output of the low-pressure high-output mercury vapor UV lamp ( $W_{uv}$ ) during the hydraulic retention time of the UV reactor is 1179 mJ (Trojan Technology, London, ON). The UV lamp surface area ( $S_{uv}$ ) is 1302 cm<sup>2</sup>.  $E$  is the energy of one mole of photons at the wavelength of 254 nm ( $4.72 \times 10^8$  mJ),  $V$  is the volume of the UV reactor (9.8 L). Consequently,  $I_o$  was calculated as  $1.27 \times 10^{-5} \text{ L}^{-1} \text{ s}^{-1}$ .

**Appendix C-2 Table of rate constants and elemental reactions for kinetics modeling**

No.	Reaction	Rate Constant	Reference
1	$H_2O_2 \xrightarrow{h\nu} 2OH^\cdot$	$1.0 \times 10^{-3} \text{ s}^{-1}$	Calculated
2	$S_2O_8^{2-} \xrightarrow{h\nu} 2SO_4^{\cdot-}$	$1.4 \times 10^{-3} \text{ s}^{-1}$	Calculated
3	$HOCl \xrightarrow{h\nu} OH^\cdot + Cl^\cdot$	$3.9 \times 10^{-3} \text{ s}^{-1}$	Calculated
4	$ClO^- \xrightarrow{h\nu} Cl^\cdot + O^{\cdot-}$	$3.2 \times 10^{-3} \text{ s}^{-1}$	Calculated
5	$NOM \xrightarrow{h\nu} OH^\cdot + \text{products}$	$1.8 \times 10^{-10} \text{ s}^{-1}$	Calculated
6	$S_2O_8^{2-} + OH^\cdot \rightarrow S_2O_8^{\cdot-}$	$1.4 \times 10^7 \text{ M}^{-1} \text{ s}^{-1}$	1
7	$S_2O_8^{2-} + SO_4^{\cdot-} \rightarrow S_2O_8^{\cdot-} + SO_4^{2-}$	$6.6 \times 10^5 \text{ M}^{-1} \text{ s}^{-1}$	2
8	$S_2O_8^{2-} + Cl^\cdot \rightarrow S_2O_8^{\cdot-} + Cl$	$8.8 \times 10^6 \text{ M}^{-1} \text{ s}^{-1}$	3
9	$S_2O_8^{2-} + CO_3^{\cdot-} \rightarrow S_2O_8^{\cdot-} + CO_3^{2-}$	$3.0 \times 10^7 \text{ M}^{-1} \text{ s}^{-1}$	4
10	$S_2O_8^{2-} + SO_5^- \rightarrow S_2O_8^{\cdot-} + SO_5^{2-}$	$1.0 \times 10^5 \text{ M}^{-1} \text{ s}^{-1}$	Assumed
11	$SO_5^{2-} + H^+ \rightarrow HSO_5^-$	$5.0 \times 10^{10} \text{ M}^{-1} \text{ s}^{-1}$	4
12	$SO_5^{2-} + SO_4^{\cdot-} \rightarrow SO_5^- + SO_4^{2-}$	$1.0 \times 10^8 \text{ M}^{-1} \text{ s}^{-1}$	5
13	$HSO_5^- \rightarrow H^+ + SO_5^{2-}$	$2.0 \times 10^1 \text{ s}^{-1}$	4
14	$HSO_5^- + OH^\cdot \rightarrow H_2O + SO_5^{\cdot-}$	$1.7 \times 10^7 \text{ M}^{-1} \text{ s}^{-1}$	6
15	$SO_4^{\cdot-} + H_2O \rightarrow HSO_4^{2-} + OH^\cdot$	$6.6 \times 10^2 \text{ s}^{-1}$	7
16	$SO_4^{2-} + Cl^\cdot \rightarrow SO_4^{\cdot-} + Cl^-$	$2.5 \times 10^8 \text{ M}^{-1} \text{ s}^{-1}$	5
17	$SO_4^{\cdot-} + OH^- \rightarrow SO_4^{2-} + OH^\cdot$	$7.0 \times 10^7 \text{ M}^{-1} \text{ s}^{-1}$	8
18	$SO_4^{\cdot-} + Cl^- \rightarrow SO_4^{2-} + Cl^\cdot$	$3.0 \times 10^8 \text{ M}^{-1} \text{ s}^{-1}$	5
19	$SO_4^{\cdot-} + OH^\cdot \rightarrow HSO_5^-$	$1.0 \times 10^{10} \text{ M}^{-1} \text{ s}^{-1}$	5
20	$SO_4^{\cdot-} + HSO_5^- \rightarrow SO_5^{\cdot-} + SO_4^{2-} + H^+$	$1.0 \times 10^6 \text{ M}^{-1} \text{ s}^{-1}$	5
21	$HSO_4^- \rightarrow H^+ + SO_4^{2-}$	$1.2 \times 10^{-2} \text{ s}^{-1}$	Calculated
22	$SO_4^{\cdot-} + SO_4^{\cdot-} \rightarrow S_2O_8^{2-}$	$7.0 \times 10^8 \text{ M}^{-1} \text{ s}^{-1}$	5
23	$SO_5^- + SO_5^- \rightarrow S_2O_8^{2-} + O_2$	$2.2 \times 10^8 \text{ M}^{-1} \text{ s}^{-1}$	5
24	$SO_5^- + SO_5^- \rightarrow SO_4^{\cdot-} + SO_4^{\cdot-} + O_2$	$2.1 \times 10^8 \text{ M}^{-1} \text{ s}^{-1}$	5
25	$SO_5^- + HO_2 \rightarrow O_2 + HSO_5^-$	$5.0 \times 10^7 \text{ M}^{-1} \text{ s}^{-1}$	9
26	$H_2O_2 \rightarrow H^+ + HO_2^-$	$1.3 \times 10^{-1} \text{ s}^{-1}$	4
27	$H^+ + HO_2^- \rightarrow H_2O_2$	$5.0 \times 10^{10} \text{ M}^{-1} \text{ s}^{-1}$	4
28	$H_2O_2 + SO_4^{\cdot-} \rightarrow HO_2 + HSO_4^-$	$1.2 \times 10^7 \text{ M}^{-1} \text{ s}^{-1}$	10
29	$H_2O_2 + SO_4^{\cdot-} \rightarrow HO_2 + SO_4^{2-} + H^+$	$1.2 \times 10^7 \text{ M}^{-1} \text{ s}^{-1}$	11
30	$H_2O_2 + O_2^{\cdot-} \rightarrow OH^\cdot + OH^- + O_2$	$1.3 \times 10^{-1} \text{ M}^{-1} \text{ s}^{-1}$	12
31	$H_2O_2 + O^{\cdot-} \rightarrow O_2^- + H_2O$	$4.0 \times 10^8 \text{ M}^{-1} \text{ s}^{-1}$	13
32	$H_2O \rightarrow H^+ + OH^-$	$1.0 \times 10^{-3} \text{ s}^{-1}$	4
33	$H^+ + OH^- \rightarrow H_2O$	$1.0 \times 10^{11} \text{ M}^{-1} \text{ s}^{-1}$	4
34	$H^+ + O_2^{\cdot-} \rightarrow HO_2^-$	$5.0 \times 10^{10} \text{ M}^{-1} \text{ s}^{-1}$	14
35	$OH^\cdot + H_2O_2 \rightarrow HO_2 + H_2O$	$2.7 \times 10^7 \text{ M}^{-1} \text{ s}^{-1}$	13
36	$OH^\cdot + OH^- \rightarrow O^{\cdot-} + H_2O$	$1.2 \times 10^{10} \text{ M}^{-1} \text{ s}^{-1}$	13
37	$O^{\cdot-} + H_2O \rightarrow OH^\cdot + OH^-$	$1.8 \times 10^5 \text{ s}^{-1}$	13
38	$O^{\cdot-} + HO_2^- \rightarrow O_2^- + OH^-$	$4.0 \times 10^8 \text{ M}^{-1} \text{ s}^{-1}$	13
39	$O^{\cdot-} + O_2 \rightarrow O_3^{\cdot-}$	$3.6 \times 10^9 \text{ M}^{-1} \text{ s}^{-1}$	13
40	$O^{\cdot-} + O_2^{\cdot-} + H^+ \rightarrow OH^- + O_2$	$6.0 \times 10^8 \text{ M}^{-1} \text{ s}^{-1}$	15
41	$O_3^{\cdot-} \rightarrow O_2 + O^{\cdot-}$	$2.6 \times 10^3 \text{ s}^{-1}$	16
42	$OH^\cdot + O^{\cdot-} \rightarrow HO_2^-$	$1.0 \times 10^{10} \text{ M}^{-1} \text{ s}^{-1}$	13
43	$OH^\cdot + HO_2^- \rightarrow HO_2 + OH^-$	$7.5 \times 10^9 \text{ M}^{-1} \text{ s}^{-1}$	17
44	$OH^\cdot + HO_2 \rightarrow H_2O + O_2$	$6.6 \times 10^9 \text{ M}^{-1} \text{ s}^{-1}$	18

45	$OH^\cdot + O_2^- \rightarrow OH^- + O_2$	$7.0 \times 10^9 \text{ M}^{-1} \text{ s}^{-1}$	19
46	$OH^\cdot + OH^\cdot \rightarrow H_2O_2$	$3.6 \times 10^9 \text{ M}^{-1} \text{ s}^{-1}$	20
47	$OH^\cdot + Cl^- \rightarrow ClOH^-$	$4.3 \times 10^9 \text{ M}^{-1} \text{ s}^{-1}$	21
48	$OH^\cdot + HSO_4^- \rightarrow H_2O + SO_4^-$	$1.7 \times 10^6 \text{ M}^{-1} \text{ s}^{-1}$	22
49	$HO_2^\cdot + HO_2^\cdot \rightarrow H_2O_2 + O_2$	$8.3 \times 10^5 \text{ M}^{-1} \text{ s}^{-1}$	23
50	$HO_2^\cdot + H_2O_2 \rightarrow OH^\cdot + H_2O + O_2$	$3.0 \times 10^0 \text{ M}^{-1} \text{ s}^{-1}$	24
51	$HO_2^\cdot + O_2^- \rightarrow HO_2^- + O_2$	$9.7 \times 10^7 \text{ M}^{-1} \text{ s}^{-1}$	23
52	$HO_2^\cdot \rightarrow H^+ + O_2^-$	$1.6 \times 10^5 \text{ s}^{-1}$	23
53	$ClOH^\cdot \rightarrow Cl^- + OH^\cdot$	$6.1 \times 10^9 \text{ s}^{-1}$	21
54	$ClOH^\cdot + Cl^- \rightarrow OH^- + Cl_2^-$	$1.0 \times 10^4 \text{ M}^{-1} \text{ s}^{-1}$	25
55	$ClOH^\cdot + H^+ \rightarrow Cl^\cdot + H_2O$	$2.1 \times 10^{10} \text{ M}^{-1} \text{ s}^{-1}$	21
56	$HOCl + H_2O_2 \rightarrow HCl + H_2O + O_2$	$1.1 \times 10^4 \text{ M}^{-1} \text{ s}^{-1}$	26
57	$HOCl + OH^\cdot \rightarrow ClO^\cdot + H_2O$	$2.0 \times 10^9 \text{ M}^{-1} \text{ s}^{-1}$	27
58	$HOCl + O_2^- \rightarrow Cl^\cdot + OH^- + O_2$	$7.5 \times 10^6 \text{ M}^{-1} \text{ s}^{-1}$	27
59	$HOCl + HO_2^\cdot \rightarrow Cl^\cdot + OH^- + O_2 + H$	$7.5 \times 10^6 \text{ M}^{-1} \text{ s}^{-1}$	27
60	$HOCl + Cl^\cdot \rightarrow ClO^\cdot + H^+ + Cl^-$	$3.0 \times 10^9 \text{ M}^{-1} \text{ s}^{-1}$	28
61	$HOCl + Cl^- \rightarrow Cl_2OH^-$	$1.5 \times 10^4 \text{ M}^{-1} \text{ s}^{-1}$	29
62	$Cl^\cdot + H_2O_2 \rightarrow H^+ + Cl^- + HO_2^\cdot$	$2.0 \times 10^9 \text{ M}^{-1} \text{ s}^{-1}$	30
63	$Cl^\cdot + H_2O \rightarrow ClOH^- + H^+$	$2.5 \times 10^5 \text{ s}^{-1}$	21
64	$Cl^\cdot + OH^- \rightarrow ClOH^-$	$1.8 \times 10^{10} \text{ M}^{-1} \text{ s}^{-1}$	28
65	$Cl^\cdot + Cl^- \rightarrow Cl_2^-$	$8.5 \times 10^9 \text{ M}^{-1} \text{ s}^{-1}$	30
66	$Cl^\cdot + Cl_2 \rightarrow Cl_3$	$5.3 \times 10^8 \text{ M}^{-1} \text{ s}^{-1}$	31
67	$Cl^\cdot + ClO^- \rightarrow ClO^\cdot + Cl^-$	$8.3 \times 10^9 \text{ M}^{-1} \text{ s}^{-1}$	28
68	$Cl^\cdot + Cl^\cdot \rightarrow Cl_2$	$8.8 \times 10^7 \text{ M}^{-1} \text{ s}^{-1}$	32
69	$Cl_2^- + Cl^\cdot \rightarrow Cl_2 + Cl^-$	$2.1 \times 10^9 \text{ M}^{-1} \text{ s}^{-1}$	30
70	$Cl_2^- + OH^- \rightarrow Cl^- + ClOH^-$	$4.5 \times 10^7 \text{ M}^{-1} \text{ s}^{-1}$	25
71	$Cl_2^- \rightarrow Cl^\cdot + Cl^-$	$6.0 \times 10^4 \text{ s}^{-1}$	30
72	$Cl_2^- + Cl_2^- \rightarrow 2 Cl^- + Cl_2$	$9.0 \times 10^8 \text{ M}^{-1} \text{ s}^{-1}$	30
73	$Cl_2^- + H_2O \rightarrow Cl^- + HClOH$	$1.3 \times 10^3 \text{ s}^{-1}$	33
74	$Cl_2^- + OH^\cdot \rightarrow HOCl + Cl^-$	$1.0 \times 10^9 \text{ M}^{-1} \text{ s}^{-1}$	34
75	$Cl_2^- + H_2O_2 \rightarrow HO_2^\cdot + H^+ + 2 Cl^-$	$1.4 \times 10^5 \text{ M}^{-1} \text{ s}^{-1}$	27
76	$Cl_2^- + HO_2^\cdot \rightarrow O_2 + H^+ + 2 Cl^-$	$3.1 \times 10^9 \text{ M}^{-1} \text{ s}^{-1}$	27
77	$Cl_2^- + O_2^- \rightarrow O_2 + 2 Cl^-$	$2.0 \times 10^9 \text{ M}^{-1} \text{ s}^{-1}$	27
78	$HClOH \rightarrow H^+ + ClOH^-$	$1.0 \times 10^8 \text{ s}^{-1}$	33
79	$HClOH \rightarrow Cl^\cdot + H_2O$	$1.0 \times 10^2 \text{ s}^{-1}$	33
80	$HClOH + Cl^- \rightarrow Cl_2^- + H_2O$	$5.0 \times 10^9 \text{ M}^{-1} \text{ s}^{-1}$	33
81	$H^+ + Cl^- \rightarrow HCl$	$5.0 \times 10^{10} \text{ M}^{-1} \text{ s}^{-1}$	4
82	$HCl \rightarrow H^+ + Cl^-$	$8.6 \times 10^{16} \text{ s}^{-1}$	4
83	$ClO^- + H_2O_2 \rightarrow Cl^- + H_2O + O_2$	$1.7 \times 10^5 \text{ M}^{-1} \text{ s}^{-1}$	26
84	$ClO^- + OH^\cdot \rightarrow ClO^\cdot + OH^-$	$8.8 \times 10^9 \text{ M}^{-1} \text{ s}^{-1}$	27
85	$ClO^- + O_2^- + H_2O \rightarrow Cl^\cdot + 2 OH^- + O_2$	$2.0 \times 10^8 \text{ M}^{-1} \text{ s}^{-1}$	27
86	$Cl_2 + Cl^- \rightarrow Cl_3^-$	$2.0 \times 10^4 \text{ M}^{-1} \text{ s}^{-1}$	35
87	$Cl_2 + O_2^- \rightarrow O_2 + Cl_2^-$	$1.0 \times 10^9 \text{ M}^{-1} \text{ s}^{-1}$	27
88	$Cl_2 + HO_2^\cdot \rightarrow H^+ + O_2 + Cl_2^-$	$1.0 \times 10^9 \text{ M}^{-1} \text{ s}^{-1}$	36
89	$Cl_2 + H_2O \rightarrow HOCl + Cl^- + H^+$	$2.2 \times 10^0 \text{ s}^{-1}$	29
90	$Cl_2 + H_2O_2 \rightarrow 2 HCl + O_2$	$1.3 \times 10^4 \text{ M}^{-1} \text{ s}^{-1}$	27
91	$Cl_2OH^- \rightarrow HOCl + Cl^-$	$5.5 \times 10^9 \text{ s}^{-1}$	29
92	$Cl_3^- \rightarrow Cl_2 + Cl^-$	$1.1 \times 10^5 \text{ s}^{-1}$	35
93	$Cl_3^- + HO_2^\cdot \rightarrow Cl_2^- + HCl + O_2$	$1.0 \times 10^9 \text{ M}^{-1} \text{ s}^{-1}$	36
94	$Cl_3^- + O_2^- \rightarrow Cl_2^- + Cl^- + O_2$	$3.8 \times 10^9 \text{ M}^{-1} \text{ s}^{-1}$	27
95	$H_2CO_3 \rightarrow HCO_3^- + H^+$	$2.5 \times 10^4 \text{ s}^{-1}$	4

96	$H_2CO_3 + OH^- \rightarrow CO_3^{2-} + H_2O + H^+$	$1.0 \times 10^6 M^{-1}s^{-1}$	37
97	$HCO_3^- + H^+ \rightarrow H_2CO_3$	$5.0 \times 10^{10} M^{-1}s^{-1}$	4
98	$HCO_3^- \rightarrow CO_3^{2-} + H^+$	$2.5 \times 10^0 s^{-1}$	27
99	$HCO_3^- + OH^- \rightarrow CO_3^{2-} + H_2O$	$8.6 \times 10^6 M^{-1}s^{-1}$	13
100	$HCO_3^- + Cl^- \rightarrow CO_3^{2-} + HCl$	$2.2 \times 10^8 M^{-1}s^{-1}$	38
101	$HCO_3^- + Cl_2^- \rightarrow 2 Cl^- + H^+ + CO_3^{2-}$	$8.0 \times 10^7 M^{-1}s^{-1}$	27
102	$HCO_3^- + SO_4^{2-} \rightarrow CO_3^{2-} + SO_4^{2-} + H^+$	$9.1 \times 10^6 M^{-1}s^{-1}$	39
103	$CO_3^{2-} + H^+ \rightarrow HCO_3^-$	$5.0 \times 10^{10} M^{-1}s^{-1}$	27
104	$CO_3^{2-} + OH^- \rightarrow CO_3^{2-} + OH^-$	$3.9 \times 10^8 M^{-1}s^{-1}$	13
105	$CO_3^{2-} + Cl^- \rightarrow CO_3^{2-} + Cl^-$	$5.0 \times 10^8 M^{-1}s^{-1}$	38
106	$CO_3^{2-} + Cl_2^- \rightarrow CO_3^{2-} + 2 Cl^-$	$1.6 \times 10^8 M^{-1}s^{-1}$	27
107	$CO_3^{2-} + ClO^- \rightarrow CO_3^{2-} + ClO^-$	$6.0 \times 10^2 M^{-1}s^{-1}$	40
108	$CO_3^{2-} + SO_4^{2-} \rightarrow CO_3^{2-} + SO_4^{2-}$	$2.5 \times 10^6 M^{-1}s^{-1}$	41
109	$CO_3^{2-} + H_2O_2 \rightarrow HCO_3^- + HO_2^-$	$4.3 \times 10^5 M^{-1}s^{-1}$	42
110	$CO_3^{2-} + HO_2^- \rightarrow CO_3^{2-} + HO_2^-$	$3.0 \times 10^7 M^{-1}s^{-1}$	42
111	$CO_3^{2-} + HO_2^- \rightarrow HCO_3^- + O_2^-$	$3.0 \times 10^7 M^{-1}s^{-1}$	1
112	$CO_3^{2-} + OH^- \rightarrow product$	$3.0 \times 10^9 M^{-1}s^{-1}$	43
113	$CO_3^{2-} + CO_3^{2-} \rightarrow product$	$3.0 \times 10^7 M^{-1}s^{-1}$	43
114	$CO_3^{2-} + O_2^- \rightarrow CO_3^{2-} + O_2$	$6.0 \times 10^8 M^{-1}s^{-1}$	43
115	$CO_3^{2-} + 2Br^- \rightarrow CO_3^{2-} + Br_2^-$	$3.4 \times 10^4 M^{-1}s^{-1}$	40
116	$CO_3^{2-} + ClO^- \rightarrow CO_3^{2-} + ClO^-$	$5.1 \times 10^5 M^{-1}s^{-1}$	44
117	$Br^- + OH^- \rightarrow BrOH^-$	$1.1 \times 10^{10} M^{-1}s^{-1}$	27
118	$Br^- + SO_4^{2-} \rightarrow Br^- + SO_4^{2-}$	$3.5 \times 10^9 M^{-1}s^{-1}$	45
119	$Br^- + H^+ \rightarrow + HBr$	$5.0 \times 10^{10} M^{-1}s^{-1}$	4
120	$Br^- + HOCl \rightarrow BrCl + OH^-$	$1.3 \times 10^{-1} M^{-1}s^{-1}$	46
121	$Br^- + Cl_2 \rightarrow BrCl_2^-$	$6.0 \times 10^9 M^{-1}s^{-1}$	35
122	$Br^- + ClOH^- \rightarrow BrCl^- + OH^-$	$1.0 \times 10^9 M^{-1}s^{-1}$	27
123	$Br^- + Cl^- \rightarrow BrCl^-$	$1.2 \times 10^{10} M^{-1}s^{-1}$	27
124	$Br^- + Cl_2^- \rightarrow BrCl^- + Cl^-$	$4.0 \times 10^9 M^{-1}s^{-1}$	35
125	$Br^- + CO_3^{2-} \rightarrow Br^- + CO_3^{2-}$	$1.0 \times 10^5 M^{-1}s^{-1}$	38
126	$Br^- + O^- \rightarrow product$	$2.2 \times 10^8 M^{-1}s^{-1}$	47
127	$BrCl_2^- \rightarrow Cl_2 + Br^-$	$9.0 \times 10^3 s^{-1}$	35
128	$BrCl_2^- + Br^- \rightarrow Br_2Cl^- + Cl^-$	$3.0 \times 10^8 M^{-1}s^{-1}$	35
129	$HBr \rightarrow H^+ + Br^-$	$5.0 \times 10^{19} s^{-1}$	4
130	$Br_2 + Br^- \rightarrow Br_3^-$	$9.6 \times 10^8 M^{-1}s^{-1}$	27
131	$Br_2 + HO_2^- \rightarrow Br_2^- + O_2 + H^+$	$1.1 \times 10^8 M^{-1}s^{-1}$	27
132	$Br_2 + O_2^- \rightarrow Br_2^- + O_2$	$5.6 \times 10^9 M^{-1}s^{-1}$	27
133	$Br_2 + H_2O \rightarrow HOBr + H^+ + Br^-$	$9.7 \times 10^1 s^{-1}$	27
134	$Br_2 + H_2O_2 \rightarrow HBr + O_2$	$1.3 \times 10^3 M^{-1}s^{-1}$	48
135	$Br_2 + Cl^- \rightarrow Br_2Cl^-$	$5.0 \times 10^4 M^{-1}s^{-1}$	27
136	$Br_2Cl^- \rightarrow + Br_2 + Cl^-$	$3.8 \times 10^4 s^{-1}$	27
137	$Br_2Cl^- + Cl^- \rightarrow BrCl_2^- + Br^-$	$1.0 \times 10^5 M^{-1}s^{-1}$	27
138	$Br_3^- \rightarrow Br_2$	$5.5 \times 10^7 s^{-1}$	27
140	$Br_3^- + HO_2^- \rightarrow Br_2^- + HBr + O_2$	$1.0 \times 10^7 M^{-1}s^{-1}$	27
141	$Br_3^- + O_2^- \rightarrow Br_2^- + Br^- + O_2$	$3.8 \times 10^9 M^{-1}s^{-1}$	27
142	$OBr^- + H^+ \rightarrow HOBr$	$5.0 \times 10^{10} M^{-1}s^{-1}$	4
143	$OBr^- + H_2O_2 \rightarrow Br^- + H_2O + O_2$	$1.2 \times 10^6 M^{-1}s^{-1}$	49
144	$OBr^- + OH^- \rightarrow BrO^- + OH^-$	$4.5 \times 10^9 M^{-1}s^{-1}$	27
145	$OBr^- + O_2^- + H_2O \rightarrow Br^- + 2 OH^- + O_2$	$2.0 \times 10^8 M^{-1}s^{-1}$	27
146	$OBr^- + CO_3^{2-} \rightarrow CO_3^{2-} + BrO^-$	$4.3 \times 10^7 M^{-1}s^{-1}$	50
147	$OBr^- + O^- + H^+ \rightarrow OH^- + BrO^-$	$2.9 \times 10^9 M^{-1}s^{-1}$	51

148	$HOBr \rightarrow H^+ + OBr^-$	$7.9 \times 10^1 \text{ s}^{-1}$	4
149	$HOBr + Br^- + H^+ \rightarrow Br_2 + H_2O$	$5.0 \times 10^9 \text{ M}^{-1} \text{ s}^{-1}$	52
150	$HOBr + HO_2^- \rightarrow Br^- + H_2O + O_2$	$7.6 \times 10^8 \text{ M}^{-1} \text{ s}^{-1}$	49
151	$HOBr + H_2O_2 \rightarrow HBr + H_2O + O_2$	$1.5 \times 10^4 \text{ M}^{-1} \text{ s}^{-1}$	1
152	$HOBr + OH^- \rightarrow BrO\cdot + H_2O$	$2.0 \times 10^9 \text{ M}^{-1} \text{ s}^{-1}$	27
153	$HOBr + O_2^- \rightarrow BrOH^- + O_2$	$3.5 \times 10^9 \text{ M}^{-1} \text{ s}^{-1}$	49
154	$HOBr + HO_2 \rightarrow BrOH^- + H^+ + O_2$	$3.5 \times 10^9 \text{ M}^{-1} \text{ s}^{-1}$	27
155	$HOBr + Cl^- \rightarrow BrCl + OH^-$	$5.6 \times 10^2 \text{ M}^{-1} \text{ s}^{-1}$	46
156	$Br\cdot + H_2O \rightarrow BrOH^- + H^+$	$1.4 \times 10^0 \text{ s}^{-1}$	28
157	$Br\cdot + OH^- \rightarrow BrOH^-$	$1.1 \times 10^{10} \text{ M}^{-1} \text{ s}^{-1}$	53
158	$Br\cdot + Br^- \rightarrow Br_2^-$	$1.2 \times 10^{10} \text{ M}^{-1} \text{ s}^{-1}$	27
159	$Br\cdot + Br\cdot \rightarrow Br_2$	$1.0 \times 10^9 \text{ M}^{-1} \text{ s}^{-1}$	27
160	$Br\cdot + OBr^- \rightarrow Br^- + BrO\cdot$	$4.1 \times 10^9 \text{ M}^{-1} \text{ s}^{-1}$	28
161	$Br\cdot + H_2O_2 \rightarrow HO_2 + Br^- + H^+$	$4.0 \times 10^9 \text{ M}^{-1} \text{ s}^{-1}$	27
162	$Br\cdot + HO_2 \rightarrow H^+ + O_2 + Br^-$	$1.6 \times 10^8 \text{ M}^{-1} \text{ s}^{-1}$	27
163	$Br\cdot + CO_3^{2-} \rightarrow Br^- + CO_3^-$	$2.0 \times 10^6 \text{ M}^{-1} \text{ s}^{-1}$	27
164	$Br\cdot + HCO_3^- \rightarrow Br^- + CO_3^-$	$1.0 \times 10^6 \text{ M}^{-1} \text{ s}^{-1}$	27
165	$Br\cdot + Cl^- \rightarrow BrCl^-$	$1.0 \times 10^8 \text{ M}^{-1} \text{ s}^{-1}$	27
166	$Br_2^- + H_2O_2 \rightarrow HO_2 + 2Br^- + H^+$	$5.0 \times 10^2 \text{ M}^{-1} \text{ s}^{-1}$	27
167	$Br_2^- \rightarrow Br\cdot + Br^-$	$1.9 \times 10^4 \text{ s}^{-1}$	27
168	$Br_2^- + Br_2^- \rightarrow Br_2 + 2Br^-$	$1.9 \times 10^9 \text{ M}^{-1} \text{ s}^{-1}$	27
169	$Br_2^- + Br\cdot \rightarrow Br_2 + Br^-$	$2.0 \times 10^9 \text{ M}^{-1} \text{ s}^{-1}$	27
170	$Br_2^- + HO_2 \rightarrow O_2 + 2Br^- + H^+$	$1.0 \times 10^8 \text{ M}^{-1} \text{ s}^{-1}$	48
171	$Br_2^- + HO_2 \rightarrow HO_2$	$4.4 \times 10^9 \text{ M}^{-1} \text{ s}^{-1}$	27
172	$Br_2^- + O_2^- \rightarrow O_2 + 2Br^-$	$1.7 \times 10^8 \text{ M}^{-1} \text{ s}^{-1}$	48
173	$Br_2^- + OBr^- \rightarrow BrO\cdot + 2Br^-$	$6.2 \times 10^7 \text{ M}^{-1} \text{ s}^{-1}$	27
174	$Br_2^- + OH\cdot \rightarrow HOBr + Br^-$	$1.0 \times 10^9 \text{ M}^{-1} \text{ s}^{-1}$	48
175	$Br_2^- + OH^- \rightarrow BrOH^- + Br^-$	$2.7 \times 10^6 \text{ M}^{-1} \text{ s}^{-1}$	48
176	$Br_2^- + CO_3^{2-} \rightarrow 2Br^- + CO_3^-$	$1.1 \times 10^5 \text{ M}^{-1} \text{ s}^{-1}$	27
177	$Br_2^- + HCO_3^- \rightarrow 2Br^- + CO_3^- + H^+$	$8.0 \times 10^4 \text{ M}^{-1} \text{ s}^{-1}$	27
178	$Br_2^- + Cl^- \rightarrow BrCl^- + Br^-$	$4.3 \times 10^6 \text{ M}^{-1} \text{ s}^{-1}$	35
179	$Br_2^- + Cl_2^- \rightarrow Br_2 + 2Cl^-$	$4.0 \times 10^9 \text{ M}^{-1} \text{ s}^{-1}$	27
180	$BrOH^- \rightarrow OH\cdot + Br^-$	$3.3 \times 10^7 \text{ s}^{-1}$	53
181	$BrOH^- \rightarrow Br\cdot + OH^-$	$4.2 \times 10^6 \text{ s}^{-1}$	53
182	$BrOH^- + H^+ \rightarrow Br\cdot + H_2O$	$4.4 \times 10^{10} \text{ M}^{-1} \text{ s}^{-1}$	53
183	$BrOH^- + Br^- \rightarrow Br_2^- + OH^-$	$1.9 \times 10^8 \text{ M}^{-1} \text{ s}^{-1}$	53
184	$BrOH^- + Cl^- \rightarrow BrCl^- + OH^-$	$1.9 \times 10^8 \text{ M}^{-1} \text{ s}^{-1}$	27
185	$Br_2OH^- + H^+ \rightarrow Br_2 + H_2O$	$2.0 \times 10^{10} \text{ M}^{-1} \text{ s}^{-1}$	54
186	$Br_2OH^- \rightarrow HOBr + Br^-$	$5.0 \times 10^9 \text{ s}^{-1}$	54
187	$BrCl + H_2O \rightarrow HOBr + Cl^- + H^+$	$1.0 \times 10^5 \text{ s}^{-1}$	27
188	$BrCl + H_2O_2 \rightarrow HBr + HCl + O_2$	$1.3 \times 10^4 \text{ M}^{-1} \text{ s}^{-1}$	27
189	$BrCl + O_2^- \rightarrow BrCl^- + O_2$	$4.0 \times 10^9 \text{ M}^{-1} \text{ s}^{-1}$	27
190	$BrCl + HO_2 \rightarrow BrCl^- + O_2 + H^+$	$5.0 \times 10^8 \text{ M}^{-1} \text{ s}^{-1}$	27
191	$BrCl + Cl^- \rightarrow BrCl_2^-$	$1.0 \times 10^6 \text{ M}^{-1} \text{ s}^{-1}$	27
192	$BrCl + Br^- \rightarrow Br_2Cl^-$	$3.0 \times 10^8 \text{ M}^{-1} \text{ s}^{-1}$	27
193	$BrCl^- + OH\cdot \rightarrow BrCl + OH^-$	$1.0 \times 10^9 \text{ M}^{-1} \text{ s}^{-1}$	27
194	$BrCl^- + HO_2 \rightarrow Br^- + Cl^- + O_2 + H^+$	$1.0 \times 10^9 \text{ M}^{-1} \text{ s}^{-1}$	27
195	$BrCl^- + O_2^- \rightarrow Br^- + Cl^- + O_2$	$6.0 \times 10^8 \text{ M}^{-1} \text{ s}^{-1}$	27
196	$BrCl^- + H_2O_2 \rightarrow Br^- + HCl + HO_2$	$5.0 \times 10^3 \text{ M}^{-1} \text{ s}^{-1}$	27
197	$BrCl^- + OH^- \rightarrow Br^- + ClOH^-$	$3.0 \times 10^6 \text{ M}^{-1} \text{ s}^{-1}$	27
198	$BrCl^- + OH^- \rightarrow BrOH^- + Cl^-$	$2.0 \times 10^7 \text{ M}^{-1} \text{ s}^{-1}$	27

199	$BrCl^- + HCO_3^- \rightarrow Br^- + HCl + CO_3^{2-}$	$3.0 \times 10^6 M^{-1}s^{-1}$	27
200	$BrCl^- + CO_3^{2-} \rightarrow Br^- + Cl^- + CO_3^{2-}$	$6.0 \times 10^6 M^{-1}s^{-1}$	27
201	$BrCl^- + BrCl^- \rightarrow Br^- + Cl^- + BrCl$	$4.7 \times 10^9 M^{-1}s^{-1}$	27
202	$BrCl^- + Cl_2^- \rightarrow 2Cl^- + BrCl$	$2.0 \times 10^9 M^{-1}s^{-1}$	27
203	$BrCl^- + Br_2^- \rightarrow Br_2 + Cl^- + Br^-$	$4.0 \times 10^9 M^{-1}s^{-1}$	27
204	$BrCl^- \rightarrow Cl^- + Br^-$	$2.0 \times 10^3 s^{-1}$	55
205	$BrCl^- \rightarrow Cl^- + Br^-$	$6.1 \times 10^4 s^{-1}$	55
206	$BrCl^- + Br^- \rightarrow Br_2^- + Cl^-$	$8.0 \times 10^9 M^{-1}s^{-1}$	35
207	$BrCl^- + Cl^- \rightarrow Cl_2^- + Br^-$	$1.1 \times 10^2 M^{-1}s^{-1}$	35
208	$Br_2Cl^- \rightarrow BrCl + Br^-$	$1.7 \times 10^4 s^{-1}$	27
209	$Br_2Cl^- \rightarrow BrCl + Cl^-$	$1.7 \times 10^5 s^{-1}$	35
210	$NOM + OH^\cdot \rightarrow product$	$7.2 \times 10^4 (mg/L)^{-1}s^{-1}$	56
211	$NOM + SO_4^{\cdot-} \rightarrow product$	$2.5 \times 10^4 (mg/L)^{-1}s^{-1}$	57
212	$NOM + Cl^\cdot \rightarrow product$	$1.3 \times 10^4 (mg/L)^{-1}s^{-1}$	58
213	$NOM + Cl_2^{\cdot-} \rightarrow product$	$1.0 \times 10^2 (mg/L)^{-1}s^{-1}$	Assumed
214	$NOM + CO_3^{\cdot-} \rightarrow product$	$3.7 \times 10^2 (mg/L)^{-1}s^{-1}$	56
215	$NOM + Br^\cdot \rightarrow product$	$1.0 \times 10^4 (mg/L)^{-1}s^{-1}$	*
216	$NOM + Br_2^{\cdot-} \rightarrow product$	$1.0 \times 10^2 (mg/L)^{-1}s^{-1}$	*
217	$NOM + BrCl^{\cdot-} \rightarrow product$	$1.0 \times 10^2 (mg/L)^{-1}s^{-1}$	*
218	$HOCl + Aniline \rightarrow product$	$9.0 \times 10^3 M^{-1}s^{-1}$	*
219	$HOCl + 17\beta - estrodiol \rightarrow product$	$2.5 \times 10^2 M^{-1}s^{-1}$	*
220	$HOCl + sulfamethoxazol \rightarrow product$	$1.0 \times 10^2 M^{-1}s^{-1}$	*
221	$HOCl + carbamazepine \rightarrow product$	$1.0 \times 10^2 M^{-1}s^{-1}$	*

---

\* Rate constants are estimated (detail in Text S3)

### Appendix C-3 Probe method to determine steady state concentration of radicals

Nitrobenzene, benzoic acid and N,N-dimethylaniline were utilized to probe the steady state concentration of HO<sup>•</sup>, SO<sub>4</sub><sup>•-</sup>, Cl<sup>•</sup>, Cl<sub>2</sub><sup>•-</sup> and CO<sub>3</sub><sup>•-</sup>. The control experiments showed a negligible direct photo-degradation for all probe compounds. Nitrobenzene exclusively reacts with HO<sup>•</sup>, therefore is the best probe for HO<sup>•</sup>. First, the experimentally observed pseudo first order decay rate of nitrobenzene ( $k_{obs}$ ) was obtained and [HO<sup>•</sup>]<sub>ss</sub> was calculated based on Equation 1.

$$-\ln\left(\frac{[NB]_t}{[NB]_0}\right) = k_{HO-NB}[HO^{\bullet}]_{ss}t \quad (\text{Eq. 1})$$

[NB]<sub>t</sub> is the concentration of nitrobenzene at time t; [NB]<sub>0</sub> is the initial concentration of nitrobenzene;  $k_{HO-NB}$  is the first-order rate constant between HO<sup>•</sup> and nitrobenzene, *i.e.*,  $3.2 \times 10^9 \text{ M}^{-1}\text{s}^{-1}$ ).<sup>59</sup>

[CO<sub>3</sub><sup>•-</sup>]<sub>ss</sub> is calculated based on equation 2 analogously.

$$-\ln\left(\frac{[N,NDMA]_t}{[N,NDMA]_0}\right) = k_{CO_3-N,NDMA}[CO_3^{\bullet-}]_{ss}t \quad (\text{Eq. 2})$$

$k_{CO_3-NB}$  is the first order rate constant between CO<sub>3</sub><sup>•-</sup> and N,N-dimethylaniline ( $1.4 \times 10^9 \text{ M}^{-1}\text{s}^{-1}$ ).<sup>60</sup>

[Cl<sup>•</sup>]<sub>ss</sub> and [SO<sub>4</sub><sup>•-</sup>]<sub>ss</sub> were simultaneously calculated using Equation 3 and 4

$$-\ln\left(\frac{[BA]_t}{[BA]_0}\right) = (k_{HO-BA}[HO^{\bullet}]_{ss} + k_{SO_4-BA}[SO_4^{\bullet-}]_{ss} + k_{Cl-BA}[Cl^{\bullet}]_{ss})t \quad (\text{Eq. 3})$$

$$-\ln\left(\frac{[1,4D]_t}{[1,4D]_0}\right) = (k_{HO-1,4D}[HO^{\bullet}]_{ss} + k_{SO_4-1,4D}[SO_4^{\bullet-}]_{ss} + k_{Cl-1,4D}[Cl^{\bullet}]_{ss})t \quad (\text{Eq. 4})$$

$k_{HO-BA}=4.3 \times 10^9 \text{ M}^{-1}\text{s}^{-1}$ ;  $k_{SO_4-BA}=1.2 \times 10^9 \text{ M}^{-1}\text{s}^{-1}$ ;  $1.4 \times 10^9 \text{ M}^{-1}\text{s}^{-1}$ ,  $k_{Cl-BA}=1.8 \times 10^{10} \text{ M}^{-1}\text{s}^{-1}$ ).<sup>61-63</sup>

In the UV/S<sub>2</sub>O<sub>8</sub><sup>2-</sup>, the contribution of Cl<sub>2</sub><sup>•-</sup> to benzoic acid and 1,4-dioxane degradation was minimal because the steady state concentration of Cl<sub>2</sub><sup>•-</sup> was low and its reactivity with the contaminants was lower than Cl<sup>•</sup>.<sup>61</sup> In UV/HOCl system, the steady-state concentration of Cl<sub>2</sub><sup>•-</sup> could be high enough to make significant contribution to contaminant degradation because the reverse reaction of ClOH<sup>•-</sup> with Cl<sup>-</sup> (Reaction 54 in **Appendix C-2**) produced a significant amount of Cl<sub>2</sub><sup>•-</sup>. Therefore, [Cl<sup>•</sup>]<sub>ss</sub> and [Cl<sub>2</sub><sup>•-</sup>]<sub>ss</sub> were simultaneously calculated using the following equations:

$$-\ln \left( \frac{[BA]_t}{[BA]_0} \right) = (k_{HO-BA}[HO^{\bullet}]_{ss} + k_{Cl_2-BA}[Cl_2^{\bullet-}]_{ss} + k_{Cl-BA}[Cl^{\bullet}]_{ss})t \quad (\text{eq 5})$$

$$-\ln \left( \frac{[1,4D]_t}{[1,4D]_0} \right) = (k_{HO-1,4D}[HO^{\bullet}]_{ss} + k_{Cl_2-1,4D}[Cl_2^{\bullet-}]_{ss} + k_{Cl-1,4D}[Cl^{\bullet}]_{ss})t \quad (\text{eq 6})$$

$$k_{Cl_2-BA} = 1.0 \times 10^6 - 1.0 \times 10^8 \text{ M}^{-1}\text{s}^{-1}, k_{Cl_2-1,4D} = 1.0 \times 10^6 - 1.0 \times 10^8 \text{ M}^{-1}\text{s}^{-1} \text{ (Appendix C-4)}.$$

#### Appendix C-4 Rate constants of reactions involving radicals

Nitrobenzene, benzoic acid and N,N-dimethylaniline were utilized to probe the steady state concentration of  $HO^\bullet$ ,  $SO_4^{\bullet-}$ ,  $Cl^\bullet$ ,  $Cl_2^{\bullet-}$  and  $CO_3^{\bullet-}$ . The control experiments showed a negligible direct photo-degradation for all probe compounds. Nitrobenzene exclusively reacts with  $HO^\bullet$ , therefore is the best probe for  $HO^\bullet$ . First, the experimentally observed pseudo first order decay rate of nitrobenzene ( $k_{obs}$ ) was obtained and  $[HO^\bullet]_{ss}$  was calculated based on Equation 1.

$$-\ln\left(\frac{[NB]_t}{[NB]_0}\right) = k_{HO-NB}[HO^\bullet]_{ss}t \quad (\text{Eq. 1})$$

$[NB]_t$  is the concentration of nitrobenzene at time  $t$ ;  $[NB]_0$  is the initial concentration of nitrobenzene;  $k_{HO-NB}$  is the first-order rate constant between  $HO^\bullet$  and nitrobenzene, *i.e.*,  $3.2 \times 10^9 \text{ M}^{-1}\text{s}^{-1}$ ).<sup>59</sup>

$[CO_3^{\bullet-}]_{ss}$  is calculated based on equation 2 analogously.

$$-\ln\left(\frac{[N,NDMA]_t}{[N,NDMA]_0}\right) = k_{CO_3-N,NDMA}[CO_3^{\bullet-}]_{ss}t \quad (\text{Eq. 2})$$

$k_{CO_3-NB}$  is the first order rate constant between  $CO_3^{\bullet-}$  and N,N-dimethylaniline ( $1.4 \times 10^9 \text{ M}^{-1}\text{s}^{-1}$ ).<sup>60</sup>

$[Cl^\bullet]_{ss}$  and  $[SO_4^{\bullet-}]_{ss}$  were simultaneously calculated using Equation 3 and 4

$$-\ln\left(\frac{[BA]_t}{[BA]_0}\right) = (k_{HO-BA}[HO^\bullet]_{ss} + k_{SO_4-BA}[SO_4^{\bullet-}]_{ss} + k_{Cl-BA}[Cl^\bullet]_{ss})t \quad (\text{Eq. 3})$$

$$-\ln \left( \frac{[1,4D]_t}{[1,4D]_0} \right) = (k_{HO-1,4D}[HO\cdot]_{ss} + k_{SO_4-1,4D}[SO_4^{\cdot-}]_{ss} + k_{Cl-1,4D}[Cl\cdot]_{ss})t \quad (\text{Eq. 4})$$

$$k_{HO-BA}=4.3 \times 10^9 \text{ M}^{-1}\text{s}^{-1}; k_{SO_4-BA}=1.2 \times 10^9 \text{ M}^{-1}\text{s}^{-1}, \text{ Neta et al, 1977); } 1.4 \times 10^9 \text{ M}^{-1}\text{s}^{-1}, k_{Cl-BA}=1.8 \times 10^{10} \text{ M}^{-1}\text{s}^{-1}. \text{ }^{6163}$$

In the UV/S<sub>2</sub>O<sub>8</sub><sup>2-</sup>, the contribution of Cl<sub>2</sub><sup>•-</sup> to benzoic acid and 1,4-dioxane degradation was minimal because the steady state concentration of Cl<sub>2</sub><sup>•-</sup> was low and its reactivity with the contaminants was lower than Cl<sup>•</sup>.<sup>61</sup> In UV/HOCl system, the steady-state concentration of Cl<sub>2</sub><sup>•-</sup> could be high enough to make significant contribution to contaminant degradation because the reverse reaction of ClOH<sup>•</sup> with Cl<sup>-</sup> (Reaction 54 in **Appendix C-2**) produced a significant amount of Cl<sub>2</sub><sup>•-</sup>. Therefore, [Cl<sup>•</sup>]<sub>ss</sub> and [Cl<sub>2</sub><sup>•-</sup>]<sub>ss</sub> were simultaneously calculated using the following equations:

$$-\ln \left( \frac{[BA]_t}{[BA]_0} \right) = (k_{HO-BA}[HO\cdot]_{ss} + k_{Cl_2-BA}[Cl_2^{\cdot-}]_{ss} + k_{Cl-BA}[Cl\cdot]_{ss})t \quad (\text{eq 5})$$

$$-\ln \left( \frac{[1,4D]_t}{[1,4D]_0} \right) = (k_{HO-1,4D}[HO\cdot]_{ss} + k_{Cl_2-1,4D}[Cl_2^{\cdot-}]_{ss} + k_{Cl-1,4D}[Cl\cdot]_{ss})t \quad (\text{eq 6})$$

$$k_{Cl_2-BA}= 1.0 \times 10^6 - 1.0 \times 10^8 \text{ M}^{-1}\text{s}^{-1}, k_{Cl_2-1,4D}=1.0 \times 10^6 - 1.0 \times 10^8 \text{ M}^{-1}\text{s}^{-1} \text{ (Appendix C-4).}$$

## Appendix C-5 Rate constants of reactions involving radicals

The rate constants for all six compounds were mostly obtained from NIST database.<sup>64</sup> When the value was not available, a range of the rate constant was estimated base on existing known values for similar compounds. For example, the reaction mechanism of Cl<sup>•</sup> and Br<sup>•</sup> are very similar to HO<sup>•</sup>, and the rates are comparable to the rates of HO<sup>•</sup>,<sup>37,64</sup> thus a  $\pm 10\%$  of HO<sup>•</sup> rate was assigned to Cl<sup>•</sup> or Br<sup>•</sup>. The estimation also based on the reaction mechanism of the specific radical with different type of molecules. For example, Cl<sup>•</sup> reacts fast with aromatic compounds and amine containing compounds ( $10^9$ - $10^{10}$  M<sup>-1</sup>s<sup>-1</sup>),<sup>64</sup> moderately fast with unsaturated aliphatic compounds ( $10^8$ - $10^9$  M<sup>-1</sup>s<sup>-1</sup>) and slow with saturated aliphatic compounds including chlorinated or brominated compounds ( $10^4$ - $10^6$  M<sup>-1</sup>s<sup>-1</sup>). Br<sup>•</sup> has high reaction rates with aromatic compounds ( $10^9$ - $10^{10}$  M<sup>-1</sup>s<sup>-1</sup>) and low reactivity with aliphatic alcohols ( $10^4$ - $10^6$  M<sup>-1</sup>s<sup>-1</sup>).<sup>64</sup>

A relatively high reactivity also applies to Cl<sub>2</sub><sup>•-</sup>, ClBr<sup>•-</sup>, Br<sub>2</sub><sup>•-</sup> and CO<sub>3</sub><sup>•-</sup>.<sup>4,58</sup> Therefore, a  $\pm 10\%$  rate was assigned based on known rates for any of the above radicals. With a comparison of available rate constants from the NIST database, Cl<sub>2</sub><sup>•-</sup> has high reaction rates ( $10^8$  M<sup>-1</sup>s<sup>-1</sup>) with unsaturated aliphatic compounds than with aromatic ( $10^6$ - $10^8$  M<sup>-1</sup>s<sup>-1</sup>). Low reactivity with unsaturated carboxylic ( $10^6$  M<sup>-1</sup> s<sup>-1</sup>). CO<sub>3</sub><sup>•-</sup> reacts fast with compounds containing amines ( $10^8$ - $10^9$  M<sup>-1</sup>s<sup>-1</sup>),<sup>64</sup> but low reactivity with aromatic compounds ( $10^4$ - $10^6$  M<sup>-1</sup>s<sup>-1</sup>). The rates of direct oxidation by HOCl were estimated when the literature values were not available. For example, the oxidation rates for aniline, 17 $\beta$ -estradiol, sulfamethoxazole and carbamazepine by HOCl was estimated based on their known

reaction rates with O<sub>3</sub>.<sup>65</sup> The direct oxidation of 1,4-dioxane by HOCl is negligible based on experimental verification.

## Reference:

---

- <sup>1</sup> Buxton, G. V.; Salmon, G. A.; Wood, N. D. A pulse radiolysis study of the chemistry of oxysulphur radicals in aqueous solution. *In Physico-Chemical Behaviour of Atmospheric Pollutants*. **1990**, 245-250.
- <sup>2</sup> Jiang, P. Y.; Katsumura, Y.; Domae, M.; Ishikawa, K.; Nagaishi, R.; Ishigure, K.; Yoshida, Y., Pulse radiolysis study of concentrated phosphoric acid solutions. *Journal of the Chemical Society. Faraday Transactions*. **1992**, 88 (22), 3319-3322.
- <sup>3</sup> Yu, X. Y., Bao, Z. C., Barker, J. R., Free radical reactions involving Cl, Cl<sub>2</sub><sup>-</sup>, and SO<sub>4</sub><sup>-</sup> in the 248 nm photolysis of aqueous solutions containing S<sub>2</sub>O<sub>8</sub><sup>2-</sup> and Cl<sup>-</sup>. *The Journal of Physical Chemistry A*. **2004**, 108 (2), 295-308.
- <sup>4</sup> Yang, Y.; Pignatello, J. J.; Ma, J.; Mitch, W. A. Comparison of halide impacts on the efficiency of contaminant degradation by sulfate and hydroxyl radical-based advanced oxidation processes (AOPs). *Environmental Science & Technology*. **2014**, 48 2344-2351.
- <sup>5</sup> Das, T., Reactivity and role of SO<sub>5</sub><sup>-</sup> radical in aqueous medium chain oxidation of sulfite to sulfate and atmospheric sulfuric acid generation. *The Journal of Physical Chemistry A*. **2001**, 105 (40), 9142-9155.
- <sup>6</sup> Maruthamuthu, P.; Neta, P., Radiolytic chain decomposition of peroxomonophosphoric and peroxomonosulfuric acids. *The Journal of Physical Chemistry*. **1977**, 81 (10), 937-940.
- <sup>7</sup> Herrmann, H.; Reese, A.; Zellner, R., Time-resolved UV/VIS diode-array absorption spectroscopy of SO<sub>x</sub><sup>-</sup> (x=3, 4, 5) radical anions in aqueous solution. *Journal of Molecular Structure*. **1995**, 348, 183-186.
- <sup>8</sup> Peyton, G. R. The free-radical chemistry of persulfate-based total organic carbon analyzers. *Marine Chemistry*. **1993**, 41 (1-3), 91-103.
- <sup>9</sup> Yermakov, A. N.; Zhitomirsky, B. M.; Poskrebyshev, G. A.; Stoliarov, S. I. Kinetic study of SO<sub>5</sub><sup>-</sup> and HO<sub>2</sub> radicals reactivity in aqueous phase bisulfite oxidation. *The Journal of Physical Chemistry*. **1995**, 99 (10), 3120-3127.
- <sup>10</sup> Wine, P. H.; Tang, Y.; Thorn, R. P.; Wells, J. R.; Davis, D. D. Kinetics of aqueous phase reactions of the SO<sub>4</sub><sup>-</sup> radical with potential importance in cloud chemistry. *Journal of Geophysical Research: Atmospheres*. **1989**, 94 (1984–2012), 1085-1094.
- <sup>11</sup> Maruthamuthu, P.; Neta, P. Phosphate radicals. Spectra, acid-base equilibria, and reactions with inorganic compounds. *The Journal of Physical Chemistry*. **1978**, 82 (6), 710-713.

- 
- <sup>12</sup> Weinstein, J.; Bielski, B. H. J. Kinetics of the interaction of perhydroxyl and superoxide radicals with hydrogen peroxide. The Haber-Weiss reaction. *Journal of the American Chemical Society*. **1979**, *101* (1), 58-62.
- <sup>13</sup> Buxton, G. V.; Greenstock, C. L.; Helman, W. P.; Ross, A. B. Critical review of rate constants for reactions of hydrated electrons, hydrogen atoms and hydroxyl radicals ( $\cdot\text{OH}/\text{O}^-$  in aqueous solution. *Journal of Physical and Chemical Reference Data*. 1988, *17* (2), 513-886.
- <sup>14</sup> Ilan, Y.; Rabani, J. On some fundamental reactions in radiation chemistry: Nanosecond pulse radiolysis. *International Journal for Radiation Physics and Chemistry*. **1976**, *8* (5), 609-611.
- <sup>15</sup> Sehested, K.; Holcman, J.; Bjergbakke, E.; Hart, E. J. Ultraviolet spectrum and decay of the ozonide ion radical,  $\text{O}_3^-$ , in strong alkaline solution. *The Journal of Physical Chemistry*. **1982**, *86* (11), 2066-2069.
- <sup>16</sup> Elliot, A. J.; McCracken, D. R. Effect of temperature on  $\text{O}^\infty$  reactions and equilibria: A pulse radiolysis study. *International Journal of Radiation Applications and Instrumentation. Part C. Radiation Physics and Chemistry*. **1989**, *33* (1), 69-74.
- <sup>17</sup> Christensen, H.; Sehested, K.; Corfitzen, H. Reactions of hydroxyl radicals with hydrogen peroxide at ambient and elevated temperatures. *The Journal of Physical Chemistry*. **1982**, *86* (9), 1588-1590.
- <sup>18</sup> Sehested, K.; Rasmussen, O. L.; Fricke, H. Rate constants of OH with  $\text{HO}_2$ ,  $\text{O}_2^-$ , and  $\text{H}_2\text{O}_2^+$  from hydrogen peroxide formation in pulse-irradiated oxygenated water. *The Journal of Physical Chemistry*. **1968**, *72* (2), 626-631.
- <sup>19</sup> Beck, G. Elektrische leitfähigkeitsmessungen zum nachweis geladener zwischenprodukte der pulsradiolyse. *International Journal for Radiation Physics and Chemistry*. **1969**, *1* (3), 361-371.
- <sup>20</sup> Elliot, A. J. A pulse radiolysis study of the temperature dependence of reactions involving H, OH and  $\text{e}^-_{\text{aq}}$  in aqueous solutions. *International Journal of Radiation Applications and Instrumentation. Part C. Radiation Physics and Chemistry*. **1989**, *34* (5), 753-758.
- <sup>21</sup> Jayson, G.; Parsons, B.; Swallow, A. J. Some simple, highly reactive, inorganic chlorine derivatives in aqueous solution. Their formation using pulses of radiation and their role in the mechanism of the Fricke dosimeter. *Journal of the Chemical Society. Faraday Transaction 1: Physical Chemistry in Condensed Phases*. **1973**, (69), 1597- 1607.
- <sup>22</sup> Heckel, E.; Henglein, A.; Beck, G. Pulsradiolytische untersuchung des radikalaniums  $\text{SO}_4\cdot^-$ . *Berichte der Bunsengesellschaft für physikalische Chemie*. **1966**, *70* (2), 149-154.

- 
- <sup>23</sup> Bielski, B. H. J.; Cabelli, D. E.; Arudi, R. L.; Ross, A. B. Reactivity of HO<sub>2</sub>/O<sub>2</sub><sup>-</sup> radicals in aqueous solution. *Journal of Physical and Chemical Reference Data*. **1985**, *14* (4), 1041-1100.
- <sup>24</sup> Koppenol, W. H.; Butler, J.; van Leeuwen, J. W. The haber-weiss cycle. *Photochemistry and Photobiology*. **1978**, *28* (4-5), 655-658.
- <sup>25</sup> Grigorev, A. E.; Makarov, I. E.; Pikaev, A. K. Formation of Cl<sub>2</sub><sup>-</sup> in the bulk solution during the radiolysis of concentrated aqueous-solutions of chlorides. *High Energy Chemistry*. **1987**, *21* (2), 99-102.
- <sup>26</sup> Connick, R. E. The interaction of hydrogen peroxide and hypochlorous acid in acidic solutions containing chloride ion. *Journal of the American Chemistry Society*. **1947**, *69* (6), 1509-1514.
- <sup>27</sup> Matthew, B. M.; Anastasio, C. A chemical probe technique for the determination of reactive halogen species in aqueous solution: Part 1 - bromide solutions. *Atmospheric Chemistry and Physics*. **2006**, *6* (9), 2423-2437.
- <sup>28</sup> Klänig, U. K.; Wolff, T. Laser flash photolysis of HClO, ClO<sup>-</sup>, HBrO, and BrO<sup>-</sup> in aqueous solution. Reactions of Cl<sup>-</sup> and Br<sup>-</sup> Atoms. *Berichte der Bunsengesellschaft für physikalische Chemie*. **1985**, *89* (3), 243-245.
- <sup>29</sup> Wang, T. X.; Margerum, D. W. Kinetics of reversible chlorine hydrolysis: temperature dependence and general-acid/base-assisted mechanisms. *Inorganic Chemistry*. **1994**, *33* (6), 1050-1055.
- <sup>30</sup> Yu, X. Y.; Barker, J. R. Hydrogen peroxide photolysis in acidic aqueous solutions containing chloride ions. I. Chemical mechanism. *The Journal of Physical Chemistry A*. **2003**, *107* (9), 1313-1324.
- <sup>31</sup> Bunce, N. J.; Ingold, K. U.; Landers, J. P.; Luszyk, J.; Scaiano, J. C. Kinetic study of the photochlorination of 2, 3-dimethylbutane and other alkanes in solution in the presence of benzene. First measurements of the absolute rate constants for hydrogen abstraction by the "free" chlorine atom and the chlorine atom-benzene. pi-complex. Identification of these two species as the only hydrogen abstractors in these systems. *Journal of the American Chemical Society*. **1985**, *107* (19), 5464-5472.
- <sup>32</sup> Wu, D.; Wong, D.; Dibartolo, B. Evolution of Cl<sub>2</sub><sup>-</sup> in aqueous NaCl solution. *Journal of Photochemistry*. **1980**, *14* (4), 303-310.
- <sup>33</sup> Mcelroy, W. J. A laser photolysis study of the reaction of SO<sub>4</sub><sup>-</sup> with Cl<sup>-</sup> and the subsequent decay of Cl<sub>2</sub><sup>-</sup> in aqueous-solution. *Journal of Physics*. **1990**, *94* (6), 2435-2441.

- 
- <sup>34</sup> Wagner, I.; Karthaeuser, J.; Strehlow H. On the decay of the dichloride anion  $\text{Cl}_2^-$  in aqueous solution. Ber. Bunsenges. *The Journal of Physical Chemistry*. **1986**, *90*, 861-867.
- <sup>35</sup> Ershov, B.G. Kinetics, mechanism and intermediates of some radiation-induced reactions in aqueous solutions. *Uspekhi. Khimii*. **2004**, *73* (1), 107-120.
- <sup>36</sup> Bjergbakke, E.; Navaratnam, S.; Parsons, B. J.; Swallow, A. J. Reaction between hydroperoxo radicals and chlorine in aqueous solution. *Journal of the American Chemical Society*. **1981**, *103* (19), 5926-5928.
- <sup>37</sup> Grebel, J. E.; Pignatello, J. J.; Mitch, W. A. Effect of halide ions and carbonates on organic contaminant degradation by hydroxyl radical-based advanced oxidation processes in saline waters. *Environmental Science & Technology*. **2010**, *44* (17), 6822-6828.
- <sup>38</sup> Mertens, R.; von Sonntag, C. Photolysis ( $\lambda = 354$  nm) of tetrachloroethene in aqueous solutions. *Journal of Photochemistry and Photobiology A: Chemistry*. **1995**, *85*, (1), 1-9.
- <sup>39</sup> Dogliotti, L.; Hayon, E. Flash photolysis of persulfate ions in aqueous solutions. Study of the sulfate and ozonide radical anions. *The Journal of Physical Chemistry*. **1967**, *71* (8), 2511-2516.
- <sup>40</sup> Huie, R. E.; Clifton, C. L.; Neta, P. Electron transfer reaction rates and equilibria of the carbonate and sulfate radical anions. *International Journal of Radiation Applications and Instrumentation. Part C. Radiation Physics and Chemistry*. **1991**, *38* (5), 477-481.
- <sup>41</sup> Padmaja, S.; Neta, P.; Huie, R. E. Rate constants for some reactions of inorganic radicals with inorganic ions. Temperature and solvent dependence. *International Journal of Chemical Kinetics*. **1993**, *25* (6), 445-455.
- <sup>42</sup> Draganić, Z. D.; Negron-Mendoza, A.; Sehested, K.; Vujošević, S. I.; Navarro-Gonzales, R.; Albarran-Sanchez, M. G.; Draganić, I. G. Radiolysis of aqueous solutions of ammonium bicarbonate over a large dose range. *International Journal of Radiation Applications and Instrumentation. Part C. Radiation Physics and Chemistry*. **1991**, *38* (3), 317-321.
- <sup>43</sup> Crittenden, J. C.; Hu, S.; Hand, D. W.; Green, S. A. A kinetic model for  $\text{H}_2\text{O}_2/\text{UV}$  process in a completely mixed batch reactor. *Water Research*, **1999**, *33* (10), 2315-2328.
- <sup>44</sup> Alfassi, Z. B.; Huie, R. E.; Mosseri, S.; Neta, P. Kinetics of one-electron oxidation by the  $\text{ClO}$  radical. *International Journal of Radiation Applications and Instrumentation. Part C. Radiation Physics and Chemistry*. **1988**, *32* (1), 85-88.

- 
- <sup>45</sup> Redpath, J. L.; Willson, R. L. Chain reactions and radiosensitization: model enzyme studies. *International Journal of Radiation Biology*. **1975**, *27* (4), 389-398.
- <sup>46</sup> Sander, R.; Vogt, R.; Harris, G. W. Crutzen, P. J. Modelling the chemistry of ozone, halogen compounds, and hydrocarbons in the arctic troposphere during spring. *Tellus B*. **1997**, *49* (5), 522-532.
- <sup>47</sup> Rabani, J.; Zehavi, D. Pulse radiolytic investigation of O<sub>aq</sub>-radical ions. *The Journal of Physical Chemistry*. **1971**, *75* (11), 1738-1744.
- <sup>48</sup> Wagner, I.; Strehlow, H.; On the flash photolysis of bromide ions in aqueous solutions. *Berichte der Bunsengesellschaft für physikalische Chemie*. **1987**, *91* (12), 1317-1321.
- <sup>49</sup> von Gunten, U.; Oliveras, Y. Kinetics of the reaction between hydrogen peroxide and hypobromous acid: implication on water treatment and natural systems. *Water Research*. **1997**, *31* (4), 900-906.
- <sup>50</sup> Buxton, G. V.; Dainton, F. S. The radiolysis of aqueous solutions of oxybromine Compounds; the spectra and reactions of BrO and BrO<sup>-2</sup>. *Proceedings of the Royal Society of London. Series A. Mathematical and Physical Sciences*. **1968**, *304* (1479), 427-439.
- <sup>51</sup> Czapski, G.; Treinin, A. Flash photolysis of the oxybromine anions. *Israel Journal of Chemistry*. **1969**, *7* (3), 351-359.
- <sup>52</sup> Eigen, M.; Kustin, K.; The kinetics of halogen hydrolysis. *Journal of the American Chemical Society*. **1962**, *84* (8), 1355-1361.
- <sup>53</sup> Zehavi, D.; Rabani, J. Oxidation of aqueous bromide ions by hydroxyl radicals. Pulse radiolytic investigation. *The Journal of Physical Chemistry*. **1972**, *76* (3), 312-319.
- <sup>54</sup> Eigen, M.; Kustin, K. The kinetics of halogen hydrolysis. *Journal of the American Chemical Society*. **1962**, *84* (8), 1355-1361.
- <sup>55</sup> Donati, A. Spectroscopic and Kinetic Investigations of Halogen Containing Radicals in the Tropospheric Aqueous Phase (Doctoral dissertation). 2002.
- <sup>56</sup> Jasper, J. T.; Sedlak, D. L. Phototransformation of wastewater-derived trace organic contaminants in open-water unit process treatment wetlands. *Environmental Science & Technology*. **2013**, *47* (19), 10781-10790.
- <sup>57</sup> Lutze, H. V.; Kerlin, N.; Schmidt, T. C. Sulfate radical-based water treatment in presence of chloride: Formation of chlorate, inter-conversion of sulfate radicals into hydroxyl radicals and influence of bicarbonate. *Water Research*. **2015**, *72*, 349-360.

- 
- <sup>58</sup> Fang, J.; Fu, Y.; Shang, C. The roles of reactive species in micropollutant degradation in the UV/free chlorine system. *Environmental Science & Technology*. **2014**, *48* (3), 1859-1868.
- <sup>59</sup> Neta, P.; and Dorfman, L. M. *Pulse radiolysis studies. XIII. Rate constants for the reaction of hydroxyl radicals with aromatic compounds in aqueous solutions*. Ohio State Univ., Columbus: 1968.
- <sup>60</sup> Lilie, J.; Henglein, A.; Hanrahan, R. J. *Reactions of the carbonate radical anion with organic and inorganic solutes in aqueous solution*. 176th Meeting American Chemical Society. Miami Beach, Fla. 1978.
- <sup>61</sup> Neta, P.; Madhavan, V.; Zemel, H.; Fessenden, R. W. Rate constants and mechanism of reaction of sulfate radical anion with aromatic compounds. *Journal of the American Chemical Society*. **1977**, *99* (1), 163-164.
- <sup>62</sup> Mártire, D. O.; Rosso, J. A.; Bertolotti, S.; Le Roux, G. C.; Braun, A. M.; Gonzalez, M. C. Kinetic study of the reactions of chlorine atoms and Cl<sub>2</sub><sup>-</sup> radical anions in aqueous solutions. II. toluene, benzoic acid, and chlorobenzene. *The Journal of Physical Chemistry A*. **2001**, *105* (22), 5385-5392.
- <sup>63</sup> Wander, R.; Neta, P.; Dorfman, L. M. Pulse radiolysis studies. XII. Kinetics and spectra of the cyclohexadienyl radicals in aqueous benzoic acid solution. *The Journal of Physical Chemistry*. **1968**, *72* (8), 2946-2949.
- <sup>64</sup> NIST Standard Reference Database 40: NDRL/NIST Solutions Kinetics Database V. 3.0, Gaithersburg, MD.
- <sup>65</sup> Huber, M. M.; Canonica, S.; Park, G. Y.; von Gunten, U. Oxidation of pharmaceuticals during ozonation and advanced oxidation processes. *Environmental Science & Technology*. **2003**, *37* (5), 1016-1024.